Imperial College London

A thesis entitled

On the influence of physical and chemical structure on charge transport in disordered semiconducting materials and devices

by

Samuel Foster

Submitted for the degree of

Doctor of Philosophy

of the

Imperial College of Science, Technology and Medicine

London, United Kingdom

January 2013

Dedicated to Dad and Gran, who I would like to have seen it,
and Mum, who will be the first to read it.

The work described in this thesis was undertaken in the Experimental Solid State Physics group in the Department of Physics at Imperial College London from October 2008 – January 2013, under the supervision of Professor Jenny Nelson.

Except where specific reference is made to the contributions of others,
the work presented herein is my own.

Abstract

Achieving fast charge carrier transport in disordered organic semiconductors is of great importance for the development of organic electronic devices. Disordered organic materials generally show low charge carrier mobilities due to their inherent energetic and configurational disorder, and the presence of chemical and physical defects. Efforts to improve mobility typically involve chemical design and materials processing to control macromolecular conformation and/or induce greater crystalline or liquid crystalline order. Whilst in many cases fruitful, these approaches have not always translated into higher bulk mobilities in devices. Addressing the adverse effect on mobility of specific types of disorder or specific defects has proven difficult due to problems distinguishing the many such features spectroscopically and controlling their formation in isolation.

In the three experimental Chapters following, we attempt to make clear links between the charge carrier mobility and the presence of specific structural defects or sources of energetic or configurational disorder. In the first experimental study, we investigate hole transport in a family of polyfluorenes based on poly(9,9-dioctylfluorene) (PFO). By controlling the phase formation of the materials through processing and by virtue of their chemical design, we examine the effect on transport of distinct material phases. Remarkably, we are able to isolate the effect of the single chain conformation of PFO known as the beta-phase and show that when embedded in a glassy PFO matrix it acts as a strong hole trap, reducing the mobility of the bulk material by over two orders of magnitude. By fabricating a device with negligible beta-phase, we demonstrate the highest time-of-flight mobility in PFO to date, at over 3×10^{-2} cm^2/Vs. This study provides the first clear and unambiguous example of the effect on transport of a distinct conformational defect in a conjugated polymer. We also demonstrate the adverse effect on mobility of crystallinity in the polyfluorenes. We suggest that our findings may generalise to other systems in the sense that the mobility may be limited by a minority population of structural traps, which may include highly ordered, crystalline regions. Significant mobility improvements may then be more easily achieved by removing the minority ordered phases than by increasing their concentration. We believe that this approach offers an alternative paradigm by which higher mobilities may be obtained in general, and in particular in systems where crystallinity is undesirable.

In the second experimental study, we study charge transport in the fullerene derivatives [6,6]-phenyl-C61-butyric acid methyl ester (PCBM), bis-PCBM and tris-PCBM. The fullerene multi-adducts bis-PCBM and tris-PCBM are of interest as alternative OPV acceptor materials with the potential to increase open-circuit voltage. However, most OPV blends employing the multi-adducts have failed to improve upon those employing PCBM. This is thought to be a result of the inferior electron transport properties of the multi-adducts, due to either (i) higher energetic disorder in the multi-adducts due to the presence of isomers with varying LUMO energies or (ii) higher configurational disorder due to a lower degree of order in molecular packing in the multi-adducts than in PCBM. We distinguish the effects of energetic and configurational disorder using temperature-dependent ToF and FET measurements. We find that differences in configurational disorder appear negligible, and that the reduced mobility in the multi-adducts is due predominantly to the energetic disorder resulting from the presence of a mixture of isomers with varying LUMO energies.

In the third and final experimental study, we examine the charge transport properties of polymer:PCBM blends for OPV, focusing on the PTB7:PCBM and P3HT:PCBM systems. In particular, we address the question of why state-of-the-art OPV systems such as PTB7:PCBM perform so much worse at large active layer thicknesses than P3HT:PCBM. We find that low electron mobility is the main cause of this difference. The electron mobility in PTB7:PCBM blends, at 10^{-5} – 10^{-4} cm^2/Vs, is 1–2 orders of magnitude lower than the electron mobility in annealed P3HT:PCBM, at over 10^{-3} cm^2/Vs. The hole mobility, in contrast, is the same to within a factor of approximately three. We hypothesise that the low tendency of PTB7 to order leads to a low degree of phase separation in the blend and to a poorly connected, disordered PCBM phase. We find that increasing the PCBM fraction is very effective in improving electron transport and electrical Fill Factor, but strongly reduces absorption. We suggest that a key challenge for OPV researchers is thus to achieve better connectivity and ordering in the fullerene phase in blends without relying on either (i) a large excess of fullerene or (ii) strong crystallisation of the polymer.

Acknowledgements

This thesis would not have been possible without the valuable input of very many colleagues and friends. I would like to take this opportunity to thank everyone who has provided me with guidance, assistance or company over the last four years.

Above all, I am indebted to my supervisor, Professor Jenny Nelson. I am immensely grateful for her unrelenting support and creative ideas when experiments were not working, and for her enthusiasm in the results when they did. My time at Imperial has been enriched by the numerous opportunities outside my PhD towards which she has directed me, in particular the work at the Grantham Institute.

Many thanks also to Professor Donal Bradley, who was a great source of inspiration and expertise in my work on polyfluorenes, and who helped me greatly in setting up the research visit to Sumitomo.

My PhD would not have been quite the same if I had not carried out much of it alongside Mark Faist, with whom it was always enjoyable and stimulating to work. I also thank all my collaborators working under Jenny and Donal, particularly Jarvist Frost, Thomas Kirchartz, Florian Steiner, Yaqub Chaudhary, Alex Perevedentsev, Arthur Losquin and Ruidong Xia.

A large part of this work benefits from a collaboration with the OFET group of Professor Thomas Anthopoulos, and in particular with Jeremy Smith, James Ball and John Labram. Much of the rest relies on the materials science expertise of Dr Natalie Stingelin and her group, and in particular the great patience of Ester Buchaca-Domingo, Paul Westacott and Liyang Yu in helping me process and characterise my materials. I also thank Dr Paul Stavrinou for interesting discussions on the polyfluorenes. An important acknowledgment should be made to Gihan Ryu, who showed me how to make the beta-phase.

All those years back I benefitted from the very professional training of Peter Levermore, Amy Ballantyne, Sachetan Tuladhar, Xuhua Wang and Panos Keivanidis.

I would also like to thank all those who made H724 so lively, including many of those above and also Dave, Clare, George, Anne, Florian, Thilini, Wei and many others.

A big thank you to Bhavna, Carolyn, Juraci, Claudia and Becky in the Group Office for keeping everything working so smoothly.

An entire Chapter of this thesis was carried out at Sumitomo Chemical in Tsukuba, Japan. I was overwhelmed by the warmth and generosity of my hosts there, and by their technical abilities. Many thanks to my supervisors Doi-san and Miyake-san for arranging my visit and welcoming me into the group, and to Ohnishi-san for hosting me on an earlier visit. I was only able to navigate my way through the intricacies of Japanese life and the kanji in the laboratory thanks to the infinite patience of Oguma-san. Okachi-san, Kimura-san, Kato-san, Mitani-san and Kim-san take credit for helping me collect much of my data. Thanks also to Yoshimura-san, Kitano-san, Tsuchida-san, Ohya-san, Kashiki-san, Asada-san, Anryu-san, Kanesaka-san, Takamori-san and the Sumitomo Football team for making my time there so fun.

I was lucky to be able to spend a productive and enjoyable month in the unique laboratory of Professor Paul Smith in ETH Zurich. Many thanks to his student Felix Koch who spent much time running around to accommodate my experiments. On an earlier trip to meet our collaborators at SCUT in China, I learned much from Dr Hongbin Wu, Zhicai He and Chengmai Zhong, who were also perfect hosts.

Finally, thank you for listening, and I hope you can give the following thesis a reason to exist!

Contents

List of Figures

List of Tables

Chapter 1

Context

For the past fifty years, the semiconductor industry and its vast array of now-ubiquitous products have been built on inorganic semiconducting materials such as silicon and gallium arsenide. While these materials still dominate the electronics industry, recent decades have seen a growing research effort to develop organic semiconducting materials, polymers or small molecules based on a conjugated carbon backbone. Organic electronics presents the opportunity to generate new applications for existing technologies, and products with a range of novel properties. The wide variety of potential advantages of organic electronics include mechanical flexibility; mechanical robustness; wide tuneability of optoelectronic properties by chemical design; low material cost; fabrication by solution deposition and perhaps even roll-to-roll production; the resulting low device production cost; and the resulting low embedded energy of products, among others.

Organic small molecular materials are already widely used for xerography; organic light-emitting diodes (OLEDs) based on small molecules and polymers are breaking through into lighting and display applications; and organic transistors (OTFTs) and organic photovoltaics (OPVs) are not far behind, having entered the market in niche areas.

In general terms, the challenges for developers of organic semiconducting materials relate to achieving sufficient control over the rich variety of chemical and structural forms that the materials may take during synthesis and processing. It is not surprising that high chemical purity and a high level of structural order is more difficult to achieve in an assembly of macromolecules synthesised in a chemist's flask and deposited from solution than in an atomic crystal grown slowly from the melt. Chemical and physical stability of the organic materials in devices post-deposition is also an issue.

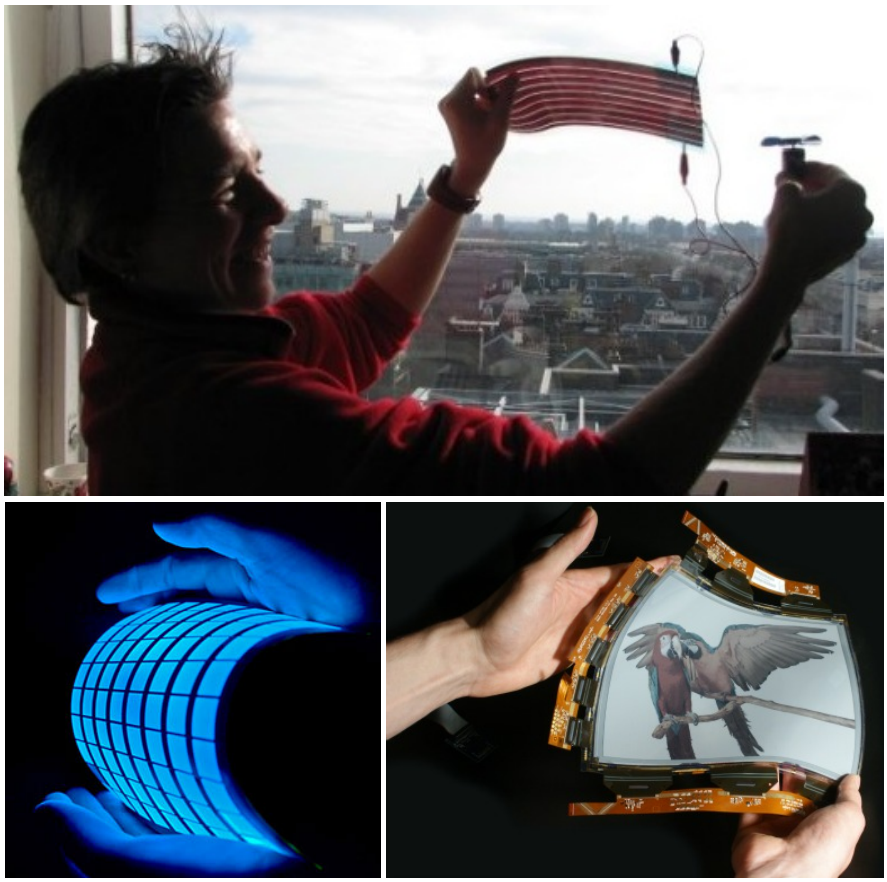

Figure 1.1: Applications of organic electronics. Top: prototype OPV module at Imperial College (picture courtesy of Sachetan Tuladhar). Bottom left: GE's roll-to-roll OLED lighting (picture from www.electronichouse.com). Bottom right: Plastic Logic's OTFT backplane driving an E-Ink Corp. e-reader display (picture from www.manufacturingdigital.com).

However, the field of organic electronics is still in period of rapid change and improvement, and there is confidence that many of the challenges to commercialisation can be overcome.

A key property of a semiconductor for optoelectronics, and the focus of this thesis, is charge carrier transport. Charge carrier transport is strongly affected by the high level of disorder and high concentration of defects in organic semiconducting materials, meaning that carrier mobilities are typically several orders of magnitude lower than those in their inorganic counterparts. Low carrier mobility currently constrains the application of many organic electronic technologies. Suitable materials with higher mobilities would benefit the development of, for example, organic photovoltaics; electrically-driven polymer lasers; light-emitting transistors; and light-emitting diodes for optical communications.

At the high mobility end of organic materials, molecular single crystals can show mobilities of up

to 40 cm^2/Vs [1], but single crystals are not compatible with flexible devices or with cost-effective solution deposition. The highest mobilities of solution-processable polymer semiconductors have improved to $3 - 6$ cm^2/Vs in 2012 [2, 3], making them competitive with metal oxide materials, which are also solution processable and flexible, and their closest competitors for application in transistor backplanes. For application in devices other than transistors, lower mobilities than this are expected to be sufficient for commercialisation. However, the requirement for certain properties other than high mobility – such as suitable energetic structure and compatibility with a donor or acceptor partner for OPV materials; and efficient luminescence for polymer lasing materials – means that leading materials for those applications lag further behind in mobility.

With these additional constraints on materials, a deeper understanding of the prerequisites for good charge transport properties in organic semiconductors is highly desirable. In particular, arriving at a better understanding of the effect of disorder and defects on charge transport will be invaluable in informing the synthesis of new materials and their processing into devices. As will be outlined in greater detail in the following sections, it has proven difficult to find the effect of particular forms of disorder and defects. This is largely a result of the sheer variety of chemical and structural forms in the materials under study, and an inability to fingerprint them or control their formation in isolation. In addition, since by far the most common approach to increasing mobility in organic systems – increasing crystalline or liquid crystalline order – is not suitable for all applications, alternative paradigms for achieving sufficiently good charge transport properties are desirable. It is hoped that this thesis demonstrates some progress in this direction.

It is also important to acknowledge the scientific context of this study. Knowledge of the mechanisms limiting charge transport in disordered organic systems, apart from the evident technological relevance, is of great academic interest. Since the first studies of charge transport in disordered organic systems for xerography [4], a large base of literature has grown around the subject. A variety of analytical models and key assumptions on the topic remain to be fully tested. The question of what fundamentally limits the mobility in disordered organic semiconductors – the role of intra-chain versus inter-chain charge transport; band-like transport versus hopping; the nature of charge trapping species; the importance of planarity, extended conjugation and the effect of conjugation breaking; the tolerable type and level of energetic and spatial disorder – is expected to stimulate generations of researchers to come.

Chapter 2

Background

2.1 Charge transport in disordered organic semiconductors

Organic semiconducting materials have an almost infinite variety of structures and chemistry, and may come in the form of small molecules (with typical molecular weight M_w of $100 - 1,000$) or greatly extended polymer chains (typical M_w of $10,000 - 1,000,000$). The feature common to all is that they are based on a hydrocarbon $\pi-$conjugated backbone, in many cases with small amounts of oxygen, nitrogen or sulphur [5]. The carbon atoms in the backbone achieve extended $\pi-$conjugation, in general, by virtue of the formation of sp^2-hybridised molecular orbitals. This is illustrated in Figure 2.1. In this configuration, only three of the four valence electrons in carbon are highly localized in $\sigma-$bonding orbitals, leaving one electron per carbon atom more weakly bound and more de-localised in a $\pi-$bonding orbital [6].

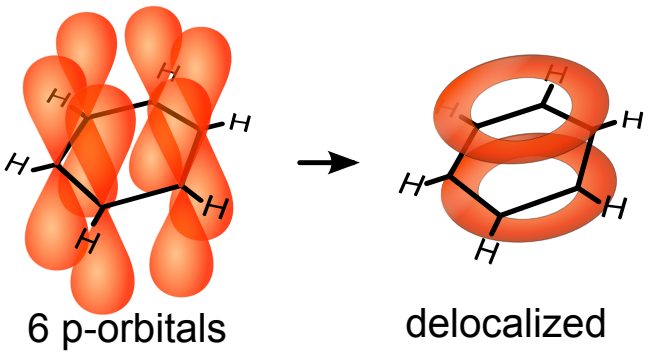

Figure 2.1: Illustration of $\pi-$conjugation of valence p-orbitals associated with the six carbon atoms of a benzene ring. Note that conjugation of the highly directional orbitals requires that they are aligned as shown. The directionality also means that effective conjugation with a second benzene ring would require the two benzene rings to be near to co-planar.

As a result of the conjugation of many such carbon atoms, the electrons in the more de-localised $\pi-$orbitals may become extended over a number of units. The energetic dividend for $\pi-$conjugation, which requires the overlap of near-parallel $\pi-$orbitals, imparts on the materials a driving force for planarity of the backbone. Depending on the suitability of the structure of the molecule for conjugation, the $\pi-$electrons extend to a greater or lesser degree across the backbone until conjugation is broken chemically or physically. Typically, conjugation may occur over the whole of a small organic molecule, and over approximately $2-10$ units of a conjugated polymer [5]. The conjugation length is limited by defects, which may simply be conformational fluctuations along the chain. Thus, it will depend firstly on the intrinsic chemical structure of the molecule, but also on extrinsic factors such as the degree of disorder 'frozen' into the material during processing and on the presence of impurities or other species, as well as the temperature and pressure.

It is important to note that in the usual case – without doping or excess injected charge – the materials described above are (like undoped silicon) insulating. Although the electrons in the $\pi-$orbitals are de-localised across a number of carbon 'hosts', they are not free carriers, as they are still contributing to bonding. The energy gap between the highest occupied molecular orbital (HOMO) and the lowest unoccupied molecular orbital (LUMO) is typically $1.5-3$ eV, meaning that the intrinsic carrier concentration at room temperature (where kT = 0.025 eV) is vanishingly small. Thus, the intrinsic conductivity of the materials is very low. In reality, extrinsic dopants increase the carrier density, and impart some conductivity to the materials. With some exceptions, however, the conjugated organic materials of the type studied in this thesis are on the whole only weakly and unintentionally doped, showing low carrier concentrations at room temperature ($10^{15}-10^{16}$ cm^{-3}). Thus, even assuming a high carrier mobility of 10^{-1} $\mathrm{cm}^2/\mathrm{Vs}$, the conductivity remains below $10^{-4}-10^{-5}$ $(\Omega\,\mathrm{cm})^{-1}$, orders of magnitude lower than, for example, metals at approx. 10^{6} $(\Omega\,\mathrm{cm})^{-1}$ and sea water at approx. 10^{-1} $(\Omega\,\mathrm{cm})^{-1}$. Hence, in order to create significant current, charge carriers must be created within the material. This may be achieved either by injecting a carrier directly from external sources (electrodes) or by promoting an electron across the HOMO–LUMO gap by the absorption of a photon. Then, the extrinsically-generated charge carrier may be able to take advantage of the de-localised nature of the lowest unoccupied states and transit through the material. Thus, the materials are termed semiconducting.

Nonetheless, the process of charge transport within organic semiconducting materials is very differ-

ent from the analogous process in inorganic semiconductors such as doped polycrystalline silicon. This thesis is concerned with the way charge carriers move through the conjugated states of organic semiconducting materials, both small molecules and polymers, for application in optoelectronic devices. What follows is a brief review of the properties of these materials relevant for our discussion.

2.1.1 The electronic properties of organic semiconducting materials

A key defining feature of conjugated organic polymers and molecules, and one which most strongly distinguishes them from crystalline inorganic semiconductors, is the localisation of excitations, both charged and uncharged [7]. This is illustrated in Figure 2.2. This arises due to strong electron-phonon coupling, allowed by the 'soft', physically flexible nature of the materials. An excitation on the polymer or molecule will interact with the surrounding medium in such a way as to create a physical distortion of the molecule to lower the overall system energy. This localisation effect is always reinforced by, and often masked by, additional sources of disorder within the material (see Section 2.1.3).

The basic charge carrier in organic semiconducting materials is a polaron, consisting of a hole or an electron with its accompanying molecular distortion (for example [8, 9]). For brevity, hole polarons and electron polarons are usually still referred to as holes and electrons. If the excitation is electrical, such as direct injection of a charge from an electrode, the basic excitation will already be polaronic. An optical excitation leads to the formation of both an electron polaron and a hole polaron. The localised nature of the 'geminate pair' of polarons means that they experience strong Coulomb attraction, and in order to achieve separated polarons a large electric field is required to overcome this attraction. A Coulombically-bound electron polaron-hole polaron pair such as this is termed an 'exciton'. The property of localisation clearly impacts greatly on the ability of excitations to move across and between molecules and to interact with other excitations. All organic electronic devices require the motion of charges, as polarons, from one place to another within the material. Understanding the mechanisms governing charge transport in organic semiconducting materials is therefore of great importance.

2.1.2 Marcus theory of electron transfer

The most informative theory describing the process of charge transport in organic semiconducting materials at the molecular level is Marcus theory. Developed to describe the electron transfer process

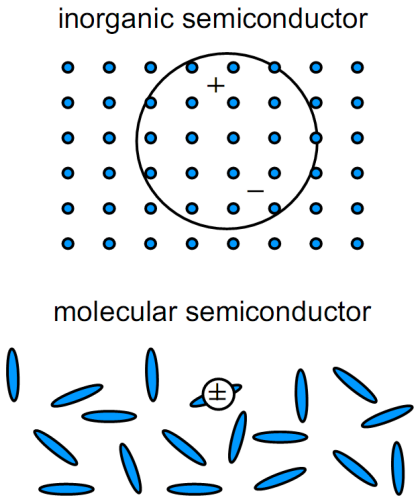

Figure 2.2: Figure courtesy of Nelson and Benson [5]. Illustration of the localised nature of charges in a molecular organic semiconductor. In this case, disorder in orientation and packing reinforces the localisation effect due to the relaxation of the 'soft' material in the presence of an excitation. Conformational freedom and packing disorder in polymeric systems leads to a similar result.

in chemical reactions and biological systems, the theory incorporates the effects of the necessary molecular distortions during charge transfer processes in organic materials. In particular, it requires that the charge transfer only takes place after the molecular configuration has re-organised from the initial to the final state. Thus, the theory is able to describe the polaronic nature of charges, with their accompanying molecular distortion. In general, therefore, charge transfer requires an activation energy to bring the initial and final sites into a non-equilibrium, distorted state. At this point, the polaron may 'hop' onto the final site, the sites subsequently relaxing into their equilibrium configurations for the new polaron position. Marcus theory gives the electron transfer rate k_{et} as:

$$k_{et} = \frac{2\pi}{\hbar} |J|^2 \frac{1}{\sqrt{4\pi\lambda k_b T}} \exp\left(-\frac{(\lambda + \Delta G^\circ)^2}{4\lambda k_b T}\right) \tag{2.1}$$

where $|J|^2$ is the electronic coupling between the initial and final states, λ is the re-organisation energy (which is always positive) and ΔG° is the total Gibbs free energy change for the electron transfer (which may be positive or negative).

The electron transfer process is thus a thermally activated one in the case of both energetically upward and downward transfer events. Charge transport in conjugated polymers may therefore be described as phonon-assisted hopping. Activation is required even in the absence of disorder, since electron transfer requires the reorganisation of the surrounding molecular structure. In solid films

of real materials, however, charge transport will take place under the influence of additional sources of disorder, which will lead to further variations in the energy and configuration of hopping sites.

2.1.3 Effect of energetic and configurational disorder on transfer rate

First, we define energetic and configurational disorder in general terms, without reference to a particular formalism. Within a particular formalism, such as the disorder formalism discussed below, the terms have mathematical definitions. Energetic disorder describes the width of the density of states (DoS) within a material. Since the occupational DoS (ODoS) depends on temperature as well as the shape of the DoS, energetic disorder leads to a temperature-dependent contribution to a property such as carrier mobility. Configurational disorder describes the degree of and/or variation in overlap of the molecular orbitals within a material, and leads to a temperature-independent contribution to a property such as carrier mobility. These categories of disorder can be related to the terms in the Marcus equation. An increase in energetic disorder will lead to an increase in the magnitude of the average root mean square Gibbs free energy change ΔG° (energetic offset) for electron transfer within the material. It can be seen that an increase in the average Gibbs free energy change will lead to much slower 'upward' hops (and perhaps slower 'downward' hops depending on the relative size of ΔG° and λ), leading to slower electron transport averaged over a large number of hops. The configurational disorder is directly related to the electronic coupling $|J|^2$. Poor and highly variable overlap of neighbouring wavefunctions, meaning a low electronic coupling for a large fraction of electron transfer steps, will also strongly decrease electron transport. Changes in configurational disorder may also change the reorganisation energy λ, but this effect will be small compared with the effect on $|J|^2$.

Energetic disorder may result from a variation in chemical stucture of different functional groups in a material or different materials within a bulk film, which give rise to variations in the polaron energy and a broadening of the DoS. Even across groups with the same chemical structure, energetic disorder will arise from local variations in polymer chain conformation, interactions between the many dipolar groups within the polymer or molecule and the presence of impurities, defects and end groups [10, 9, 11, 12]. A typical width of the DoS in disordered organic semiconductors is around 0.1 eV [13, 14, 15, 16, 17, 18]. These sources of energetic disorder increase the activation required for transport, often masking the underlying activation due to the polaronic nature of charged excitations.

Configurational disorder concerns the spatial extent of polarons, and will vary with chemical structure and processing. Since polarons occupy the conjugated segments of molecules, large spatial separation between those conjugated segments within or between molecules will lead to low electronic coupling $|J|^2$ for transfer between those segments. Spatially disordered packing of molecules or polymers whose ordering is hindered by their chemical structure, by the processing method used or by the presence of another material, will show large configurational disorder.

Energetic and configurational contributions to disorder may be separated by temperature-dependent studies. The transfer rate may be written as the product of a term relating to configurational disorder only, the $|J|^2 \frac{1}{\sqrt{4\pi\lambda k_b T}}$ term, and a term relating to the energetic disorder, the $\exp\left(-\frac{(\lambda+\Delta G^\circ)^2}{4\lambda k_b T}\right)$ term (which also contains some information on the configurational disorder through λ). It can be seen that as $T \rightarrow \infty$, the exponential term containing the energetic disorder term tends to unity, leaving only the configurational disorder terms in the electron transfer rate. This simply says that as $T \rightarrow \infty$, there is enough thermal energy to activate any electron transfer, and the rate depends only on the electronic coupling. Studying the behaviour of the mobility with temperature therefore allows a separation of the two effects. This may be demonstrated more clearly within a particular formalism. The formalism most commonly applied to measurements of charge transport in disordered organic systems is the disorder formalism.

2.1.4 The disorder formalism and hopping within the DoS

The dynamics of charges in systems dominated by disorder have been well-studied as a result of their relevance for doped organic semiconductors and photoconductors for xerography. The Gaussian Disorder Model (GDM) was developed by Bässler and co-workers to describe the situation where the overall energetic disorder dominates the activation energy due solely to the polaronic nature of transport [13, 19].

In the GDM, an injected charge is viewed as hopping through a cubic lattice of sites. The energetic disorder described above is represented using a Gaussian DoS. The DoS is unoccupied except for the injected charge, and hence the GDM describes systems with low carrier density. The DoS $g(E)$ is described by:

$$g(E) = \frac{N_0}{\sqrt{2\pi}\sigma} e^{-E^2/2\sigma^2} \tag{2.2}$$

for the width of the Gaussian distribution σ (defined as the energetic disorder) and a constant for normalisation to the total number of states N_0. In the basic model, the sites are spatially distributed on a grid or lattice to give a fixed site separation. In a common extension, the site separations are also allowed to vary about their mean, leading to a statistical variation in electronic overlap.

Bässler et al. set up a Monte Carlo simulation where the injected charge 'hops' under the influence of an applied field F within an empty DoS, carrying out a random walk. The hopping rate in the GDM is not derived from Marcus theory. Rather, the much simpler Miller-Abrahams [20] hopping rate $v_{i\to j}$ between sites i and j is used, given by:

$$v_{i\to j} = v_0\, e^{-2\gamma r_{ij}}\, e^{-(E_j - E_i)/kT} \quad E_j > E_i \tag{2.3}$$

$$v_{i\to j} = v_0\, e^{-2\gamma r_{ij}} \quad E_i > E_j \tag{2.4}$$

with an attempt-to-jump frequency v_0; an exponential term describing the electronic overlap with jump distance r_{ij}; the inverse localisation radius γ; and a Boltzmann term to describe the retardation of hopping for energetically upward hops with initial and final site energies E_i and E_j. As a result of the Boltzmann term for upward hops, energetically downward hops are favoured. Thus, the charge is injected at some energy, and relaxes, through hopping, to a dynamic equilibrium energy in the states located below the centre of the DoS.

The Monte Carlo simulation led to the following expressions for the mobility in the limit of high fields (typically above 3×10^5 V/cm):

$$\mu = \mu_0 e^{(-2\sigma/3kT)^2} \times e^{C[(\sigma/kT)^2 - \Sigma^2]\sqrt{F}} \quad \Sigma \geq 1.5 \tag{2.5}$$

$$\mu = \mu_0 e^{(-2\sigma/3kT)^2} \times e^{C[(\sigma/kT)^2 - 2.25]\sqrt{F}} \quad \Sigma < 1.5 \tag{2.6}$$

where σ is the width of the Gaussian density of states (the energetic disorder) as above, and Σ is the parameter representing configurational disorder. While Σ is not a physically well-defined parameter in the GDM, these equations serve to demonstrate the different behaviour with temperature of the energetic and configurational contributions to disorder. As $T \rightarrow \infty$, the energetic disorder terms vanish, and only the configurational disorder term remains non-zero (for non-zero electric field). Hence, judicious plotting of the data allows the energetic and configurational terms to be determined separately.

It was also shown that the ODoS probability function resulting from the injection of the charge into the Gaussian DoS is a Gaussian of the same width σ, but displaced by an energy $(-\sigma^2/kT)$ below the centre of the DoS. This leads to a strong temperature dependence of charge transport, for two reasons: (a) the equilibrium energy decreases with decreasing temperature, and (b) at lower temperature there is also less energy available from phonon interactions for activation. Hence, many fewer sites become accessible at lower temperature. In terms of Equation 2.3, the final term has both the explicit T-dependence and a further dependence in the average value of E_i. Therefore, the expected temperature dependence of the mobility is of the form $\ln \mu \propto 1/T^2$. This is commonly verified experimentally [19, 21, 22].

The concept of a 'transport energy' has been useful in modelling experimental data [23, 19]. This can be described qualitatively as the energy to which activation is required in order for effective hopping transport to occur. Somewhat more precisely, it corresponds to the energy to which carriers in lower energy sites are most likely to be activated, discounting sites from which 'backward' hops (which should not be counted as transport hops) are likely to occur. The energetic scheme, showing transport energy E_{trans} and injection energy E_{inj}, is shown in Figure 2.3. Whilst we do not make use of the full description here, the concept is useful for visualising various aspects of hopping transport, including, for example, the effects of a broadened DoS, of increased carrier concentration and of charge carrier trapping (see below).

The electric field dependence of the mobility can also be predicted with a simple energetic picture. Consider a charge sitting in a local energy minimum in an electric field F, as in Figure 2.4. For electron hopping to the next local minimum, the charge requires activation up to the maximum

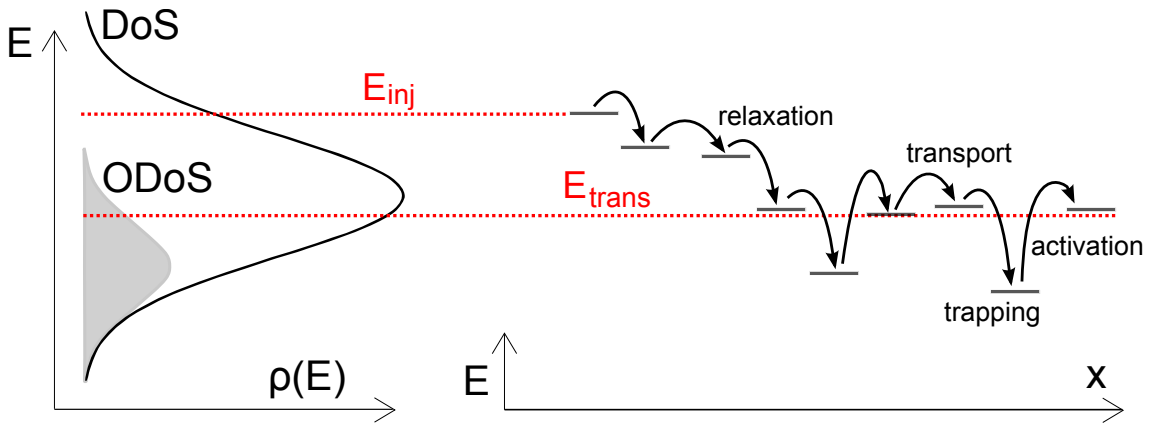

Figure 2.3: Schematic showing the process of transport via hopping through a disordered organic semiconductor. A charge injected at an energy E_{inj} into one of the higher states in an empty DoS will relax to lower energies by hopping (on average) to lower energy states. After it has relaxed, it will hop between states with an occupation probability according to the ODoS, with the same width as the DoS but lower in energy. The transport energy E_{trans} represents the energy to which a charge must be activated to undergo further hopping transport. When below the transport level, the charge may be considered to be trapped.

site energy located some distance from the present position (neglecting tunnelling for simplicity). We define the activation energy E_a in the absence of an electric field. The electric field F will tilt the DoS in the direction of the field, reducing the activation energy for a hop in that direction by an amount $\beta\sqrt{F}$, where $\beta = \sqrt{q^3/\pi\epsilon_0\epsilon_r}$ for the electric charge q. This results in the characteristic Poole-Frenkel field-dependence of the mobility $\mu = \mu_0 \exp^{\beta}\sqrt{F}$ observed in a very wide range of disordered materials.

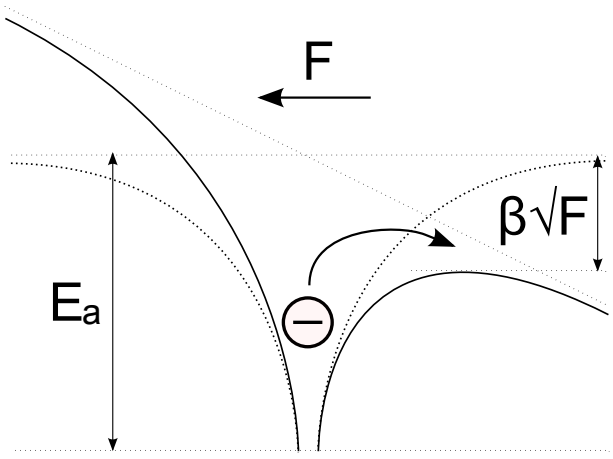

Figure 2.4: Illustration of the Poole-Frenkel effect, whereby an electric field F reduces the barrier to hopping between energy minima by an amount $\beta\sqrt{F}$ as described in the text.

The GDM is quite successful in predicting the experimentally observed behaviour of disordered organic systems at low carrier densities in terms of their field- and temperature-dependence over certain ranges. It is also able to describe the phenomenon of dispersive transport [24, 25]. Disper-

sive transport occurs when there is insufficient time for the energy of carriers to equilibrate during transit, and carriers show a wide distribution in transit time. This is common in systems with a long tail of sites in the DoS, and hence is often indicative of a high level of energetic disorder. Dispersive transport is easily observed in the time domain in experiments such as time-of-flight (see Section 2.2.1).

Certain outputs of the GDM can be rationalised physically, and used to make useful comparisons between materials. The most useful output is the disorder parameter σ, which may be correlated to the width of the DoS, and hence to the degree of energetic disorder [14, 26]. The zero-field, infinite-temperature prefactor mobility μ_0 is occasionally used to compare the intrinsic mobilities of a series of materials removing the effect of energetic disorder [27]. It should be noted that as a description of transport in disordered media the GDM has a number of limitations. In particular, (i) it does not correctly predict the transport behavior at low electric fields and that (ii) it cannot account for polaronic effects since it does not model phonons or any interactions between the charge and the transporting material. However, these limitations are beyond the scope of the work presented in this thesis. Due to its successes and to its simplicity the GDM is one of the most widely used models for charge transport in disordered organic systems at low carrier densities. Accordingly, it will be used in this thesis to compare the effects of disorder on charge transport across material and sample sets using the time-of-flight method.

In this thesis, however, we also make use of field-effect transistor (FET) mobility measurements. A key feature of charge transport in the field-effect transistor configuration is a high carrier density. Hence, the GDM is not an appropriate formalism in this case. The typical method for analysis of FET mobility data is outlined below.

2.1.5 Alternative transport models typically used for FET measurements

The essential features of the GDM for comparison with alternative models for charge transport in organic materials are a Gaussian DoS; an unoccupied DoS to represent low carrier density; and a Miller-Abrahams hopping rate. It was seen above that these features lead to a temperature dependence of the mobility of the form $\ln\mu \propto 1/\mathrm{T}^2$.

It is commonly observed in FET mobility measurements that the temperature dependence of the

mobility is better fit to an 'Arrhenius' plot of the form:

$$ln\mu = -\frac{E_a}{k_B T} + ln\mu_0 \tag{2.7}$$

with infinite-temperature mobility μ_0 and characteristic activation energies E_a of 10s to 100s meV.

The models developed for charge transport in FETs consistent with the Arrhenius form are numerous. However, those applied to charge transport in disordered organic materials are typically based, like the GDM, on thermally-activated hopping [28, 22]. Also like the GDM, models of this type employ a Miller-Abrahams transfer rate [20, 29, 22]. The models typically diverge from the GDM regarding the choice of shape and/or occupation of the DoS. The Arrhenius form follows from hopping in an exponential tail of the DoS, and thus has often been considered incompatible with a Gaussian DoS. However, Coehoorn et al. have shown that for sufficiently high charge carrier density within a Gaussian DoS of width σ and accounting for Fermi-Dirac statistics, the mobility μ tends towards the Arhennius form $\ln\mu \propto 1/\mathrm{T}$ [22]. The 'crossover' from a $\ln\mu \propto 1/\mathrm{T}^2$ dependence to a $\ln\mu \propto 1/\mathrm{T}$ dependence was found to be centred around a carrier density at which the Fermi energy $\mathrm{E}_F = -\sigma^2/\mathrm{k}_B\mathrm{T}$ measured from the centre of the Gaussian DoS. It may therefore be the case that the GDM and the various 'activated hopping' models leading to an Arhennius form are compatible, and are simply approximations of the same transport model in different carrier density regimes. A deeper discussion of the validity of the various transport models is beyond the scope of this work, but it is sufficient to note that the data in this thesis is analysed within both the GDM (for ToF data) and the activated hopping model (for FET data) as appropriate for the different carrier density conditions.

2.1.6 Effect on transport of charge-trapping species

Here, it is useful to introduce the concept of a charge-trapping site, or 'trap'. The defining property of a trap is an asymmetry in the time taken for the site to become occupied and the time taken for it to become empty again, with the latter process the slower. In the Miller-Abrahams electron transfer description as used in the GDM and the other 'activated hopping' models this is very easily understood. Since energetically upward hops require activation, whereas downward hops do not, the asymmetry will be satisfied simply when the site has a relatively lower energy than its neighbours.

In the Marcus electron transfer description the picture is complicated by the fact that both upward and downward hops are activated, but nonetheless it remains clear that an upward jump is strongly penalised at finite temperature. The term 'trap' usually refers, therefore, to a site significantly lower in energy than the sites surrounding it.

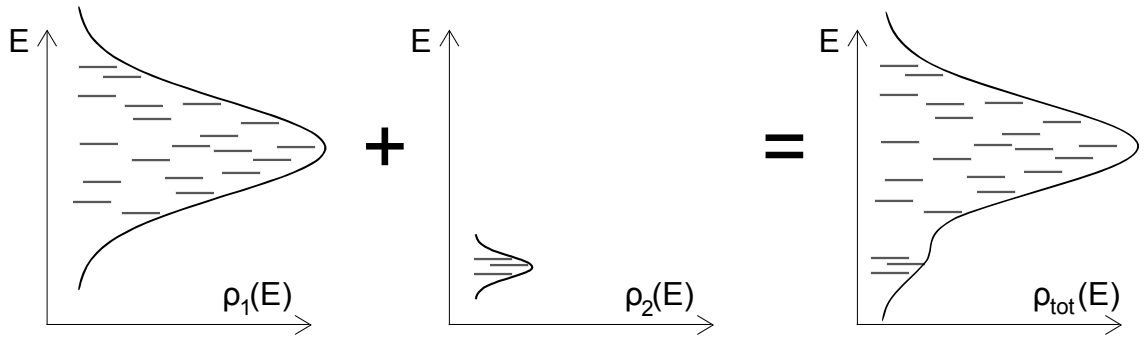

Figure 2.5: Schematic showing the effect on the DoS of a distinct set of states located at a lower energy. The effect of such states will be to trap carriers at energies well below the transport level of the DoS. If the states are sufficiently numerous, they will severely reduce the average mobility.

As described above, the GDM treats disorder in the system by employing a Gaussian DoS, representing lower energy states extending into the nominal energy 'gap' between LUMO and HOMO. States towards lower energies in the Gaussian DoS, as illustrated in Figure 2.5, will act as traps relative to those higher in the DoS. Since the energy difference involved is generally not so large – the traps are shallow – the de-trapping time may not be so large, and charges in these lower energy states may still contribute significantly to the transport. Depending on the number of such traps relative to the charge carrier density, however, they may act to reduce the effective, average mobility of the carriers. The distinction between transport sites and shallow traps is thus rather blurred.

Distinct from shallow traps – typically caused by disorder in molecular packing and conformation and fluctuation in dipolar interactions, for example – are deep traps. This term is used to refer to states of significantly lower energy than those contributing to transport. These may be caused by distinct defects in the material, which may be chemical (for example due to oxidation) or physical (for example due to a distinct and strong conformational change, as will be seen in Chapter 4), by the presence of impurities such as oxygen or water. De-trapping times of a charge located within these traps may be so long that it makes sense to describe the charge as fully immobile. Systems in which this type of trap is important have inspired an alternative model for transport within disordered organic materials, developed by Arkhipov and co-workers [23, 30]. Following from the concept of

the transport energy within the GDM, this approach focuses on the nature of transport as being activated from purely localised, low energy sites to transport sites at higher energies towards the centre of the DoS. The model defines an effective transport energy, which simplifies the numerical calculation of mobility as compared with averaging over carrier hopping rates.

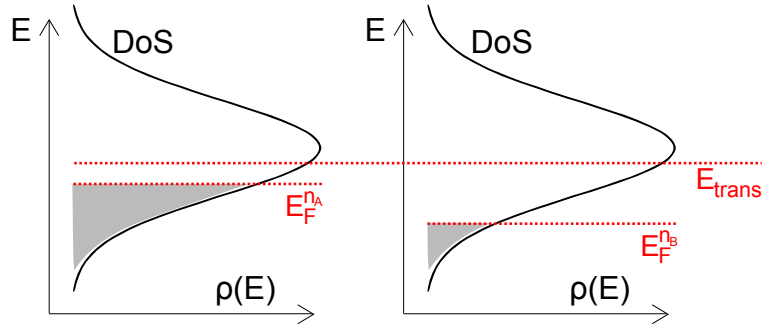

Figure 2.6: Schematic showing the effect on the DoS of carrier concentration. The grey area indicates the occupied states (on average) for carrier concentrations $n_A > n_B$. The upper red line represents the transport level E_{trans} as described above, and the lower red line represents the Fermi level E_F (the energy of the highest occupied state). The larger the energetic separation between E_{trans} and E_F, the slower will be the transport at finite temperature.

The broad energetic distribution of sites for polaron occupation has consequences for the measurement of carrier mobility. Since a broad DoS leads to a Fermi level strongly dependent on the charge density, and the position of the Fermi level relative to the effective transport energy influences the rate of transport, the mobility is also strongly dependent on the charge density. This can be interpreted as an increase in mobility due to the filling of traps. Measurements of the same material in space-charge-limited current measurements (see Section 2.2.4), with carrier densities of the order $10^{14} - 10^{16}$ cm^{-3}, and in field-effect transistors, with carrier densities of the order $10^{17} - 10^{20}$ cm^{-3}, have shown variations in mobility of up to three orders of magnitude [31, 29]. A mobility variation of nearly two orders of magnitude was also demonstrated in the same study in field-effect transistors with a range of carrier densities [31]. Hence, the comparison of mobility at relatively low carrier density (for example from ToF measurements) with that at high carrier density (for example from FET measurements) is a useful indicator of the degree of disorder and trapping within the system.

2.1.7 Hierarchical scales of charge transport – intrinsic and bulk mobility

As described above, charge trapping may occur due to disorder, through variation in polymer or molecular conformation, or to the presence of impurities and defects. Since charge trapping acts as a bottleneck for transport, the phenomena above mean that the observed charge transport properties of a material depend strongly on the scale, geometry and time-scale of measurement. The mobility

measured on a short, conjugated length of polymer chain over times shorter than the scattering time, for example, may be many orders of magnitude higher than the mobility measured when the charge carrier has passed between different polymer chains, or across grain boundaries, or has been captured and released by some defect.

An observation of the different scales of charge transport within a material is claimed to have been made using the time-resolved electric field-induced second harmonic (TREFISH) generation technique [32]. The group carrying out the experiment identified three regimes of charge transport over different time-scales after polymer excitation. The first two regimes involved very high carrier mobility from around $10^0 - 10^{-3}$ cm^2/Vs, and the third a much lower mobility below 10^{-4} cm^2/Vs. These regimes could not be explained by carrier relaxation in a single DoS as presented in Bässler's Monte Carlo simulations, as the dynamics observed were too fast [32, 13]. They therefore (tentatively) attributed these regimes to carrier motion first within conjugated chain segments, then along the chain over distances larger than the conjugation length, and finally – over longer times – between different chains. This is illustrated in Figure 2.7.

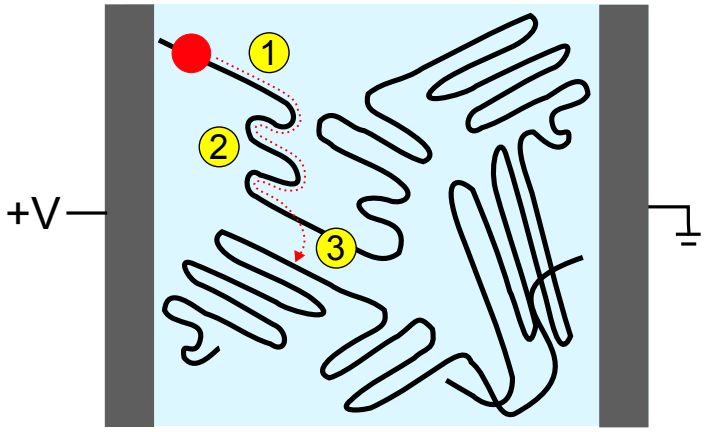

Figure 2.7: Illustration of the hierarchical scales of transport in polymeric conductors and semiconductors. Process 1 is transport within a single conjugated segment on a single polymer chain; process 2 is transport between conjugated segments on a single chain; process 3 is transport between two separate chains. The first two processes represent intra-chain transport; the third represents inter-chain transport.

In optoelectronic devices such as photovoltaics and transistors, charge transport is necessarily a bulk phenomenon, where the charge carrier will be required to pass between conjugated segments through regions with a variety of chain conformations, and between different polymer chains. Along this path, the carrier is likely to be exposed to a variety of trapping species such as conformational or

other physical chain defects [33, 34], chemical defects or impurities, or grain boundaries. Therefore, the mobility along a single conjugated segment of polymer or molecule – what may be thought of as the microscopic or intrinsic mobility – will not be observed in a real device. Rather, the macroscopic or bulk mobility observed in the device depends more critically on the degree of disorder and the concentration of trapping species in the material. Reducing the limiting influence of these factors in order to increase the mobility closer towards the intrinsic mobility is therefore the challenge for researchers. Controlling the morphology – the conformational, packing and phase behaviour of the materials – by variations in chemical structure and processing is the primary way in which this can be achieved. Researchers have been able to control morphology by changes in polymer backbone or side-chain chemical structure [35, 27, 16, 36, 37], molecular weight [38, 39, 40, 41, 42] and regioregularity [38, 43, 44], and with changes in processing solvent, deposition method, solution concentration, temperature, pressure, and by using processing additives, amongst other methods [12].

2.1.8 The structure-mobility relationship: optimising materials and morphology for high mobility

The hierarchical scales of transport can also be seen by comparing the mobilities measured on the same materials by different methods. The reader is referred to the following section for information on the key techniques used to measure mobility in disordered organic semiconductors. We use some results here without further explanation of method. As described above, intra-chain charge transport is very rarely seen experimentally in measurement of bulk materials. The transient microwave conductivity method does not require bulk transport (see Section 2.2.2). Since the measurement involves probing the conductivity response of the sample to an oscillating electromagnetic field, all carriers moving within the sample will contribute to the signal. This allows intra-chain charge transport to be observed over short timescales.

The Siebbeles group at Delft have carried out TRMC mobility measurements on a variety of conjugated polymers. Since these measurements probe to some extent the 'intrinsic' transport properties of the material – the mobility over short length and time scales rather than across a bulk sample – the synthesised results are useful to discuss the structure-mobility relations related to individual polymer chains.

Material	**TRMC** μ / cm^2/Vs	**[Ref.]**	**Bulk** μ_{hole} / cm^2/Vs	**[Ref.] (Method)**
P3HT	0.02	[45]	10^{-1}	[46] (FET)
			$\approx 10^{-4}$	[44] (ToF)
			10^{-5} – 10^{-4}	[40] (ToF)
			10^{-4}	[47] (SCLC)
MEH-PPV	0.2–0.5	[48]	10^{-6} – 10^{-5}	[49] (ToF)
	0.4	[45]	10^{-7}	[50] (SCLC)
			10^{-5}	[51] (FET)
PFO	45 (stretched)	[52]	$\approx 10^{-4}$	[53] (ToF)
	$\approx$ 1 (coiled)	[52]	$\approx 10^{-2}$	[54] (ToF)
			10^{-4} – 10^{-3}	[14] (ToF)
			10^{-5} – 10^{-2}	[55] (FET)
			10^{-5}	[56] (SCLC)
MeLPPP	600 (isolated)	[57]	8×10^{-4}	[35] (ToF)
	30 (solid film)	[58]		

Table 2.1: Non-exhaustive survey of mobility measurements on an illustrative set of materials to demonstrate the large difference between intra-chain and bulk mobility and the variation in bulk mobility with processing and measurement method. References are given in the table.

Table 2.1 details the TRMC mobilities (representing an effective mobility for both holes and electrons) for a selection of conjugated polymers in solution. It can be seen that the TRMC mobilities range from around 10^{-2} cm^2/Vs in P3HT, to 10^{-1} cm^2/Vs for MEH-PPV, to $10^0 - 10^1$ cm^2/Vs in PFO to nearly 10^3 cm^2/Vs in the ladder-type polymer MeLPPP. As described by the authors [45, 57, 37], the trend can be rationalized by a consideration of the degree of planarity in the polymer chains. Increased planarity is expected to lead to a larger conjugation length with fewer 'kinks' and lower disorder, and thus to a higher mobility along the chain. PFO has a chemical structure which reduces the torsional freedom of the chain as compared with P3HT and the PPVs, primarily as a result of the bridging carbon atom per two benzene rings, and with some planarising effect of the bulkier side-chains. MeLPPP takes this further, by linking all units in the polymer chain with a bridging carbon atom, extending planarity much further along the chain.

It was expected that the increased planarity of polymer chains would also lead to higher bulk mobilities, both through the increased intra-chain mobility and through an improved inter-chain interaction allowed by the reduced steric hindrance of planar chains relative to disordered chains [59, 60, 61, 62]. However, as shown in Table 2.1, typical bulk hole mobilities from the literature for the same materials do not follow a clear trend. Furthermore, they are orders of magnitude lower

than the TRMC values. Bulk electron transport is no better, and in some cases far worse than the hole transport [63, 53, 64, 40, 14, 65, 66]. Further, the bulk hole mobilities found for the materials have varied widely and often improved incrementally over time (with improved synthesis, varying molecular weight and different processing). In fact, the material which has shown the highest bulk mobility of those listed is P3HT, which shows the lowest TRMC mobility. It has become clear that this is because the bulk mobilities are rarely limited by the intra-chain mobility, and are instead limited by inter-molecular charge transfer and/or additional charge trapping species. These phenomena are not usually probed by TRMC. This reflects a general finding in the field that device performances are as dependent on synthesis and processing method as on molecular formula [12]. The most striking 'anomaly' in the table, P3HT, offers a good case study in this regard.

The high bulk mobilities measured in P3HT have been achieved as a result of strategies promoting close intermolecular interaction, and improving the order within the material over larger scales. The approach is based around the close packing made possible in P3HT by controlling regio-regularity, and helped by the sterically non-disruptive linear side chain. When prepared carefully in the solid state to promote crystallinity, this allows a very favourable overlap of $\pi-$systems between neighbouring chains, which allows a high inter-chain charge transfer rate. Some studies suggest that charges within well-ordered P3HT domains are delocalised over several chains [9]. Despite the lower intra-chain mobility in the system relative to the PPV, PFO and PPP polymers – a result of lower planarity of the chain – the bulk mobility in an FET measurement was found to be up to 0.1 cm^2/Vs for the most regio-regular samples, even higher than the mobility found by TRMC [46, 38]. This approach has led to other successful examples of high bulk mobilities being demonstrated in semi-crystalline and LC polymer films displaying longer-range order, including measurements on single crystalline domains [38, 67, 68, 69, 70], and FET mobilities in conjugated polymers have recently reached $3 - 6$ cm^2/Vs [2, 3].

Nonetheless, such high mobilities have not been achieved in the majority of conjugated polymers. Further, the approach taken for P3HT and the other cases above is not desirable for a number of applications. In particular, the close $\pi - \pi$ interactions in these systems tends to be detrimental for luminescence. Applications such as polymer lasing, light-emitting transistors and light-emitting diodes for optical communications will require both high mobility and efficient luminescence. Therefore, there have been vigorous efforts to identify the source of the transport bottleneck in highly

luminescent systems such as the PPVs, the polyfluorenes and related materials, with the aim of liberating the 'intrinsic' bulk mobility from the limits imposed by defects or other traps. However, the existence of a wide variety of chemical and physical candidates for trapping and the difficulty in 'fingerprinting' them and controlling their formation in isolation means that this has proven a difficult task. Identification of species or mechanisms for charge trapping in disordered organic materials is one important theme of this thesis.

Specific details on the relevant structure-mobility relationships for the particular material sets studied in this thesis will be given in the coming chapters.

2.2 Techniques used to measure charge transport

A great many techniques have been employed to study the charge transport in organic semiconducting materials, each appropriate in certain situations and with advantages and disadvantages. Below are the most relevant for our purposes, with the amount of detail reflecting the importance of the method in the following chapters. The practical experimental details relating to the data collected first-hand will be given separately in Chapter 3.

2.2.1 Time-of-flight photocurrent

The time-of-flight photocurrent method is a direct and unambiguous way of observing the speed of charge carrier motion within a material. As illustrated in Figure 2.8, a thick sandwich of the material is placed between two non-injecting electrodes, at least one of which should be transparent or semi-transparent, and a constant d.c. bias is applied. A short laser pulse is then applied to the sample. The aim is to create a sheet of electron-hole pairs near the illuminated electrode, subsequently to be separated by the applied field. One carrier type is then collected (or trapped) at the illuminated electrode, and the other carrier type swept across the device and collected at the back electrode, at which time the system returns to steady-state. In this way, the photoexcitation induces a displacement current over the timescale of the transit of the photoinduced carriers.

The resulting photocurrent transient can be displayed on an oscilloscope. If the absorption depth is thin relative to the film thickness, the pulse short relative to the carrier transit time, and the photo-generated charge density low enough that it does not significantly perturb the uniform elec-

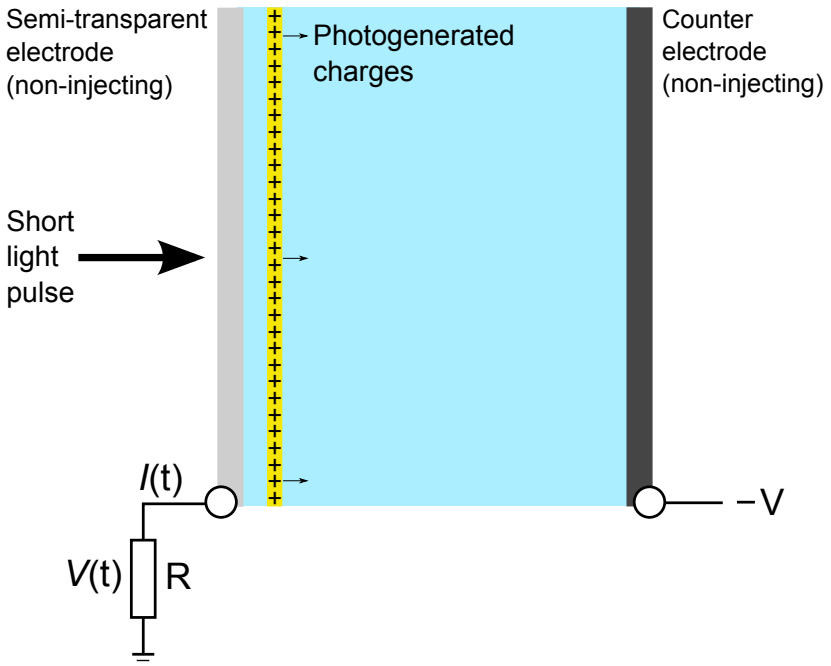

Figure 2.8: Schematic of the time-of-flight setup.

tric field, the photocurrent transient may in certain cases resemble the form seen in Figure 2.9a. The time for the transit can be clearly observed as the time at which the current begins to decrease rapidly. Whether or not the transient resembles the form in Figure 2.9a, even when the above criteria are met, will depend on the nature of transport within the material and its 'dispersiveness'. Since transport in disordered organic systems may take place in states with a broad range of energies, the transiting carriers may have a broad distribution of drift velocities. In the case that they have a single fixed drift velocity – fully non-dispersive transport – the photocurrent transient will resemble Figure 2.9a, where it is only broadened by the finite absorption depth and the diffusion of the carriers. In the case that the drift velocities are distributed over an ever broader range due to disorder – as the transport becomes more and more dispersive – the transient will resemble some variant of Figure 2.9a, Figure 2.9b or Figure 2.9c. Depending on how severely dispersive is the transport, an estimate of the transit time may still be made, often with the help of a log-log plot as shown in Figure 2.9d, where the transit time is taken as the 'knee' of the curve.

We note that in the case of highly dispersive transport, when no transit time 'knee' can be observed, it is possible to derive an estimate of the transit time by the so-called 'integral method' [63]. In this case, the signal is electronically integrated such that it corresponds to the cumulative charge collected rather than the instantaneous current, and the transit time is taken as the point at which

half of the total charge has been collected. This method extends the range of samples which can be measured by the ToF method, but since the transient in this case is rather featureless, it does not offer the direct, unambiguous measurement of the ToF measurement in 'normal' mode. However, our work in Chapter 5 offers support for use of the integral method in certain circumstances.

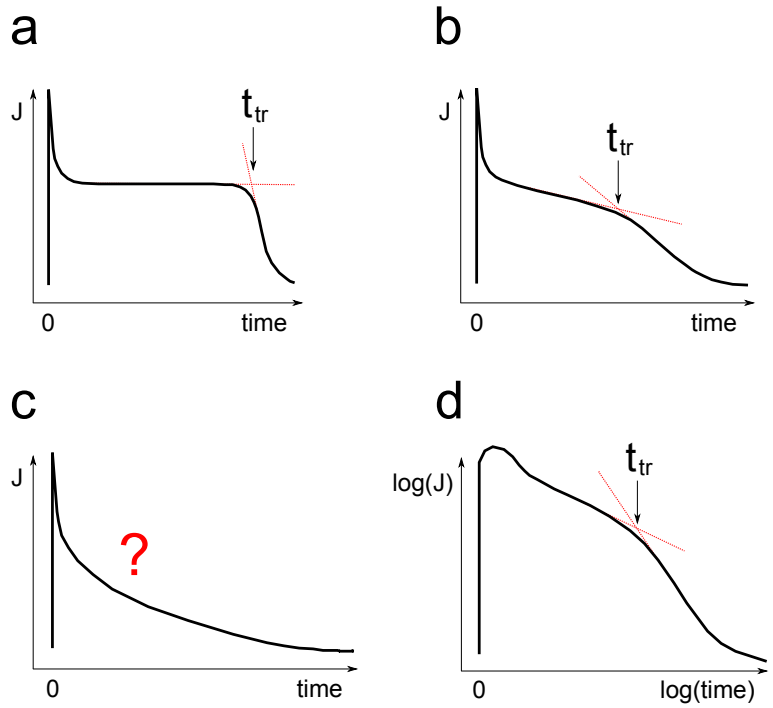

Figure 2.9: Types of transients which may be observed in a ToF experiment. In transients showing non-dispersive transport such as (a) the transit time is easily determined in a linear-linear plot as shown. In transients showing slightly dispersive transport such as (b) the transit time is less well defined, but may still be easily determined in a linear-linear plot if the 'knee' – the point of change in the decay kinetics – is clear. Transients showing more dispersive transport such as (c) will have to be plotted on a log-log plot as in (d), where the 'knee' may be more easily observed. Even more highly dispersive transport, where the 'knee' is not visible even on a log-log plot, may require the integral mode. In that case, the charge collected is integrated electronically and the transit time given by the time taken for half of the total charge to reach the collecting electrode.

Successful measurement of the mobility also requires that the transit time is longer than the RC time constant of the system, and hence thicker films are desirable. Hence, the ToF method may prove difficult for very high mobility materials. However, it has been very successful with many organic materials, and is widely used.

Once the transit time τ can be inferred from the photocurrent transient, the mobility μ is derived via the simple expression

$$\mu = d^2/V\tau \tag{2.8}$$

for the film thickness d and an applied field $E = V/d$. The mobility is typically calculated for a range of applied fields, in order to find the strength of the field dependence, which relates to the disorder in the material. However, the field-dependence of the mobility is itself temperature-dependent. A fuller characterisation of the disorder in the material via the GDM, for example, therefore requires a field-dependent and temperature-dependent measurement. The advantages of the ToF method are that, in successful cases, it allows very direct observation of the transit time and the mobility, leaving little room for ambiguity of results, and also provides extra information in terms of the dispersiveness of transport. The disadvantages are that it requires a much thicker film than is used in most optoelectronic devices, which may have consequences for the accuracy of morphology representation; that it corresponds to a high field drift regime, which may not reflect the transport mechanism in certain devices very closely; and that in some cases transport is either too dispersive or too fast for this method to allow the mobility to be derived.

2.2.2 Pulse-radiolysis transient microwave conductivity

Developed initially to measure conductivity changes in pulse-irradiated liquids [71], the transient microwave conductivity method was applied to the measurement of mobility in polymer systems largely in response to the issues outlined in the above section, namely that macroscopic d.c. mobility measurements are sensitive to bulk phenomena such as molecular packing, disorder and defects (for example, see [45, 72]). TRMC was applied with the intention of probing the 'intrinsic' charge transport properties of isolated polymer chains in solution. This is made possible by measuring the absorption response of very high frequency a.c. microwave radiation by charge carriers. The method does not require electrodes. Charge carriers are created on the polymer by a pulse of high energy electrons from a van der Graaff generator. The change in conductivity as a result of the creation of charged excitations on the polymer is monitored through the absorption of the microwave radiation. The high frequency mobility can be derived once the time-dependent charge concentration in the system has been calculated from the kinetics of the change in conductivity. As described above, this method is designed to probe intrinsic transport properties of materials, and hence may not be directly relevant to device operation. The method is also analytically demanding. However,

it provides important information on the intra-chain mobility and hence on the structure of the materials, and forms an interesting comparison with other mobility measurement methods.

2.2.3 Field-effect transistor

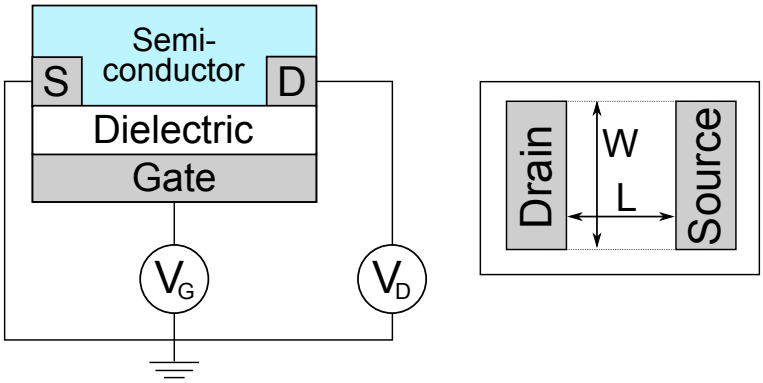

Figure 2.10: Schematic of the field-effect transistor configuration.

The carrier mobility may also be derived using the electrical characteristics of a field-effect transistor, shown schematically in Figure 2.10. Measurement of the mobility from a field-effect transistor is a steady-state, rather than transient technique. In the framework developed for inorganic transistors, the mobility is proportional to the current between the source and drain electrodes in the linear and saturation regimes of operation. We define the gate voltage V_G, the threshold voltage at which the current turns on V_T, the channel width W, the channel length L and the capacitance of the gate dielectric C. The equation relating the mobility μ to the source-drain current I_D within the linear regime, where $V_D \ll (V_G - V_T)$ and $V_G > V_T$, is

$$I_D = \mu_{lin} C V_D (V_G - V_T) \times \frac{W}{L} \tag{2.9}$$

where $V_D \ll (V_G - V_T)$ and $V_G > V_T$. The mobility μ_{lin} may then be calculated from

$$\mu_{lin} = \frac{L}{WCV_D} \cdot \frac{\partial I_D}{\partial V_G} \tag{2.10}$$

In the saturation regime, where $V_D > (V_G - V_T)$

$$I_D = \mu_{sat} C (V_G - V_T)^2 \times \frac{W}{2L} \tag{2.11}$$

The mobility may then be calculated from

$$\mu_{sat} = \frac{L}{WC} \cdot \frac{\partial^2 I_D}{\partial V_G^2} \tag{2.12}$$

The source-drain current I_D flows in the plane of the device, in a very narrow region within just a few nanometres of the gate dielectric. This is in contrast to the current in time-of-flight (and in the majority of optoelectronic devices except transistors), which flows perpendicular to the plane and through the bulk of the material. This is one reason why care must be taken when comparing mobility values derived from different measurements. The different geometries of transport may lead to very different results in systems showing strong alignment and anisotropy in mobility, for example regioregular P3HT [38]. The geometry of the current flow in a transistor also means that the electrical properties are subject to the interference of the gate dielectric. Dielectrics with low defect densities are required to avoid charge trapping effects which will strongly distort the mobility measurement.

A second important difference between the field-effect transistor and time-of-flight methods is the charge carrier density present in the transporting region. These carrier concentrations are often several orders of magnitude larger than those in time-of-flight measurements and in other optoelectronic devices. As described above in Section 2.1.6, it has been shown [31] that the mobility in disordered organic materials can increase rather strongly with the carrier density. Hence, it is likely that the mobility derived from a field-effect transistor measurement may be higher than that corresponding to the operation of other devices, such as photovoltaics.

Finally, in contrast to the time-of-flight and transient microwave conductivity measurements, this measurement requires good injection at the source electrode and good extraction at the drain electrode. This can preclude accurate measurement in materials with HOMO/LUMO levels poorly matched to available contact metal work functions, and in less extreme cases may still present complications due to the influence of contact resistances.

Nonetheless, field-effect transistor measurements remain one of most effective and widely used meth-

ods to derive carrier mobilities, and even where the absolute value may overestimate the mobility as found in other types of device, trends across various materials may be preserved. The advantages of the method are flexibility regarding film thickness; the ability to screen a large number of devices rather quickly; and the ability to measure a very wide range of mobilities, not being limited by equipment response or by the effects of dispersive transport.

2.2.4 Space-charge-limited current

Another steady-state technique to measure mobility is the space-charge-limited current (SCLC) method. As in FET measurements, the mobility is derived from a current-voltage scan. However, the method measures charge transport in a different regime. In this case, the appropriate regime is the space-charge-limit. Space-charge-limited currents may be seen when the following conditions apply [73, 74, 75]:

- Low mobility
- Strongly unbalanced transport
- Sufficient injection
- Dominance of injected charges over intrinsic charges

The first condition is generally applicable to disordered organic materials. The second condition may apply naturally in the case that the hole and electron mobilities differ widely (by several orders of magnitude). Alternatively, it may be ensured in any given material by choosing selective contacts in order to promote the injection of one type of carrier, and block the injection of the other type. Likewise, sufficient injection is ensured by appropriate choice of electrodes. The fourth condition is more difficult to guarantee, since many organics have variable levels of doping which are non-trivial to quantify. Therefore, it is often the case that space-charge-limited current measurements are justified by the self-consistency of the measurement over a range of parameters.

If the above conditions are fulfilled, the unbalanced transport means that one polarity of carrier is predominant in the device. This leads to the formation of a space-charge which may only be supported by the formation of screening charge distributions held on the electrodes. However, the amount of charge that can be screened has a fundamental limit according to the capacitance of the device. Hence, the current in the device is limited by its capacitance. The space-charge-limited

current in a trap-free insulator (that is, one with no intrinsic carrier concentration) is given by the Mott-Gurney equation:

$$J = \frac{9}{8}\epsilon\epsilon_0\mu\frac{V^2}{d^3} \tag{2.13}$$

A modification to this – useful for disordered organic systems – was performed by Murgatroyd [76]. In systems with a distribution of shallow traps, an additional contribution to the voltage dependence of the current is expected via the Frenkel effect. The Frenkel effect accounts for additional charges becoming mobile with increasing voltage as a result of the lowering of the barrier for de-trapping by an electric field. These charges, once mobile, contribute to the current. The functional form of the equation is then [76]

$$J = \frac{9}{8}\epsilon\epsilon_0\mu\, e^{0.89\beta\sqrt{V/d}}\,\frac{V^2}{d^3} \tag{2.14}$$

Although Murgatroyd describes the stronger field dependence of the current as originating from an increase in the number of free charges resulting from a decrease in trapped charge (with mobility independent of electric field), the parametric form of the equation given above is commonly interpreted as describing a field-dependent mobility (implicitly assuming a field-independent carrier density). For this reason, the mobility term μ is often written μ_0, where the subscript indicates that the mobility applies to the condition of zero electric field. In that interpretation, the mobility at field E is written as $\mu(E) = \mu_0 e^{0.89\beta\sqrt{E}}$.

A disadvantage of the space-charge-limited current method is a significant degree of uncertainty around the applicability of the model to the given situation. In the case that intrinsic carrier density is non-zero, deviations from the model may be expected. However, it is highly non-trivial to determine the balance of intrinsic and injected charge [77]. In addition, the method requires very efficient injection from the contacts. In conditions of insufficient injection the space-charge-limit will not apply. Therefore, measurements should be carefully checked for self-consistency (for example the scaling with thickness) and repeatability. However, the method offers the advantage of a close representation to the operation of devices such as photovoltaics, with out-of-plane transport through the bulk of the material, flexibility in film thickness (providing injection is good enough to

support high currents) and a more similar charge carrier concentration as compared with field-effect transistor measurements. For these reasons, this is one of the most common methods used to derive mobility in disordered organic systems.

2.2.5 Complex impedance spectroscopy

Complex impedance spectroscopy uses an alternating, perturbative voltage to probe the response of a system at different frequencies. This allows the various charge relaxation processes within the system occurring at different voltages or over different time-scales to be isolated. The technique is widely applicable for measurement or observation of various processes. For the purpose of measuring mobility, a sample in a device configuration is required, with the material under study sandwiched between injecting electrodes (either bipolar or unipolar devices may be used).

The device is held at some (d.c.) voltage V, corresponding to a point on the steady-state current-voltage curve. A small excitation voltage $v_{ac}(\omega)$ is then applied, with the condition that the steady-state current response should be well-approximated by a linear function over the resultant voltage range $V - v_{ac}$ to $V + v_{ac}$. The a.c. current response $i_{ac}(\omega)$ is then monitored, allowing the derivation of the complex impedance $Z(\omega) = v_{ac}(\omega)/i_{ac}(\omega)$, both resistive and capacitative parts. V may of course be varied to probe different regimes within the system, but the power of the technique lies in the variation of the frequency of the excitation voltage. Phenomena which occur over a characteristic time-scale τ will 'switch-on' in the frequency region around $1/\tau$. The effective mobility in the system may therefore be derived by observing the characteristic time over which the carriers begin to transit the device. At high frequencies, injected charges will be unable to reach the collecting electrode before the field has reversed and they are collected at the same electrode. In this regime, the impedance response is seen as capacitative, as the charge injecting and collection is fully reversible. At some critical frequency going towards lower frequencies, the reversal in the field is slow enough that the faster carriers have just enough time to transit the device. This is no longer a capacitance, but a resistive loss, since the carriers are not returned to the original electrode. This transition can be clearly seen in the frequency response of the complex impedance, and an effective transit time may be interpolated. This can then be used in the same way as a time-of-flight transit time to calculate an effective mobility μ, using Equation 2.8 to give

$$\mu = \frac{d^2}{V\tau}$$

for the film thickness d. The advantage of this method is that good data can be quite unambiguous regarding the mobility extraction, since the charge transiting process has the characteristic signature as described. The method can also, like the space-charge-limited current method, represent the situation in a device such as a photovoltaic cell rather well, with vertical transport through the bulk and a similar carrier density. The film thickness is only limited by the time response of the setup and the effectiveness of shielding in reducing interference from circuitry inductance, for example. For lower mobility materials therefore, thin films of 100 nm, as in many devices, may be used, but for higher mobility materials ($>10^{-4}$ cm^2/Vs) it is often found that thicker films are required. Nonetheless, films can usually be thinner than in time-of-flight experiments. Finally, the method gives an effective mobility, and does not distinguish between electrons and holes. The individual mobilities may be found if electrodes can ensure unipolar devices, but this may not be trivial and may present a challenge to the use of the method. As a result of the non-trivial analysis required to derive mobility from impedance measurements, this method is not one of the most commonly used. However, it offers a potentially less ambiguous result than some of the methods outlined above.

2.3 Charge transport in organic photovoltaics

As background to Chapter 6, we outline here the basic working principles of an OPV device, and the importance of charge transport for OPV. Since only Chapter 6 includes OPV data, we aim for a fairly brief treatment. As we will focus on the charge transport processes in OPV devices, the reader is referred to review articles [5, 78, 79] for more detailed coverage of the other important processes in OPV systems. The devices under study in this report are polymer:fullerene bulk heterojunction (BHJ) devices. Polymer:fullerene BHJ devices have been the state-of-the-art for solid-state OPVs for more than a decade [80]. In 1995, Yu et al. made OPV devices based on a blend of the polymer MDMO-PPV and the fullerene PCBM, achieving a power conversion efficiency of 2.9% under monochromatic light at 430 nm with intensity 20 mW/cm^2 [81]. It was found that a judicious blending of two material components to form an internal network of heterojunctions allowed much more efficient separation of excitons into charge carriers than could be achieved with the polymer component alone. Photovoltaic conversion in an OPV device involves the following steps:

1. Absorption of a photon in the active layer to form an exciton

2. Diffusion of the exciton towards a heterojunction

3. Separation of electron and hole polaron across the heterojunction

4. Transport of the polarons through the different phases to opposite electrodes

5. Extraction of the polarons at the electrodes

Figure 2.11 shows these five basic processes required for photovoltaic conversion in OPV bulk heterojunction devices. On the right the scheme is shown spatially, and on the left the scheme is shown energetically. Each of the basic processes in OPV operation requires optimisation, and will otherwise lead to losses in the number or energy of the carriers.

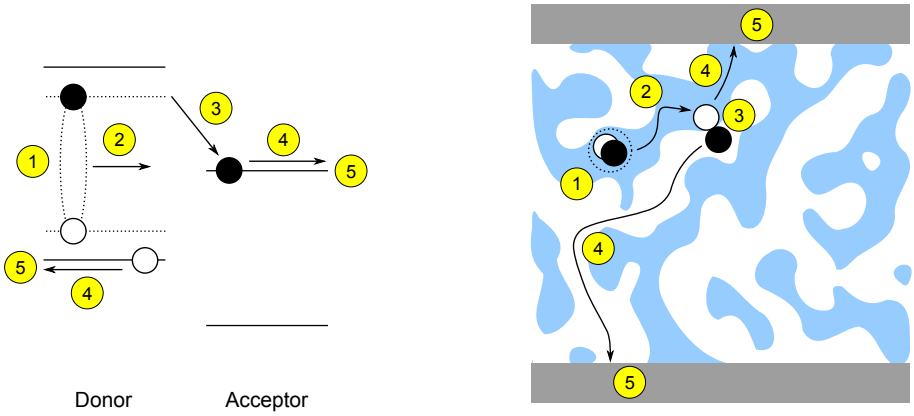

Figure 2.11: Schematic of the processes in an operating organic photovoltaic device, with numbered labels as described in the main text.

2.3.1 Losses during OPV operation

Absorption

The first process above, the absorption of the OPV material, is a key area of research in OPV. Whilst the polymers used for OPV generally have strong absorption (large oscillator strength) and an absorption depth at the peak wavelength of around 100 nm, the wavelength range of absorption is not particularly broad, and does not overlap particularly well with the solar spectrum. Research is thus underway to extend the range of absorption of OPV materials further into the infra-red whilst simultaneously preserving efficient charge separation and collection.

Charge separation

The requirement for efficient charge formation from the generated excitons places a strong constraint on the extent of intermixing of the components. Exciton diffusion lengths are typically $1 - 20$ nm

[82, 83], and hence the length-scale of phase separation should not be much larger, or exciton recombination will be the primary loss mechanism. Once the exciton has reached a heterojunction, it must be ensured that charge separation occurs. Another important loss mechanism is that of geminate recombination, whereby partially separated charges cannot escape the Coulomb field of the pair, and recombine rather than become fully separated charges in the distinct phases. Minimising geminate recombination is a key current challenge for OPV, and there is currently vigorous research into the mechanisms involved and how to design materials to best avoid it. However, we do not focus on this process here.

Charge transport and collection

Once the charges have been separated and geminate recombination has been avoided, the charges must be transported through the bulk for collection at their respective electrodes. It is intuitive that a high mobility allows each charge to reach the corresponding electrode for collection more quickly. However, the main process competing with collection is also strongly dependent on charge transport. That competing process is one of nongeminate recombination, whereby electron and hole polarons on different molecules, having originated from different excitons, meet and recombine in the bulk. In fact, it is thought that in state-of-the-art OPV devices nongeminate recombination is the major loss mechanism in operating conditions [84, 85, 86, 87, 88]. Since the balance between collection and bimolecular recombination is strongly dependent on the charge transport properties of the blend, as well as the carrier lifetime, blend morphology and device thickness, we discuss this in more detail in Section 2.3.3.

Charge extraction

It is important that the electrodes promote charge selectivity. Ideally, the desired charge carrier should be extracted without number or energetic loss, and the opposite charge carrier should be blocked. This is typically achieved by choosing an electrode material which forms an Ohmic contact with one material for one carrier, either acceptor LUMO for the cathode or donor HOMO for the anode. The large energetic separation between acceptor LUMO and donor HOMO should then ensure reasonable selectivity. Nonetheless, the presence of the undesired charge carrier at an electrode is likely to lead to losses through recombination with the opposite carrier both next to the electrode and on the electrode surface. Thus, blend morphology also has a role to play in minimising losses at the electrodes. Typical electrode combinations for high efficiency OPV devices currently

include PEDOT:PSS as anode with a low work function metal such as Ba or Ca, a metal fluoride such as LiF, an n-type metal oxide such as TiO_x or in one case a polymer interlayer [89], each typically capped with Al, as cathode. Various disadvantages of these materials, such as chemical instability and in some cases the requirement for vapour deposition, means alternative electrode materials are another important topic of research in OPV. However, we do not focus further on these here.

2.3.2 Light JV curve and definitions

Successful completion of these steps allows work to be extracted from incident light. For work to be done, the device must supply current and voltage to the external load. Figure 2.12 shows the dependence of current through a good OPV device under illumination on voltage across the device. We here define three quantities which combine to give the maximum power provided by the device, and relate to the shape of the current-voltage curve: open-circuit voltage V_{oc}, short-circuit current J_{sc} and Fill Factor FF. The factorisation of the power into these quantities turns out to be useful to characterise solar cells, but the quantities should not be thought of as independent.

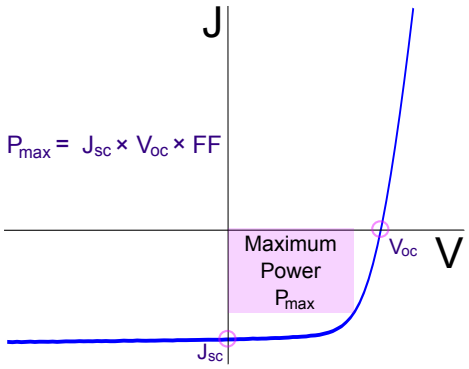

Figure 2.12: Illustration of the solar cell parameters as defined by the JV curve under illumination. The JV curve intersects the axes at J_{sc} and V_{oc}. The FF is given by the ratio of the maximum power point P_{max} in the power-generating fourth quadrant and the product $V_{oc} \times J_{sc}$.

In Figure 2.12, it can be seen that in reverse bias (negative voltages), the current collected from a good OPV device is almost constant. This reflects the fact that in reverse bias, when the external voltage acts as a strong driving force for collection of charges (in competition with recombination), the efficiency of the process is nearly 100%. At J_{sc}, where the external voltage is zero, the current in a good solar cell will still be large, as a result of the designed asymmetry of the system. The electrodes of the cell are chosen such that they are highly selective, the anode forming an Ohmic contact

with the donor HOMO and the cathode with the acceptor LUMO, assisting extraction. Since the asymmetry is usually energetic, there is usually a significant internal field driving extraction at J_{sc}. Other asymmetries, such as the vertical composition of the blend [90] and even the direction of illumination [91], may also assist net current flow. However, as the external voltage becomes positive $V > 0$, the internal field and the driving force for collection both decrease. An increasing number of carrier are then lost to recombination, and the current collected decreases more quickly (for example, see [87]). V_{oc} is defined as the point where no net current flows, and all generated charges recombine.

At some point along the curve between J_{sc} and V_{oc}, the product $J \times V$ is maximised. This represents the maximum power P_{max} which can be collected by the device. This leads to the definition of $FF = P_{max}/(J_{sc} \times V_{oc})$. The FF can hence be seen as an indicator of the ability of the device to collect charge in the critical region where the driving force for collection is small.

2.3.3 Balance between charge collection and nongeminate recombination

As stated above, it has been established that nongeminate recombination, in competition with charge collection, is commonly the dominant loss mechanism in state-of-the-art OPV devices [84, 85, 86, 87, 88]. Here, we briefly outline the current understanding of the mechanisms involved, with particular reference to the influence of charge transport.

Influence of charge transport on collection and nongeminate recombination

Regarding charge collection, it is clear that a higher mobility allows each charge to reach the corresponding electrode more quickly. The relevant quantity is the $\mu\tau$ product, with mobility μ and charge carrier lifetime τ. The product of the mobility, lifetime and electric field $\mu\tau E$ represents a characteristic distance over which charges travel before recombination. The mobility determines the speed with which a charge may move in the electric field, for example to reach the collection electrode and escape recombination. The lifetime describes the timescale of the dominant loss process for a carrier, including the effects of nongeminate recombination.

However, the rate of recombination (and thus the carrier lifetime τ) is itself, in general, dependent on the charge transport properties of the blend. Models of nongeminate recombination commonly start from a Langevin description of bimolecular recombination, where both charges move in an isotropic medium and recombine with a certain probability when they approach within a certain

distance [92]. Thus, higher mobility may be expected to lead to a higher rate of recombination and a reduced lifetime. In this case, the overall effect on the balance of collection and recombination of an increasing mobility is intuitively less clear. In high efficiency OPV systems, however, very significant deviations from the Langevin description are commonly observed. A number of groups have observed nongeminate recombination orders of magnitude lower than predicted by a Langevin model [93, 94, 95, 96, 97, 98]. This has been attributed to (i) the non-uniform spatial distribution of the carriers in operating devices, where the concentration of electrons is higher at the cathode than at the anode, and vice versa for holes [93, 99]; and (ii) the spatial separation of electrons and holes in the phase-separated blend morphology [94, 96]. We note that there have been recent demonstrations of non-Langevin recombination in systems without clear phase separation as observed by TEM [98]. This phenomenon remains an interesting topic of study.

Charge transport properties may further influence the balance between charge collection and recombination by altering the charge density conditions. Since the local recombination rate is proportional to the local product of the density of electrons and holes, this can be a significant effect. Deep charge traps within either material will lead to immobile charges which are effectively never collected, and hence to higher carrier densities. For example, Etzold et al. have shown that energetic disorder in PCDTBT and its blends with PCBM leads to trapped charge and increases the nongeminate recombination rate [88]. Morana et al. have suggested that recombination of holes with electrons trapped on isolated PCBM clusters is an important mechanism limiting charge collection in PCPDTBT:PCBM blends [100]. In such cases, poor charge transport properties thus have the potential simultaneously to increase recombination rate and reduce charge collection rate, leading to drastically lower device efficiencies.

With the development of OPV, there have been many experimental reports of increased mobility leading to increased device efficiency. Such correlations have been established in systems including MDMO-PPV:PCBM with different PCBM fractions [101]; OC_1C_{10}-PPV:PCBM with different PCBM fractions [102]; annealed and non-annealed P3HT:PCBM [47]; PCPDTBT:PCBM with or without octanedithiol additive and with different PCBM fractions [100]; PCPDTBT or its silicon bridged counterpart Si-PCPDTBT with PCBM [103]; Si-PCPDTBT with PCBM or bis-PCBM [104]; and P3HT with PCBM, bis-PCBM or tris-PCBM [105, 26], amongst other systems.

It may thus be wondered whether an increase in mobility always leads to an increase in device efficiency. This question has been addressed by several groups [106, 107, 108]. The consensus appears to be that in the great majority of practical cases an increase in mobility will lead to an increase in efficiency. Caveats to this include (i) cases where certain recombination mechanisms, such as recombination at the electrode surface, are strongly enhanced for high mobilities; and perhaps (ii) cases where the mobilities of the two carriers are strongly imbalanced. Regarding (i), Kirchartz et al. [108] have shown that in the case of fast recombination at the electrode surface, there may exist an optimum mobility defined by the balance between charge collection and surface recombination. The applicability of this limit to OPV systems has not been demonstrated experimentally. An earlier study by Mandoc et al. [107] claimed that considering only bulk Langevin-type recombination, further increases in mobility above a certain mobility may lead to a decrease in the open-circuit voltage as the carrier densities are reduced towards zero. Kirchartz et al. showed, however, that this analysis, without a further mobility-dependent recombination pathway such as surface recombination, is not valid. Regarding (ii), it has been shown that if the mobility of one carrier greatly exceeds that of the other, there will be a build-up within the bulk of the lower mobility charge carrier. This constitutes a space-charge, which will act to limit the photocurrent which can be extracted by the device [74, 109, 110]. It may thus be postulated that further increases in the high mobility carrier may in this case lead to a reduction in device efficiency. Whilst there are isolated studies demonstrating the existence of the space-charge-limit in OPVs [75], a systematic demonstration of the effect of imbalanced mobilities on charge collection efficiency has yet to be performed.

Charge collection versus light absorption: an optimisation problem

It can be seen that the requirements for efficient charge collection and strong light absorption lead to an optimisation problem. Thicker active layers are desirable to maximise absorption, but will place stricter constraints on the $\mu\tau$ product, as the charges have to travel further in the same time to avoid recombination. It will be seen in Chapter 6 that this is highly relevant to current state-of-the-art OPV systems where the thickness of devices is limited to around 100 nm, resulting in the waste of around 1/3 of the incident useable light [111].

Effect of blend morphology on charge collection efficiency

The carrier mobilities within an OPV device are, of course, limited by all the factors described in Section 2.1.3, including energetic and spatial disorder and the presence of impurities, defects and

end groups. However, polymer:fullerene devices have the further complication that the transport layer is a blend of two materials, each of which is required to transport a particular charge carrier towards a particular electrode. Macroscopic features such as the connectivity and vertical distribution of the two phases thus become important. In addition, the presence of a second material has the potential to disrupt the packing and ordering behaviour of the first material dramatically, potentially leading to different transport properties in the blend film versus the single-component film. A relatively close inter-mixing of the phases cannot be avoided due to the requirement for the majority of excitons to reach a heterojunction within several nanometres of the position of formation for charge separation.

The term 'blend morphology' is thus used to encompass both the structural features of the individual materials and the architecture of the blend. Since this influences the charge separation efficiency, the mobility of the two charge carriers, the rate of recombination and the efficiency of collection at the electrodes, optimisation of the blend morphology is one of the key challenges for developers of OPV.

Fill Factor as indicator of charge collection efficiency

From the discussion in Section 2.3.2, it may be seen that a high FF is an indicator of the ability of the OPV device to collect charges when the driving force for collection is low; that is, it indicates that charge collection outcompetes nongeminate recombination at low applied fields. It is clear, then, that the FF is an interesting parameter from the point of view of charge transport. In optimised devices, the FF can be used to compare the efficiency of charge collection across a series of devices. This has been described in some detail in the case of P3HT:PCBM by Mauer et al. [86] and by Dibb et al. [112]. Mauer et al. studied temperature- and light intensity-dependent current-voltage curves alonside transient absorption measurements. The group was able to reproduce the observed FF values closely using a model of field- and temperature-independent free charge generation followed by kinetic competition between charge collection and nongeminate recombination. Dibb et al. used transient absorption spectroscopy, charge extraction and transient photovoltage experiments to show that the low observed FF in PCPDTBT:PCBM devices versus P3HT:PCBM devices is due to enhanced nongeminate recombination. However, Dibb et al. also showed that in APFO-3:PCBM devices, the low observed FF is a result of strongly field-dependent geminate recombination. In general, then, care should be taken since the FF is affected by a number of factors aside from bulk

charge transport.

Since the subject of Chapter 6 is based around correlations between mobility and FF, we attempt here a brief, non-exhaustive, summary of the possible causes of a low FF:

- Inefficient charge collection due to low mobility-lifetime product of charge carriers
- Inefficient charge collection due to imbalance in mobilities and formation of space charge
- Field-dependent charge separation at the heterojunction
- Inefficient charge collection due to poor extraction at electrode(s)
- Low shunt resistance due to leakage pathways (constituting a current opposing the photocurrent)
- High external series resistance (from external contacts)

Optimisation of the Fill Factor by varying the electrodes or the film thickness, for example, can help to identify the mechanism of a low FF. The relationship between charge transport and the FF in OPV blend systems will be discussed further in Chapter 6.

2.4 Outline of this thesis

Achieving good charge carrier transport in disordered organic semiconductors is of great importance for technological application in plastic electronic devices such as solar cells, transistors and electrically-pumped lasers. In solar cells, for example, good charge transport properties are required so that collection of electrons and holes outcompetes recombination; in various transistor applications, high mobility is necessary to achieve large enough currents for device performance to compete with existing inorganic technologies; and in electrically-pumped lasers, high mobility allows the excitation density threshold to be reached before the build-up of space-charge prevents further charge injection.

We have described above the challenges for researchers aiming to improve charge transport properties in disordered organic materials. We summarise the key challenges relevant to this thesis briefly below.

1. 'Soft' organic materials generally show low charge carrier mobilities compared with inorganic materials due to their inherent energetic and configurational disorder, chemical and physical defects.

2. Using changes in chemical design and/or materials processing to increase crystalline or liquid crystalline order, whilst in many cases a fruitful approach, has not always succeeded. Attempts such as increasing the polymer chain planarity (see Section 2.1.8) and increasing the crystalline fraction within a film [41] have not always led to bulk mobility improvements.

3. Determining the effect on mobility of specific types of disorder or specific defects has proven difficult due to the wide variety of such features within a single system; the problems distinguishing them spectroscopically; and the challenges to controlling their formation in isolation.

4. Achieving high mobility in systems within which the approach of increasing crystalline or liquid crystalline order is not desirable has been even more challenging. Cofacial $\pi-\pi$ ordering tends to erode the efficiency of luminescence, for example, hindering the development of high mobility materials for light emitting transistors and polymer lasers.

5. The development of high mobility materials for OPV involves further complications due to the requirement for a closely interpenetrating blend of two materials. In order to achieve efficient

transport of both electrons and holes through their respective phases, careful and sometimes complex processing is required. The charge collection challenge continues to limit efficiencies today.

The subject of this thesis is the influence of physical and chemical structure on charge transport in disordered organic semiconducting materials and devices. In the three experimental Chapters following, we aim to address several key areas where our understanding of charge transport in organic materials is incomplete. In each case, we attempt to tie clear observations of changes in charge carrier mobility to specific structural defects or sources of energetic or configurational disorder.

In Chapter 4, we investigate hole transport in a family of polyfluorenes, namely poly(9,9-dioctylfluorene) (PFO), poly(9,9-dioctylfluorene-co-9,9-dihexylfluorene) (F8:F6) and poly(9,9-dioctylfluorene-co-9,9-di(2-methyl)butylfluorene) (F8:F4/1), a material set of technological interest as efficient blue emitters. By controlling the phase formation of the materials by processing and by virtue of their chemical design, we are able to examine the effect on transport of distinct material phases. Remarkably, we are able to isolate the effect of the single chain conformation of PFO known as the beta-phase and show that when embedded in a glassy PFO matrix it acts as a strong hole trap, reducing the mobility of the bulk material by over two orders of magnitude. By fabricating a device with negligible beta-phase, we demonstrate the highest time-of-flight mobility in PFO to date. This study provides the first clear and unambiguous example of the effect on transport of a distinct conformational defect in a conjugated polymer, and explains the mechanism behind the original observation of greatly enhanced mobility in F8:F4/1 [16]. We also demonstrate the adverse effect on mobility of crystallinity in the polyfluorenes. While the beta-phase conformation is far from a general property of conjugated polymers, we suggest that our findings may generalise to other systems in the sense that the charge transport properties may be limited by a minority population of structural traps, which may include highly ordered, crystalline regions. Significant mobility improvements may then be more easily achieved by removing the minority phases within the samples than by increasing their concentration. We believe that this approach offers an alternative paradigm by which higher mobilities may be obtained in general, and in particular in systems where crystallinity is undesirable.

In Chapter 5, we study charge transport in the fullerene derivatives [6,6]-phenyl-C61-butyric acid methyl ester (PCBM), bis-PCBM and tris-PCBM. The fullerene multi-adducts bis-PCBM and tris-

PCBM have attracted attention recently as alternative OPV acceptor materials with the potential to increase V_{oc} and PCE. While bis-PCBM has been used successfully in a blend with P3HT to increase V_{oc} and PCE relative to the P3HT:PCBM blend [113], OPV blends employing the multi-adducts with other donor materials have generally failed to improve upon those employing PCBM. This is thought to be a result of the inferior electron transport properties of the multi-adducts, due to either (i) higher energetic disorder in the multi-adducts due to the presence of isomers with varying LUMO energies [26, 105] or (ii) higher configurational disorder due to a lower degree of order in molecular packing in the multi-adducts than in PCBM [105]. However, the relative importance of these two factors remains unknown. We attempt to distinguish between the effects of energetic and configurational disorder using temperature-dependent ToF and FET measurements. The ToF measurements are ultimately unsuccessful in this regard, but the FET measurements allow a full comparison of energetic and configurational disorder in the three fullerenes. We find large variations in the energetic disorder between the fullerenes, consistent with the variation in LUMO distributions predicted theoretically by Frost et al. [114]. Further, we find that differences in configurational disorder appear negligible. We therefore conclude that the reduced mobility in bis-PCBM and tris-PCBM compared with PCBM is due predominantly to the effects of energetic disorder resulting from the presence of a mixture of isomers with varying LUMO energies. Design rules for novel OPV acceptors of any type must include a consideration of energetic disorder introduced through the production of isomers.

In Chapter 6, we examine the charge transport properties of polymer:PCBM blends for OPV. We focus on the PTB7:PCBM system, studying the P3HT:PCBM and PCPDTBT:PCBM systems for comparison. In particular, we set out to address the question of why state-of-the-art OPV systems such as PTB7:PCBM perform so much worse at large active layer thicknesses than P3HT:PCBM. We find that low electron mobility is the main cause of the poor performance of PTB7:PCBM relative to P3HT:PCBM. The electron mobility in PTB7:PCBM blends is found to be 1–2 orders of magnitude lower than the electron mobility in annealed P3HT:PCBM, while the hole mobility, in contrast, was found to be the same to within a factor of approximately three. We hypothesise that the low electron mobility is due to the low degree of phase separation of PTB7 and PCBM in the blend, leading to a poorly connected and disordered PCBM phase. We suggest that the low degree of phase separation is a result of the low tendency of the PTB7 polymer to crystallise as compared with P3HT. We investigate methods to address the low electron mobility in PTB7:PCBM blends, including

varying the PCBM fraction and using solvent additives such as DIO. We find that increasing the PCBM fraction in PTB7:PCBM blends without DIO is very effective in improving electron transport (without significantly affecting hole transport), as confirmed by the correlation between SCLC electron and hole mobility and FF. We find that the use of DIO, however, does not improve electron mobility, and does not solve the problem of poor performance at large film thicknesses. We suggest that a key challenge for OPV researchers is thus to achieve better connectivity and ordering in the fullerene phase in blends without relying on either (i) a large excess of fullerene or (ii) strong crystallisation of the polymer. The rewards for such progress would be vast, as it may be estimated that the current literature record PCE of 8.4% for PTB7:PCBM [89] could be up to 50% higher if a FF of 0.6 were achieved using a film > 300 nm in thickness.

Chapter 3

Experimental Methods

This section outlines in detail the experimental procedures for the most significant techniques in collecting the data presented in this thesis. They include: (i) time-of-flight photocurrent, (ii) space-charge-limited current-voltage, (iii) dark and light current-voltage for OPV, (iv) photoluminescence spectroscopy, (v) UV-visible absorption/transmission, (vi) differential scanning calorimetry, (vii) wide angle X-ray scattering and (viii) device fabrication.

A smaller amount of data using several other techniques will be presented in this thesis. Where this applies, the important experimental information will be found alongside the data.

3.1 Time-of-flight photocurrent

The basic theory of the time-of-flight (ToF) method was outlined in Section 2.2.1. Here, we focus on the experimental setup and practical details of the measurement. The d.c. bias voltage was supplied by a high-voltage Keithley 237 source-measure unit, and could be of either polarity to probe either holes (as required for the polyfluorenes study) or electrons (as required for the fullerenes study).

Devices were fabricated as described in Section 3.9. Time-of-flight devices require blocking contacts – the reader is referred to individual chapters for details of the contacts used.

The light pulse was provided by a frequency tripled Quantel Nd:YAG pulsed laser (wavelength = 355 nm, pulse width $\approx$ 6 ns), in order to overlap with the absorption spectrum of the polyfluorenes and the fullerenes under study. The requirement for the pulse width to be much shorter than the

transit time t_{trans} is fulfilled as typical transit times presented are 500 ns – 1 ms. The requirement that the absorption depth (≈100 nm) be much smaller than the film thickness was ensured by using samples >2 μm in thickness. It is also important that the concentration of charge in the device formed by the laser pulse does not disturb the uniformity of the electric field. This was ensured by the use of neutral density filters where required. For each transient, the Labview program collecting the data was used to estimate the total charge collected Q (as the integral under the current-time curve). The value of Q was compared to the amount of charge which would be needed to compensate the applied field, that is $Q_0 = CV$ for device capacitance C and applied voltage V, and the intensity adjusted such that $Q/Q_0 < 0.1$.

For room temperature measurements, the device was contained in a sample chamber with a nitrogen overpressure. For temperature-dependent measurements, the device was contained in a helium-exchange-gas Oxford InstrumentsTM Optistat cryostat with a quartz glass optical access. The instrument operation temperature range is 77–500K, and the temperature was controlled using an Oxford Instruments ITC503 Temperature Controller Unit. For all measurements the signal was displayed on a computer-controlled 500 MHz Tektronix TDS 3052 oscilloscope and collected by a Labview program.

The photocurrent signal was observed through the voltage drop across a resistor in series with the device. Since the response time of the system is dependent on this resistance (as well as the system capacitance), it is necessary to choose a low enough resistance that the circuit time constant $RC \ll t_{trans}$. However, it is desirable to choose a high enough resistance to ensure a good signal-to-noise ratio. In order to improve the signal-to-noise, measurements were usually made with a home-built non-inverting amplifier constructed to offer a gain of 11. The signal was further improved by removing the coherent interference from the laser source. Since this noise was present in the system even when the light from the laser was not incident on the device (that is, when there was no photoinduced signal), it was possible to remove it effectively by subtracting the 'dark' signal from the 'light' signal, if the two traces were collected within the coherence time (usually tens of seconds was sufficient). The system could be switched between 'dark' and 'light' by using a shutter.

As described in Section 2.2.1, there is another mode in which the ToF setup can be used, namely the 'integral' mode. This is described, for example, in [63]. In this case, the load resistor is chosen such

than the circuit RC $\gg$ t_{trans}, such that the recorded signal is not the variation of the photocurrent with time, but the variation of the total charge accumulated at the back electrode.

3.2 Space-charge-limited current

The basic theory of the space-charge-limited current technique was outlined in Section 2.2.4, and so we focus on experimental details here.

Devices were fabricated at Sumitomo Chemical Co., Ltd as described in Section 3.9. Space-charge-limited devices require careful optimisation of the contacts to ensure sufficient injection of the desired carrier, and effective blocking of the other carrier – the reader is referred to Chapter 6 for details of the contacts used.

The space-charge-limited current measurement setup is very simple, consisting only of a Keithley 2400 SourceMeter unit to supply a voltage to and measure the steady-state current response of a device. All measurements were performed at room temperature. All measurements, unless otherwise stated, were performed in forward bias, where the ITO side of the device was biased positively. The devices were encapsulated in nitrogen without exposure to the air after deposition of the top contacts and subsequently measured in atmosphere. Unless otherwise stated, devices were measured in the absence of illumination by covering in aluminium foil.

Analysis of the data was performed by fitting in OriginLab's OriginPro 8 licensed to Imperial College. The raw current-voltage data was first corrected for external series resistance (mainly from the ITO contact), by subtracting from the voltage series the voltage drop $V_s = I \times R_s$ across the fixed resistance R_s for each data point (each with a different current value I and hence different voltage drop across the series resistance). The data was then, unless otherwise stated, fitted to a Murgatroyd function (as described in Section 2.2.4, and sometimes known as a 'Modified Mott-Gurney ' function) of the following form, allowing for a built-in voltage V_{bi} resulting from the different work functions of the contacts:

$$J = \frac{9}{8}\epsilon\epsilon_0\mu_0 \; e^{0.89\beta\sqrt{(V-V_s-V_{bi})/d}} \; \frac{(V-V_s-V_{bi})^2}{d^3} \tag{3.1}$$

3.3 Dark and light current-voltage for OPV

Devices were fabricated at Sumitomo Chemical Co., Ltd as described in Section 3.9. Dark current measurements were taken using a Keighley 2400 SourceMeter unit to supply a voltage to and measure the steady-state current response of a device. All measurements were performed at room temperature. Scans were generally taken from 1.5 V reverse bias to 1.5 V forward bias. Solar-simulated current-voltage measurements were taken with a Jasco xenon lamp solar simulator (AM 1.5D) at an illumination intensity of approximately 1000 Wm^{-2}. Devices were encapsulated in nitrogen without exposure to the air after deposition of the top contacts and subsequently measured in atmosphere.

3.4 Photoluminescence

Photoluminescence (PL) spectroscopy involves measuring the radiative emission of a sample upon optical excitation. Typically, the response of a sample is measured over a range of wavelengths. The resulting emission spectrum potentially contains a large amount of information relating to the structure of the material and the processes of energy and charge transfer occurring within it. In Chapter 4, PL is used to identify the presence or absence of certain structural features and energy transfer processes in the polyfluorene family, and in Chapter 6 it is used as an indicator of charge generation in polymer:fullerene blends.

In Imperial College, a Spex Fluoromax Jobin Yvon spectrofluorometer was used. The optical excitation is formed by focusing light from a 150 W continuous output xenon arc lamp onto the input of a monochromator, inside which the light is split into its component wavelengths by a multiple-slit grating. The setup is controlled by Datamax software, allowing the slit widths of the excitation spectrometer and the emission spectrometer to be varied, to control the band-pass of the incident light and the collected signal respectively. Wider slits lead to a higher signal-to-noise ratio, but to decreased spectral resolution. Part of the incident beam is collected before it is incident on the sample, and this light is sent to a reference silicon photodiode, in order to calibrate the beam for the xenon lamp output, the monochromator and variations in the power supply. The rest of the beam is incident on front surface of the sample (in this case a solid film), whose position is fixed by a sample holder, and should remain fixed throughout the acquisition of the emission spectrum in order to compare the intensity of emission at different wavelengths. Here, the beam is incident directly on

the sample, and the angle between the sample plane and the beam chosen such that the reflected beam does not enter the emission spectrometer. Even with the reflected beam thus removed, the angle of incidence strongly affects the signal intensity due to changes in path length within the sample and hence to self-absorption effects. The emission spectrometer contains an R928P photomultiplier tube which is read by a photon-counting module. The signal is then further corrected for the emission monochromator and emission spectrometer response. The resulting spectrum is the type shown in this thesis.

Where absolute measurements of photoluminescence intensity are required (such as for PL quantum efficiency measurements), use of an integrating sphere is recommended; however, this was not required for the purposes of this thesis and hence is not discussed further.

In Sumitomo Chemical Co., Ltd, spectrofluorometers with a very similar working principle were used. For the data in Chapter 6, a Horiba Jobin Yvon Fluorolog was used in the cases of PTB7 and PCPDTBT, and a Jasco FP-6500 spectrofluorometer in the case of P3HT.

3.5 Absorption/transmission

Organic materials absorb primarily over the ultraviolet, visible and near-infrared range. Measurement of the transmission spectrum of a material – used to derive the absorption – is a simple and common measurement which can provide useful information on the energy of optical transitions in the material.

The transmission of a sample is measured by comparing the attenuation of incident light through the sample and a reference. Light from a light source (typically a halogen lamp and a deuterium lamp) is split into two identical beams, sent through a monochromator and sent along two paths with equal optical length, one passing through the sample and the other through the reference. The ratio of the two beams at a particular wavelength gives the transmission T of the sample, which is defined as the fraction of incident light transmitted $T = I/I_0$, for incident intensity I_0 and transmitted intensity I. Transmission T is a function of wavelength, $T = T(\lambda)$. Typically, therefore, the measurement is performed over a range of wavelengths to form an transmission spectrum.

Here, samples were typically solid films prepared on Spectrosil B (TM) substrates, used for their increased transparency into the ultraviolet versus glass. No sample was placed in the reference position. Instead, the absorption of the substrate was accounted for by taking a separate transmission spectrum of a blank Spectrosil B (TM) substrate in the sample position, again with no reference, and manually subtracting the resulting spectrum from other spectral data. Defining the transmission of both sample and substrate as $T_{sample+substrate}$ and that of the substrate only as $T_{substrate}$, the transmission of the sample is given as $T_{sample} = T_{sample+substrate}/\ T_{substrate}$.

Data is often presented int he form of absorbance A (also called optical density OD) rather than transmission T. The absorbance is defined as $A = -\log_{10}(T) = -\log_{10}(I/I_0)$. The absorbance of the sample, with the above labelling, is then $A_{sample} = -\log_{10}(T_{sample+substrate}/\ T_{substrate})$, or equivalently $A_{sample} = A_{sample+substrate} - A_{substrate}$.

The absorbance of a sample increases with its thickness. In order to remove the thickness dependence to compare films of different thickness more effectively, a material property is defined as the absorption coefficient alpha. The Beer-Lambert Law, where it holds, relates the transmission T of a sample to its thickness d via $T = e^{-\alpha d}$. This gives the relation with absorbance $A = \alpha d/\ln(10)$, that is a linear dependence with thickness.

In Imperial College, absorption spectra were measured using a Shimadzu UV-2550 spectrometer, with a wavelength range of 200 nm to 1100 nm with optical density measurement capability $0.01 < A < 5$. The data in Chapter 6 were taken in Sumitomo Chemical Co., Ltd using a Jasco V-670 spectrophotometer.

3.6 Differential scanning calorimetry

Differential scanning calorimetry (DSC) is a probe of phase transitions in materials. It exploits the fact that, as a result of the different free energies of the initial and final phases (of a first-order phase transition), typically large amounts of heat energy are released (for exothermic transitions) or absorbed (for endothermic transitions) during the phase transition at fixed temperature. DSC experiments in the Department of Materials at Imperial College and in the Polymer Technology Division at ETH Zurich were in both cases carried out using a Mettler Toledo DSC822e.

The material for study is placed in a small aluminium crucible (in this thesis and typically), together comprising the study sample. The study sample and a reference sample with well-known heat capacity (usually an empty crucible, as in this thesis) are placed in thermal contact with two separate heaters. The temperatures of the study sample and the reference sample, and the heat flows to the two samples, are recorded by two thermocouples and the data fed into a controller unit. Usually, the temperature of the system is set by the controller unit to increase or decrease linearly with time (commonly 10–20°C/min), with the study sample and reference sample remaining at almost the same temperature throughout the experiment. The difference in the amount of heat required to raise the temperature of the two samples to the same temperature is then used to calculate the heat capacity of the material under study. Phase transitions are observed as changes in the heat capacity with temperature.

The primary output of a DSC measurement is a plot of heat flow (normally the difference in heat flow from the study sample and reference sample heaters) versus temperature, where temperature is directly proportional to time. The plot is commonly used to observe the presence or absence of certain phase transitions – for example, whether the material has a glass transition (that is, whether it acts as a glass over some temperature range), or whether it crystallises – and at which temperature they occur. The plot may be used for more advanced purposes. Integrating the area under the curve in the neighbourhood of the changes in heat flow, for example, allows the total enthalpy of the phase change to be calculated. This may allow a comparison of the extent of crystallisation of a sample, for example.

A schematic of such a plot is shown in Figure 3.1. Characteristic heat flow profiles of the main phase transitions in polymers are shown as examples. The plot shows heat flows to the sample (endothermic changes) plotted positive on the y-axis against temperature on the x-axis. It can be seen that the glass transition is typically observed as a simple increase in the heat flow to the sample for a given temperature change. This is because the heat capacity of a polymer is higher above its glass transition. A crystallisation, in contrast, is typically observed as an inverted peak. This is because crystallisation is an exothermic process, and during the transition less heat is needed for a given temperature rise. Melting is an endothermic process, where more heat is required for a given temperature rise, and so this is seen as a peak in the heat flow.

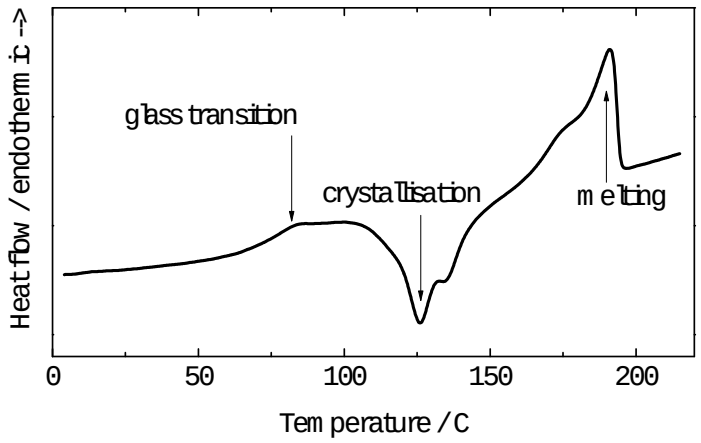

Figure 3.1: Example differential scanning calorimetry trace with key features as described in the text.

3.7 Wide-angle X-ray diffraction

Wide angle X-ray diffraction was performed at ETH Zurich using an Oxford Diffraction Xcalibur PX instrument using molybdenum K_α radiation (wavelength 0.0709 nm). Diffraction was performed in two configurations in order to probe the structure of the samples in all dimensions. The distance between the sample and the detector was in all cases 130 mm. The nomenclature used is defined as shown in Figure 3.2.

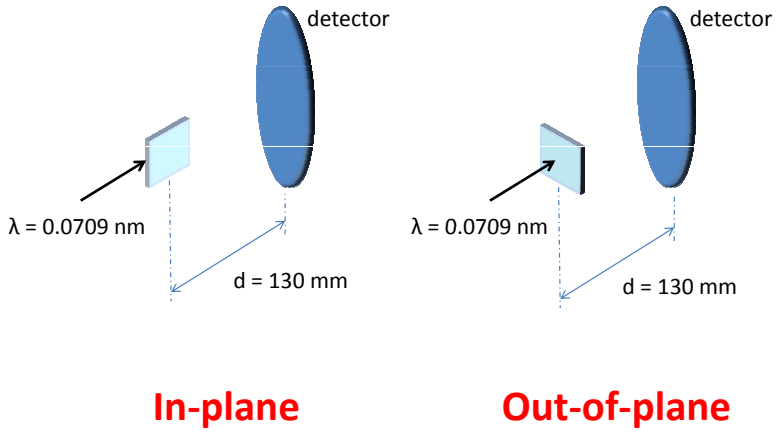

Figure 3.2: Illustration of the 'in-plane' and 'out-of-plane' XRD configurations as defined here. In the 'in-plane' configuration the incident beam is in the plane of the film; in the 'out-of-plane' configuration it is normal to the plane of the film.

3.8 Density gradient column

In density gradient column measurements, a fluid column with a continuous density gradient is set up by mixing two fluids of different density in a controlled manner. The samples under study may then be dropped into the fluid, their position along the column equilibrating according to the film density. The density profile of the column is calibrated using a set of plastic test samples of known density.

Density gradient column measurements were performed at ETH Zurich using an American Density Materials system.

3.9 Device fabrication

Here, we outline a typical fabrication procedure for a device consisting of an organic layer sandwiched between two electrical contacts, in the form used for the majority of the device measurements in this thesis (including time-of-flight, space-charge-limited current and OPV, but not field-effect transistor measurements). Where the fabrication steps differ significantly for different methods, it is indicated below, and the reader is referred to the individual Chapters for further details.

3.9.1 Device fabrication at Imperial College

For devices made at Imperial College, the starting point is a 12 mm $\times$ 12 mm square glass substrate patterned with an 8 mm $\times$ 12 mm stripe of indium-tin oxide (ITO). The bottom electrode comprised either the bare ITO, or the ITO covered with some other material chosen to better inject or block carriers according to the requirements. On top of the bottom electrode, the active layer was formed, usually by spin-coating, or otherwise by drop-casting or wire bar-coating from solution. After that, the top electrode was deposited by thermal evaporation of either aluminium or gold. The thermally evaporated top electrode was deposited through a shadow mask in order to define six separate pixels each of area 0.045 cm^2.

All fabrication steps prior to thermal deposition of the top contacts, unless otherwise stated, were carried out in ambient conditions in a cleanroom. The thermal deposition, as described, was performed under vacuum.

1. Cleaning ITO substrates
   (a) Rinse in acetone to remove photoresist
   (b) Ultrasonic bath in detergent (Hellmanex II, 2 wt% in de-mineralised water, 10 mins)
   (c) Ultrasonic bath in acetone (10 mins)
   (d) Ultrasonic bath in isopropanol (10 mins)
   (e) Dry in covered petri dish on hotplate
   (f) Immediately before the next step, treat with UV ozone in plasma asher (100W, 3 mins)
2. Completion of bottom electrode
   (a) EITHER leave bare ITO
   (b) OR deposit PEDOT:PSS
      i. Spin-coat PEDOT:PSS layer to thickness of 40–60 nm
      ii. Immediately before deposition of the active layer, heat PEDOT:PSS layer at 150°C for 15 mins
3. Deposition of active layer
   (a) Prepare solutions by dissolving the as-received materials in an organic solvent, typically toluene, chlorobenzene or chloroform
   (b) Stir solutions and heat below the boiling point of the solvent until thoroughly dissolved (typically 30 mins – 2 hours for OPV and space-charge-limited devices, and more than 4 hours for more concentrated solutions for time-of-flight devices)
   (c) Deposit active layer on the bottom electrode by spin-coating, drop-casting or wire bar-coating
4. Deposition of top contact
   (a) Load samples into vacuum system and wait until pressure is below 6×10^{-6} mbar
   (b) Thermally evaporate top layer
      - EITHER thermally evaporate aluminium at a rate 0.1–1 nm/s to thickness 60–100 nm
      - OR thermally evaporate gold at a rate 0.01–0.1 nm/s to a thickness of 40–100 nm

Before testing, a contact to the ITO bottom electrode must be made. This is achieved by wiping or scratching off the other layers at one side of the device, and applying silver paint. Silver paint is also added to the area of each pixel not overlapping with the ITO stripe. These steps allow good electrical contact to the pins in the sample chamber.

3.9.2 Device fabrication at Sumitomo Chemical Co.

For devices made at Sumitomo Chemical Co. Ltd, the starting point was a 20 mm × 50 mm glass substrate patterned with ITO as shown. The bottom electrode comprised either the bare ITO, or the ITO covered with some other material chosen to better inject or block carriers according to the device. On top of the bottom electrode, the active layer was formed by spin-coating from solution. After that, the top electrode was deposited. In certain cases this comprised of a further solution processed layer, but in all cases was completed by thermal evaporation of one or more layers, with the top layer being a relatively air-stable metal. The thermally evaporated top electrode was deposited through a shadow mask in order to define four separate pixels each of area 0.04 cm^2.

All fabrication steps up to the thermal deposition of contacts, unless otherwise stated, were carried out in ambient conditions in a cleanroom, which also contained the thermal deposition system. The thermal deposition, as described, was performed under vacuum. The thermal deposition system incorporated a glovebox for encapsulation, such that devices could be encapsulated without exposure to the atmosphere after deposition of the contacts.

1. Cleaning ITO substrates
    (a) ITO substrates pre-cleaned in ultrasonic bath with acetone and IPA and kept in nitrogen
    (b) Immediately before the next step, treat with UV ozone in plasma asher (100 W, 20 mins)
2. Completion of bottom electrode
    (a) EITHER leave bare ITO
    (b) OR deposit PEDOT:PSS
        i. Spin-coat PEDOT:PSS layer to thickness of 40–60 nm
        ii. Immediately before deposition of the active layer, heat PEDOT:PSS layer at 200°C for 10 mins

(c) OR deposit dense TiO_x layer

i. Spin-coat layer from 0.37 wt% solution of Ti-isopropoxide in ethanol to thickness of 30–100 nm

ii. Heat at 200°C for 10 mins

3. Deposition of active layer

(a) Prepare solutions by dissolving the as-received materials in an organic solvent, typically toluene, chlorobenzene or chloroform

(b) Stir solutions and heat below the boiling point of the solvent until thoroughly dissolved (typically 30 mins – 2 hours)

(c) Deposit active layer on the bottom electrode by spin-coating

4. Deposition of top contact

(a) EITHER deposit a layer of dense TiO_x

i. Spin-coat layer from 0.37 wt% solution of Ti-isopropoxide in ethanol to thickness of 30–100 nm

ii. NO heating step for top TiO_x layer

(b) OR add no further solution-processed layers

(c) Load samples into vacuum system and wait until pressure is below 5×10^{-7} mbar

(d) Thermally evaporate one or more layers

- LiF evaporated at a rate of 0.01 nm/s to a thickness of 0.3 nm
- NaF evaporated at a rate of 0.01 nm/s to a thickness of 0.3 nm
- Ca evaporated at a rate of 0.1-0.5 nm/s to a thickness of 30 nm
- Al evaporated at a rate of 0.1-0.5 nm/s to a thickness of 60 nm
- Au evaporated at a rate of 0.01-0.1 nm/s to a thickness of 60 nm

5. Encapsulation

(a) Transfer to nitrogen-filled encapsulation glovebox

(b) Seal with cover-glass using UV-fixing epoxy

Chapter 4

On the influence on charge transport of conformational and structural defects and disorder in a family of polyfluorenes

4.1 Summary

We investigate hole transport in a family of polyfluorenes, namely poly(9,9-dioctylfluorene) (PFO), poly(9,9-dioctylfluorene-co-9,9-dihexylfluorene) (F8:F6) and poly(9,9-dioctylfluorene-co-9,9-di(2-methyl)butylfluorene) (F8:F4/1). By controlling the formation of distinct material phases in films by processing and by virtue of their chemical design, and by fingerprinting the phases using spectroscopic, thermal and structural techniques, we are able to examine the effect of particular material phases on time-of-flight and field-effect transistor mobility. Remarkably, we are able to isolate the effect of the single chain conformation of PFO known as the beta-phase. We show that when embedded in a glassy PFO matrix it acts as a hole trap, reducing the mobility of the bulk material by over two orders of magnitude. By fabricating a device with negligible beta-phase, we demonstrate the highest time-of-flight mobility in PFO to date at over 3×10^{-2} cm^2/Vs at room temperature. Furthermore, we observe this in a glassy film with no indication of crystalline or liquid crystalline order. This study provides the first clear and unambiguous example of the effect on transport of a distinct conformational defect in a conjugated polymer. This also explains the mechanism behind

the original observation by Yap et al. of greatly enhanced mobility in F8:F4/1 [16], in which the beta-phase is unable to form. We also study the effect of crystallinity on mobility, and find that samples into which crystallinity has been introduced by thermal annealing exhibit mobilities of approximately 10^{-3} cm^2/Vs, one order of magnitude lower than glassy samples, but approximately one order of magnitude higher than any sample containing the beta-phase.

While the beta-phase conformation is not a general property of conjugated polymers, we suggest that our findings may generalise to other systems in the sense that the charge transport properties may be limited by a minority population of structural traps. Such traps may include highly ordered, crystalline regions as well as beta-phase-like conformational defects. In those cases, as in this study, significant mobility improvements may be more easily achieved by removing the minority phases within the samples than by increasing their concentration. In other words, an increase in the minority fraction of crystalline or conformational order may, within certain systems, have the effect of reducing the bulk mobility. We believe that the approach of removing minority phases – even if they are highly ordered – offers an alternative paradigm by which higher mobilities may be obtained in general, and in particular in systems where crystallinity is undesirable. Such systems include, for example, those requiring high luminescence quantum efficiency or mechanical flexibility.

4.2 Scope of this Chapter

The research presented here is intended to provide insight into the mechanism of the enhanced charge carrier mobility observed in the polyfluorene copolymer F8:F4/1 relative to PFO by Yap et al. [16]. The high mobility in F8:F4/1 was achieved, remarkably, in a glassy film with the efficient luminescence properties typical of the family of polyfluorenes based on PFO. It is hoped that finding the mechanism responsible for the enhanced mobility in F8:F4/1 will allow us to derive a more complete picture of the factors determining mobility in the polyfluorene family. An understanding of the factors determining mobility in the polyfluorenes is of great interest for researchers pursuing higher mobilities in conjugated polymers in general, and in systems where crystallinity is undesirable and where efficient luminescence is highly desirable in particular. Indeed, it is hoped that our work will provide inspiration towards an alternative paradigm within which to design high mobility materials for applications such as polymer lasing, light-emitting transistors and light-emitting diodes for optical communications.

The chemical structures of the materials studied here are shown in Figure 4.1. We study two F8:F4/1 copolymers of the same chemical structure as in the study of Yap et al., but both of the alternating variety, with molecular weights of approximately M_w=50k and 300k respectively. Yap's F8:F4/1 polymers had molecular weights of approximately M_w=400k. The F8:F4/1 polymers studied here were initially chosen both to reproduce the findings of Yap et al., and to study the effect of molecular weight. We also study a new polymer, F8:F6, an alternating copolymer with alternate units containing a pair of linear hexyl side-chains. F8:F6 was chosen to examine the effect of shorter side-chains than the octyl side-chain in PFO (but still linear), and in some sense represents an 'intermediate' case. It is of interest whether this polymer demonstrates an enhanced mobility relative to PFO. Finally, we study PFO.

As discussed below in Section 4.3.1, the polyfluorene family has shown a wide range of charge transport properties depending on processing route and side-chain structure. First, in Section 4.4, we compare the transport, spectroscopic and microstructural properties of the three materials when spin-coated at room temperature. We consider both FET and ToF mobilities, at low and high carrier densities respectively, in order to probe the effect of charge trapping species. We perform DSC, cross-polarised light microscopy, X-ray diffraction, transmission and photoluminescence measure-

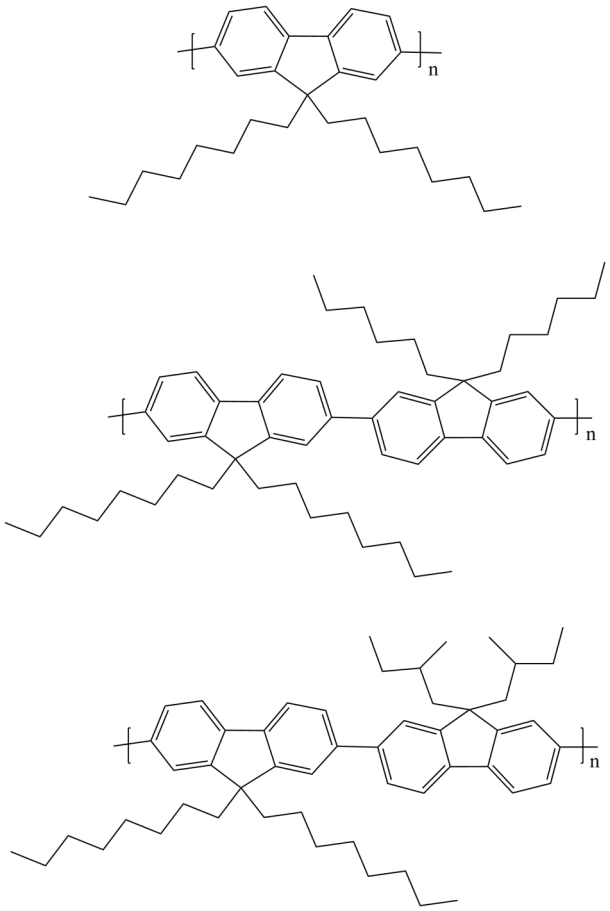

Figure 4.1: Chemical structures of the materials studied in this Chapter. Top: poly(9,9-dioctylfluorene) (PFO). Centre: poly(9,9-dioctylfluorene-co-9,9-dihexylfluorene (F8:F6). Bottom: poly(9,9-dioctylfluorene-co-9,9-di(2-methyl)butylfluorene) (F8:F4/1).

ments to obtain the baseline properties of the three materials and compare their phase behaviour. In particular, we probe the tendency of the materials to crystallise and to form the beta-phase.

In Section 4.5, we go on to use this information to control the microstructure of films of the three materials. By careful control over processing parameters, we are able to obtain films of PFO and F8:F6 with ToF hole mobilities as high as that of F8:F4/1, above 10^{-2} cm^2/Vs. We identify each of these films as having a glassy microstructure, both glassy liquid crystalline and – most surprisingly – glassy isotropic. In Section 4.6, we study the high mobility glassy isotropic PFO film in greater detail. We are able to show, using a combination of variable angle spectroscopic ellipsometry, transmission, photoluminescence and microscopy measurements, that the high mobility is possible due to the absence of the beta-phase conformation and a very low crystalline fraction. By re-introducing the beta-phase alone, we are able to show that the beta-phase acts to reduce the ToF hole mobility by two orders of magnitude to around 10^{-4} cm^2/Vs. We show that the beta-phase has the same

effect on high mobility liquid crystalline PFO films, reducing the mobility from 10^{-2} cm^2/Vs to 10^{-4} cm^2/Vs. To our knowledge, this is the first time that the charge trapping effect of a single conformational defect has been elucidated. We describe quantum chemical modelling and Monte Carlo transport simulations done in this group to rationalise the mobility decrease as a result of the formation of extended planarised segments within the polyfluorene chain.

In Section 4.7, we build a more complete picture of charge transport in the polyfluorene family by studying the effect of crystallinity and beta-phase in isolation and covering the accessible phase space. We show that the ToF hole mobility of polyfluorene films generally lies in one of three regimes: approximately 10^{-4} cm^2/Vs when the film contains a non-negligible fraction of beta-phase; approximately 10^{-3} cm^2/Vs when the film contains negligible beta-phase but significant crystallinity; and above 10^{-2} cm^2/Vs when the film contains negligible beta-phase and negligible crystallinity. Using these findings, we remark on the important mechanisms governing charge transport in the polyfluorene family, and how the findings may be generalised to inform material synthesis and device fabrication in other materials systems.

The experimental data in this Chapter was collected by me alone, with several exceptions as follows. Field effect transistors were made and characterised with the help of Jeremy Smith. Some of the optical and emission data was collected in collaboration with Alex Perevedentsev. The differential scanning calorimetry, X-ray diffraction and density gradient column data were collected in collaboration with the groups of Natalie Stingelin in the Department of Materials at Imperial College and Paul Smith at ETH Zurich, with the help of Ester Buchaca-Domingo and Felix Koch in particular. VASE data was collected by Mariano Campoy-Quiles. The modelling work was done predominantly by Jarvist Frost, Florian Steiner and Jenny Nelson.

4.3 Background

4.3.1 Polyfluorenes offer a case study in novel routes to achieving high mobility

Polyfluorenes and oligofluorenes have been extensively studied as a result of their great diversity of properties of interest both fundamentally and technologically, as blue emitters [115, 116, 117]. Their charge transport properties are no exception: polyfluorenes (and oligofluorenes) have been studied as model systems for developing an understanding of the relationship between chemical

design, microstructure and carrier mobility.

It is clear that the rich phase behaviour of PFO, including isotropic and liquid crystalline glasses, the beta-phase conformation and crystalline phases, has been an important driver of the interest in the materials as a model system. The critical dependence of charge transport in conjugated organic materials on the morphology – the conformational, packing and phase behaviour of the material – has long been recognised. As discussed in the Background chapter, it is well-founded that the high level of disorder present in conjugated organic materials is an important contributing factor to their inferior charge transport properties relative to the best of their inorganic counterparts [35, 21, 67, 118, 14]. Typical sources of disorder in organic systems include conformational freedom, disorder in packing and the occurrence of chemical and physical defects, impurities and end groups [9, 11, 12].

Efforts to improve charge transport in conjugated polymers have therefore focused on reducing disorder by controlling conformation, packing and the formation of defects and impurities. One common strategy has been to design and synthesise polymers with increased planarity within the chain, and hence increased conjugation length. It is expected that this may increase both intra-chain transport (a direct result of increased conjugation) [59, 60, 61, 62] and inter-chain transport (by reducing steric hindrance to allow closer interactions between neighbouring chains) [36]. Polyfluorenes are one example of this strategy. They offer a higher degree of planarity than the earliest conjugated polymers studied for their optoelectronic properties, which were based on polyphenylenevinylene (PPV) [119, 120]. Indeed, the first measurement of hole mobility in PFO was the highest demonstrated in a conjugated polymer at that time [53]. Polymers such as the indenofluorenes and ladder-type polyphenylenes exhibit a planarity enforced by the bridging of larger numbers of benzene rings, which may extend across the whole molecule [121, 60, 122, 35, 123, 36]. Hertel et al. demonstrated a mobility of 8×10^{-4} cm^2/Vs in the ladder polymer MeLPPP, a value slightly higher than that of the (non-ladder-type) PPV polymers, and that of PFO as in [53].

However, the mobility achieved in these and other materials has varied widely and often improved incrementally over time (with improved synthesis, varying molecular weight and different processing), such that the mobility trend between the above classes of polymers is not a uniform one as it first appeared [54, 14, 16]. Further, the performance of such materials in bulk films has, in fact,

fallen well short of the hoped-for level, and mobilities in films of these materials remain orders of magnitude below those measured in transient microwave conductivity (TRMC) measurements in solution [45, 72, 52, 58, 124, 57] (which do follow a more uniform trend with chain planarity, as shown in Table 2.1). It has become clear that the shortfall between expected and achieved mobility is, in many cases, due to the fact that the mobility is limited not by the intrinsic on-chain mobility or by the fastest inter-chain hops, but by the presence of trapping species (either intrinsic or extrinsic). However, it has proven difficult to demonstrate the influence on transport properties of such species in isolation, due to the large number of potential contributing factors and the challenge of distinguishing them spectroscopically.

Other strategies towards increasing mobility have focused on improving the packing of an assembly of chains, without the need for the intrinsic planarity in the chain. A classic example is that of the polythiophenes, such as P3HT, as outlined in Section 2.1.8. Despite the large torsional freedom of P3HT [45], careful control of the regularity of the pendant alkyl groups can lead to highly effective self-organisation with strong intermolecular interactions [46, 38]. This strategy amounts to promoting either long-range crystalline or long-range liquid crystalline order, and has proven a successful strategy in polymers systems based on thiophenes and bi-thiophenes [46, 38, 68, 69], thiophene-thiazolothiazoles [70] and cyclopentadithiophene-benzothiadiazoles [2, 3], for example. Bulk mobilities in the field-effect transistor configuration, in semi-crystalline or liquid crystalline polymer films, have risen from 0.1 cm^2/Vs to over 5 cm^2/Vs in the last decade. It may thus be concluded that up to now controlling packing has been more effective than controlling intra-chain structure in the pursuit for high mobility.

However, such high mobilities have remained out of reach for applications such as polymer lasing [16], due to the simultaneous requirement of efficient luminescence. Increased intermolecular interaction and overlap of neighbouring π–orbital systems tends to promote the quenching of luminescence. The mobility in isotropic polymer films, with more separated polymer chains, has until recently been limited to around 10^{-3}–10^{-4} cm^2/Vs [53, 63, 125]. As a result, there have recently been efforts to develop alternative paradigms for increasing the carrier mobility above this limit. To this end, researchers at Imperial College have demonstrated two poly(9,9-dialkylfluorene) copolymers of statistical and alternating type, here both referred to as F8:F4/1 [16]. Synthesised at Sumitomo Chemical Co., these copolymers have the same backbone as PFO, but with some fraction of the

octyl side-chain pairs replaced with pairs of shorter, branched methyl-butyl side-chains. The group was able to demonstrate a greatly enhanced mobility as compared with PFO – over 10^{-2} cm^2/Vs by ToF – in glassy films, whilst preserving the excellent luminescence properties characteristic of the polyfluorenes. This was tentatively attributed to the effect of changes in the side-chain structure in facilitating inter-chain charge transfer, but this was not proven. Hence, the polyfluorenes present an exciting subject for the study of novel routes to achieving high mobility in conjugated polymers. This is the context in which the current study was undertaken.

4.3.2 Properties of the beta-phase in polyfluorene

PFO belongs to the 'hairy rod' class of polymers, with a semi-rigid backbone and a reasonably dense set of side-chains arranged around it. It is semi-crystalline, and up to now two similar but distinct crystalline phases have been elucidated, usually labelled α and α' [126, 117]. It has a melting temperature above around 160°C, above which it exhibits a glassy nematic liquid crystalline phase, often labelled N, up to around 300°C where the melt becomes isotropic [127]. On spin-coating, some mixture of these phases is typically formed as a result of the 'freezing-in' of thermodynamically less stable phases. The majority of the volume of a spin-coated film is usually in the form of a glassy matrix, either nematic or isotropic, and the crystalline forms may be introduced by thermal annealing. Spin-coated films have also been shown to contain a further phase, invariably termed the β-phase (beta-phase). Since the beta-phase is key to this chapter, it is outlined in some detail here.

Grell and co-workers demonstrated that, through various processing routes, samples of PFO can be made to exhibit high degrees of intra-chain order [128, 129]. The distinct conformation now termed the beta-phase has been identified as a segment of extended conjugation within a single polymer chain [128, 129, 130, 131, 132, 133, 134]. Several studies have shown that the structure can be induced by processes leading to stress within the polymer film, such as swelling of the polymer in the vapour of a good solvent, such as toluene [129, 135, 136, 132, 133, 134], slow cooling and heating routines [129], preparation using a poor solvent [128, 124] and use of solvent mixtures [137]. Through X-ray measurements, the beta-phase was elucidated as a 'planar zigzag', or 2_1 helical structure [129]. The key element to the structure of the beta-phase is the planarity of the monomeric units, with close to zero torsional displacement of adjacent units across the beta-phase segment, as illustrated in Figure 4.2. Da Como et al. have studied the process of beta-phase formation on

exposure to toluene vapour [134], monitoring the polarisation anisotropy of the fluorescence. The group found that the formation of beta-phase was strongly correlated to the initial shape of the polymer chain, with the planar structure of the beta-phase (with zero torsional displacement across monomer units) more likely to occur in already extended (that is, co-linear) chains. They found that the process of inducing the planar beta-phase structure by exposure to toluene, however, did not have the effect of inducing chain extension. That is, 'bent' chains in which the beta-phase was formed remained 'bent'. It was found that even in 'bent' chains the conjugation was not disrupted. This finding suggests that although the beta-phase is preferentially formed in extended (co-linear) polymer chains, the process of formation of the beta-phase does not involve a rearrangement of the chain other than the re-ordering of monomeric torsional angles in a single chain. This highlights the distinct nature of the beta-phase from the crystalline phases of PFO, the formation of which involves a rearrangement of multiple polymer chains into a crystal structure.

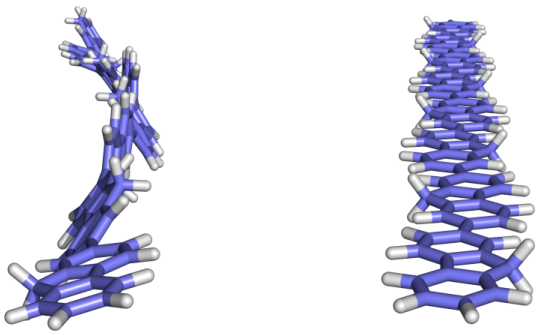

Figure 4.2: Illustration of the beta-phase structure in fluorene octamers (side-chains not shown for clarity). Shown are fully glassy phase (left) and fully beta-phase (right) fluorene octamers. We note that although the beta-phase segment shown here is co-linear, the key characteristic of the beta-phase, as described below and in [134], is thought to be the near-zero torsional angle between adjacent units rather than the co-linearity of the units. Figure courtesy of Jarvist M. Frost.

The beta-phase is not common to all polyfluorene materials, and indeed has been found only in a small subset of the family. Bright et al. have studied a series of poly(9,9-dialkylfluorenes), with linear alkyl side-chains varying in length from 6 to 10 carbon atoms [138]. They were only able – via thermal cycling – to observe the beta-phase in the polyfluorenes with alkyl side-chains containing 7, 8 and 9 carbon atoms. The beta-phase was induced most strongly with side-chains of length 8, that is, PFO itself. The result is in excellent agreement with an earlier molecular modelling simulation suggesting that the beta-phase conformer was unstable for alkyl side-chains composed of six or fewer carbon atoms [139]. It was suggested that the beta-phase is particular to a small

subset of polyfluorenes due to the requirement of a close balance between the factors determining the likelihood of dimerisation of the polymer backbones, those being the steric hindrance of the alkyl chains (longer chains mean more disorder and make dimerisation less likely) and the van der Waals forces available to stabilise planarization of the backbones (longer chains mean more stabilisation).

Tsoi et al. have studied the beta-phase in oligomers of 9,9-dioctylfluorene, in order to identify a minimum length of stability for the conformation [140]. The group were able to produce the beta-phase in a fluorene pentamer (five units), but it was necessary to disperse the pentamer in a PMMA matrix to do so, and attempts to produce beta-phase by exposing a pure film of the pentamer to toluene vapour were unsuccessful. Neither method was able to produce the beta-phase in a trimer (three units), suggesting that either four or five 9,9-dioctylfluorene units is the minimum required to stabilise the structure.

It is important to note that in bulk samples, even in thin films where the beta-phase has been very strongly induced, the beta-phase is always found as a minority phase intimately embedded within a surrounding glassy matrix. Phases are typically mixed even within one polymer chain [134]. In one recent study outlining a highly effective method to induce beta-phase [137], the beta-phase was found to amount to less than 45% of the film's volume. In all other studies where the fraction of beta-phase was quantified, that fraction was less than 25%, and without extensive processing specifically to induce the beta-phase it commonly amounts to less than a few percent of the volume [136, 141, 142, 140].

Samples containing the beta-phase have been shown to exhibit an interesting variety of photophysical properties [128, 129, 143, 136, 131, 144, 141, 142, 126, 132, 139, 145, 146]. A key property of the beta-phase is an extended charge conjugation length [129, 143, 141]. A number of experimental studies have found beta-phase segments to be energetically favourable for excitons as compared with the isotropic phase, with strong energy transfer occurring between the phases [143, 136, 131, 141], and there is experimental evidence of the same for polarons [143, 136, 124]. The formation of beta-phase segments within a bulk polymer film can be readily identified by a red-shifted and well-resolved photoluminescence spectrum and the appearance of a distinct absorption peak at approximately 430–437 nm [128, 129, 132, 137, 147]. It should be noted that the crystalline phases of PFO show a red-shifted absorption edge, but this extends continuously from the absorption edge

of the glassy film, where the absorption feature of the beta-phase is well-separated and fixed in wavelength [128, 132]. It has been shown that a small fraction of beta-phase within a bulk PFO film can dominate the emission behaviour [143, 136, 131, 141]. Ariu et al. estimated from emission spectra from samples rich in beta-phase (composing 13% of the bulk film) that >99% of excitons absorbed in the glassy matrix were transferred to beta-phase regions, in a time shorter than 5 ps [131]. In an earlier paper, a similar result was obtained with as little as 1–2% of the film in the beta-phase [136].

The charge transport behaviour of the polyfluorene family has received a significant amount of attention. We note that up to now, the great majority of transport measurements on PFO have used the ToF method, due to the high ionisation potential of 5.8 eV [148] and the resulting difficulties in achieving good hole injection, as required for methods such as field-effect transistor (FET) measurements, dark injection space-charge-limited current (SCLC) measurements and fitting to current-voltage curves. The first study to characterise charge transport in PFO, that of Redecker et al. [53], found a relatively high ToF hole mobility (for the time) of around 4×10^{-4} cm^2/Vs in a field of 5×10^5 V/cm, in a film spin-coated from toluene. Soon after this result was published, the same group discovered that the mobility of holes in PFO films could be enhanced by more than an order of magnitude by exploiting the liquid crystalline properties of the material to produce aligned polymer films on polyimide, quenched into a nematic liquid crystal glass [54]. The ToF mobility of holes in such films was found to be very high, at approximately 9×10^{-3} cm^2/Vs in a field of 4×10^4 V/cm. We note that a similar approach was taken by Chen et al. using fluorene oligomers, which could be aligned in the nematic phase very effectively to exhibit ToF mobilities (for both electrons and holes) above 10^{-2} cm^2/Vs. Kreouzis et al. [14] have examined the enhancement in hole mobility in PFO films by crystallization through thermal annealing at 120–140°C for 15 hours, leading to reduced energetic disorder within the Gaussian Disorder formalism and a maximum RT mobility of just over 10^{-3} cm^2/Vs.

Nicolai et al. were recently able to achieve sufficient hole injection into the HOMO of PFO, using a molybdenum trioxide layer, to be able to observe SCLC in a thin spin-coated film [56]. They were thus able to extract a mobility of just over 10^{-5} cm^2/Vs in a field of around 10^6 V/cm. The morphology of the spin-coated film was not elucidated.

The effect on charge transport of the beta-phase in particular, in contrast to its photophysical behaviour, has not received a great deal of attention. As one exception to this, the charge transport within segments of beta-phase has been considered by Prins et al. by the TRMC method [124]. In this experiment, all carriers moving within the sample – not only those which can be collected – contribute to the signal. The current from ns to ms timescale can be probed. By comparing the responses of a film of PFO rich in beta-phase and a film of a branched side-chain polyfluorene exhibiting no beta-phase, the group found evidence of higher charge mobility within beta-phase PFO regions than in isotropic PFO regions.

As described above, a recent paper by Yap et al. [16] presented two F8:F4/1 copolymers, which exhibited very high ToF hole mobilities above 10^{-2} cm^2/Vs. Further, the measurements were performed on glassy samples showing no evidence of crystallinity. No liquid crystallinity was reported. The intention was to promote a system with generally well-separated polymer chains containing a small number of preferential inter-chain charge transfer sites, to simultaneously inhibit photoluminescence quenching and yet allow efficient bulk charge transport. This mechanism of the mobility enhancement, however, was not proven. The results of the study of Yap et al. nonetheless demonstrated the potential for the polyfluorene family to achieve a hole mobility above 10^{-2} cm^2/Vs, even higher than that of the aligned nematic glass of Redecker, without complex or high-temperature processing routes.

4.4 A comparison of the transport, spectroscopic and morphological properties of spin-coated films of PFO, F8:F6 and F8:F4/1

4.4.1 Comparison of ToF and FET mobility in films spin-coated at RT

First, we outline the basic charge transport properties of PFO, F8:F6 and F8:F4/1. As described in Section 2.1.6, a comparison of ToF and FET mobility measurements is informative regarding the factors contributing to the particular transport properties of the material. The higher charge carrier concentration in FETs should lead to a lower sensitivity than in ToF to tail states in the DoS. Providing that the FET mobility is not limited by trapping near the dielectric interface or by insufficient charge injection, differences in the ToF and FET mobilities may be indicative of the presence of minority charge trapping species in the transporting material.

Figures 4.3 and 4.4 show the ToF and FET hole transport data of the three materials in films spin-coated from toluene at room temperature, with no further treatment. The ToF films were 5–10 μm thick, and the FET films around 100 nm thick. The ToF mobilities shown correspond to applied fields of approximately 10^5 V/cm. The FET mobilities shown are calculated in the saturation regime at gate voltages V_G of -50 V. The ToF data in Figure 4.3 shows clearly the wide variation in mobilities observed within the polyfluorene family. At a field of approximately 10^5 V/cm, it can be seen that the mobilities span over two orders of magnitude, from approximately 10^{-4} cm^2/Vs for PFO to above 10^{-2} cm^2/Vs for the higher molecular weight F8:F4/1 copolymer. The F8:F6 copolymer shows, at a field of approximately 10^5 V/cm, a mobility of approximately 10^{-3} cm^2/Vs. The FET measurements show a different behaviour. It can be seen that in thin films in the FET configuration, all three materials studied, including PFO itself, display a mobility of approximately 10^{-2} cm^2/Vs. Indeed, all three materials studied displayed approximately the same mobility within experimental error.

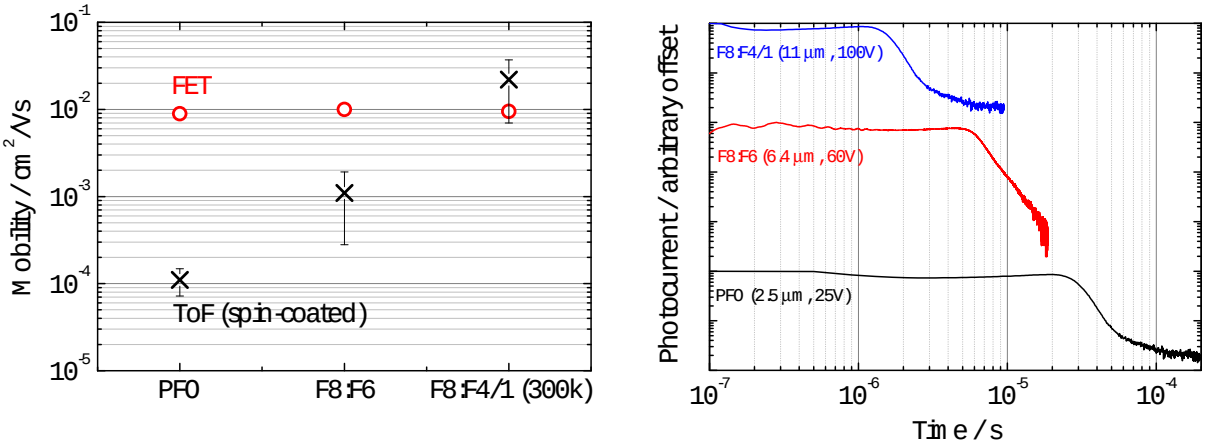

Figure 4.3: Left: comparison of the room temperature ToF and FET hole mobilities of PFO, F8:F6 and F8:F4/1. ToF mobilities are shown for applied fields of approximately 10^5 V/cm, and FET mobilities correspond to the saturation regime at a gate voltage V_G of -50 V. Right: ToF transients corresponding to the mobility values given on the left.

The ToF data for PFO and F8:F4/1 is consistent with previous publications [53, 14, 16]. Due to the difficulty in injecting holes into PFO there is, to our knowledge, only one previous publication detailing FET measurements on polyfluorenes [55]. We note that our FET mobility value for PFO is apparently not consistent with that previous study. The study found a maximum FET mobility in PFO of 6×10^{-3} cm^2/Vs in an aligned nematic sample, but the corresponding mobility in a mainly

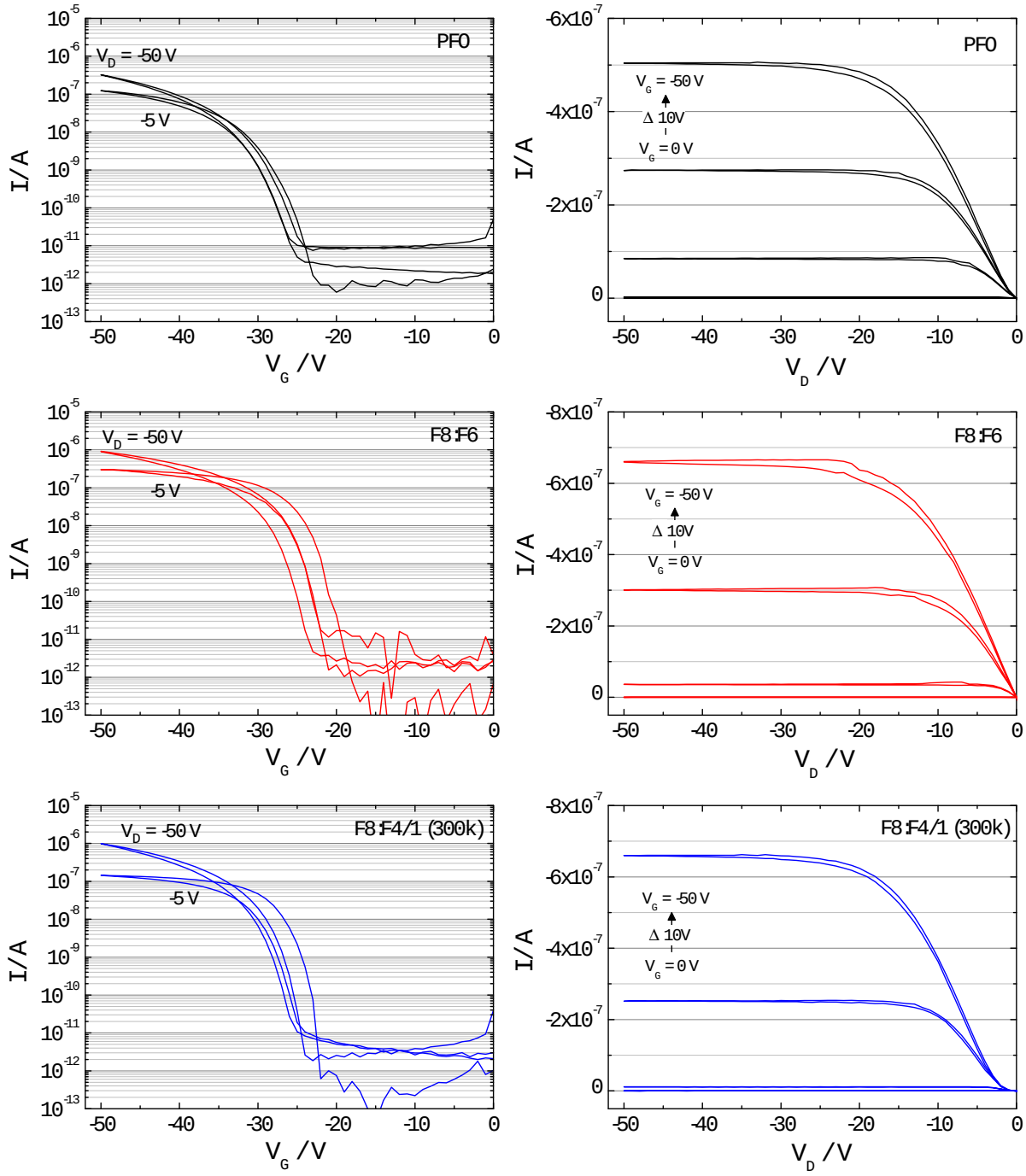

Figure 4.4: FET transfer (left) and output (right) curves for PFO (top), F8:F6 (middle) and F8:F4/1 (bottom). Transfer curves are shown for source-drain voltages V_D of -50 V and -5 V. Output curves are shown for gate voltages V_G between 0 V and -50 V at 10 V intervals. Channel lengths were 50μm for PFO and F8:F4/1, 40 μm for F8:F6. Channel widths were 1000 μm for PFO and F8:F4/1, 1500 μm for F8:F6. The F8:F4/1 data shown here corresponds to the M_w= 300k sample.

glassy isotropic sample (nominally in the same morphology as our spin-coated thin film) was much lower, at around 3.3×10^{-4} cm^2/Vs. The origin of this difference cannot be conclusively explained. It is possible that a difference in film morphology is responsible, in light of the data to be presented in this Chapter. It is also possible that the lower mobility found in glassy isotropic samples results

Material	σ / meV	Σ	μ_0 / cm^2/Vs	C / 10^{-4}(cm/V)$^{0.5}$
F8:F6	84(5)	2.4 (0.1)	0.028 (0.010)	2.8 (0.3)
F8:F4/1 (50k)	69 (2)	2.2 (0.2)	0.11 (0.04)	3.1 (0.1)
F8:F4/1 (300k)	65 (2)	1.9 (0.1)	0.24 (0.03)	3.1 (0.1)

Table 4.1: Parameters resulting from a GDM analysis of the temperature-dependent ToF data for F8:F6 and the M_w= 50k and M_w= 300k samples of F8:F4/1. For corresponding parameters for PFO, the reader is referred to the detailed study of Kreouzis et al. [14].

from small variations in the large injection barrier from the Au electrodes, which at 0.7–0.8 V is expected to be non-Ohmic, as suggested by the slightly non-linear output characteristics, and may lead to an underestimation of the mobility. Following Nicolai et al. [56], we have made use of molybdenum trioxide to fabricate FETs using molybdenum trioxide with improved output characteristics. We note that slightly non-linear output characteristics were still observed, to a lesser extent, in some, but not all, of our samples (see Figure 4.4). In any case, our measurements clearly demonstrate the potential for mobilities above 10^{-2} cm^2/Vs to be achieved in non-liquid crystalline, non-aligned samples in the FET configuration.

The observation of widely-varying ToF mobility values for these materials, in contrast to their very similar FET mobility values, implies the existence of a broader tail in the density of states in PFO and F8:F6 than in F8:F4/1. In other words, it may be that the difference in ToF mobility between the materials is related to the presence of trapping species rather than to some more 'intrinsic' material property. This finding suggests the possibility of observing as high a ToF mobility in PFO and F8:F6 as in F8:F4/1, if the population of trapping species can be sufficiently reduced.

We have also studied the temperature dependence of the ToF mobility of the copolymers F8:F6 and F8:F4/1, and analysed the results within the framework of the Gaussian Disorder Model. The data is summarised in Table 4.1. We can compare the disorder parameters σ extracted for the copolymers with typical values for PFO as found in the literature. Values of σ for unannealed films of PFO have been found as 82–95 meV [14, 149]. Yap et al. also performed GDM analysis on an alternating F8:F4/1 copolymer (M_w=400k), and found a value for σ of 57 meV. The values found here for F8:F4/1 are therefore roughly consistent, at 65 meV for the M_w=300k copolymer and 69 meV for the M_w=50k copolymer. This also hints at some molecular weight dependence of the disorder. The value found here for F8:F6 of 84 meV is towards the lower end of the range for PFO. The GDM

analysis is therefore in qualitative agreement with the hypothesis following the room temperature ToF and FET measurements that PFO films exhibit a broader DoS with a higher population of deep traps than F8:F4/1. F8:F6 films, on the basis of the small amount of data presented so far, appear in some way to represent an intermediate case.

In order to begin to identify the nature of the trapping species, it is first necessary to form a better picture of the properties of the materials, including their phase behaviour and the microstructure of the solid state films. The next section outlines these 'baseline' material properties.

4.4.2 Differential scanning calorimetry

Yap and co-workers, within the group at Imperial College, were the first to report a comparison of the transport properties of PFO and F8:F4/1 materials. The authors noted that all samples tested were in a glassy state, but did not characterise the morphology or phase behaviour. We have studied the phase behaviour of our series of polyfluorenes, firstly, by DSC. Figure 4.5 shows a summary of the results. The plots for PFO, F8:F6 and F8:F4/1, all taken with scan rates of 20°C/min on as-received samples, show striking differences. The DSC traces of PFO are consistent with previous measurements [127, 126, 132], showing an endotherm corresponding to the glass transition temperature T_g at around 50–60°C and an endotherm corresponding to the melting temperature T_m at around 160–170°C. The polymer can be seen to demonstrate a strong tendency to crystallise both on heating form the glassy form and on cooling from the nematic melt, leading to exotherms at around 120–125°C. As expected for a system with shorter side-chains and the concomitant increased interaction between neighbouring chains, T_g and T_m for F8:F6 are shifted to slightly higher temperatures, at 70–90°C and 170–190°C respectively. However, the behaviour of F8:F6, under the same conditions as PFO, has a more significant difference. While the polymer clearly crystallises on heating above T_g, it shows here little or no tendency to crystallise on cooling below T_m. It is presumed that this reduced tendency to crystallise is a result of the decreased translational symmetry of the system and the resulting increase in disorder. The behaviour of F8:F4/1 (shown here is the M_w=300k copolymer) is different again. The only clear transition observable is the glass transition at 100–110°C. The polymer shows little or no tendency to crystallise on either the heating or the cooling scan. We also note the absence of a clear transition to the nematic (or isotropic) melt, suggesting there is little change in the organisation of the material on melting. We note that the very low tendency towards crystallisation of the F8:F4/1 copolymer is

not particularly surprising. The branched side-chain means that there will be a number of isomers of the monomer, the steric influence of which will suppress the ordering of neighbouring chains.

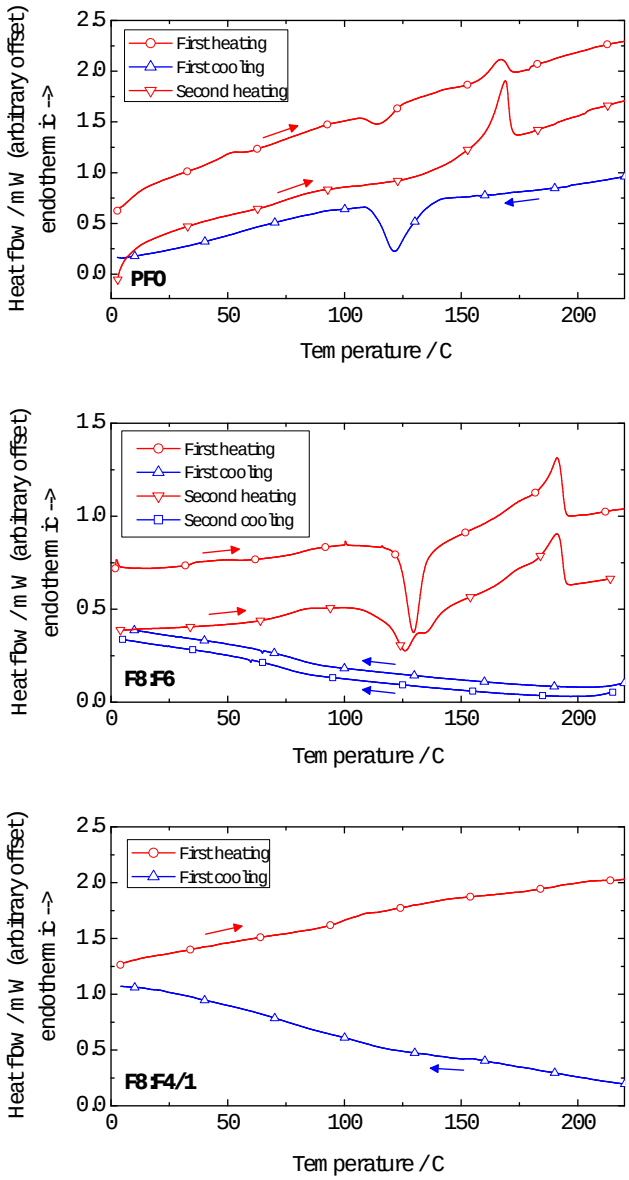

Figure 4.5: Differential scanning calorimetry plots for 'as-received' samples of PFO (top), F8:F6 (centre) and F8:F4/1 (M_w=300k) (bottom). The positive direction corresponds to endothermic heat transfer. The transitions are described in the text.

4.4.3 Microscopy under cross-polarised light

The phase behaviour and the relative tendency for the polymers to crystallise were also examined by microscopy under crossed polarised light. We present images taken with the analyser perpendicular to the polariser. In the absence of scattering no light passes to the viewer, and the image appears completely dark. If light is transmitted, it is attributed to scattering from some anisotropy, such

as a region of crystallinity or liquid crystallinity. Figure 4.6 shows images of representative regions of thick films (4–6 μm) of the three copolymers spin-coated from toluene at room temperature. Each of the images was taken with the same magnification and exposure time, with the same image processing performed on each, as described in the caption. The bar chart shows the mean camera signal intensity across each of the raw images, on a scale from 0 to 255. The image of the PFO film displays a highly heterogeneous microstructure with a high concentration of scattering centres on the scale of 100–1000 nm. A comparable concentration of scattering centres and heterogeneity is seen in the F8:F6 film. The camera intensity is even high than for the PFO film. By contrast, F8:F4/1 displays a much-reduced concentration of scattering centres and less heterogeneity, and the camera intensity is significantly reduced relative to PFO and F8:F6. It is proposed that the scattering centres are crystallites. Hence, the absence of light scattering from the F8:F4/1 sample suggests that the film is fully isotropic. This is in agreement with the DSC traces of F8:F4/1, which showed no evidence of crystallisation. Further, none of the samples studied here suggest the presence of liquid crystallinity, the domains of which have a characteristic appearance under cross-polarised light. It appears that the PFO and F8:F6 films consist of some fraction crystalline material within a glassy isotropic matrix, and the F8:F4/1 film consists almost entirely of glassy isotropic material.

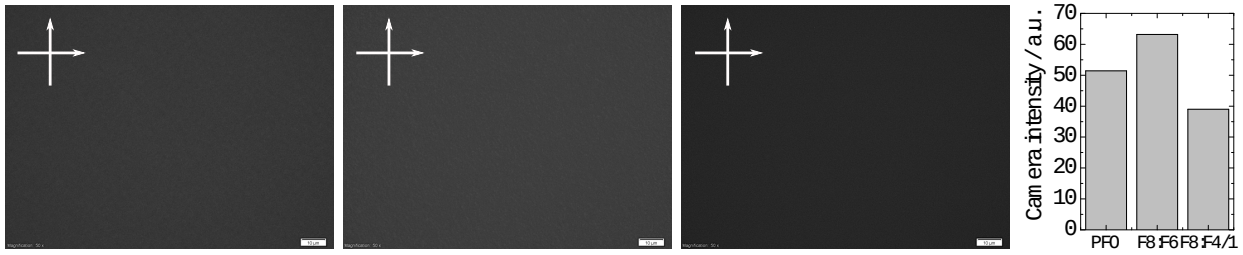

Figure 4.6: Cross-polarised light micrographs in transmission (50x magnification) and camera intensity for films of PFO (left), F8:F6 (centre) and F8:F4/1 (right) spin-coated at room temperature. All films are 4–6 μm in thickness. The scale bar is 10 μm. All cross-polarised light micrographs shown in this Chapter were taken with the same experimental parameters (exposure time 500 ms, gain 5 dB, fixed light intensity) using an Olympus microscope and have been subjected to identical image processing (uniform brightening and contrast enhancement) using Photoscape v6.3.2 graphics editing software. The camera intensity value is a mean intensity level across the raw image on a scale between 0 and 255, calculated using ImageJ software version 1.46.

4.4.4 X-ray diffraction

As a further probe of crystallinity, X-ray diffraction was performed on the same 4–6 μm thick films spin-coated from toluene at room temperature. Both in-plane and out-of-plane scattering orienta-

tions were studied (see Figure 3.2 for definitions). The diffraction micrographs are shown in Figure 4.7. The degree of scattering in all samples is fairly weak. We note that the in-plane signal is generally stronger than the out-of-plane signal due to the larger path length travelled by the beam. This path length, however, may vary between films due to small differences in the incidence angle, and so the signal intensity should not be regarded as a measure of intrinsic scattering strength. Further, the in-plane signal from the F8:F4/1 film was collected over a longer period than the other samples (see figure caption). The PFO film exhibits several fairly weak reflections. The two main peaks are likely to correspond to the length and width of the fluorene monomer with the chain in 'ribbon' form, as described by Grell et al. [129]. There appears to be one further reflection at an intermediate distance, and no other clear structure. The fact that so few reflections are visible – and that they correspond either to 'intra-chain' distances or nearest neighbour distances only – indicates that the ordering is rather weak and short-range. The F8:F6 film shows a very similar spectrum, with the peak positions the same within error. The F8:F4/1 film shows the same basic structure, with the peak positions slightly shifted towards larger separation distances, perhaps reflecting the disorder in packing due to the branched side-chains. We note that the F8:F4/1 film shows an additional clear radially-symmetric feature corresponding to a distance of around 0.2 nm. The source of this is unknown – perhaps an impurity in the film or introduced during measurement – but in any case the distance is far too short to correspond to some molecular packing distance, and hence we ignore it. One difference observable from the in-plane images, which show a higher signal intensity in the direction perpendicular to the film plane, is that the F8:F6 and F8:F4/1 have a slightly increased tendency to align parallel to the substrate plane (but with no preferred in-plane direction).

Summarising the structural data for the spin-coated F8:F4/1 films, the thermal properties show little tendency for the polymer to crystallise, cross-polarised light microscopy on the device films themselves show no indications of crystallinity or liquid crystallinity, and XRD studies on similar films show no evidence of order except for a slight tendency towards alignment in the plane of the substrate (which is also seen for F8:F6). All the data presented so far are consistent with films of spin-coated F8:F4/1 being in a glassy isotropic phase with a slight preference for in-plane alignment, but no strong structural ordering. The films of PFO and F8:F6 spin-coated at RT show some degree of crystallinity in cross-polarised light microscopy. The microscopy and XRD studies together suggest polycrystallinity with domains 100–1000 nm in size, and only short-range order on the nm scale.

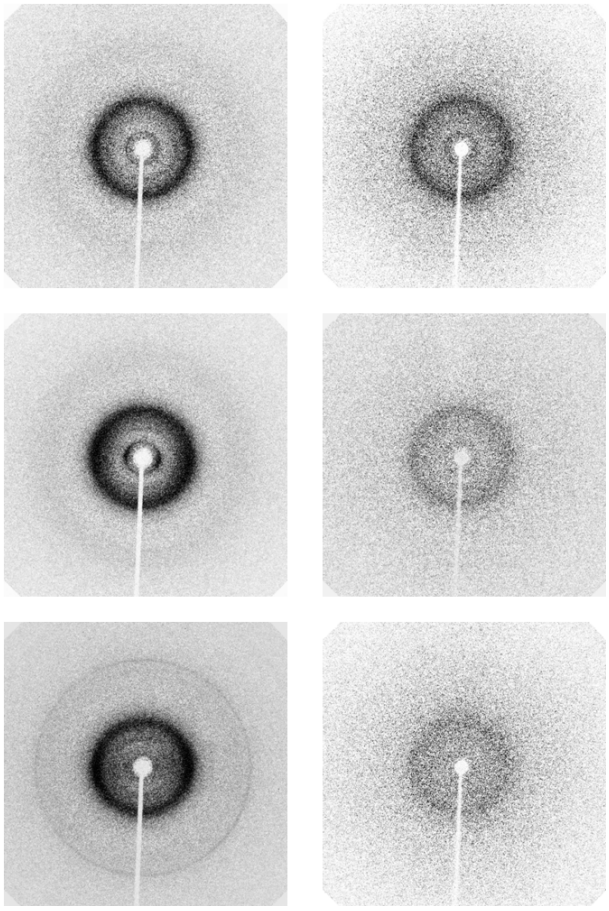

Figure 4.7: X-ray diffractograms of PFO (top), F8:F6 (centre) and F8:F4/1 (bottom) films spin-coated at room temperature, taken using an Oxford Diffraction Excalibur PX instrument using molybdenum K_α radiation. Images from both in-plane (left) and out-of-plane (right) configurations are shown (see Figure 3.2 for definitions). All diffractograms were collected with 1200s integration time except for that of in-plane F8:F4/1 which was collected with 3600s integration time.

4.4.5 Transmission and photoluminescence spectroscopy

In order to better identify the phases or species present in the films, we turn to spectroscopy. The photoluminescence and absorption spectroscopic characteristics of the polyfluorenes, in particular PFO, have been extensively studied [129, 131, 126, 132], and allow the isotropic, crystalline, liquid crystalline and beta-phases to be distinguished. We note that in almost all cases real samples are a mixture of phases. Therefore, the spectroscopic data should be interpreted with care. Absorption spectroscopy is fairly unambiguous, showing a roughly linear relationship between the concentration of the different component phases present and the absorbance (although different component phases may have different absorption coefficients). However, in photoluminescence an efficient energy transfer from glassy phase and crystalline phase to beta-phase means that even a small amount of beta-phase within a mixed film will dominate the emission. Ariu et al. have demonstrated near-complete energy transfer from the isotropic phase to the beta-phase with as little as 1–2% of the

volume of the film in beta-phase [136, 131].

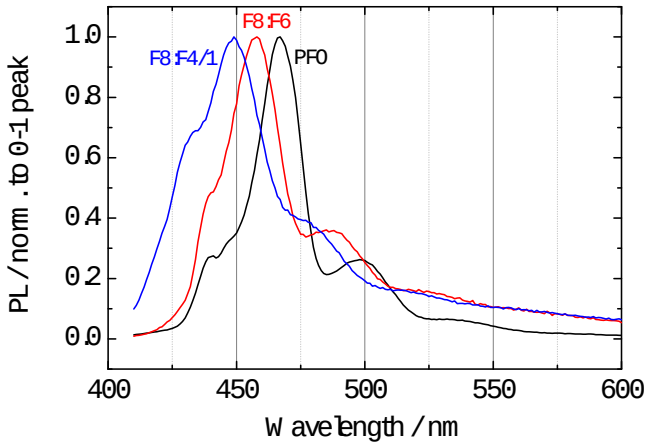

Figure 4.8: Emission spectra of thick (4–6 μm) films of PFO, F8:F6 and F8:F4/1 spin-coated at room temperature. As described in the text, the 0–1 peak positions indicate that while beta-phase dominates the emission from the PFO film, it is absent from the emission of F8:F6 and F8:F4/1.

Figure 4.8 shows the emission spectra of thick films of the materials. Thick films saturate the absorption measurement across most of the absorption range, so absorption measurements are not shown here. The emission spectra of thick films show a much-reduced intensity of the 0–0 peak relative to the 0–1 peak. This is a result of self-absorption in the film in the region below 450 nm, which is significant due to the large film thickness, and varies between films due to variations in the path length as well as in the absorption strength in that region dependent on the presence of the beta-phase and tail states. Hence, we concentrate on the position of the 0–1 peak seen here at 450–470 nm, where the absorption of the film is essentially zero. It can be seen that the 0–1 peak of the PFO film occurs at around 467 nm. This identifies the emission clearly as coming from the beta-phase [129, 131, 126, 132, 133, 138, 134, 140]. The emission spectrum of the F8:F6 material has not previously been characterised. The 0–1 peak of the F8:F6 film occurs at a wavelength of around 458 nm, significantly blue-shifted relative to the beta-phase 0–1 peak in PFO. A 0–1 peak wavelength of 458 nm has been observed to originate from one of the crystalline phases of PFO [126]. The indication of the presence of crystalline material in the F8:F6 film is consistent with the images under cross-polarised light. This also suggests the absence of beta-phase in the F8:F6 film, since (as occurs in PFO) energy transfer to the beta-phase from the crystalline phase would be expected if it were present. We therefore tentatively conclude that the beta-phase is absent in the F8:F6 film, and that emission is dominated instead by crystalline regions with a similar structure to

one of the PFO crystalline phases. The 0–1 peak of the F8:F4/1 film is at a still lower wavelength at around 449 nm. Emission at this wavelength is characteristic of the glassy phases of PFO, with glassy isotropic and glassy nematic liquid crystalline phases showing 0–1 peaks in the range 446–453 nm [129, 131, 126, 132]. We emphasise, however, that the cross polarised micrograph of the same F8:F4/1 film in Figure 4.6 suggests that the film is not in a liquid crystalline state. We conclude that the F8:F4/1 film is in a glassy isotropic state, with some degree of in-plane alignment as indicated by the XRD data, but no strong structural ordering. There is a clear absence of crystalline phases and of the beta-phase.

4.4.6 Absence of beta-phase conformation in F8:F6 and F8:F4/1

The above photoluminescence measurements show that while the emission from thick spin-coated films of PFO is dominated by the beta-phase, the emission from thick spin-coated films of F8:F6 and F8:F4/1 contains no contribution from the beta-phase. It is important to establish whether or not the beta-phase is a property of PFO alone, or whether it can be found in F8:F6 and F8:F4/1 after appropriate processing.

PFO, F8:F6 and F8:F4/1 have been studied here by Alex Perevedentsev for their propensity to form the beta-phase, or a similar species. Films of the polymers were processed in various ways known to induce the beta-phase in PFO, including processing from mixed solvents and exposing to toluene vapour [129, 135, 136, 132, 137]. The presence or absence of beta-phase was monitored using photoluminescence and transmission spectroscopy, looking for the characteristic red-shift in emission and, in particular, the distinct absorption feature as observed for PFO. While such processing was able to induce large fractions of beta-phase in the PFO films, no indications of beta-phase were found in films of F8:F6 or F8:F4/1.

4.5 Controlling microstructure through processing variations to enhance mobility in PFO and F8:F6

The previous section outlined the ‘baseline’ properties – the morphological, spectroscopic and basic charge transport properties – of PFO, F8:F6 and F8:F4/1. It was demonstrated that, spin-coating the films at room temperature, the three materials show approximately the same FET mobility, but

widely varying ToF mobilities. It was hypothesised that this is due to an increased concentration of trapping species in the low energy tail of the DoS in PFO and, to a lesser extent, F8:F6 relative to F8:F4/1, a suggestion supported by temperature-dependent mobility measurements. The highest time-of-flight mobility, over 10^{-2} cm^2/Vs at room temperature, was observed in the F8:F4/1 film. This film was seen to be highly uniform and glassy, with some degree of chain alignment but showing no evidence of monodomain liquid crystallinity, and with a very low concentration of crystalline material. In contrast, F8:F6 and PFO films showed a significant concentration of crystalline material and a higher degree of heterogeneity. The PFO film, showing the lowest ToF mobility, also demonstrated emission from the beta-phase. No evidence of beta-phase was observed in either F8:F6 or F8:F4/1. The presence of the various phases therefore appears to impact very strongly on the charge transport properties of the films. In this section, we explore two methods of processing found to increase the mobility in films of PFO and F8:F6.

4.5.1 High mobility nematic LC phase in PFO

The highest time-of-flight mobility measured in PFO in the literature is that in Redecker's aligned liquid crystalline phase film [54]. Using fluorene oligomers, Chen et al. have also been able to show very high time-of-flight mobility, for both holes and electrons, in aligned liquid crystalline samples [150, 151]. Determining the key property of the LC phase which allows the high mobility may offer insight into the mobility enhancement mechanism in F8:F4/1.

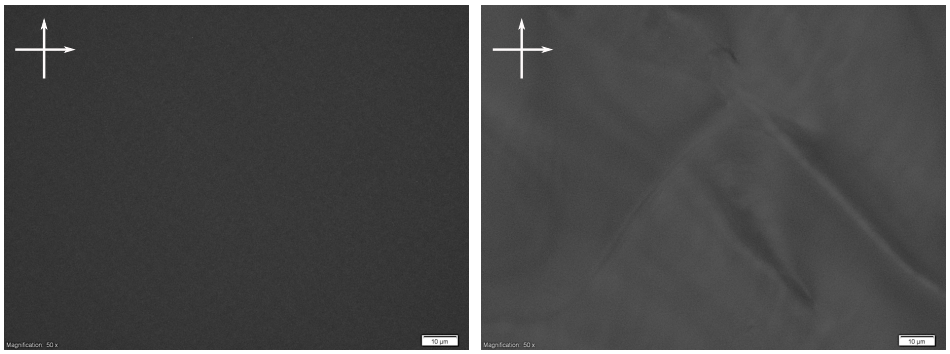

Figure 4.9: Cross-polarised light micrographs in transmission (50x magnification) of films of PFO spin-coated at room temperature (left) and quenched from the nematic melt (right). The scale bar is 10 μm. All cross-polarised light micrographs shown in this Chapter were taken with the same experimental parameters (exposure time 500 ms, gain 5 dB, fixed light intensity) using an Olympus microscope and have been subjected to identical image processing (uniform brightening and contrast enhancement) using Photoscape v6.3.2 graphics editing software.

We first fabricated an LC phase film of PFO by heating a spin-coated film above T$_m$ into the nematic

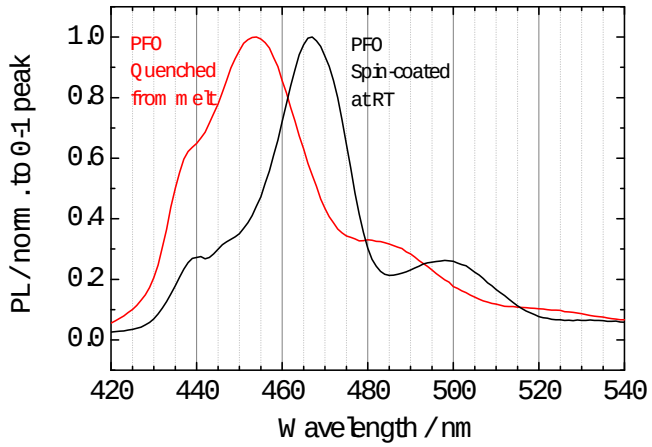

Figure 4.10: Emission spectra of thick films of PFO spin-coated at room temperature and quenched from the nematic melt.

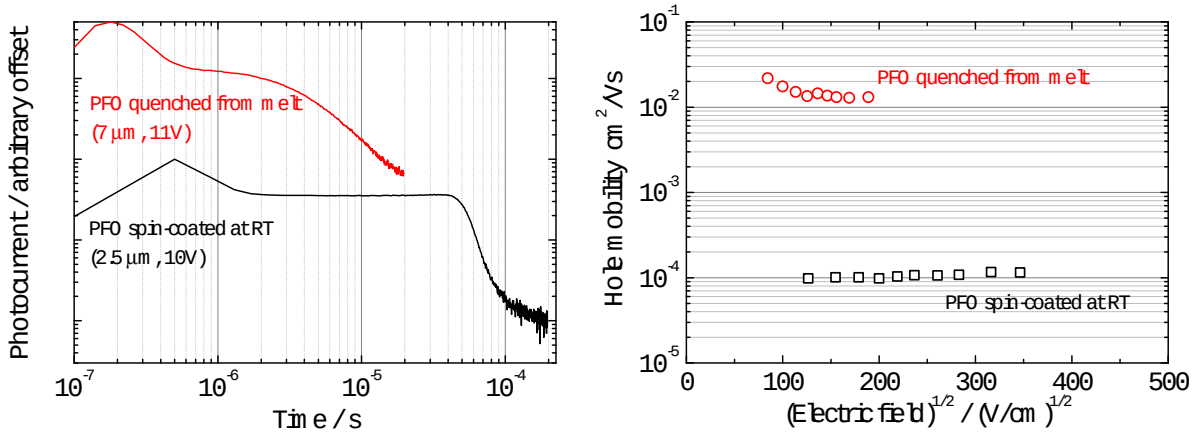

Figure 4.11: ToF transients (left) and mobility data (right) for PFO spin-coated at room temperature and quenched from the nematic melt.

melt, and quenching the film rapidly to room temperature on a metal surface. It is important to note that no further efforts were made to align the film in a particular direction, in contrast to the studies described above [54, 150, 151]. The appearance of the film under cross-polarised light in shown in Figure 4.12. The characteristic 'Schlieren' texture in the image shows regions of different brightness, corresponding to domains within which the polymer chains are aligned in a common direction. Different domains have a different alignment direction. The domains can be seen to be large, on the order of 10s μm, larger than the length scale over which transport occurs. The emission spectrum, shown in Figure 4.14 alongside the emission spectrum of a spin-coated film as in the previous section, shows a broad 0–1 peak at 453 nm, consistent with the nematic LC phase [129, 126, 132]. Figure 4.11 shows the ToF data from the LC phase film and a spin-coated film. It is worth noting that the optical appearance of the film is largely glassy, but with some degree of 'cloudiness' from scattering. This indicates that the quenching process may not have been fully complete, and that a

small degree of crystalline ordering has occurred. However, the cross-polarised light images and the emission spectrum confirm the predominance of the nematic LC phase within the film. Indeed, the mobility of the same LC phase film is over 10^{-2} cm^2/Vs, around two orders of magnitude higher than the spin-coated film. The mobility of the LC phase film is as high as, and even slightly higher than, that of Redecker's aligned LC sample. The domains of various alignment direction could not be probed individually for their transport properties. However, it appears that the most important feature of the LC phase film is the formation of a uniform, near-monodomain phase (relative to the transport distance). A single domain contains no grain boundaries or heterogeneities, which would be expected to act as trapping centres. The enhanced mobility in LC phase samples hints at the importance of removing phase heterogeneity for bulk charge transport.

4.5.2 High mobility nematic LC phase in F8:F6

At this point, it is of interest to examine the corresponding LC phase of F8:F6, and whether we can enhance the mobility in the same way as for PFO. Further, the thermal properties of F8:F6, as shown in Figure 4.5, show that F8:F6 has a much-reduced tendency to crystallise on cooling through T_m as compared with PFO. It may be expected that this allows a more homogeneous LC phase than in the case of LC PFO, and whether this may lead to a higher mobility. Figure 4.12 shows a cross-polarised light micrograph for an LC phase sample of F8:F6, fabricated by heating a spin-coated sample above T_m and cooling rapidly to room temperature on a metal surface. It is seen that an LC phase with domains of the order 10 μm is formed. It is notable that in the case of F8:F6, the optical appearance of the film is highly glassy, indicating that the quenching of the nematic melt was near-complete, and a lower degree of crystalline ordering was formed compared with the LC PFO case. This is consistent with the reduced tendency of F8:F6 to crystallise on cooling as seen in the DSC data. Figure 4.13 shows the in-plane and out-of-plane XRD data of the sample. The in-plane XRD data for LC F8:F6 shows, like for F8:F6 spin-coated at RT, an increased signal intensity in the direction perpendicular to the film plane. However, this effect is stronger in the LC phase film than in the spin-coated film, indicating a stronger alignment in the substrate plane in the case of LC phase. The out-of-plane image shows that, like for the spin-coated film, there is no preferred alignment direction within the plane of the substrate. The emission spectrum is also shown alongside that from a spin-coated sample, which again shows a 0–1 peak at 453 nm, at almost exactly the same position as the 0–1 peak of the PFO LC phase.

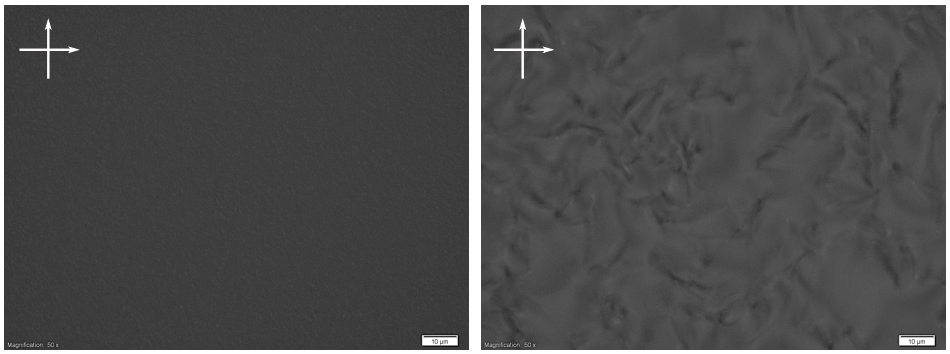

Figure 4.12: Cross-polarised light micrographs in transmission (50x magnification) of films of F8:F6 spin-coated at room temperature (left) and quenched from the nematic melt (right). The scale bar is 10 μm. All cross-polarised light micrographs shown in this Chapter were taken with the same experimental parameters (exposure time 500 ms, gain 5 dB, fixed light intensity) using an Olympus microscope and have been subjected to identical image processing (uniform brightening and contrast enhancement) using Photoscape v6.3.2 graphics editing software.

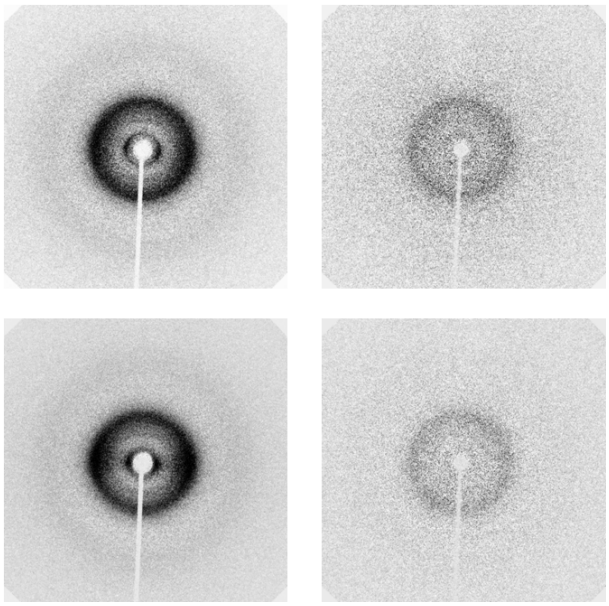

Figure 4.13: X-ray diffractograms of F8:F6 spin-coated at room temperature (top) and quenched from the nematic melt (bottom), taken using an Oxford Diffraction Excalibur PX instrument using molybdenum K_α radiation. Images from both in-plane (left) and out-of-plane (right) configurations are shown (see Figure 3.2 for definitions). All diffractograms were collected with 1200s integration time.

Figure 4.15 shows the ToF data of the F8:F6 LC phase. It can be seen that the mobility is again strongly enhanced relative to the spin-coated sample. The mobility in the F8:F6 LC phase is around 2×10^{-2} cm^2/Vs, approximately the same as in the PFO LC phase.

4.5.3 High mobility glassy isotropic phase in PFO

In order to process increasingly thick films for ToF, solutions of increasing concentration were used. During these experiments, the phenomenon of gelation of the highly concentrated solutions became evident. Gelation in PFO has been reported previously [128, 129, 152, 153]. A gel is a system that

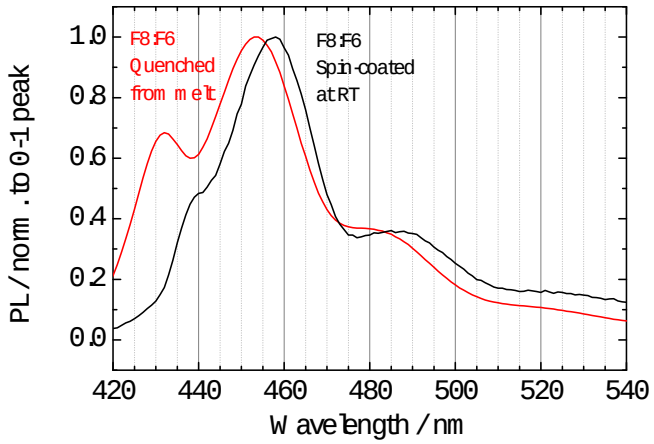

Figure 4.14: Emission spectra of thick films of F8:F6 spin-coated at room temperature and quenched from the nematic melt.

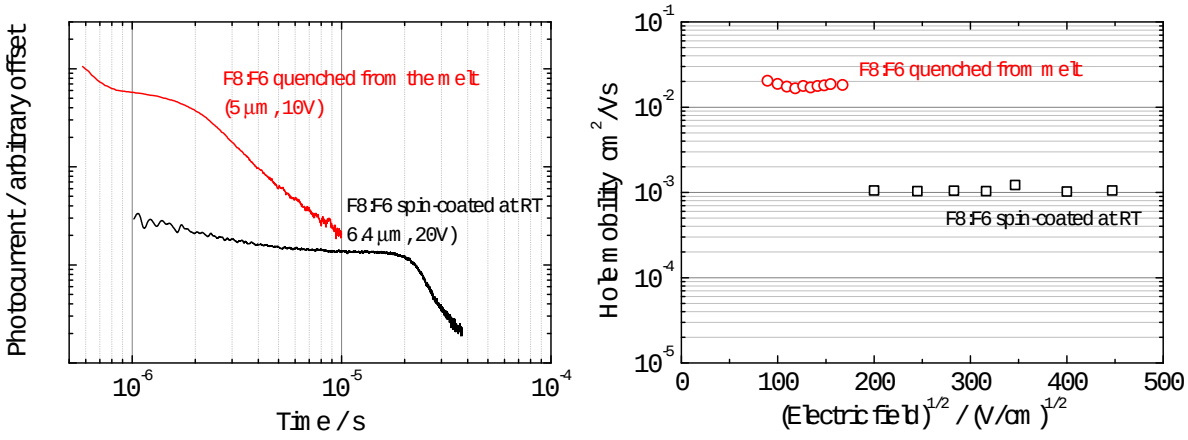

Figure 4.15: ToF transients (left) and mobility data (right) for F8:F6 spin-coated at room temperature and quenched from the nematic melt.

behaves like a solid despite the majority of its weight being in the liquid form, as a result of some form of cross-linking network within the liquid. It has been suggested that the gelation sometimes occurring in highly concentrated (approximately >10 g/l) PFO solutions occurs by a conformation change-induced physical cross-linking mechanism, involving the aggregation of neighbouring chains. It has also been suggested that the beta-phase may be the key agent in stabilising the dimerisation of chains, and gels of PFO exhibit the characteristic emission spectrum of the beta-phase [128, 129, 152, 153].

We observed that on heating the PFO gel above approximately 70–80°C, it reverted to solution form. On cooling to RT, the sample remained in solution form for some time – allowing the solution to be spin-coated – before reverting to gel form. It has been shown that the beta-phase is unstable at elevated temperatures [132, 153, 147]. In the study of Chen et al. [153], it was found by monitoring

PL in-situ that heating a gel of 3 wt% PFO in toluene above 40–45°C resulted in the dissipation of the beta-phase and a gel-solution transition, although the beta-phase emission began to decrease at even lower temperatures. It is likely that this gel-solution transition temperature will vary with solution concentration, as well as solvent, which may explain the higher temperatures required here. We note that beta-phase dissipation in a solid film may require even higher temperatures: in the study of Chen et al. [132], the dissipation of beta-phase in a solid film was observed to begin at around 85°C. In the study of Shi et al. [147], the beta-phase content of a solid film was seen to be reduced only above around 120°C and dissipated fully above around 140°C.

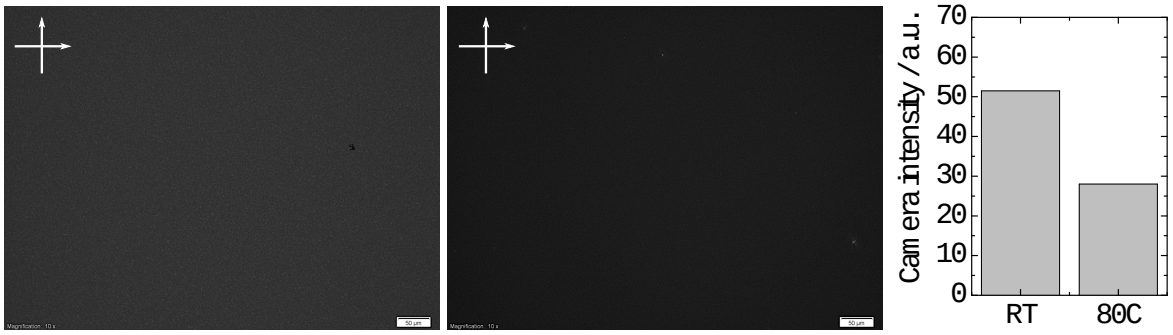

Figure 4.16: Cross-polarised light micrographs in transmission (10x magnification) of films of PFO spin-coated at room temperature (left) and spin-coated at 80°C (right). The scale bar is 50 μm. All cross-polarised light micrographs shown in this Chapter were taken with the same experimental parameters (exposure time 500 ms, gain 5 dB, fixed light intensity) using an Olympus microscope and have been subjected to identical image processing (uniform brightening and contrast enhancement) using Photoscape v6.3.2 graphics editing software. The camera intensity value is a mean intensity level across the raw image on a scale between 0 and 255, calculated using ImageJ software version 1.46.

We observed that if the highly concentrated solutions were spin-coated not after cooling to RT, but whilst still hot – within a range of temperatures between approximately 80°C and 100°C – the resulting films were highly glassy in appearance. The films spin-coated from the same solution after cooling to RT, before the recurrence of gelation (that is, the RT-spin-coated samples of Section 4.4.1), were much less glassy. Cross-polarised light micrographs are shown in Figure 4.16. The images show that, in a similar way to the F8:F4/1 film in Figure 4.6, there is a much reduced concentration of scattering centres in the film spin-coated at elevated temperature relative to that spin-coated at RT (this is the same image as that of the spin-coated film in Figure 4.6). Also shown are the XRD data for the two films. The increased width of the diffraction peaks shows that the film-spin coated at elevated temperature has poorly defined packing distances. There is an indication of a slight in-plane alignment of the chains, but this is not strong. These data show that the structure of the film spin-coated at elevated temperature is highly glassy, with no indication of

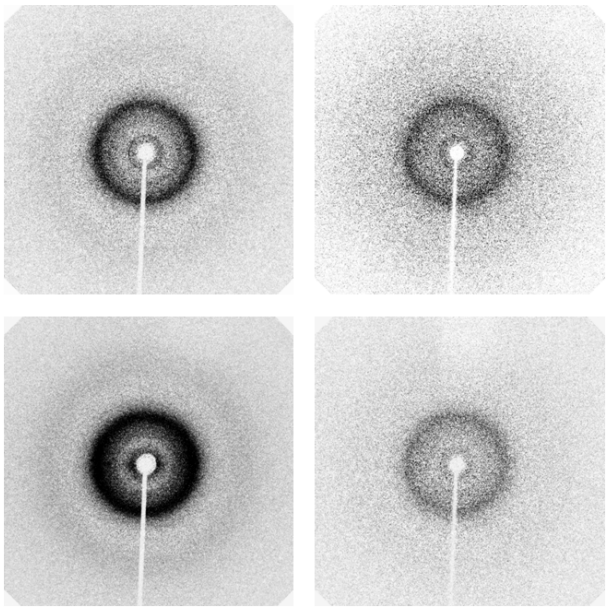

Figure 4.17: X-ray diffractograms of PFO spin-coated at room temperature (top) and spin-coated at 80°C (bottom), taken using an Oxford Diffraction Excalibur PX instrument using molybdenum K_α radiation. Images from both in-plane (left) and out-of-plane (right) configurations are shown (see Figure 3.2 for definitions). All diffractograms were collected with 1200s integration time.

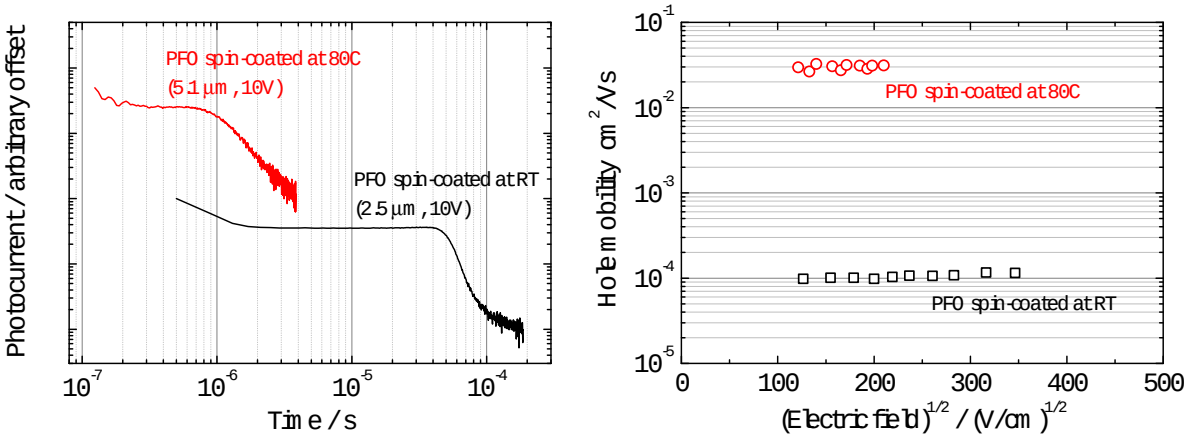

Figure 4.18: ToF transients (left) and mobility data (right) for PFO spin-coated at room temperature and spin-coated at 80°C.

significant crystalline or liquid crystalline order.

The ToF transport properties of a film spin-coated at elevated temperature (80–100°C) are shown alongside those of a film spin-coated at room temperature (the same sample as in Section 4.4.1 above). It can be seen that the process of spin-coating at elevated temperature leads to a greatly enhanced mobility of around 3×10^{-2} cm^2/Vs, with the ToF transient remaining non-dispersive. This mobility is slightly higher than that of the LC phase PFO of Redecker et al. [54] and in this study, and to our knowledge the highest mobility reported in PFO by time-of-flight or any other

bulk mobility measurement method. Further, it is highly notable that this has been demonstrated in a glassy isotropic sample, as indicated by the cross-polarised light and optical images. The next section will address the mechanism of mobility enhancement in the sample spin-coated at elevated temperature and show, remarkably, that it is made possible by suppressing the formation of the beta-phase and crystalline material within the film.

It can also be seen that the mobilities of the LC samples of both PFO and F8:F6, and the sample of PFO spin-coated at elevated temperature, at 1–3 $\times$ 10^{-2} cm^2/Vs, are very close to the mobility found in the F8:F4/1 (M_w=300k) spin-coated sample, and the mobility of all three polymers as spin-coated in FET devices. It is interesting to ask whether this indicates that some common mobility limit has been reached. This is a question which we shall return to in a later section.

4.6 Controlling chain conformation to enhance mobility in PFO – the beta-phase as a hole trap

The introductory Section 4.3.1 to this Chapter discussed the historical difficulty in disentangling the many factors limiting charge transport in disordered organic materials. These factors include the variety of polymer chain conformers, configurations and material phases, chemical defects on the chain and impurities within the sample, and the electrostatic interactions due to those structural variations. It has commonly been observed that the bulk mobility (for example, the ToF mobility) of many materials has fallen short of that expected from a 'design' point of view (eg by designing more planar polymer backbones to increase conjugation length and enhance interactions between neighbouring chains), and has remained well below the intra-chain mobility as estimated from TRMC measurements.

The material set under study here allows us for the first time to study in isolation the mobility-limiting effect of a distinct charge trapping species. We identify the charge trapping species as the beta-phase conformation of PFO. This has been possible by controlling the formation of phases in films of PFO in ways such as those described in the above section, and by making use of the distinct spectroscopic signature of the beta-phase.

4.6.1 Introducing the beta-phase into high mobility glassy isotropic PFO films

It was shown in the above section that films of PFO spin-coated from solution at an elevated temperature of 80–100°C exhibit a uniform glassy microstructure, and a high ToF mobility of around 3×10^{-2} cm^2/Vs. The method of fabrication – heating past the gel-solution transition of a highly concentrated solution and spin-coating whilst at this elevated temperature – hints towards the role of the beta-phase. This was examined further by taking emission spectra of the films, as shown in Figure 4.19. The figure shows the emission spectra of three films spin-coated at elevated temperature, alongside the spectrum of a film spin-coated at room temperature. It can be seen that the emission spectra of the films spin-coated at elevated temperature are highly variable, with the 0–1 peak position seen at wavelengths between 450 nm and 466 nm. This spans almost the full wavelength range observed for various polyfluorene films in the solid state, for emission from the glassy phase at around 446-450 nm and emission from the beta-phase at around 466-468 nm. We hypothesise that the variation is due to a small but varying beta-phase fraction within the film. Since the temperature of the solution during spin-coating was difficult to control, there may have been some variation in the completeness of dissipation of the beta-phase. As discussed above, even a very small fraction of beta-phase (≈1%) in a sample may dominate the emission [136]. Thus, it appears the samples shown may contain a 'threshold' amount of beta-phase, perhaps $< 1\%$ by volume, where the transition between emission dominated by beta-phase and by glassy matrix occurs.

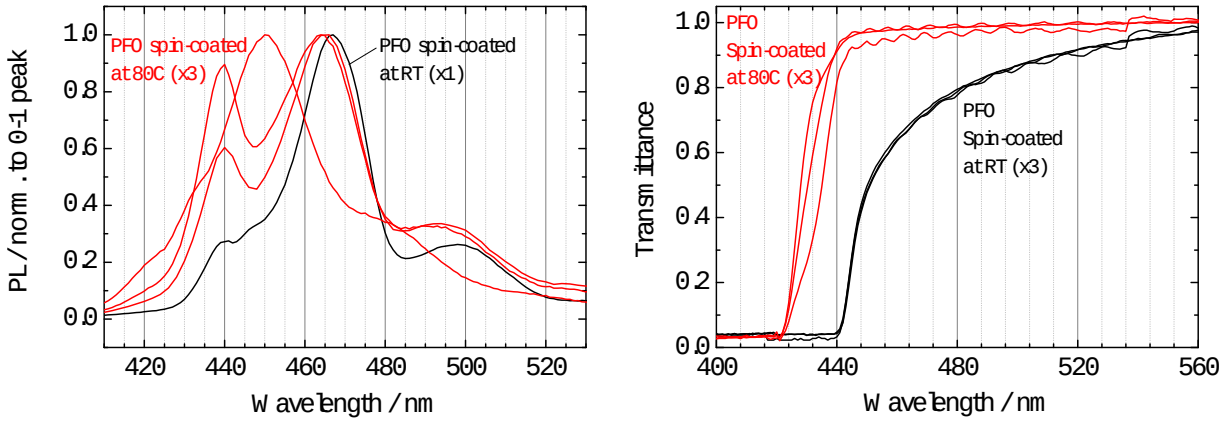

Figure 4.19: Left: Emission spectra of thick films of PFO spin-coated at room temperature (x1) and spin-coated at 80°C (x3). Right: Transmission spectra of thick films of PFO spin-coated at room temperature (x3) and spin-coated at 80°C (x3). Note that the highly-absorbing films saturate the response of the instrument above the onset of absorption. The transmission spectra are shown here to indicate the ≈20 nm shift in the onset of absorption, and the difference in the degree of scattering outside the absorption range (above ≈450 nm), for the different processing routes.

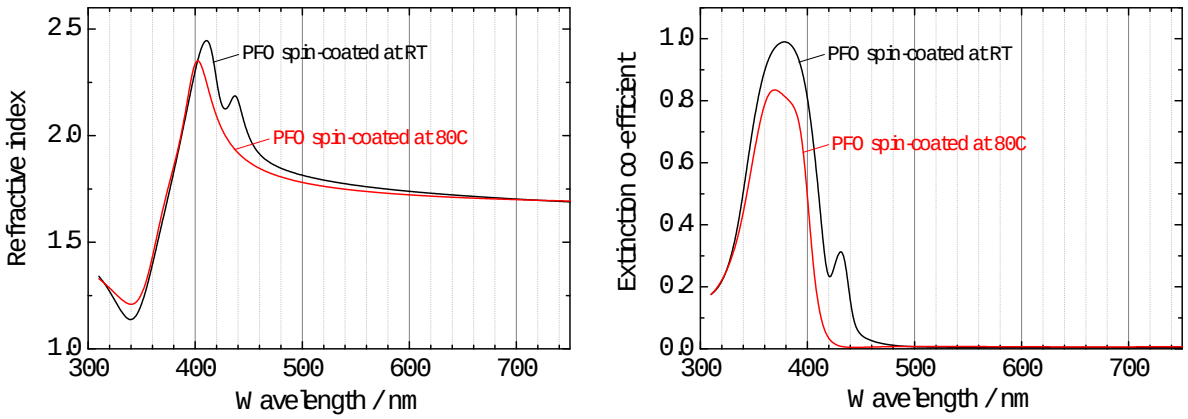

Figure 4.20: Variable angle spectroscopic ellipsometry (VASE) data for PFO spin-coated at room temperature and spin-coated at 80°C. Left: the wavelength-dependent refractive index for the two samples. Right: the imaginary part of the refractive index (the extinction co-efficient) for the two samples. The characteristic beta-phase absorption at 432–434 nm is clearly visible for the sample spin-coated at room temperature, but not for the sample spin-coated at 80°C.

It is clear that the emission spectra are therefore not the ideal tool in assessing the beta-phase content of the films, since it appears the emission is highly sensitive to a very small minority of beta-phase. It may be expected that absorption spectra would provide more a convincing assessment, since the strength of the characteristic absorption of the beta-phase can be directly related to its volume fraction. However, direct transmission spectroscopy is not particularly well-suited in this case either, since the large film thickness leads to a saturation of the response of the photometer across almost the entire wavelength range in question, as shown in Figure 4.19. Nonetheless, the spectra are consistent with the hypothesis of very low beta-phase content. Estimations of the band gap edge from Figure 4.19 suggest that the onset of absorption is approximately 20 nm lower for the samples spin-coated at elevated temperature compared with those spin-coated at RT. This difference is approximately that expected between the glassy absorption and the beta-phase absorption. However, the influence of the red-shifted absorption edge due to crystallinity - known to be present in the film spin-coated at RT - clouds the analysis. A more direct confirmation is desirable. To achieve this, we have employed variable angle spectroscopic ellipsometry (VASE), in collaboration with Mariano Campoy at ICMAB-CSIC in Barcelona. Since this technique is based on polarization dependent reflectivity data, we can access the absorption of thick films without saturating the signal, as in the transmission experiment. Figure 4.20 shows the refractive index of the two films spin-coated at elevated temperature and at RT, as deduced from VASE. Also shown is the extinction coefficient, the imaginary part of the refractive index, which is employed to study the absence or presence of beta-phase. The data clearly shows the presence of the characteristic beta-phase

absorption peak at 432–434 nm in the film spin-coated at RT, and the complete absence of the same peak in the film spin-coated at elevated temperature. This confirms the effect of spin-coating at elevated temperature of drastically reducing the beta-phase content in the film.

Therefore, we have observed high mobility in a glassy film of PFO with very low beta-phase content. This has been compared with the two orders of magnitude lower mobility in a PFO film with a significant fraction of beta-phase and a significant concentration of scattering centres corresponding to regions of crystalline order. At this stage, we cannot attribute the enhancement in mobility solely to the absence of beta-phase or the absence of the crystalline phases. In order to do so, we require a method to control the formation of one of these species independently of the other. Fortunately, such a method has already been described. The swelling of PFO chains in toluene vapour has been used to introduce beta-phase into samples in several studies [129, 135, 136, 132, 134]. In these studies there is no evidence of increased crystallinity after the toluene vapour exposure. Further, as described in Section 4.3.2, Da Como et al. have shown that formation of the beta-phase by exposure to toluene does not involve rearrangements of the polymer chain other than re-ordering of the torsional angles between adjecent monomeric units [134]. 'Bent' chains in which beta-phase was formed remained 'bent'. This observation makes it very unlikely that the toluene exposure treatment can increase the crystallinity in the sample, which would involve the large-scale rearrangement of multiple polymer chains into the crystal structure.

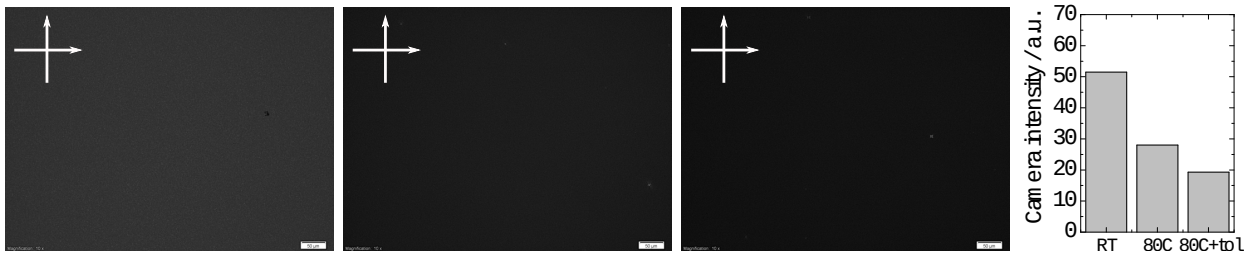

Figure 4.21: Cross-polarised light micrographs in transmission (10x magnification) and camera intensity for films of PFO spin-coated at room temperature (left); spin-coated at 80°C (centre); and spin-coated at 80°C and subsequently exposed to toluene vapour (right). The scale bar is 50 μm. All cross-polarised light micrographs shown in this Chapter were taken with the same experimental parameters (exposure time 500 ms, gain 5 dB, fixed light intensity) using an Olympus microscope and have been subjected to identical image processing (uniform brightening and contrast enhancement) using Photoscape v6.3.2 graphics editing software. The camera intensity value is a mean intensity level across the raw image on a scale between 0 and 255, calculated using ImageJ software version 1.46.

These observations in the literature are supported by our cross-polarised light images, optical images and transmission spectra of treated films. Films of PFO spin-coated both at RT and at elevated

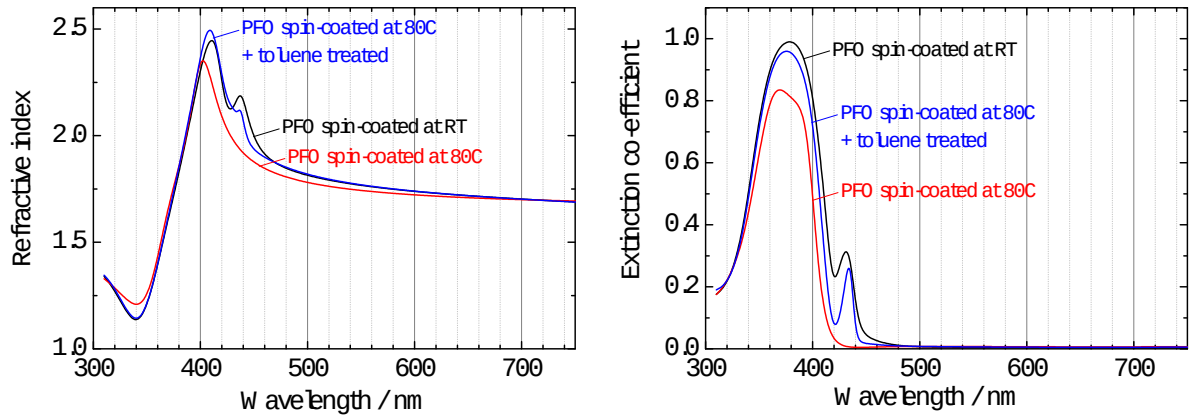

Figure 4.22: Variable angle spectroscopic ellipsometry (VASE) data for PFO spin-coated at room temperature; spin-coated at 80°C; and spin-coated at 80°C and subsequently exposed to toluene vapour. Left: the wavelength-dependent refractive index for the samples. Right: the imaginary part of the refractive index (the extinction co-efficient) for the samples. The characteristic beta-phase absorption at 432–434 nm not visible in the sample spin-coated at 80°C is clearly visible after exposeure to toluene vapour.

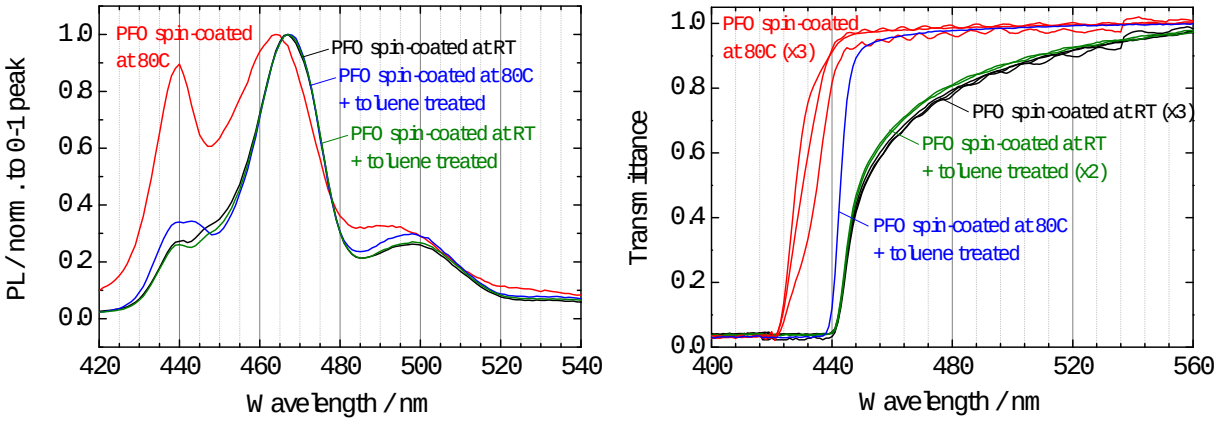

Figure 4.23: Left: Emission spectra of thick films of PFO spin-coated at room temperature; spin-coated at room temperature and subsequently exposed to toluene vapour; spin-coated at 80°C; and spin-coated at 80°C and subsequently exposed to toluene vapour. Right: Transmission spectra of thick films of PFO spin-coated at room temperature (x3); spin-coated at room temperature and exposed to toluene vapour (x2); spin-coated at 80°C (x3); and spin-coated at 80°C and subsequently exposed to toluene vapour (x1). The toluene treatment causes a shift in the absorption onset of the sample spin-coated at 80°C but does not change the degree of scattering above ≈450 nm. The toluene treatment does not change the transmission of the sample spin-coated at room temperature.

temperature were treated with toluene vapour for one hour. This was achieved by placing the samples on a stage in a dish of toluene and covering with a large beaker. The apparatus was placed on a hotplate at 50°C until toluene was seen to condense on the sides of the beaker, at which point the heat was reduced to room temperature for the remainder of the exposure period. The various optical and spectroscopic data of the resulting films is shown in Figure 4.23. The VASE data in Figure 4.22 clearly shows that the toluene treatment has introduced the characteristic beta-phase absorption at 430–437 nm which was absent in the film spin-coated at elevated temperature. The

toluene-treated film spin-coated at RT (not shown) showed no significant difference in VASE from the film spin-coated at RT. It can be seen that the appearance under cross-polarised light of the film spin-coated at elevated temperature is unchanged after the toluene vapour exposure. The resulting film is also uniformly glassy, with no evidence of crystalline or liquid crystalline order. The transmission spectra of the films can also be compared in the transparency region at wavelengths longer than approximately 450 nm. It can be seen that the spectra from films spin-coated at RT exhibit a long tail out to at least 550 nm, attributed to scattering from crystalline regions. The spectra from films spin-coated at elevated temperature, in contrast, show a much sharper increase in transmission outside the region of glassy phase absorption (without toluene treatment) and beta-phase absorption (with toluene treatment) respectively. Together, this evidence strongly suggests that the toluene treatment of a film spin-coated at elevated temperature results in a film with significant beta-phase content, but negligible crystalline content.

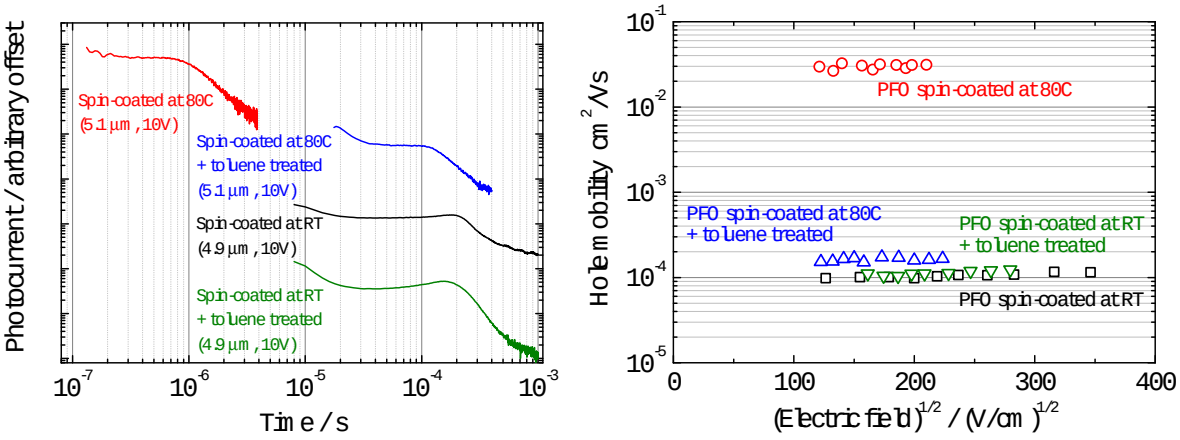

Figure 4.24: ToF transients (left) and mobility data (right) for PFO spin-coated at room temperature; spin-coated at room temperature and subsequently exposed to toluene vapour; spin-coated at 80°C; and spin-coated at 80°C and subsequently exposed to toluene vapour.

We are therefore in a position to examine the charge transport effect of the beta-phase in these films independent of the effect of the crystalline phases. The ToF data of the PFO films spin-coated at elevated temperature before and after exposure to toluene treatment is shown in Figure 4.24, alongside control films spin-coated at RT before and after toluene treatment. It can be seen that the toluene treatment reduces the mobility of the film spin-coated at elevated temperature by over two orders of magnitude from 3×10^{-2} cm^2/Vs to 2×10^{-4} cm^2/Vs. The reduced mobility of just over 10^{-4} cm^2/Vs corresponds very closely to the mobility of the film spin-coated at RT. The film spin-coated at RT and then treated with toluene shows essentially no change in mobility, and only

a small change in the shape of the transient.

4.6.2 Introducing the beta-phase into high mobility LC phase PFO films

We have also considered the effect on charge transport of introducing the beta-phase into the high mobility nematic LC phase of PFO. Since processing PFO into the LC phase involves temperatures above 200°C, it is clear that the beta-phase – which is dissipated above some temperature 85–140°C [132, 153, 147] – should be completely absent. This is supported by the emission spectrum of a film which has been quenched from the melt, such as that in Figure 4.25, which does not display the characteristic beta-phase 0–1 emission at 466–468 nm, but rather a broad 0–1 peak centred around 453–454 nm, characteristic of the LC phase. Figure 4.25 also shows the emission spectrum of the same film which has been subsequently exposed to toluene vapour. This clearly shows the characteristic emission of the beta-phase with a 0–1 peak at 467 nm, as for the film spin-coated at room temperature (shown for comparison). This confirms that energy transfer from the LC phase to the beta-phase is to be expected if the beta-phase is present. Figure 4.25 also shows the emission from the same film which, after having been treated with toluene vapour, has been heated above its melting temperature and quenched a further time in order to retrieve an LC phase with no beta-phase. The emission of this film coincides very closely with the original quenched film.

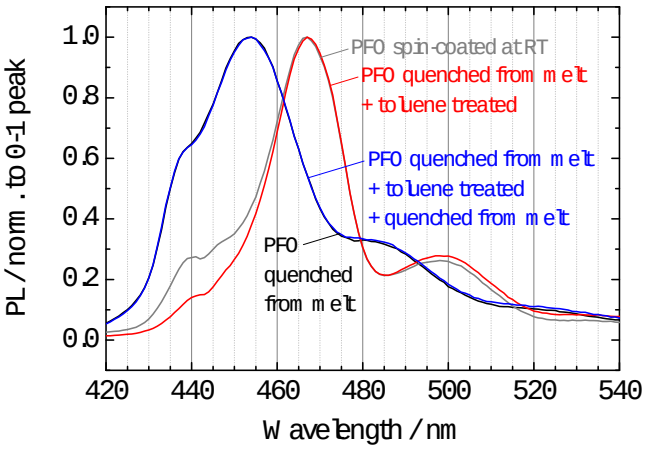

Figure 4.25: Emission spectra of thick films of PFO spin-coated at room temperature; quenched from the nematic melt; quenched from the melt and subsequently exposed to toluene vapour; and quenched from the melt for a second time after the exposure to toluene vapour.

ToF transients of the exact same samples are shown in Figure 4.26. The two fast transients from LC phase films with no beta-phase show almost the same transit time at around 3.5 μs, corresponding to mobilities of around 9×10^{-3} cm^2/Vs. The transients show slightly different shapes, attributed

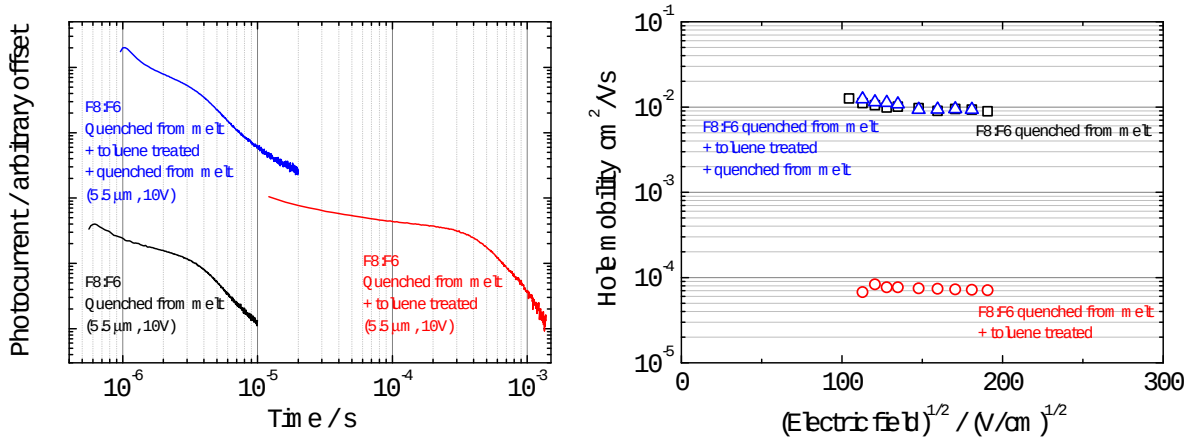

Figure 4.26: ToF transients (left) and mobility data (right) for PFO quenched from the nematic melt; quenched from the nematic melt and subsequently exposed to toluene vapour; and quenched from the melt for a second time after the exposure to toluene vapour.

to small differences in microstructure (for example LC domain size or minority crystalline content) due to the relatively uncontrolled quenching process. The LC phase film containing the beta-phase shows a transit time more than 100 times longer at around 380 μs, corresponding to a mobility of around 8×10^{-5} cm^2/Vs. Again, the limiting effect on transport of the beta-phase has been isolated. Introducing the beta-phase into the glassy LC film results in a greater-than-two orders reduction in mobility to approximately 10^{-4} cm^2/Vs, approximately the mobility of the spin-coated film. The effect is almost identical to that seen by introducing beta-phase into the glassy films spin-coated at elevated temperature.

4.6.3 Quantitative modelling of the hole trapping effect of the beta-phase

The two demonstrations above show clearly that the presence of beta-phase, independent of the effect of other conformational or structural factors, limits the ToF mobility to around 10^{-4} cm^2/Vs. This suggests that the beta-phase acts as a very strong hole trap. We have sought to rationalise this large effect with quantitative modelling methods, in order to reconcile the known structural and spectroscopic properties of the beta-phase with the transport data detailed above. The modelling work has been led by Jarvist Frost, Florian Steiner and Jenny Nelson.

First, we have examined the energetic effect of the formation of beta-phase in terms of the planarisation of the PFO chain. The experimental absorption features of the PFO glassy phase and beta-phase give some idea of the size of the energetic effect, and it may be calculated that the energetic difference between 380 nm (the glassy phase absorption peak) and 435 nm (the beta-phase

absorption peak) is approximately 400 meV. However, this corresponds to the difference in the bandgap of the two phases, which will depend on changes in both the LUMO and the HOMO and differences in exciton binding energy. To study the effect on hole transport, we require the difference in the energy of a hole in the two phases. For this, we turn to quantum chemical methods.

The approach was to take a 9,9-dioctylfluorene octamer initially in its energetically relaxed conformation, representing a chain in the 'glassy' form (albeit a single chain). In this energetic minimum, the torsional angle between neighbouring monomers is 45°. From this initial state, planarity (zero torsional angle between neighbours) was enforced over a number of successive monomers in the centre of the octamer, increasing this number from 2 to 8. The structure was then relaxed with this constraint over the torsional angles, and the electronic structure calculated using density functional theory (DFT). The HOMO was obtained using this method. The LUMO was then also obtained through a time-dependent DFT (TDDFT) calculation, using the DFT solution. It was found that the planarisation has a large effect on both the HOMO and LUMO energies. The planarisation of six units led to a rise in the HOMO energy (towards the vacuum level) of approximately 140 meV. The largest rate of change of the HOMO energy was seen to occur on planarising the first few units, with the effect beginning to saturate with the planarisation of 5–8 units. Since 140 meV is nearly six times the room temperature thermal energy, this information already indicates that the beta-phase conformation may act as a strong hole trapping species. This calculation also provides an estimate of the lower bound for the hole trap depth as 120 meV, assuming, as in [140], that the beta-phase is only stable for four or more planarised units. However, it is likely that the real trap depth is significantly higher, for the following reason. It was found that the configuration of a 90° torsional angle between neighbouring units presents a relatively small energetic penalty of around twice the thermal energy at 300K relative to the torsional energy minimum at 45°. A torsional angle of 90° corresponds to broken conjugation. Hence, it may be expected that the glassy phase within which the beta-phase is embedded will have a fairly high concentration of conjugation-breaking defects. Decreasing the average conjugation length would have the effect of shifting the hole DoS in the glassy phase to more negative energies – the HOMO of fluorene hexamers was calculated to lie around 20–30 meV deeper than the HOMO of fluorene octamers. The overall effect would be to increase the energetic separation of the glassy phase and beta-phase hole energies. Hence, the quantum chemical modelling suggests that the beta-phase within a glassy matrix represents a hole trap with a depth of at least 120–140 meV, and perhaps several 10s of meV more.

Next, the time-of-flight experiment was simulated using software developed at Imperial by Jarvist Frost, Florian Steiner and Jenny Nelson. The effective DoS for holes was constructed based on the quantum chemical calculations, consisting of a Gaussian DoS of width σ to represent the glassy phase (a variable parameter) and a single energetic state at an energy ΔE_{beta} deeper than the mean of the glassy phase Gaussian DoS to represent the beta-phase. This DoS was assigned to a 3D array of hopping sites consisting of 'polymer chains', typically 23 hopping sites in length, arranged in a (typically) $50 \times 50 \times 100$ box in a space-filling but disordered 'morphology'. A charge was 'injected' at one 50×50 face, and an 'electric field' applied such that the charge tended to hop towards the opposing 50×50 face. The transfer rate was calculated using Marcus theory, with parameters, including the re-organisation energy and the electronic transfer integral, chosen to describe the experimental values. Different transfer integrals were assigned to 'intra-chain' and 'inter-chain' hops such that intra-chain hops were faster by a factor of 100, based on the intra-chain mobility of 1 cm^2/Vs in PFO as found by TRMC [52] and the highest mobility in PFO involving inter-chain hops of around 10^{-2} cm^2/Vs (as in this study and in [54]). The time taken for the charge to transit was recorded, and the process repeated for a large number of charges. A mobility was then extracted by fitting to a constructed photocurrent curve in the same way as is done experimentally. The effect on mobility of introducing a distributed population of beta-phase segments into a glassy background phase was studied. It was found that with reasonable parameters, a two orders of magnitude reduction in the mobility could be predicted with a 10% volume fraction of the beta-phase and a ΔE_{beta} of 200 meV. This value for ΔE_{beta} is reasonable given the findings of the quantum chemical calculations described above. This result therefore confirms that the planarisation of the PFO chain can represent a hole trap deep enough to cause the two orders of magnitude reduction in mobility observed experimentally.

4.6.4 Summary

In summary, the limiting effect of beta-phase on charge transport in PFO has been demonstrated and rationalised. The planarisation of the fluorene units from the torsionally disordered glassy phase presents, according to quantum chemical calculations, an intra-chain trap state at least 120 meV (and likely several 10s of meV more) deeper in energy for hole polarons than the glassy phase. Given that the beta-phase regions are embedded within a glassy phase matrix in too low a concentration to percolate, this leads to a strong charge trapping effect. The result is a two orders of

magnitude reduction in ToF hole mobility relative to the case of transport through a purely glassy film. This is, to our knowledge, the first description of the effect on charge transport of a single, isolated conformational defect in conjugated polymers.

The intra-chain charge trapping effect of the beta-phase may be considered somewhat analogous to the intra-chain trapping effect of minority amine units observed in spirobifluorene-triarylamine copolymers [154, 155]. When the hole-transporting amine unit, with a shallower HOMO than the spirobifluorene unit, was introduced as a minority component at 10% by stoichiometry, it reduced the time-of-flight mobility by more than one order of magnitude relative to the mobility of the spirobifluorene homopolymer. Only at 50% amine by stoichiometry did the copolymer mobility exceed that of the homopolymer. A similar finding was observed by Yap et al. using fluorene-phenylenediamine copolymers [149].

In the next section, the effect on transport of crystallinity in the polyfluorenes, including the copolymers F8:F6 and F8:F4/1 is examined further. This data, together with the above findings regarding the beta-phase, will be used to offer a complete explanation for the enhancement in mobility in F8:F4/1 relative to PFO (when simply spin-coated at RT). It will also be used to form a qualitative description of charge transport in the polyfluorene family and to support an alternative paradigm for designing high mobility polymer semiconductors.

4.7 Influence of crystallinity on transport in the polyfluorenes

It is clear from the above sections that the highest mobilities achieved in polyfluorenes to date have been found in glassy samples, whether the glassy LC phase of PFO, the glassy isotropic phase of PFO or the glassy isotropic film of F8:F4/1. We have established that the beta-phase has a strong limiting effect on hole transport in PFO, reducing the mobility of these glassy films by around two orders of magnitude. The effect of crystallinity has not been addressed explicitly. Nonetheless, the hole transport properties of films containing the crystalline forms of PFO have been studied in some detail in the literature, particularly by Kreouzis et al. [14]. It was found that by thermally annealing spin-coated films of PFO, for up to 16 hours, mobilities could be increased to just over 10^{-3} cm^2/Vs. Whilst this represents a significant improvement over the mobility in spin-coated films, it remains an order of magnitude lower than that in the glassy films studied here. Particularly when

Processing route	0–0 / nm	0–1 / nm	0–2 / nm
Spin-coated at 80°C	440	**464**	491^s
Quenched from melt	438^s	**454**	482^s
Q. from melt + tol. treated + Q. from melt	439^s	**454**	483^s
Spin-coated at 80°C + annealed at 150°C	434^s	**459**	485^s
Quenched from melt + annealed at 150°C	431^s	**457**	484^s
Cooled slowly from melt	431^s	**457**	485
Spin-coated at RT + annealed at 150°C	443	**460**	489
Spin-coated at 80°C + toluene treated	441^s	**467**	498
Spin-coated at RT	441^s	**467**	498
Quenched from melt + toluene treated	441^s	**467**	498

Table 4.2: Emission peak wavelengths for all PFO films shown in Figure 4.27. Peak positions have an error of ±1 nm, except those with a superscript^s indicating a shoulder with a larger position error of ±5 nm. The values for the 0–1 peaks, which are the main point of reference, are emboldened.

compared with the glassy isotropic films of PFO (formed by spin-coating at elevated temperature), this is somewhat surprising, and in general disagreement with the approach taken in the majority of the literature, where there have been many successful attempts to increase mobility by increasing inter-chain ordering and crystallinity (such as [46, 38, 68, 2] and many more).

In this section, we collate a wide range of ToF mobility measurements on films fabricated via different processing routes, representing the accessible phases of the polyfluorene family. Using the findings from the above section, the effects of crystallinity and beta-phase can be separated experimentally. It will be shown that for all processing routes studied here, samples containing significant crystallinity, but no beta-phase, exhibit mobilities lower by approximately one order of magnitude than glassy samples without beta-phase. Reasons are proposed for this. The findings are set in the context of the past literature measurements of the polyfluorenes. Finally, we make some remarks regarding the important mechanisms governing charge transport in the polyfluorene family, and how the findings may be generalised to inform synthesis and device fabrication in other materials systems.

4.7.1 Transport properties across the phase space of PFO

Figure 4.27 shows the collected ToF data for PFO films fabricated via a number of processing routes. All data are original to this study. Emission peak data of the same samples is given in Table 4.2. Images under cross-polarised light of three crystalline forms of PFO, for comparison with the images of the other forms of PFO earlier in this Chapter, are shown in Figure 4.28. The transport data

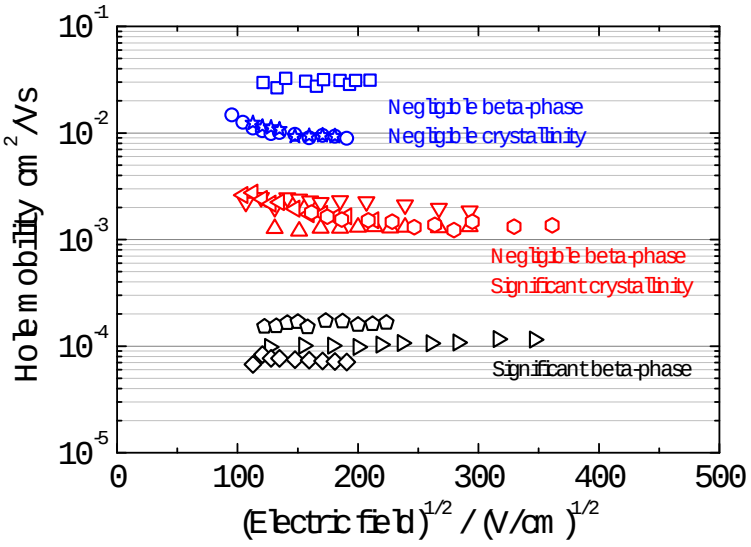

Figure 4.27: ToF mobility data for all forms of PFO studied in this Chapter (all data original to this study) Shown are data for PFO spin-coated at 80°C (squares); quenched from the melt (circles); quenched from the melt, exposed to toluene and quenched from the melt for a second time (stars); spin-coated at 80°C and annealed at 150°C (down triangles); quenched from the melt and annealed at 150°C (left triangles); cooled slowly from the melt (hexagons); spin-coated at room temperature and annealed at 150°C (up triangles); spin-coated at 80°C and exposed to toluene (pentagons); spin-coated at room temperature (right triangles); and quenched from the melt and exposed to toluene (diamonds). The colour coding represents three proposed classes of microstructure based on evidence from the emission, transmission, VASE, cross-polarised microscopy, XRD and DSC data sets, as labelled in the Figure. The emission peak positions of the same samples are given in Table 4.2.

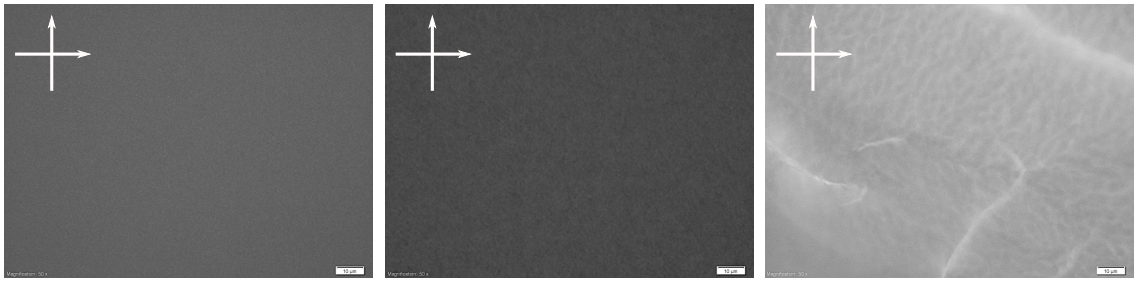

Figure 4.28: Cross-polarised light micrographs in transmission (50x magnification) of three films of PFO with significant crystallinity, for comparison with the micrographs presented earlier in the Chapter. Those shown correspond to films spin-coated at room temperature and annealed at 150°C (left); cooled slowly from the melt to promote crystallisation (centre); and quenched from the melt to RT and subsequently annealed at 150°C (right). The scale bar is 10 μm. All cross-polarised light micrographs shown in this Chapter were taken with the same experimental parameters (exposure time 500 ms, gain 5 dB, fixed light intensity) using an Olympus microscope and have been subjected to identical image processing (uniform brightening and contrast enhancement) using Photoscape v6.3.2 graphics editing software.

shows that the samples divide roughly into three groups. The group with the highest mobilities, around 10^{-2} cm^2/Vs, contains the glassy PFO samples as outlines in the sections above, both the nematic LC phase and the glassy isotropic phase fabricated by spin-coating at elevated temperature. The group with the lowest mobilities, around 10^{-4} cm^2/Vs, contains the samples with significant amounts of beta-phase, also as described in the sections above. The grouping with intermediate

mobilities of around 10^{-3} cm^2/Vs have been fabricated via a number of different thermal routes to contain various degrees and types of crystallinity, but no beta-phase, as described below.

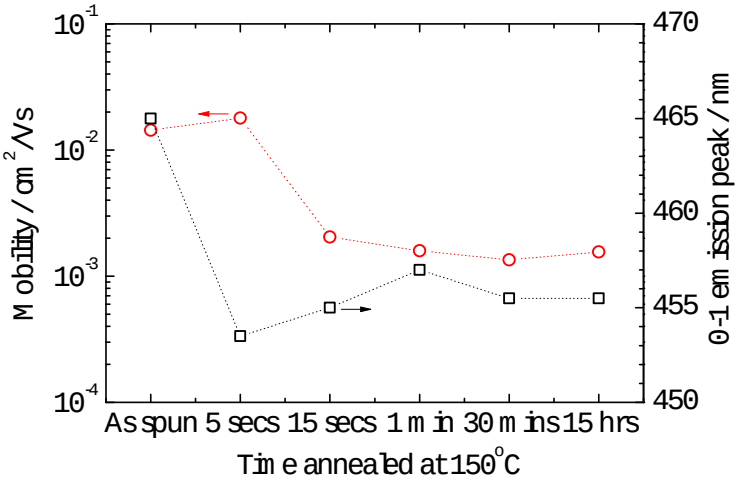

Figure 4.29: ToF mobility (circles, left axis) and 0–1 emission peak wavelength (squares, right axis) shown for a sample spin-coated at 80°C and for the same sample subsequently annealed at 150°C for the times shown on the x-axis. Times are additive.

It was shown in Section 4.6.1 that the two high mobility ($>10^{-2}$ cm^2/Vs) samples, those spin-coated at 80°C and quenched from the melt, contain negligible beta-phase. This allows us to consider the effect of introducing crystallinity in isolation – without influence from the beta-phase – by annealing those two samples above the glass transition temperature. It can be seen in Figure 4.27 that in both cases, the mobility after annealing at 150°C is reduced to approximately 10^{-3} cm^2/Vs. In the case of the film spin-coated at 80°C, the annealing procedure has been carried out for various times of 5 secs – 15 hrs, in order to examine the effect of increased perfection of crystallinity on transport. This is shown in Figure 4.29. After the initial decrease in mobility to around 10^{-3} cm^2/Vs after between 5 and 15 secs of annealing, the mobility is not observed to change significantly. The ToF transient dispersiveness was seen first to increase between 1 min and 30 mins and then to decrease after 15 hrs as the crystalline domains continued to develop and perfect. Despite the small changes in transient shape, the mobility remained constant within 20% and below 2×10^{-3} cm^2/Vs. It may be seen that after 5 secs of annealing, the 0–1 PL peak position shifts to 454 nm, indicating that the annealing has reduced the beta-phase content to a negligible amount. The mobility, however, remains above 10^{-2} cm^2/Vs until 15 secs annealing. This suggests that the development of crystalline domains between 5 secs and 15 secs annealing, independent of considerations of the beta-phase content, is responsible for the reduction in mobility.

We have also investigated the transport in a crystalline sample formed by slow cooling from the melt to 150°C. Crystallisation by cooling from the melt is expected to lead to a larger average domain size than crystallisation by heating from RT, since the polymer mobility (the physical motion of the chains) is larger at higher temperature and the driving force for nucleation smaller. A larger average grain size might be expected to be more favourable for charge transport. Figure 4.27 shows a sample cooled from the melt to 150°C over approximately one hour, and then held at that temperature for approximately 60 hrs, in order to allow the crystalline ordering to develop. However, the mobility is again of the order 10^{-3} cm^2/Vs. Therefore, we have seen that increasing the degree of crystallinity from both glassy isotropic and glassy LC phases – both by heating from RT and by cooling from the melt – reduces the mobility from around 10^{-2} cm^2/Vs to around 10^{-3} cm^2/Vs. The final PFO film with a mobility of approximately 10^{-3} cm^2/Vs is that spin-coated at room temperature and annealed from RT to 150°C. This has been studied in detail in [14].

4.7.2 Transport properties of LC and crystalline phases of F8:F6

As shown in Figure 4.30, the F8:F6 sample spin-coated at room temperature has a mobility of approximately 10^{-3} cm^2/Vs. The cross-polarised light image of this sample, shown in Figure 4.6, shows a significant concentration of scattering centres (similar to PFO spin-coated at room temperature). As described in Section 4.4.6, the F8:F6 sample shows no tendency to form a beta-phase-like conformation under the processing conditions which lead to its formation in PFO. We note that none of the F8:F6 samples show an emission as red-shifted as beta-phase PFO, which shows a 0–1 peak at around 467 nm. As shown in Figure 4.30, the F8:F6 sample spin-coated at RT has a 0–1 peak at around 457 nm, very close to the position of the 0–1 emission from the PFO crystalline phases. Given the similarity of the 0–1 emission to that of the crystalline phases of PFO, the observation of significant crystallinity in the cross-polarised light images and the observation that the beta-phase is not readily formed in F8:F6, we may deduce that the emission in the F8:F6 sample spin-coated at room temperature is dominated by the crystalline phase of F8:F6. We may also deduce that this phase has a similar structure to the crystalline phase of PFO. This is consistent with the mobility of the sample which, at around 10^{-3} cm^2/Vs, is very similar to the mobility of the PFO samples containing significant crystallinity but no beta-phase.

The LC phase F8:F6 sample was annealed at 150°C in order to introduce crystallinity. As shown in

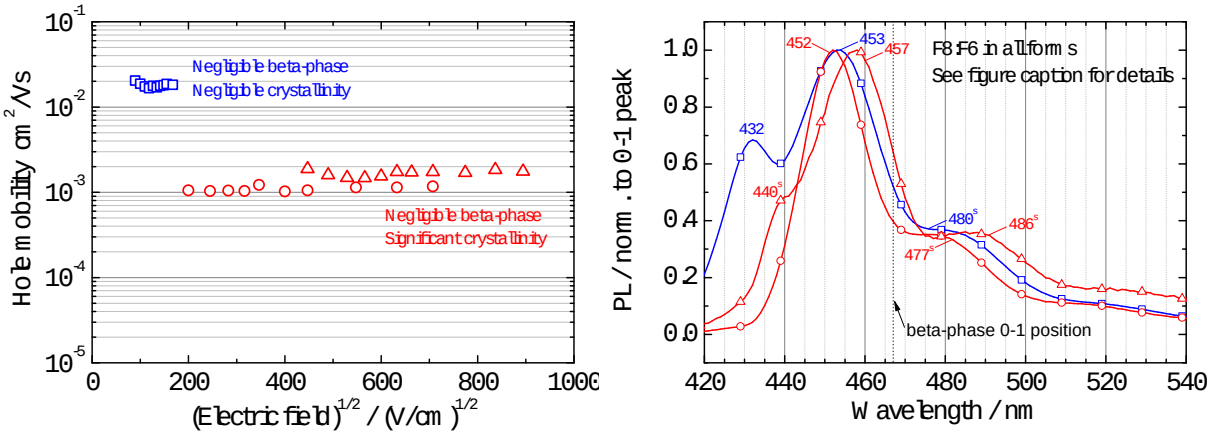

Figure 4.30: Left: ToF mobility data for all forms of F8:F6 studied in this Chapter. Shown are data for F8:F6 quenched from the nematic melt (squares); quenched from the nematic melt and annealed at 150°C (triangles); and spin-coated at room temperature (circles). The colour coding and labelling is as for the forms of PFO in Figure 4.27. Right: Emission spectra of thick films of F8:F6 quenched from the nematic melt (squares); quenched from the nematic melt and annealed at 150°C (circles); and spin-coated at room temperature (triangles). The emission peak positions in nm are labelled.

Figure 4.30, it was found that the mobility was, once again, reduced after annealing to approximately 1–2 $\times$ 10^{-3} cm^2/Vs. It remained at this level for the 15 hours over which the annealing study was carried out. These measurements are suggestive of a common mobility-limiting mechanism in PFO and F8:F6, related to the presence of the crystalline phase.

4.7.3 Molecular weight dependence of mobility in F8:F4/1

As described in Section 4.4.6, F8:F4/1 also shows no tendency to form a beta-phase-like conformation under the processing conditions which lead to its formation in PFO. Further, the DSC data show that the polymer has a much-reduced tendency relative to PFO to crystallise both on heating above T_g and cooling below T_m. Consistent with this, it can be seen that the sample of F8:F4/1 spin-coated at RT shows a much-reduced concentration of scattering centres, and exhibits predominantly a glassy isotropic phase. The ToF mobility in a F8:F4/1 sample with M_w=400k was shown by Yap et al. to be above 10^{-2} cm^2/Vs in simple RT-spin-coated films. We have reproduced a mobility above 10^{-2} cm^2/Vs for the M_w=300k sample. We have also studied a lower molecular weight F8:F4/1 sample with M_w=50k, which demonstrates a slightly reduced mobility of around 5 $\times$ 10^{-3} cm^2/Vs as shown in Figure 4.31. Reasons for the M_w-dependence are proposed in the following section.

In the next section we propose a qualitative description of charge transport in the polyfluorene

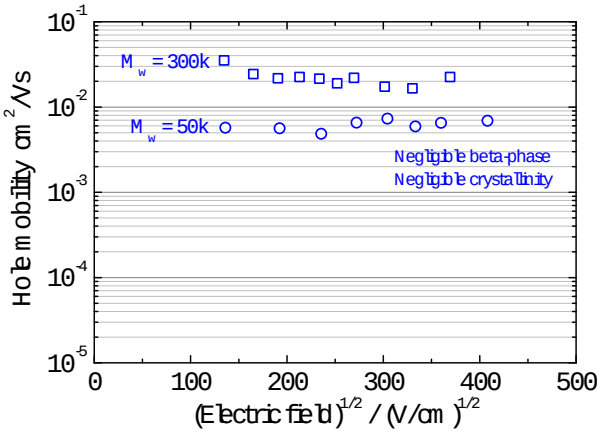

Figure 4.31: ToF mobility data for the two F8:F4/1 samples studied in this Chapter, with M_w=50k (circles) and 300k (squares).

family to explain the mobility data presented above. Before this is outlined, we describe a null result which was proposed as an alternative explanation for the variation in mobilities, relating to the density of the films. In the study of Yap et al., a significant increase in the refractive index was observed in F8:F4/1 relative to PFO. It was suggested that this was consistent with the reduction in relative alkyl content, and was calculated to correspond to an approximately 25% increase in film density. Given that this implies an decrease average separation of neighbouring conjugated backbones, it may be hypothesised that the mobility should correlate with film density (this was not explicitly hypothesised by Yap et al.). A correlation of mobility and film density has been observed previously by Sims et al. in fully-converted and partially-converted films of PDMeOPV [156]. In order to test this hypothesis for the current material systems, we have performed direct measurements of the density of films using the density gradient column described in Section 3.8. Density measurements were carried out at ETH Zurich in collaboration with Felix Koch. Figure 4.32 shows density data for a selection of films fabricated to the same specification as those for ToF measurements. It can be seen that there is no correlation between mobility and film density for this set of materials. Hence, we conclude that the mobility variations observed are due to other factors. Our explanation is proposed in the following section.

4.7.4 Hole transport in the polyfluorene family

Crystalline domains and beta-phase chains reduce bulk hole mobility

The highest mobilities we have been able to achieve in the polyfluorenes studied (PFO, F8:F6 and F8:F4/1) have been found in glassy samples, including both glassy isotropic and glassy LC films.

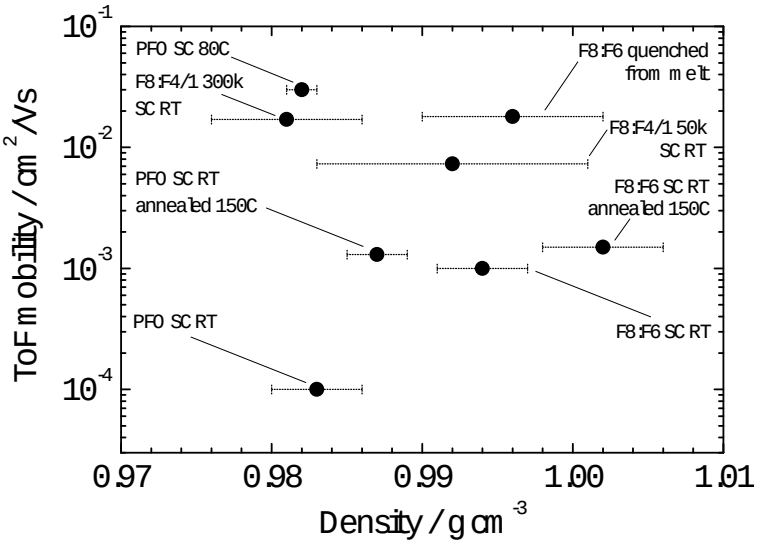

Figure 4.32: ToF mobility of various samples plotted against the density of the film as measured in a density gradient column (described in the text). Error bars, representing the standard deviation between a number of measurements, are shown for the density data. No correlation was observed between the two properties.

Similar mobilities of above 10^{-2} cm^2/Vs have been achieved in all three polyfluorenes studied, consistent with charge transport in these samples being limited by a common factor. In PFO and F8:F6, it has been shown that introducing crystallinity into the glassy samples by annealing above T_g results in a reduction in mobility to approximately 10^{-3} cm^2/Vs. This mobility is apparently fairly insensitive to the degree of crystallinity above some threshold. In PFO only, a further limit can be imposed on the mobility by the introduction of the beta-phase conformation. Introducing the beta-phase into either the glassy isotropic or the glassy LC phase sample results in a decrease in mobility to around 10^{-4} cm^2/Vs. We have shown, therefore, that the presence of either the crystalline phase or the beta-phase leads to reduced bulk sample mobilities.

Suppress crystallinity and the beta-phase to achieve high mobility

This then allows us to explain the origin of the enhanced mobility in F8:F4/1 relative to PFO, when processed simply by spin-coating at room temperature. The enhanced mobility is in fact closer to the 'intrinsic' mobility of the polyfluorene family, achieved by the suppression of charge trapping species related both to crystallinity and to the beta-phase. The absence of crystallinity and beta-phase in the spin-coated samples of F8:F4/1 is ensured by the structure of the branched side-chains. This demonstrates the power of simple chemical modification to control material phase behaviour, the sample microstructure and the resulting optoelectronic properties.

It is also interesting to speculate on the origins of the mobility enhancement in [14]. In that study, as in this, it was found that annealing spin-coated films of PFO at 100–140°C resulted in an increased mobility of around 10^{-3} cm^2/Vs and a reduced energetic disorder. Given the above findings, it is possible that both the reduced energetic disorder and the enhanced mobility are in this case due predominantly to the dissipation of the beta-phase, and not to benefits of the development of crystallinity. However, since we have been unable to remove beta-phase from spin-coated PFO films without also affecting the crystallinity of those films, this particular hypothesis cannot be confirmed.

How is high mobility in glassy isotropic samples possible?

The first point for discussion is how glassy samples – including glassy isotropic samples – of conjugated polymers are able to display a ToF mobility above 10^{-2} cm^2/Vs, which has been achieved only in a handful of cases [16, 36, 15]. Higher ToF mobilities in organics have been measured only in small molecule systems with LC, crystalline or semi-crystalline order [151], and higher mobilities in conjugated polymers have been achieved only in FET measurements, usually also reporting LC, crystalline or semi-crystalline order [46, 38, 68, 2]. We note, however, that there have been reports of high FET mobilities in films showing a comparably low level of macroscopic order [157, 158]. This is an indication that mobilities in polymer systems of the order 10^{-1} cm^2/Vs may not require particularly high levels of order. The fastest charge transport regime in polymeric materials is usually intra-chain, and so interactions with neighbouring chains may not need to be strong at every point along the chain to achieve high bulk mobility. Prins et al. have studied the intra-chain transport in PFO by TRMC, and have suggested a mobility of approximately 1 cm^2/Vs for transport through a single coiled (that is, disordered and non-planar) chain. This is lower than the corresponding mobility of 45 cm^2/Vs in a 'stretched' (ordered) chain, but still significantly higher than the bulk mobility of just over 10^{-2} cm^2/Vs in PFO presented here.

Thus, intra-chain transport in PFO is very fast even in the isotropic case, and is not expected to limit the bulk mobility. The limiting factor for bulk transport must therefore be inter-chain hopping. In order to explain the high mobility measured in F8:F4/1, Yap et al. invoked the concept of a small population of preferential inter-chain transfer sites with an unusually high orbital overlap. In this picture, polymer chains with high intra-chain mobility act as 'highways' to allow the effective sampling of these efficient transfer sites. We propose a similar picture of a population of preferential inter-chain transfer sites combined with fast intra-chain transport to enable high mobility bulk

charge transport. However, whereas in the paper of Yap et al. the preferential transfer sites were suggested to be linked to the particular side-chain structure of the F8:F4/1 copolymer, our results suggest that they are a feature of all the polymers studied, at least under certain processing conditions. Our suggestion is that the preferential inter-chain transfer sites occur with statistical significance amongst the randomised conformations of neighbouring polymer chains present within the bulk. The mobility of approximately 1–6 $\times$ 10^{-2} cm^2/Vs, which appears to be the maximum attainable by each of the materials studied here, may then be attributed to the transfer rate limit of the postulated preferential inter-chain transfer sites.

Why does more crystallinity mean lower mobility in polyfluorenes?

It was shown that samples with significant levels of crystallinity show a lower mobility than glassy samples of the same material; that is, charge transport suffers from an additional rate-limiting step when there are crystalline regions. Since even highly crystalline films contain a large fraction of disordered, glassy material, the preferential inter-chain transfer sites proposed above are likely to be available in all films. An explanation of the lower mobility in crystalline samples must account for this.

We propose two possible explanations for the low mobility in crystalline samples. The first proposed mechanism is that the crystallinity attainable in this system by conventional processing routes introduces new trapping species in the form of grain boundaries and structural defects. Transport within crystalline regions themselves may be very fast, perhaps faster than in glassy regions, but poor connectivity between isolated crystalline domains ensures a low macroscopic mobility. Rather similarly to the trapping mechanism involving beta-phase segments, the charges will tend to be stabilised in ordered crystalline regions, and hence will migrate towards these regions where possible. There will then be an energetic barrier for the charges to migrate back to the surrounding disordered region. If the crystalline region is not macroscopic, the charge may be unable to find a collection pathway, and will remain trapped. This can explain why film with significant crystalline material, but still a majority fraction of glassy material, may exhibit a lower mobility than a fully glassy film.

There are precedents for this adverse effect of crystallinity. Kline et al. have observed a similar phenomenon in films of P3HT, where lower molecular weight samples exhibited increased crystallinity

but reduced mobility. This was attributed to poor connectivity between crystalline domains, each smaller than the macroscopic length of transport being probed [67]. We caution that it is difficult in this case to separate the various effects of molecular weight, including varying degrees of crystallinity, changes in connectivity between crystalline domains and the influence of end groups. The adverse effect of grain boundaries was also reported by [159]. It is plausible that in the case of polyfluorenes, crystalline ordering cannot be achieved by conventional processing techniques to a sufficient level to lead to connected, macroscopic crystalline domains. In such a case, it would be favourable to eliminate crystallinity entirely by processing the film into a glassy form. The exciting prospect is then that even higher mobilities may be achievable via the two very different routes of (i) removing crystallinity more completely or (ii) increasing crystallinity to greater levels by some more effective method.

The second proposed mechanism is that crystallinity reduces the mobility not by presenting an additional trap, but by reducing the number and/or favourability of the preferential inter-chain transfer sites postulated above. In this case, the transport within crystalline regions is truly slower than in glassy regions, as a direct result of the re-orientation of neighbouring chains into the crystal structure. There remains no consensus on the crystal structure(s) of PFO, and hence there have been few attempts to calculate the intermolecular transfer integrals in the PFO phases. It is conceivable that the side-chains in polyfluorene, which protrude out of the π-conjugated plane from the sp^3-hybridised bridging carbon atom, hinder close packing of the backbone and lead only to a moderate transfer integral within a regularly ordered structure. A demonstration of this was presented by Athanasopoulos et al., where it was shown using a crystal structure based on dioctylfluorene trimers that torsional disorder between neighbours could lead, surprisingly, to a higher transfer integral than certain ordered arrangements [160]. However, this analysis was performed using a highly simplified unit cell containing only one trimer, and such an outcome is expected to become less likely as a more realistic structure is modelled.

We emphasise that our data does not offer support for either of these explanations over the other, although it may be speculated that the first proposal is more likely. We note that the molecular weight dependence of the mobility in F8:F4/1 is consistent with either explanation, reflecting either the increased tendency of the low M_w polymer to crystallise, or the reduced ability of that polymer to bridge between the most efficient inter-chain sites within the bulk. Experiments to induce higher

crystalline fractions and/or measure transport within single crystalline domains, were they to be developed, would therefore be of great interest.

4.8 Conclusions and implications

We set out to explain the mechanism of mobility enhancement in F8:F4/1 relative to PFO as first observed by Yap et al. We also hoped to build a more complete picture of the charge transport properties in the polyfluorene family. We have achieved both of these aims. The mechanism for mobility enhancement in F8:F4/1 has been shown to be a suppression of the formation of minority non-glassy phases, more precisely (i) the beta-phase conformation and (ii) the crystalline phases found in spin-coated PFO films. Spectroscopic, optical, structural and thermal measurements have shown that the shorter, branched side-chain structure in F8:F4/1 prohibits the formation of an analogous beta-phase conformation, and also strongly suppresses crystallisation. The result is a glassy isotropic film through simple spin-coating at room temperature.

Compelling evidence for this has been demonstrated by achieving the high mobility of over 10^{-2} cm^2/Vs in PFO and F8:F6 though appropriate processing. The desired microstructure has been shown, indeed, to be a uniform glassy film with sufficiently low concentrations of beta-phase and crystalline material. We have been able to fabricate PFO films with very low concentrations of beta-phase and crystallinity through careful processing at elevated temperature. Films processed in this manner have shown the highest ToF mobility achieved in PFO to date, with mobilities of over 3×10^{-2} cm^2/Vs at room temperature. Further, we have been able to re-introduce either the beta-phase or crystallinity into those films in order to study the effect of those phases in isolation. Remarkably, the presence of the beta-phase alone has been shown to reduce the mobility in a glassy film by more than two orders of magnitude. This is the first time to our knowledge that the trapping effect of a single conformational defect has been elucidated.

A point of interest is the demonstration of high mobility in glassy films with low levels of structural order. All high mobility films (those with mobilities above 10^{-2} cm^2/Vs) were shown to be in a glassy form. In some cases, the films were shown to be in a near-monodomain nematic LC phase, but in the case of PFO processed at elevated temperature, high mobility was observed in a glassy film with no indication of nematic ordering. It was shown that introducing crystallinity by conventional thermal annealing methods leads invariably to a reduction in mobility to around 10^{-3} cm^2/Vs. We hypothesise that this is due to the trapping effect of microscopic, non-percolating crystalline regions and their grain boundaries. We emphasise that no researchers have yet demonstrated mobilities in

crystalline polyfluorene films much above 10^{-3} cm^2/Vs.

The approach suggested is then to maximise the uniformity of the glass, removing isolated defects and trapping species, even if those species are highly ordered regions. We suggest that this approach may be relevant to a number of material systems where the bulk mobility has fallen many orders of magnitude short of the intra-chain mobility or the mobility found from FET mobility measurements. The observation of high mobility in glassy isotropic films offers the exciting prospect of developing high mobility materials in situations where crystallinity is undesirable, such as those requiring good luminescence properties or mechanical flexibility.

We note that there remains the possibility of improvements in mobility in the polyfluorenes by the route of improving crystallinity. Our studies indicate that the crystallinity formed by conventional routes in the polyfluorenes is highly imperfect, and new techniques of processing samples with far higher crystalline fractions would be of interest fundamentally and for application.

Nonetheless, as a final remark we suggest that the concept of high 'intrinsic' carrier mobility limited by the presence of nano-morphological phase heterogeneities – including those resulting from isolated regions of increased order and crystallinity – will be relevant to a wide range of cases. Thus, we encourage a broader approach to improving charge transport in conjugated polymers. We hope that this study emphasises the potential to increase carrier mobility in new and existing materials systems by achieving a fuller understanding of the effect on charge transport of those phase heterogeneities, and by developing methods to control their formation. This presents a new paradigm within which mobility improvements in any class of material might be achieved.

Chapter 5

Effect of energetic and configurational disorder on electron transport in the fullerene multi-adducts bis-PCBM and tris-PCBM

5.1 Summary

We have used temperature-dependent electron mobility measurements to assess whether the low electron mobility in the fullerene multi-adducts bis-PCBM and tris-PCBM relative to PCBM is due primarily to (i) the energetic disorder in LUMO energies of the isomers or to (ii) the configurational disorder in molecular packing due to the additional side-chains [26, 105]. The result is expected to inform the design of new fullerenes for state-of-the-art OPV devices.

Temperature-dependent ToF measurements were attempted on films comprising the fullerenes dispersed in an inert matrix of polystyrene. The energetic and configurational disorder parameters within the Gaussian Disorder Model (GDM) were found in a PCBM:PS blend with 33 wt% PCBM as $\sigma = 86$ meV and $\Sigma = 5.2$ respectively. ToF signals of bis-PCBM and tris-PCBM blends, however, were found to be too dispersive to allow derivation of the disorder parameters within the GDM. It was therefore not possible to assess the relative importance of energetic and configurational disorder using the ToF method.

In contrast, temperature-dependent FET mobility measurements allowed the energetic and configurational disorder of all three fullerenes to be compared. The activation energies E_a derived from an Arrhenius plot at $V_G = 40$ V increase from around 100 meV for PCBM to around 160 meV for bis-PCBM to around 300 meV for tris-PCBM. The large differences in energetic disorder suggested by the FET measurements are thus consistent with the modelling and electrochemical study of Frost et al. [114], who found differences in the LUMO levels of the multi-adduct isomers of up to several 100 meV.

Further, the electron mobilities of the three fullerenes were observed to converge in the limit $T \rightarrow \infty$ towards a single mobility value, in the range 1.5–1.9 cm^2/Vs for a fixed gate voltage of 40 V. The convergence of the mobilities in the limit $T \rightarrow \infty$ implies that the effects of variation in configurational disorder are negligible compared with the effects of variation in energetic disorder. We therefore conclude that the reduced mobility in bis-PCBM and tris-PCBM compared with PCBM is due predominantly to the effects of energetic disorder resulting from the presence of a mixture of isomers with varying LUMO energies. Where separation of the isomers is precluded, therefore, the energetic disorder in the LUMO limits the achievable transport properties of fullerene multi-adducts, and thus disadvantages their use in OPV devices. Design rules for novel OPV acceptors of any type must include a consideration of energetic disorder introduced through the production of isomers.

5.2 Scope of this Chapter

One route towards higher efficiencies in OPV is raising the open-circuit voltage V_{oc}. This may be achieved by using an acceptor material with a higher LUMO energy [161, 162], provided that there is sufficient driving force for charge separation. Since the leading acceptor material is the fullerene derivative [6,6]-phenyl-C61-butyric acid methyl ester (PCBM), recent efforts to develop alternative acceptors have focused on the use of alternative fullerene derivatives [113, 26, 163, 105, 164, 165, 166, 167]. Among these are the so-called 'fullerene multi-adducts' bis-PCBM and tris-PCBM, with two and three phenyl butyric acid methyl ester (PBM) side-chains respectively, as in Figure 5.1. Aside from a single successful case of P3HT:bis-PCBM showing increased V_{oc} and

power conversion efficiency (PCE) relative to P3HT:PCBM [113], however, OPV blends employing the multi-adducts with other donor materials have generally failed to improve upon those employing PCBM [104, 168, 169].

It has been suggested that the poor results in OPV devices with multi-adducts are due to poor electron transport properties in the blends of multi-adducts with polymers [26, 105]. Two potential causes of the poor electron transport in the multi-adducts have been proposed: (i) higher energetic disorder in the multi-adducts than in PCBM due to the presence of isomers with varying LUMO energies [26, 105] and (ii) higher configurational disorder in the multi-adducts due to a lower degree of order in molecular packing than in PCBM [105]. However, the relative importance of these two factors remains unknown.

This study is intended to assess the relative importance of energetic and configurational disorder in determining the poor electron transport properties of the multi-adducts. Since the effects of energetic disorder are diminished in the limit $T \rightarrow \infty$, whereas the effects of configurational disorder remain in this limit (as described in Section 2.1.3), we use temperature-dependent mobility measurements to distinguish between the two factors. In Section 5.4.1, we attempt temperature-dependent ToF measurements. We choose ToF since this is thought to represent the geometry and carrier density conditions in OPV devices most closely. ToF measurements require thick films, and so the fullerenes are diluted in a blend with polystyrene. The influence of the PCBM fraction on the electron mobility is studied. In the case of PCBM:PS, we are able to find the energetic and configurational disorder using temperature-dependent ToF measurements, with good agreement in both the 'normal' and 'integral' modes. However, we are ultimately unable to find the disorder parameters for bis-PCBM and tris-PCBM, even using the 'integral' mode of ToF. Possible reasons for this are discussed.

In Section 5.4.3, we therefore move on to study the electron mobility by temperature-dependent FET measurements. There has been a previous comparison of the energetic disorder in PCBM and bis-PCBM by the SCLC and FET methods [26, 170], but no successful quantification of the energetic disorder in tris-PCBM. Further, FET measurements have not previously been used to probe differences in configurational disorder in the fullerenes. We are able to compare the energetic disorder in pristine films of each of PCBM, bis-PCBM and tris-PCBM in terms of the activation

energy for transport, and compare the values with the energetic disorder predicted by Frost et al. [114]. We are also able to extrapolate the temperature-dependent mobility at fixed gate voltage towards $T \rightarrow \infty$, in order to probe differences in the configurational disorder. We find that the effects of configurational disorder appear negligible, and conclude that the differences in mobility between PCBM, bis-PCBM and tris-PCBM are predominantly due to the energetic disorder resulting from the presence of isomers with different LUMO levels. The implications of this finding for the design of new fullerenes are discussed.

The ToF data in this Chapter was collected in partnership with a Masters student, Arthur Losquin, and the FET data was collected in collaboration with John Labram and James Ball in the group of Thomas Anthopoulos at Imperial College.

5.3 Background

5.3.1 Fullerene multi-adducts with higher LUMO energies offer the potential to increase V_{oc}

One route towards higher efficiencies in photovoltaics is raising the open-circuit voltage V_{oc}. It has been shown that for polymer:fullerene bulk heterojunction organic photovoltaics (BHJ OPV) V_{oc} is strongly dependent on the LUMO and HOMO levels of the acceptor and donor material respectively [161, 162]. Hence, V_{oc} may be tuned by using different donors or acceptors, provided that there is sufficient driving force for charge separation.

Alternative acceptor materials with higher LUMO levels – offering the hope of increased V_{oc} – have recently been the subject of a significant research effort. Following the discovery of photoinduced electron transfer between polymers and C60 [171, 172] and the synthesis of soluble fullerene derivatives for use in solar cells [81, 173], fullerene derivatives have been the leading acceptor materials for BHJ OPV devices. The fullerene derivatives [6,6]-phenyl-C61-butyric acid methyl ester (PCBM) and [6,6]-phenyl-C71-butyric acid methyl ester (PC71BM), each with a single methano-bridged side-chain, have been the standard acceptors of choice for all donor polymers. PCBM is pictured in Figure 5.1. Research into alternative acceptors has focused on developing alternative fullerenes with higher LUMO levels to replace PC61BM and PC71BM [113, 26, 163, 105, 164, 165, 166, 167]. The effect on the LUMO of various chemical changes to the fullerenes have been investigated, in

particular: (i) increasing the number of side-chains, to form the so-called fullerene multi-adducts; (ii) changing the chemical structure of the atom or atoms directly connected to the C60 cage, known as the 'bridge'; and (iii) changing the chemical structure of the side-chain(s) beyond the bridge.

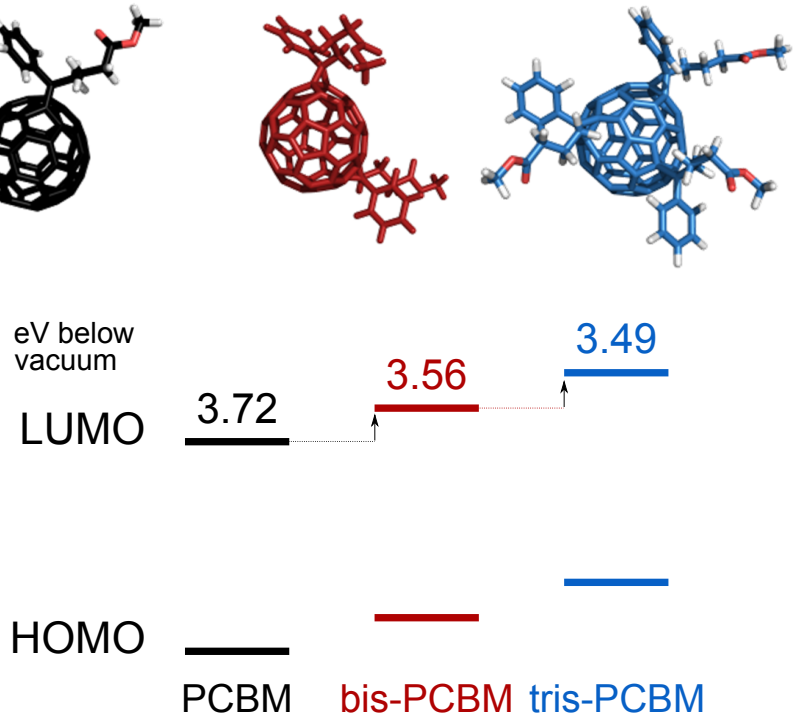

Figure 5.1: Chemical structures and energy level scheme for PCBM, bis-PCBM and tris-PCBM. LUMO values are those found by differential pulse voltammetry, taken from [114].

Frost et al. have studied the effect on the LUMO energy of each of these three strategies using time-dependent density functional theory (TD-DFT) [114, 174]. It was shown that changing the number of side-chains (that is, strategy (i) above) can lead to large increases in the LUMO energy of up to several 100 meV. For example, the addition of a second identical phenyl butyric acid methyl ester (PBM) side-chain to the PCBM molecule (to form bis-PCBM) raises the LUMO energy by around 110 meV relative to PCBM, and that the addition of a third identical PBM side-chain (to form tris-PCBM) raises the LUMO energy by around 270 meV relative to PCBM. [114]. It was found that altering the chemical structure of the bridge (that is, strategy (ii) above) can also lead to increases in the LUMO energy, though less dramatically. For example, the use of an indene bridge in place of a methano bridge was found to raise the LUMO energy by 20–40 meV. Each of these results from TD-DFT was verified by electrochemical measurement, and found to be in good agreement with experiment [114, 174]. In contrast, Frost et al. found that variations in the side-chain beyond

the bridge (that is, strategy (iii) above) do not influence the LUMO strongly. This is supported by the study of Troshin et al., who studied more than 20 different fullerene adducts with the same 'methano' bridge as PCBM but with a wide variety of side-chain structures, and found LUMO level variations (by electrochemical measurement) of less than 20 meV [175].

5.3.2 Multi-adducts may increase energetic and configurational disorder

The study of Frost et al. demonstrated another important effect of increasing the number of side-chains added to the C60 cage to produce bis-PCBM and tris-PCBM. The addition of a second PBM side-chain does not lead to a single product, but to the formation of one of a set of isomers of bis-PCBM. There is an even higher number of isomers of tris-PCBM. The presence of multiple isomers has been shown to lead to additional energetic disorder [114, 174], and may be expected to lead to additional configurational disorder. Both types of disorder may be expected to influence the charge transport properties of the material [113, 114, 105].

The increased energetic disorder in the multi-adducts versus PCBM was studied by Frost et al. [114, 174]. Their TD-DFT calculations show a range of LUMO levels of the isomers of bis-PCBM and tris-PCBM of up to several 100 meV, as shown in Figure 5.2. While the relative abundance of each isomer cannot be determined by the TD-DFT calculations, the presence of a range of LUMO levels was confirmed experimentally by DPV measurements. The width of the reduction peak observed in the DPV measurement, also shown in Figure 5.2, can be related to energetic disorder in the LUMO. The width of the PCBM peak was found to be 43±1 meV, close to the theoretical value for a reversible single-electron reduction of 38 meV [176]. Deconvolving this width from the DPV peaks for the multi-adducts allowed an estimation of the energetic disorder in LUMO level of 21±1 meV in bis-PCBM and of 51±1 meV in tris-PCBM. We note that the energetic disorder values were derived from the width of the DPV peaks using fits to a single Gaussian. It was found that the DPV peak for tris-PCBM, particular, was not well-described by a single Gaussian in the tail region. This hints towards the presence of discrete LUMO levels with energy deviating significantly from the mean. This lends support to the TD-DFT calculations which predicted variations in the LUMO for tris-PCBM of up to several 100s of meV. An energetic broadening of the density of states for electrons is expected, in the framework of Marcus theory, to increase the activation energy required for intermolecular electron transfer and therefore to lead to lower mobility at finite temperature. Changes in the DoS width of the order 20–50 meV would be significant for transport at room tem-

perature, where the thermal energy is approximately 25 meV. Isolated states up to several 100s of meV displaced from the DoS mean, if present, would have a very significant trapping effect.

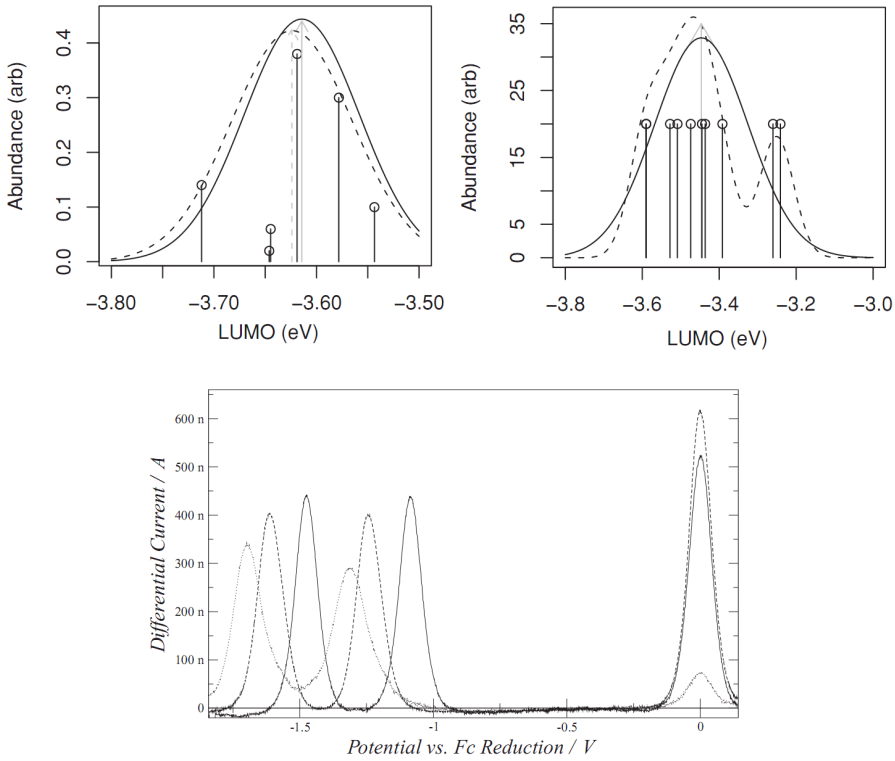

Figure 5.2: Figures reproduced from [114]. Top left: relative abundance (open circles) of bis-PCBM isomers versus the LUMO calculated from TD-DFT; superimposed Gaussian using weighted mean and variance of sampled values (full line); superimposed Gaussian using flat mean and variance from sampled values (dashed line). Top right: Calculated TD-DFT LUMO values (open circles) for the ten tris-PCBM isomers studied; superimposed Gaussian using mean and variance from sampled values (full line); superimposed convolution of the ten LUMO energies with Gaussian of σ=43 meV to simulate experimental broadening in voltammetry (dashed line). Bottom: Differential Pulse Voltammetry for PCBM (full line), bis-PCBM (dashed line) and tris-PCBM (dotted line) plotted relative to the fitted peak of the ferrocene standard reduction. See [114] for further details.

Increased configurational disorder in the multi-adducts versus PCBM may be expected by considering the molecular packing. It has been shown that for C60 the effect on mobility of disorder in molecular packing is small [177, 178, 179], but packing disorder is expected to have a much stronger effect as molecular symmetry reduces. It has been shown that PCBM in pristine films tends to form a well-ordered structure consisting of densely packed crystalline domains in random crystallographic orientation [180]. The degree of order depends upon the processing method and packing may be disrupted by the presence of other materials (such as a donor polymer), but nonetheless PCBM is able to exhibit fairly ordered and close packing. The additional side-chains of the multi-adducts may be expected to increase the average packing distance (measured between the centre of the

molecules) in two ways. Firstly, the greater volume of film taken up by the alkyl side-chains will tend to increase the average packing distance. Secondly, the variety of geometries of the isomers of the multi-adducts will tend to increase the disorder in molecular packing, which is likely to reduce packing density and increase the packing distance further. A recent study by Bouwer et al. of 'tethered' bis-PCBM, where the two PBM side-chains are in fact connected as a single unit during adduction in order to reduce the number of isomers in a single synthesis product, showed significant improvements in FF and J_{sc} versus 'untethered' bis-PCBM [181]. This supports the concept that the poor performance of multi-adducts is at least in part due to the isomeric mixture, and not to the simple presence of the additional side-chain(s). An increased separation of the conjugated parts of neighbouring molecules will lead to a decrease in wavefunction overlap of those molecules, which is expected to strongly increase the hopping time and therefore decrease the mobility. Mackenzie et al. have considered a related problem, studying the effect on mobility of increasing the length of a single side-chain attached to the C60 cage [182]. It was calculated that an increase in the intermolecular distance between two fullerenes of 1 $\mathring{A}$ can reduce the transfer rate by an order of magnitude. Disruptions in the ordering of the fullerene may therefore have an orders-of-magnitude effect on the mobility, enough to have an adverse impact on device performance.

5.3.3 OPV devices using fullerene multi-adducts usually show poor performance

PCBM, bis-PCBM and tris-PCBM show similar optical absorption and emission properties and can be processed by similar methods, and so they allow the effect of the different LUMOs to be studied directly in OPV devices. There have been a number of studies investigating the OPV performance and change in V_{oc} using fullerene multi-adducts [113, 26, 163, 105, 164, 165, 166, 167]. For example, the blend of P3HT and bis-PCBM was shown to result in a V_{oc} 150 mV higher than that of a blend of P3HT and PCBM [113]. In other studies, blends of P3HT and two other fullerene multi-adducts, bis-indene-C60 and bis-indene-C70, have been shown to produce a V_{oc} up to 250–280 mV higher than that in blends of P3HT and PC61BM and PC71BM respectively [164, 165, 183]. In these cases, the solar cell parameters J_{sc} and FF were largely unchanged, resulting in an overall increase in PCE.

However, the examples of increased PCE using bis-PCBM and bis-indene-C60 with P3HT are rare examples of the successful replacement of PCBM. No other fullerenes have shown higher overall PCE than PCBM in blends with any polymer, and even bis-PCBM and bis-indene-C60 have given lower overall PCEs in blends with polymers other than P3HT [163, 168]. Further, many groups

have been unable even to reproduce the good performance of the P3HT:bis-PCBM blend, finding a reduced J_{sc} and/or FF and a lower PCE [105, 26]. Use of tris-PCBM, the multi-adduct with three PBM side-chains, has given poor or very poor performance in blends with all polymers [105, 26, 168].

5.3.4 Fullerene multi-adducts show poor charge transport properties

In order to explain the generally poor OPV performance of multi-adducts, there have been a number of studies comparing PCBM, bis-PCBM and tris-PCBM in devices. In the study of Lenes et al. [26], a follow-up to the first publication of bis-PCBM cited above, the efficiency of P3HT:bis-PCBM devices was approximately the same as the efficiency of P3HT:PCBM devices, with the increased V_{oc} compensated by a small reduction in J_{sc}. The efficiency of P3HT:tris-PCBM devices were very poor. The group measured the electron mobility in the P3HT:multi-adduct blends using space-charge-limited current (SCLC) measurements. Fitting for a field-dependent mobility, they found zero-field electron mobilities at room temperature of just over 10^{-2} cm^2/Vs for PCBM, just over 10^{-3} cm^2/Vs for bis-PCBM and below 10^{-8} cm^2/Vs for tris-PCBM. The group attributed the lower electron mobility of the multi-adducts to shallow trapping in certain isomers with lower-lying LUMOs. The temperature dependence of the mobility was studied using an analysis based on the Gaussian Disorder Model, and energetic disorder parameters σ of 68 meV for PCBM and 94 meV for bis-PCBM were derived. The additional energetic disorder measured in bis-PCBM versus PCBM is in good agreement with the predictions of Frost et al. The low temperature electron current in the P3HT:tris-PCBM device was too low for an energetic disorder value to be derived. The group did not discuss a contribution to reduced electron mobility of increased disorder in packing or of a decrease in the orbital overlap of neighbouring fullerene molecules.

In the study of Faist et al. [105], the efficiency of P3HT:bis-PCBM devices was found to be slightly lower than that of P3HT:PCBM due to a decrease in J_{sc} and FF. P3HT:tris-PCBM devices were very poor. In order to diagnose the reductions in efficiency using multi-adducts, the group considered the effect of the additional side-chains on charge generation, blend microstructure and charge recombination. They concluded that charge generation was not significantly affected, and that the reduced performance of the multi-adducts was due to poorer charge transport properties. This was supported by FET mobility measurements performed on pristine films of the fullerenes, giving electron mobilities of 4.0×10^{-2} cm^2/Vs for PCBM, 2.7×10^{-3} cm^2/Vs for bis-PCBM and 5.5×10^{-6} cm^2/Vs for tris-PCBM. They attributed the reduction in electron mobility both to energetic disor-

der due to the isomeric mixture and to configurational disorder in the fullerene phase due to the steric hindrance of the side-chains.

For completeness, we note that Azimi et al. have recently studied blends of PCBM and bis-PCBM with a different polymer, Si-PCPDTBT [163, 104, 184]. The worse performance of the blend with bis-PCBM in this case was also attributed to a reduction in electron mobility.

It should be noted that considerations of the blend microstructure – and not only the donor and acceptor properties in isolation – are critical to the behaviour of OPV devices. Guilbert et al. have studied the microstructure and phase behaviour of blends of P3HT and PCBM, bis-PCBM and tris-PCBM. Using DSC measurements, the group found that blends of P3HT with each of the multi-adducts showed a eutectic composition with a lower polymer fraction (higher fullerene fraction) and a lower eutectic temperature than blends of P3HT and PCBM. This was attributed to weaker P3HT-fullerene interactions and to a lower fullerene melting temperature for the multi-adducts. It was suggested that the polymer:fullerene ratios typically used in OPV devices would therefore be hyper-eutectic with respect to polymer content for blends with the multi-adducts, where the ratios are typically hypo-eutectic for blends with PCBM. A hypo-eutectic composition with respect to polymer content has previously been identified as necessary for the formation of an efficient electron transporting network of fullerene crystallites [185]. Hence, the different phase behaviour may be another factor which in part explains the worse transport properties and reduced performance of OPV devices based on the multi-adducts. Nonetheless, the FET mobility measurements on pristine films described above suggest that poor electron transport is an intrinsic property of the fullerenes and not only a property of the blend morphology.

5.4 Results and Discussion

5.4.1 Time-of-flight electron mobility measurements

We initially attempted to study the electron mobility in fullerenes using the time-of-flight (ToF) method. As described in Section 2.2.1, ToF requires films much thicker than the absorption depth of the material, which in practice means thicker than approximately 1 μm. Practical measurement of the high mobility in pristine PCBM would perhaps require films even thicker than 1 μm. Films of this thickness consisting only of PCBM are difficult to fabricate, usually non-uniform and me-

chanically unstable. Following previous work, such as that of Tuladhar et al. [101, 186], we took the approach of dispersing the fullerene in an inert 'matrix' polymer, polystyrene (PS). This allowed the fabrication of uniform, mechanically stable films with thickness > 1 μm.

It was found that using PCBM fractions higher than 40 wt% led to very non-uniform films as a result of aggregation of the fullerene phase, as shown in Figure 5.3. Hence, the ToF measurements were taken using blends with PCBM fractions below 40 wt%.

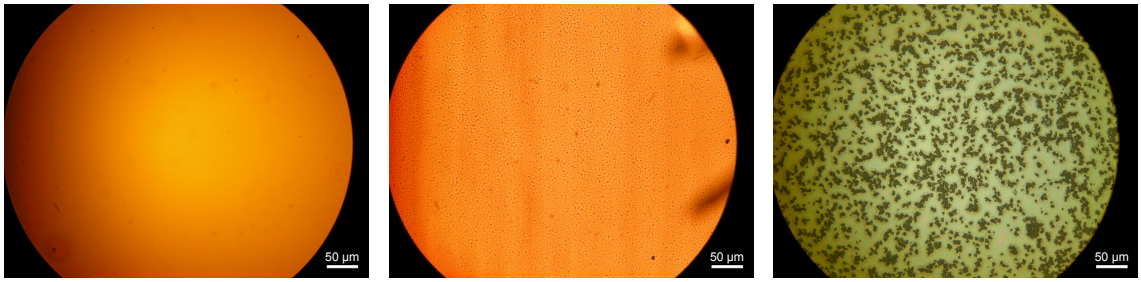

Figure 5.3: Optical images of PCBM:PS blends with 33 wt% PCBM (left), 40 wt% PCBM (centre) and 50 wt% PCBM (right). The scale bars are 50 μm.

Figure 5.4 shows the derived mobilities and sample ToF transients for a series of PCBM:PS blends with PCBM fractions between 10 wt% PCBM and 40 wt% PCBM. The mobility value for pristine PCBM as derived from SCLC in Chapter 6 is also shown. The presence of the matrix polymer reduces the mobility relative to the value for pristine PCBM. This can be attributed largely to the increased average separation of neighbouring fullerene molecules, decreasing the electronic wave-function overlap and reducing the intermolecular transfer rate. The mobility is strongly dependent on the fraction of PCBM in the film. It can be seen that below around 30–40 wt% PCBM the samples exhibit extremely dispersive transport. For these blends, the estimated transit time has a large uncertainty. For the films with 33 wt% PCBM and 40 wt% PCBM, the transit time is clearer, although the transients remain dispersive. The electron mobility falls from close to 10^{-4} cm^2/Vs for 40 wt% PCBM to below 10^{-6} cm^2/Vs for 10 wt% PCBM.

Figure 5.5 shows further ToF data from a 1.5 μm thick blend film of PCBM:PS with 33 wt% PCBM. Transients are given for a range of electric field values, along with a plot of the field dependence of the mobility. It can be seen that the field dependence of the mobility is negative. A negative field dependence is observed in systems with a very high level of configurational disorder, when configu-

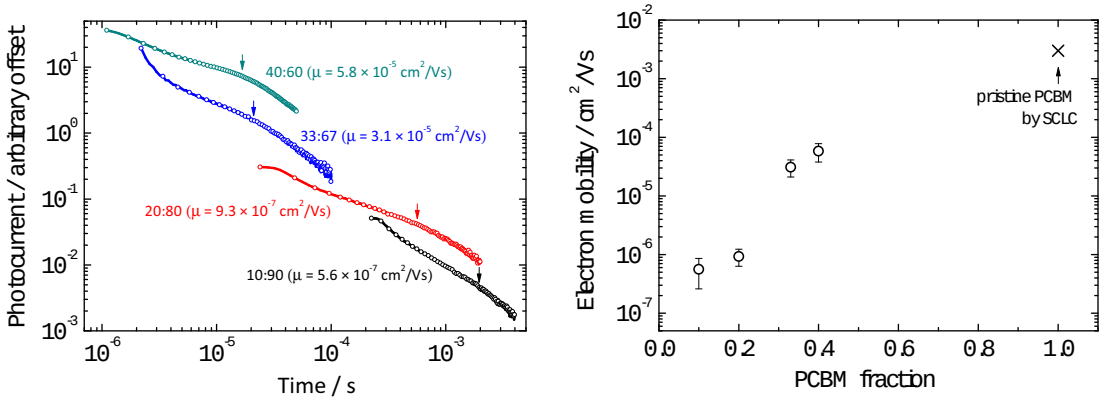

Figure 5.4: Left: ToF transients for blends of PCBM:PS with 40 wt% PCBM (green, 170 V, 4.1 μm); 33 wt% PCBM (blue, 130 V 2.9 μm); 20 wt% PCBM (red, 180 V, 3.0 μm); 10 wt% PCBM (black, 180 V , 4.2 μm). The transit times extracted by fitting asymptotes by eye are marked by arrows. Right: electron mobility in PCBM:PS films as a function of the weight fraction of PCBM. Circles correspond to values found by the ToF method as described in the text; the cross corresponds to the value found in pristine PCBM by the SCLC method. The error bars represent upper and lower limits to the mobility based on fitting to the dispersive transients.

rational disorder dominates energetic disorder (within the GDM where $\Sigma > \sigma/kT$). A negative field dependence of electron mobility in PCBM:PS was also reported by Tuladhar et al. [101]. In Monte Carlo modelling of electron transport in fullerenes with different length alkyl side-chains, Mackenzie et al. [182] saw an increasingly negative field dependence along with a decrease in mobility for longer side-chains. It is important to note that there may be a contribution to the observed negative field dependence related to the extraction of transit times from highly dispersive transients. This effect has been described by Frost et al. [187]. The standard method of deriving the transit time as the intersection of the short-time and long-time linear asymptotes in a log-log plot has been shown to lead to an underestimation of the transit time in dispersive transients as compared with the same process applied to non-dispersive transients. It is therefore likely that the low field mobilities (where transients are most dispersive) are overestimated. We note, however, that a negative field dependence was also observed on the PCBM:PS device when the mobilities were found using the 'integral mode' of ToF (see below in Section 5.4.2), which should not be susceptible to a similar fitting bias. Therefore, we suggest that the negative field dependence is due at least in part to a high level of spatial disorder in the film.

As described above, the highly dispersive transients suggest that the fullerene and polymer are closely inter-mixed in the film. The optical image of the 33 wt% PCBM (PCBM:PS) film in Figure 5.3, showing no aggregates of the fullerene on the 1–10 μm scale, suggests that this is the case. The

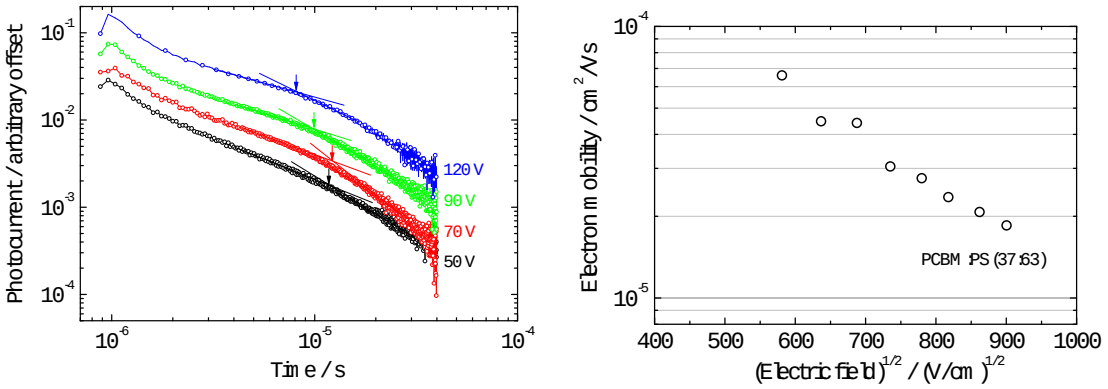

Figure 5.5: Left: selected ToF transients of the 33 wt% PCBM PCBM:PS blend film at various applied fields. The film thickness is 1.5 μm. Right: Poole-Frenkel plot for the same device.

close inter-mixing of the fullerene and polymer were confirmed by TEM imaging. Figure 5.6 shows two TEM images of PCBM:PS with 33 wt% PCBM corresponding to 20kx and 120kx magnification. There appear to be polymer-rich and fullerene-rich regions, but the two materials are clearly seen to be inter-mixed at the scale of tens of nm or less.

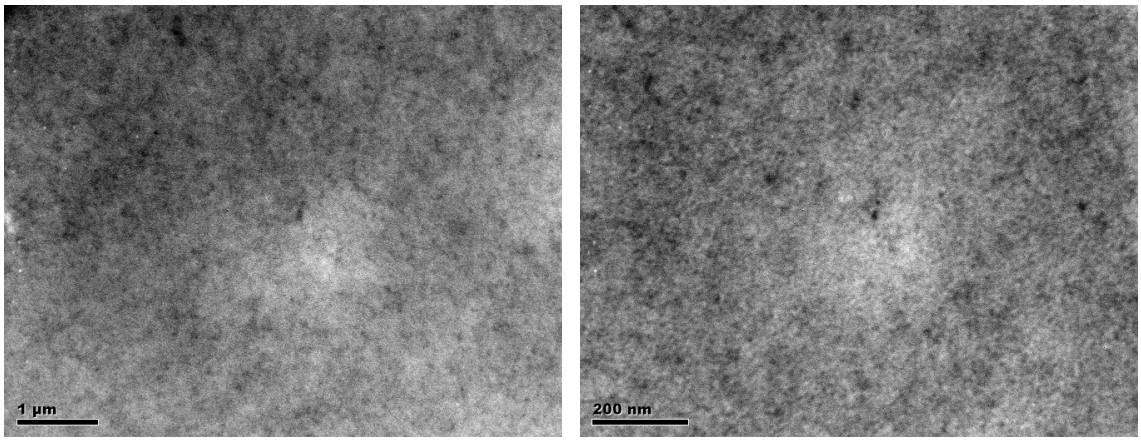

Figure 5.6: TEM images of the 33 wt% PCBM PCBM:PS blend film, with magnification of 20kx (left, scale bar 1 μm) and 120kx (right, scale bar 200 nm).

5.4.2 Energetic disorder by temperature-dependent time-of-flight

We studied the energetic disorder of the PCBM:PS with 33 wt% PCBM film by temperature-dependent ToF. Figure 5.7 shows a series of transients taken at different temperatures, each in an applied field of 7×10^5 V/cm. Temperature- and field-dependent mobility values are shown in Figure 5.8. The data can be fitted to the GDM by plotting the logarithm of the mobility against the inverse square temperature as shown in Figure 5.9. This analysis results in an energetic disorder value σ

= 86 meV. To our knowledge this is the first quantification of the energetic disorder parameter in blends of PCBM and PS, but similar values for the energetic disorder for electron transport in pristine PCBM and in blends of PCBM with other polymers have been reported. Mihailetchi et al. derived a value of 73 meV using SCLC measurements on pristine PCBM [188]; Lenes et al. reported a value of 68 meV using SCLC measurements on a blend of PCBM:P3HT (50 wt% PCBM) [26]; Tuladhar et al. found a value of 76 meV using ToF measurements on a blend of PCBM:MDMO-PPV (67 wt% PCBM) [186].

The plot of mobility against the inverse square temperature also leads to a derivation of the zero-field infinite-temperature mobility value μ_0, as in the GDM. Our measurements on a 33 wt% PCBM PCBM:PS film lead to a μ_0 value of 2×10^{-2} cm^2/Vs. In the studies listed above, Mihailetchi et al. derived a value for μ_0 by the same method, finding a value of approximately 3×10^{-2} cm^2/Vs and 10^{-1} cm^2/Vs for pristine PCBM and Tuladhar derived a value of 2.5×10^{-1} cm^2/Vs for 67 wt% PCBM PCBM:MDMO-PPV. The lower value found in our study than in the study of Tuladhar (both using ToF) may be due to the reduced PCBM fraction in our study, which is likely to increase the average nearest-neighbour distance. The spatial disorder parameter Σ was calculated to be 5.2, significantly higher than the value found by Tuladhar, equal to 2.5. This may also be attributed to the lower PCBM fraction and a larger variation in the nearest-neighbour distance. The lower value of Mihailetchi compared with that of Tuladhar may be explained by the fact that the ToF mobility is determined largely by the fastest carriers, and may in general be higher than the SCLC mobility, which is a mobility-weighted average over all carriers.

It was hoped that similar temperature-dependent ToF measurements on blends of PS with bis-PCBM and tris-PCBM could be used to find the energetic and configurational disorder and zero-field infinite-temperature mobility of the multi-adducts. As will be described in the next section, however, it was not possible to fit the bis-PCBM:PS or tris-PCBM:PS data to the GDM. Nonetheless, the attempts to obtain these data led to a useful result regarding the equivalence of the 'current' and 'integral' modes of ToF. For this reason, the attempts are outlined briefly in the next section.

Transport in bis-PCBM:PS and tris-PCBM:PS too dispersive to measure mobility

It was attempted to repeat the above analysis as performed on PCBM:PS by measuring the mobility in blends of the multi-adducts with PS. In order to give the best comparison, the fullerene

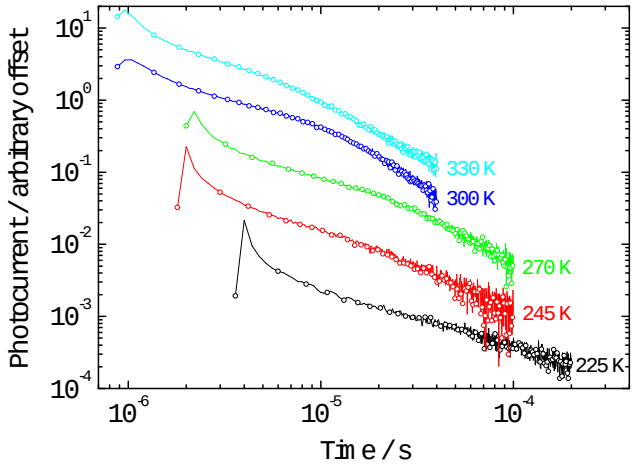

Figure 5.7: Selected ToF transients of the 33 wt% PCBM PCBM:PS blend film at a fixed field of 7×10^5 V/cm at various temperatures.

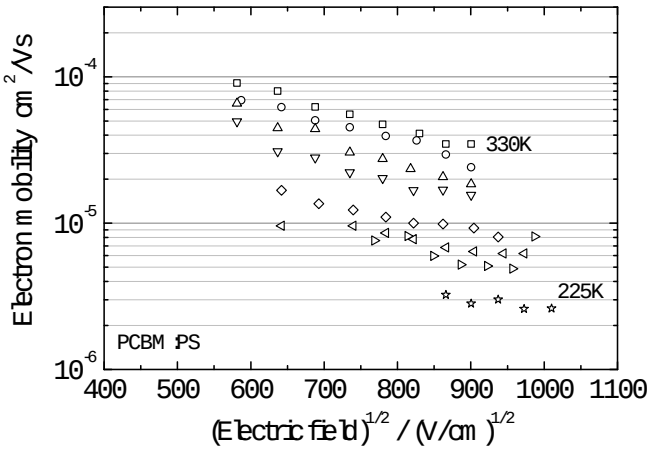

Figure 5.8: Poole-Frenkel plots for the electron mobility in the device in Figure 5.7 at 330K (squares); 315K (circles); 300K (up triangles); 285K (down triangles); 270K (diamonds); 255K (left triangles); 245K (right triangles); 225K (stars).

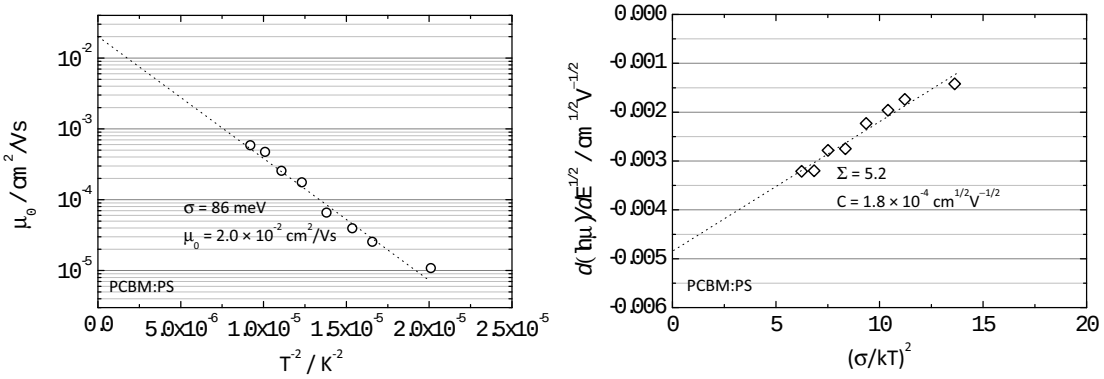

Figure 5.9: Left: Plot of zero-field mobility μ_0 versus T^{-2} to extract σ from the data within the GDM. Right: Plot to extract Σ from the data within the GDM.

fractions for the multi-adducts were adjusted relative to the PCBM fraction such that the weight fraction of conjugated C60 units remained constant across the blends of the different fullerenes. The intention was to allow the effects under study, the configurational and energetic disorder, to dominate. Fixing the weight fraction of C60 units fixes the average separation of C60 units with the assumption of uniform dispersion of all fullerenes and a constant overall density. This removes the simple effect of the lower C60 fraction in the multi-adducts, but does not address the potential effect of reduced density in the multi-adducts due to disorder in molecular packing. To compare with a PCBM content of 33 wt %, the appropriate content of bis-PCBM is 44 wt% and that of tris-PCBM is 52 wt%.

Figure 5.10 shows a typical room temperature transient of a 44 wt% bis-PCBM blend of bis-PCBM:PS, taken at 70 V using a 1.4 μm thick film. The transient is significantly more dispersive than those for PCBM:PS, and it is not possible even at high applied fields to observe the transit time 'knee' to derive a mobility value. Transients of 52 wt% tris-PCBM tris-PCBM:PS films were similar.

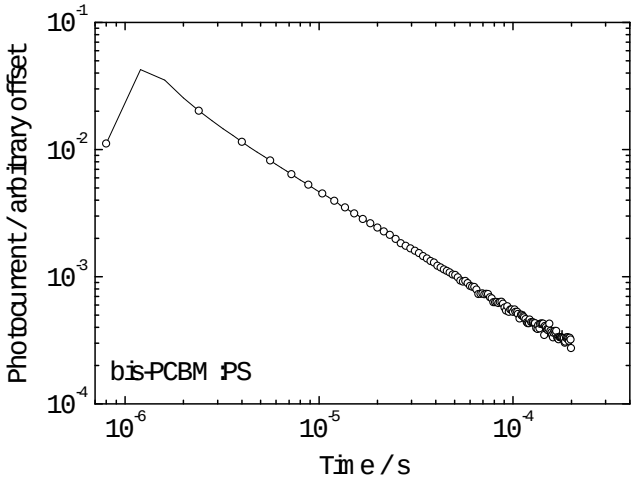

Figure 5.10: ToF transient of 44 wt% bis-PCBM bis-PCBM:PS blend film (70 V, 1.4 μm).

In Section 2.2.1, the 'integral mode' of ToF was outlined. This measurement allows the derivation of the transit time and mobility in the case of highly dispersive transients by electronically integrating the photocurrent signal and timing the collection of charge (usually taking the time for half of the charge to be collected as the 'transit time'). It was therefore deemed appropriate to use the integral mode to find the mobility of the bis-PCBM:PS and tris-PCBM:PS blends. To the best of our knowledge, however, there has been no quantitative comparison of field- and temperature-dependent

measurements taken using the integral mode and the normal 'current mode' of ToF. In fact, there are relatively few examples of the use of the integral mode to quantify mobility [189, 190, 63, 191]. It is therefore of general interest first to test the applicability of the integral mode by using it to repeat the GDM analysis for PCBM and comparing the result with the result found using the current mode, as above.

Integral mode results consistent with normal mode for PCBM:PS

Figure 5.11 shows a typical integral mode transient for a film of PCBM:PS, plotted twice on different time scales to show the short-time and long-time integrated current signals. The field- and temperature-dependent mobility data for PCBM taken using the integral mode of ToF are shown in Figure 5.12. Figure 5.13 shows fits to the GDM. The corresponding data taken using the current mode are given alongside this. It can be seen that the integral mode data are consistent with the current mode data, reproducing the field-dependences closely over all temperatures. The derived σ of 77 meV is close to the current mode value of 86 meV. The zero-field infinite-temperature mobility is approximately twice the size of the value derived from the current mode, which likely reflects a systematic offset of the transit time as derived from the different modes (for dispersive transients).

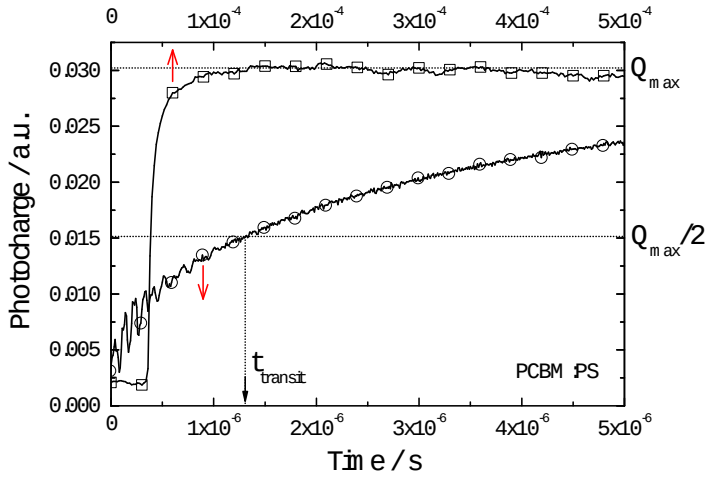

Figure 5.11: Example integral mode transient, showing the derivation of the transit time $t_{transit}$. The transient is plotted on two timescales to show the short-time (circles, bottom x-axis) and long-time (squares, top x-axis) integrated current signal. The maximum of the long-time signal is taken as the total charge collected at infinite time Q_{max}. The time at which half of this charge has been collected is then found on the short-time signal, and used as $t_{transit}$.

The consistency of the field and temperature dependence of the mobility data for PCBM:PS taken

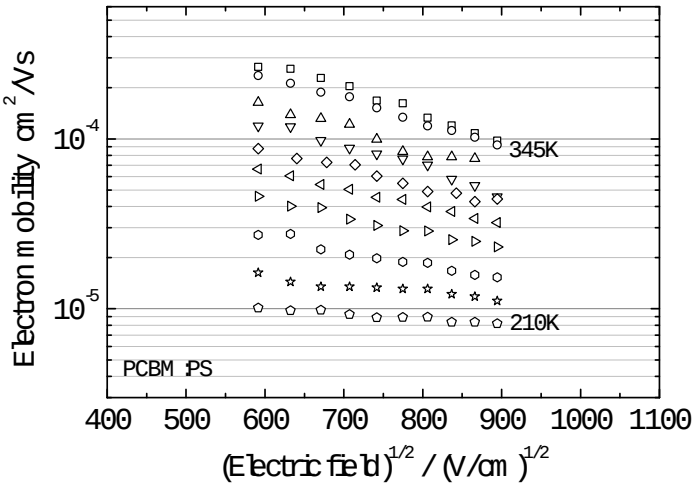

Figure 5.12: Poole-Frenkel plots for the integral mode electron mobility of PCBM:PS (33 wt% PCBM) film at 345K (squares); 330K (circles); 315K (up triangles); 300K (down triangles); 285K (diamonds); 270K (left triangles); 255K (right triangles); 240K (hexagons); 225K (stars); 210K (pentagons).

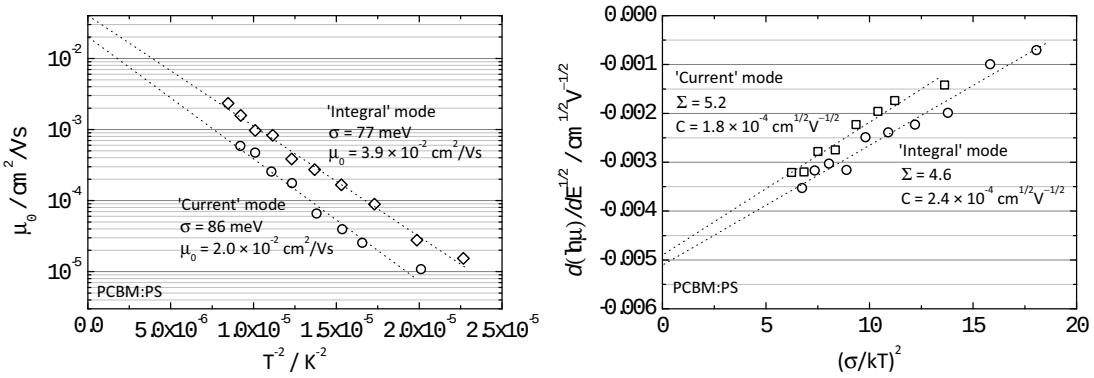

Figure 5.13: Comparison of data for 'current' and 'integral' models for PCBM:PS (33 wt% PCBM). Left: data plotted to derive σ. Right: data plotted to derive Σ.

with the integral and current modes of ToF suggests that the integral mode should give an accurate reflection of the transport properties in the other multi-adducts. We therefore attempt a GDM analysis of the multi-adducts using the integral mode.

GDM fitting not possible for bis-PCBM:PS and tris-PCBM:PS data

Figure 5.14 shows the field- and temperature-dependence of the electron mobility in bis-PCBM:PS (44 wt% bis-PCBM) and tris-PCBM:PS (52 wt% tris-PCBM), and the plots used for fitting within the GDM, with the fits for PCBM:PS shown for comparison. It can be seen, surprisingly, that the temperature dependence of the mobility of bis-PCBM:PS is weaker than for the PCBM:PS blend, and that there is almost no temperature dependence in the case of tris-PCBM:PS. In fact, that there is no acceptable fit to the GDM for either bis-PCBM:PS or tris-PCBM:PS. Neither the μ_0

versus T^{-2} plot nor the $d(ln\mu)/d\sqrt{E}$ versus T^{-2} plot is compatible with a fit to a GDM parameter.

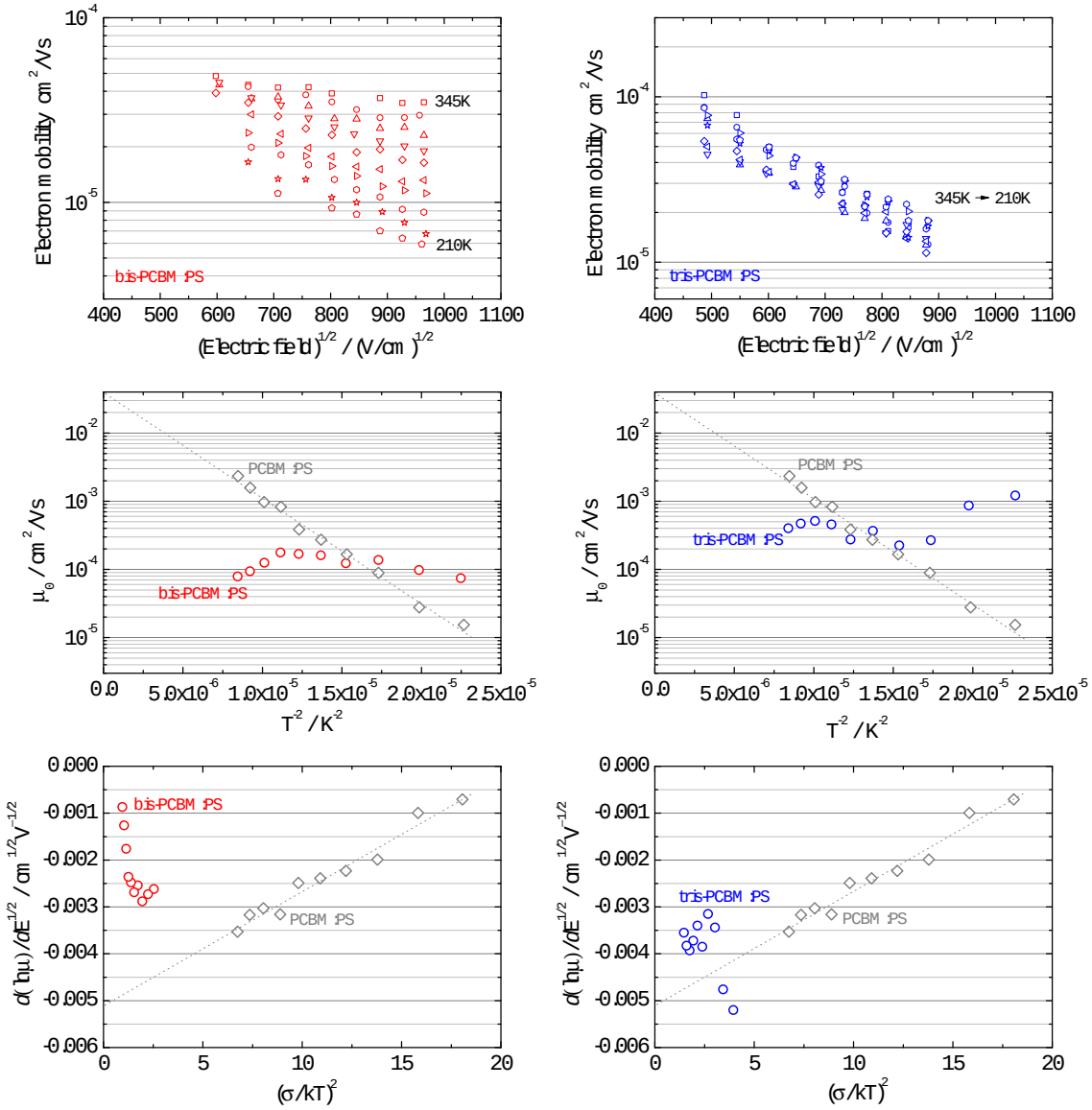

Figure 5.14: Top: Poole-Frenkel plots for the integral mode electron mobility in 44 wt% bis-PCBM bis-PCBM:PS film (left) and the 52 wt% tris-PCBM tris-PCBM:PS film (right). Curves are shown at 345K (squares); 330K (circles); 315K (up triangles); 300K (down triangles); 285K (diamonds); 270K (left triangles); 255K (right triangles); 240K (hexagons); 225K (stars); 210K (pentagons). Middle: Data plotted to derive σ for bis-PCBM:PS (left) and tris-PCBM:PS (right), with the data for PCBM:PS for comparison. No fit is shown for the bis-PCBM:PS or tris-PCBM:PS data. Bottom: Data plotted to derive Σ for bis-PCBM:PS (left) and tris-PCBM:PS (right), with the data for PCBM:PS for comparison. No fit is shown for the bis-PCBM:PS or tris-PCBM:PS data.

It is not known why the data for bis-PCBM:PS and tris-PCBM:PS do not fit the GDM, or similarly why the temperature dependence of the mobility for those blends is so weak. The experiment was repeated, and very similar results obtained. However, we may speculate on two broad possibilities. First, it may be the case that the integral mode, despite reproducing the results for PCBM very

closely, does not reflect the true transport properties in the case of bis-PCBM and tris-PCBM. The disadvantage of the method is that integrated transients are featureless and hence it cannot be confirmed that they represent ToF transport rather than some other transient phenomenon (such as dielectric relaxation). Second, it may be that in the regime of extremely dispersive transport as observed here for the bis-PCBM and tris-PCBM samples, the concept of average mobility is not a well-defined or meaningful quantity. In that case, even if the integral method reflects the dispersive transport accurately, the mobility represented by the time for half of the total charge to be collected may not change with field and temperature in the same way that the mobility calculated in less dispersive cases changes. Attempts to fit to the GDM or other models developed to describe well-behaved transport properties would then fail.

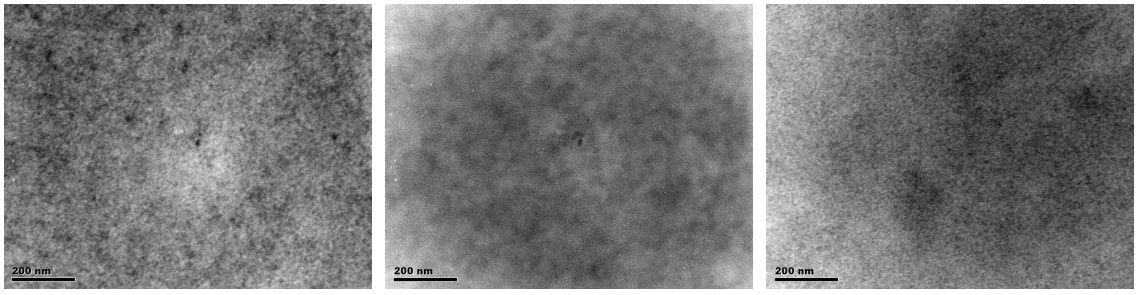

Figure 5.15: TEM images of the PCBM:PS (left), bis-PCBM:PS (centre) and tris-PCBM:PS (right) blend films, at a magnification of 20kx. The scale bar is 200 nm.

The physical reasons for either of these cases appear to be related to the very poor transport properties of the samples. It may be that blending the materials in the matrix polymer leads to a very unfavourable blend morphology without percolating pathways in the fullerene between the electrodes. In this case the time-of-flight signals may be totally dominated by electron trapping. We note that there has been an observation of increased phase separation in blends of the multi-adducts with another amorphous polymer, TFB [192]. We should note, however, that TEM images of bis-PCBM:PS and tris-PCBM:PS, as shown in Figure 5.15, do not give clear support for this, and appear to show roughly similar degrees of phase separation for the three fullerenes.

In any case, it was not possible to quantify the energetic and configurational disorder in the multi-adducts by the ToF method. We were therefore unable to address the question of whether energetic or configurational disorder is the primary reason for the poor electron transport properties. We therefore move on to consider FET measurements as a probe of the effect of energetic and configu-

rational disorder on electron transport.

5.4.3 Field-effect transistor electron mobility measurements

FET measurements have previously been used to successfully measure the mobility of all of the fullerene multi-adducts at room temperature. Temperature-dependent FET measurements have previously been performed on PCBM (and PC70BM) and bis-PCBM [193, 170], but not on tris-PCBM. The results have not previously been used to compare energetic and configurational disorder for any of the fullerenes.

FET measurements may be expected to succeed where the ToF measurements failed for two main reasons. Firstly, since the FET mobility may be derived from films less than 100 nm in thickness, pristine fullerene films may be used without the need for a matrix polymer. Secondly, derivation of the FET mobility does not require non-dispersive transport, as it is based on the magnitude of the steady-state current flow rather than on a transient feature. Hence, we expect that the FET method should not be subject to the limitations of the ToF method as discussed above. The disadvantages of the FET method are that the geometry of transport and charge carrier density are not representative of OPV devices. However, for a fundamental study of the effects of configurational and energetic disorder on transport in the fullerenes, the FET method should be suitable.

We first verify the trend of decreasing mobility with increasing number of adducts at room temperature. Figure 5.16 shows output and transfer characteristics of top-gate bottom-contact FETs of the three fullerenes measured at room temperature. Figure 5.17 shows the room temperature electron mobilities of the fullerenes in the linear regime at $V_G = 30$ V. The values are in good agreement with the literature [105]. PCBM shows a mobility of 5×10^{-2} cm^2/Vs, bis-PCBM a mobility of 3×10^{-3} cm^2/Vs and tris-PCBM a mobility of 3×10^{-5} cm^2/Vs.

5.4.4 Separating energetic and configurational disorder using temperature-dependent FET measurements

The energetic and configurational disorder in the materials was examined using temperature-dependent FET mobility measurements. As discussed in Section 2.1.3, the effects of energetic and configurational disorder may, in general, be separated by considering the limiting mobility as

T $\rightarrow \infty$. At this limit, the effects of energetic disorder are diminished, and only the effects of configurational disorder remain. Extrapolating a temperature-dependent set of data towards T $\rightarrow \infty$ should thus provide insight into the dominant effect behind the low electron mobility in the multi-adducts.

Organic FETs at sufficiently high temperature typically show activated behaviour of the mobility μ of the Arhennius form:

$$ln\mu = -\frac{E_a}{k_B T} + ln\mu_0$$

with infinite-temperature mobility μ_0 and characteristic activation energies E_a of 10s to 100s meV. The Arrhenius temperature dependence has been observed for the electron mobility in fullerenes in both FET and SCLC experiments [193, 194, 170]. As discussed in Section 2.1.5, the Arrhenius form follows both from hopping in an exponential tail of the DoS and from hopping within a Gaussian DoS at sufficiently high charge carrier density [22]. It is sufficient for our purposes to note that this form is not incompatible with the GDM as used in the analysis of the ToF data, but rather that is represents a more accurate approximation in the conditions of high carrier density likely to prevail during the FET measurement.

It has previously been suggested that a measure of the energetic disorder in a sample may be found by a consideration of both the magnitude of the activation energy E_a extracted from the Arhennius plot of the mobility data and the rate of change of E_a with gate voltage [170]. This argument is based on the observation that E_a is a function of the average energy required for an electron to hop between neighbouring transport sites. Assuming sufficient temperature for sampling of the DoS around the transport energy, E_a is therefore a function of the width of the Gaussian DoS (for a Gaussian DoS) or of the charateristic energy of the exponential tail of the DoS (for an exponential DoS). In FETs, E_a is commonly observed to reduce with increasing gate voltage. This is understood by considering the increase in the Fermi level E_F as the gate voltage increases and a higher charge carrier density is induced. Then, more states become thermally accessible and the average activation required for hopping reduces. The rate of decrease of E_a with gate voltage depends on the width of the Gaussian DoS (for Gaussian DoS) or the characteristic energy of the exponential tail of the DoS (for an exponential DoS), with a broader DoS leading to a higher rate of decrease

of E_a. Therefore, a system with higher energetic disorder is expected to show both a larger E_a and a higher rate of decrease of E_a with increasing gate voltage.

Figure 5.18 shows the FET mobility over a range of gate voltages V_G and temperatures, and the activation energy E_a of the mobility calculated from the slope of the mobility versus temperature plots as a function of V_G. It can be seen that E_a^{tris} ranges from 190 to 360 meV as V_G decreases from 80 V to 30 V. E_a^{bis} ranges from 155 to 180 meV as V_G decreases from 50 V to 25 V. E_a^{mono} ranges from 100 to 110 meV as V_G decreases from 45 V to 20 V. It is clear then that E_a increases in the order $E_a^{mono} < E_a^{bis} < E_a^{tris}$. In agreement with this, the rate of decrease of E_a with V_G increases in the same order. E_a and its rate of decrease with V_G are particularly high in the case of tris-PCBM.

It is also important to note, for comparison with photovoltaics where charge density is low, that the more relevant regime is that of low V_G. For low V_G, E_a for tris-PCBM rises very steeply. This data therefore gives strong evidence for a significant increase in energetic disorder in bis-PCBM relative to PCBM, and a large increase in energetic disorder in tris-PCBM relative to PCBM and bis-PCBM. The additional energetic disorder relative to PCBM of the order 50–70 meV for bis PCBM and 100–250 meV for tris-PCBM, are roughly consistent with the energetic disorder predicted to result from the range of isomer LUMOs by Frost et al. using TD-DFT, as in Figure 5.2 [114].

Figure 5.18 also shows the extrapolation of the FET mobility data to infinite temperature ($1/T \rightarrow 0$) for $V_G = 40$ V (for PCBM, bis-PCBM and tris-PCBM) and $V_G = 25$ V (for PCBM and bis-PCBM). It can be seen that at $V_G = 40$ V the infinite-temperature mobility μ_0 is approximately equal (in the range 1.5–1.9 cm^2/Vs) for all three fullerenes. At $V_G = 25$ V, where there is no data for tris-PCBM due to the low mobility, μ_0 is approximately equal (in the range 3.5–4.1 cm^2/Vs) for PCBM and bis-PCBM. This tells us that for fixed gate voltage, μ_0 is essentially equal for all three fullerenes. This suggests that essentially the entire difference in mobility at finite temperature is due to the effects of energetic disorder, which is diminished at high temperature. The effects of configurational disorder, which remain at high temperature, appear much less important. This is therefore strong evidence that the differences in mobility between PCBM, bis-PCBM and tris-PCBM are overwhelmingly due to the energetic disorder resulting from the mixture of isomers with different LUMO levels. No significant effect on the mobility of configurational disorder relating to

less dense and disordered molecular packing in the fullerene phase is observed.

5.5 Conclusions

In summary, we have used temperature-dependent ToF and FET measurements to assess the relative importance of energetic and configurational disorder in determining the poor electron transport properties of the fullerene multi-adducts bis-PCBM and tris-PCBM. Poor electron transport properties have previously been suggested as the primary reason for the poor performance of the multi-adducts in OPV devices [26, 105]. The same studies have proposed that the poor electron transport properties may be due to one or both of the following sources of disorder: (i) higher energetic disorder in the multi-adducts versus PCBM due to the presence of a mixture of isomers with varying LUMO energies and (ii) higher configurational disorder in the multi-adducts due to increased disorder in the molecular packing. However, the relative importance of these two factors has not until now been investigated.

ToF measurements were performed on blends of the fullerenes with the inert matrix polymer polystyrene, which was necessary to ensure optically thick films. Temperature-dependent ToF measurements on a 33 wt% PCBM PCBM:PS blend were used to derive energetic and configurational disorder parameters within the GDM of $\sigma = 86$ meV and $\Sigma = 5.2$ respectively. ToF signals of bis-PCBM and tris-PCBM blends, however, were found to be too dispersive to allow derivation of the mobility by the current mode. The ToF integral mode was therefore employed. However, despite the integral mode closely reproducing the field- and temperature-dependent mobility data for PCBM, it did not allow the energetic and configurational disorder parameters to be derived for bis-PCBM or tris-PCBM. The reasons for this are not understood, but it appears that it is a result of a very high degree of charge trapping in the multi-adduct:PS blends. In any case, it was not possible from the ToF studies to determine the dominant cause of the low mobility in the multi-adducts.

In contrast, temperature-dependent FET mobility measurements allowed the energetic and configurational disorder of all three fullerenes to be studied. The large spread in transport properties of the fullerenes at room temperature observed in the literature [105] was reproduced, with mobilities of 5×10^{-2} cm^2/Vs cm2/Vs, 3×10^{-3} cm^2/Vs and 3×10^{-5} cm^2/Vs found for PCBM, bis-PCBM and tris-PCBM respectively. Temperature- and gate voltage-dependent measurements were able to provide gate voltage-dependent activation energies E_a for all three fullerenes. By considering both E_a and the rate of change of E_a with gate voltage V_G as measures of the energetic distribution of

localised states, the levels of energetic disorder in the fullerenes were compared. It was found that tris-PCBM exhibited the largest energetic disorder by some margin. At a fixed gate voltage V_G = 40 V, E_a^{tris} = 300 meV, E_a^{bis} = 160 meV and E_a^{mono} = 100 meV. The rate of change of E_a with V_G was found to decrease in the same order. The large differences in energetic disorder suggested by the FET measurements are consistent with the modelling and electrochemical study of Frost et al. [114], who found differences in the LUMO levels of the multi-adduct isomers of up to several 100 meV.

An extrapolation of the FET mobility data at fixed gate voltage V_G = 40 V showed that as $T \to \infty$ the differences in the mobility of the three fullerenes diminishes. At V_G = 40 V, all three fullerenes showed an infinite-temperature mobility μ_0 in the range 1.5–1.9 cm^2/Vs – equal within the experimental error. The effect on mobility of the variation in configurational disorder, which remains at high temperature, thus appears negligible. This is therefore strong evidence that the differences in mobility between PCBM, bis-PCBM and tris-PCBM at room temperature are predominantly due to the energetic disorder resulting from the presence of isomers with different LUMO levels. No significant effect on the mobility of a variation in configurational disorder in the fullerene phase has been observed. Where separation of the isomers is precluded, therefore, the presence of isomers with different LUMO levels presents a strict limit on the achievable transport properties of fullerene multi-adducts, and thus on their use in OPV devices. Design rules for novel OPV acceptors of any type must include a consideration of energetic disorder introduced through the production of isomers.

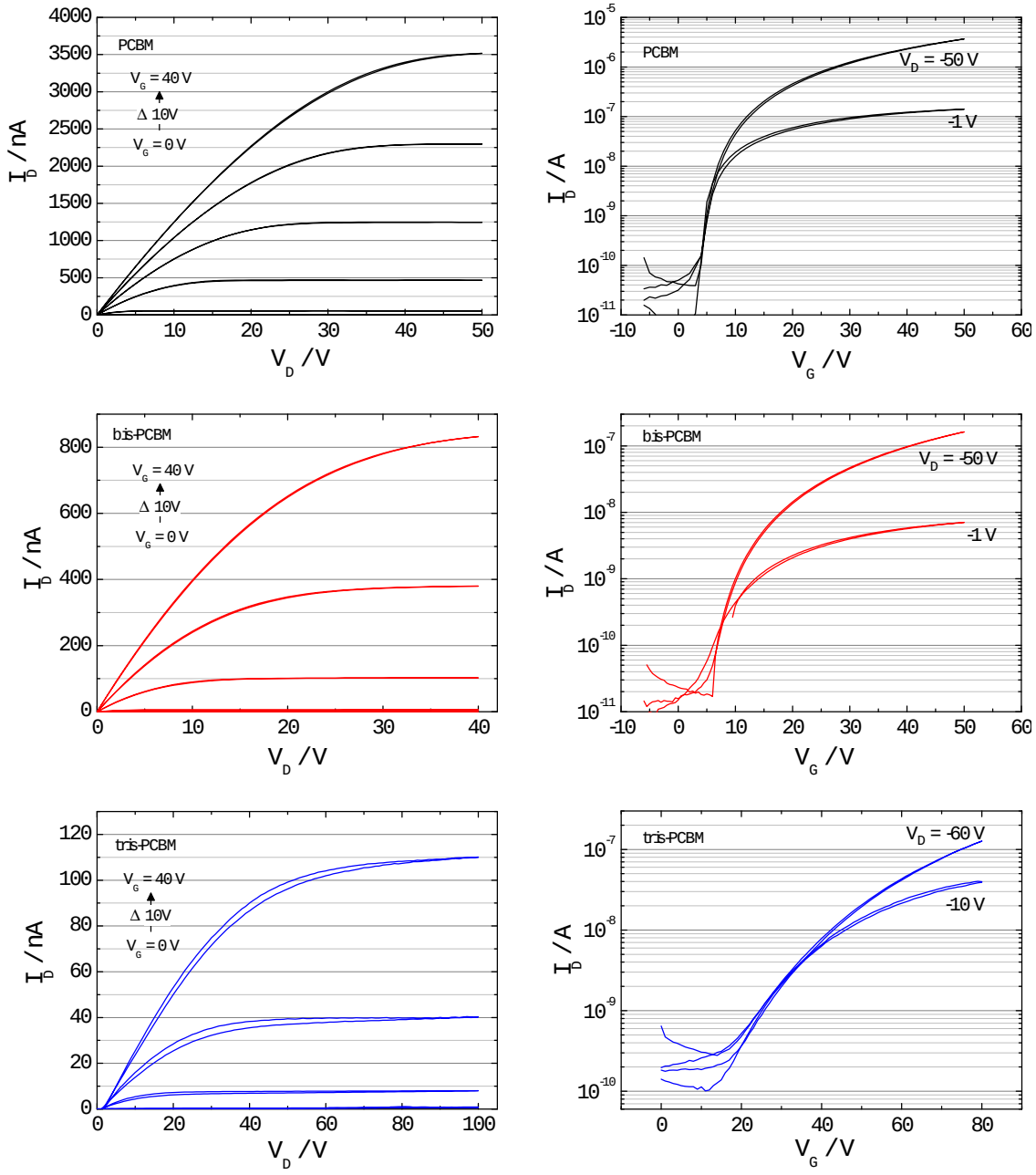

Figure 5.16: Left: Output characteristics of top-gate bottom-contact FETs made using PCBM (top), bis-PCBM (middle) and tris-PCBM (bottom) for gate voltages V_G of 0 V, 10 V, 20 V, 30 V and 40 V. Right: transfer characteristics of the same FETs. Curves for PCBM and bis-PCBM are shown for source-drain voltages V_D of -1 V and -50 V, and for tris-PCBM for source-drain voltages of -10 V and -60 V. In each case, the channel length is 30 μm, the channel width 1 mm and the capacitance approximately 8 nFcm^{-2}.

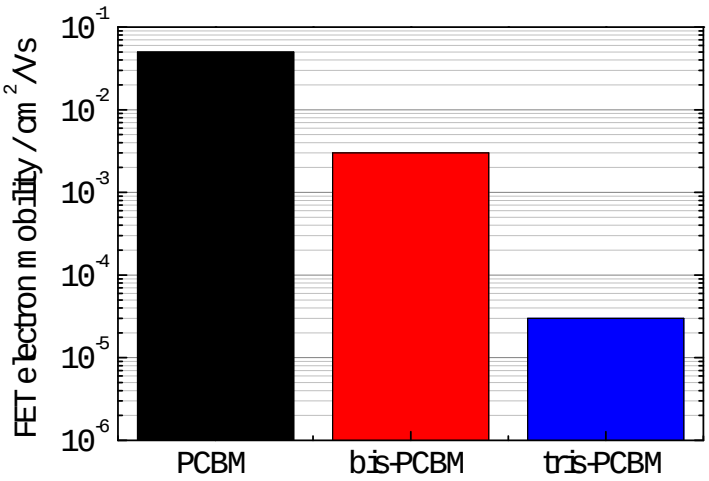

Figure 5.17: Room temperature FET mobilities of all three fullerenes as extracted from the linear regime of the output characteristics at $V_G = 30$ V. The channel length is 30 μm, the channel width 1 mm and the capacitance approximately 8 nFcm^{-2}.

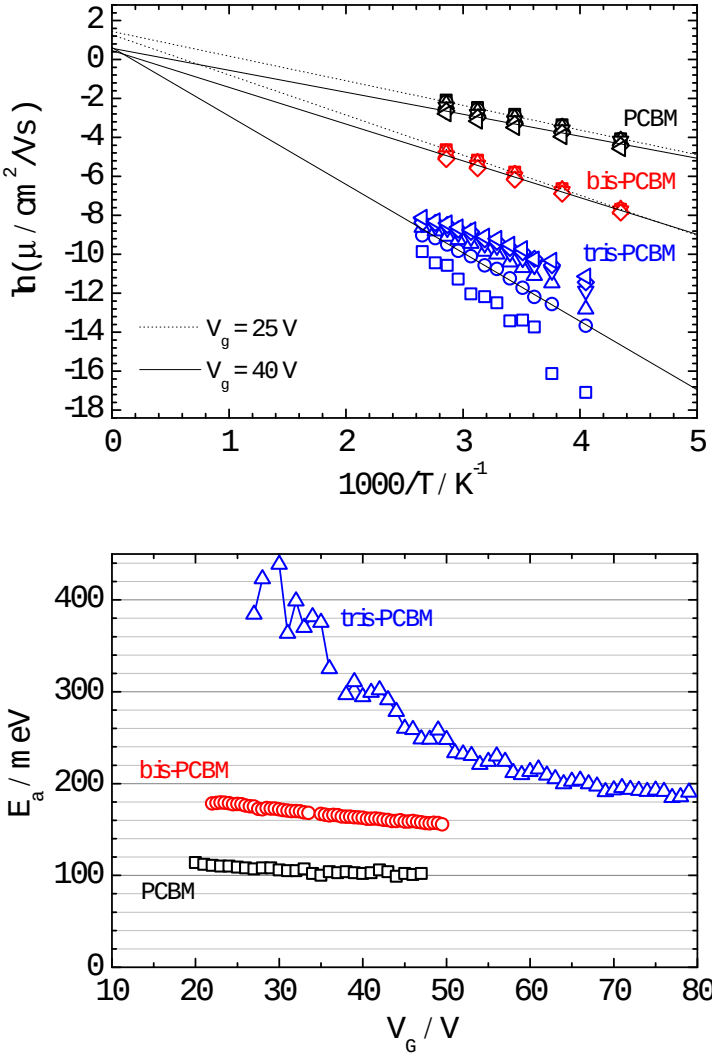

Figure 5.18: Top: Logarithmic mobility versus 1/T plots for all three fullerenes, over a range of gate voltages. The gate voltages shown for PCBM are 20 V (squares), 25 V (circles), 30 V (up triangles), 35 V (down triangles), 40 V (diamonds) and 45 V (left triangles); for bis-PCBM 25 V (squares), 30 V (circles), 35 V (up triangles), 40 V (down triangles) and 45 V (diamonds); for tris-PCBM 30 V (squares), 40 V (circles), 50 V (up triangles), 60 V (down triangles), 70 V (diamonds) and 80 V (left triangles). Also shown are fit lines extrapolated to $1/T \rightarrow 0$ for PCBM, bis-PCBM and tris-PCBM at $V_G = 40$ V (solid lines) and for PCBM and bis-PCBM at $V_G = 25$ V (dotted lines). Bottom: E_a as a function of gate voltage V_G for PCBM, bis-PCBM and tris-PCBM.

Chapter 6

Electron collection as a limit to polymer:PCBM solar cell efficiency: effect of blend microstructure on carrier mobility and device performance

6.1 Summary

We have carried out a detailed and systematic study to correlate carrier mobility with OPV device performance, concentrating on the PTB7:PCBM system and comparisons with the P3HT:PCBM and PCPDTBT:PCBM systems (chemical structures are given in Figure 6.1). In particular, we address the question of why state-of-the-art OPV systems such as PTB7:PCBM perform so much worse at large active layer thicknesses than P3HT:PCBM. The primary finding of this study is that low electron mobility is the main cause of the poor performance of PTB7:PCBM relative to P3HT:PCBM at larger film thicknesses. We have found that the electron mobility in PTB7:PCBM blends is 1–2 orders of magnitude lower than the electron mobility in annealed P3HT:PCBM for all film thicknesses up to 400 nm. The hole mobility, in contrast, was found to be the same to within a factor of approximately three in all devices studied.

We have confirmed that electron collection is the primary limiting factor in PTB7:PCBM blends by studying the effect of increasing fullerene content. We have shown that increasing the PCBM content from the PCE-optimised value of 60 wt% to 80 wt% allows a thickness dependence almost as good as that of annealed P3HT:PCBM, and a FF close to 0.6 above 300 nm. Using SCLC measurements, we have correlated this improvement to an increase in electron mobility, with almost no change observed in hole mobility. Although in this case the loss in absorption due to the replacement of polymer with fullerene overcompensates the gain in electron collection, the result confirms that by improving only the electron transport efficient electron and hole collection is possible for PTB7:PCBM devices greater than 300 nm in thickness.

The low electron mobility in PTB7:PCBM is proposed to result from the low degree of phase separation of PTB7 and PCBM in the blend, likely due to the low tendency of the polymer to crystallise. A low degree of phase separation is confirmed by our transmission electron microscopy (TEM) and photoluminescence (PL) quenching experiments. We find that for PTB7:PCBM, unlike for PCPDTBT:PCBM, solvent additives such as ODT and DIO do not lead to increased phase separation. Use of DIO does lead to a higher FF and PCE in PTB7:PCBM at low film thicknesses for some PCBM fractions, but we show that this improvement is not explained by an increase in either hole or electron mobility. A key challenge for OPV researchers is thus to develop improved methods to ensure connectivity and ordering in the fullerene phase in blends without relying on either (i) a large excess of fullerene or (ii) strong crystallisation of the polymer. It may be estimated that approximately one third of the incident available light in state-of-the-art devices is wasted due to the requirement for active layers to be no more than 100 nm in thickness [111], and hence that PCEs up to 50% larger than the current values for 100 nm devices may be within reach.

6.2 Scope of this Chapter

We address the question of why state-of-the-art OPV systems such as PTB7:PCBM perform so much worse at large active layer thicknesses than P3HT:PCBM. We have shown that the FF of PTB7:PCBM devices decreases steeply from above 0.6 at 100 nm thickness to approximately 0.4 for thicknesses greater than 300 nm. Annealed P3HT:PCBM devices, in contrast, are able to show a FF greater than 0.6 for thicknesses up to 300–400 nm. It appears obvious that this is a problem of charge collection, but it is not obvious whether it is primarily a result of lower carrier mobility or

an increased recombination rate or both. Further, it is not obvious whether the difference concerns some intrinsic feature of the polymer or a feature of the blend microstructure. A better understanding of the factors limiting charge collection in state-of-the-art OPV devices is critical in the pursuit of higher device efficiency. It may be estimated that approximately one third of the incident available light in state-of-the-art devices is wasted due to the requirement for active layers to be no more than 100 nm in thickness [111], and hence that efficiency gains of up to 50% may be at stake.

In order to reveal the mechanisms limiting charge collection in PTB7:PCBM at large thicknesses, and hence the maximum achievable PCE of the system, we carry out a range of thickness-dependent, composition-dependent and processing-dependent charge transport and OPV device measurements in PTB7:PCBM, P3HT:PCBM and PCPDTBT:PCBM (chemical structures are given in Figure 6.1). In Section 6.4.1, we demonstrate the charge collection problem in PTB7:PCBM blends (processed with DIO as for the champion recipe) as compared with annealed P3HT:PCBM blends. In Sections 6.4.2–6.4.4 we then focus on the measurement of carrier mobility by the space-charge limited current (SCLC) method, verifying the results carefully against literature data for the P3HT:PCBM and PCPDTBT:PCBM systems. Using SCLC, we demonstrate that the electron mobility in PTB7:PCBM blends (also processed with DIO) is up to two orders of magnitude lower than in annealed P3HT:PCBM, while the hole mobility is roughly the same. In Section 6.4.5, by studying the microstructure of the PTB7:PCBM and P3HT:PCBM blends using photoluminescence (PL) and transmission electron microscopy (TEM) measurements, we derive a hypothesis that the low electron mobility in PTB7:PCBM is a result of a low degree of phase separation and the concomitant disruption to connectivity and ordering in the fullerene phase.

In Section 6.4.6, we test our hypothesis by carrying out a series of PCBM concentration-dependent SCLC mobility and OPV device measurements. We demonstrate that in this system, the electron mobility increases strongly with PCBM content. This is also correlated to an increase in FF. Furthermore, we show that PCBM-rich blends (80 wt% PCBM) show a thickness dependence of FF approximately as good as annealed P3HT:PCBM. This strongly suggests that electron mobility is a key limit to the PCE in the PTB7:PCBM system.

In Section 6.4.7, we then study the effect on electron collection of processing PTB7:PCBM with DIO, which leads to a strong increase in FF and PCE of PTB7:PCBM at intermediate PCBM

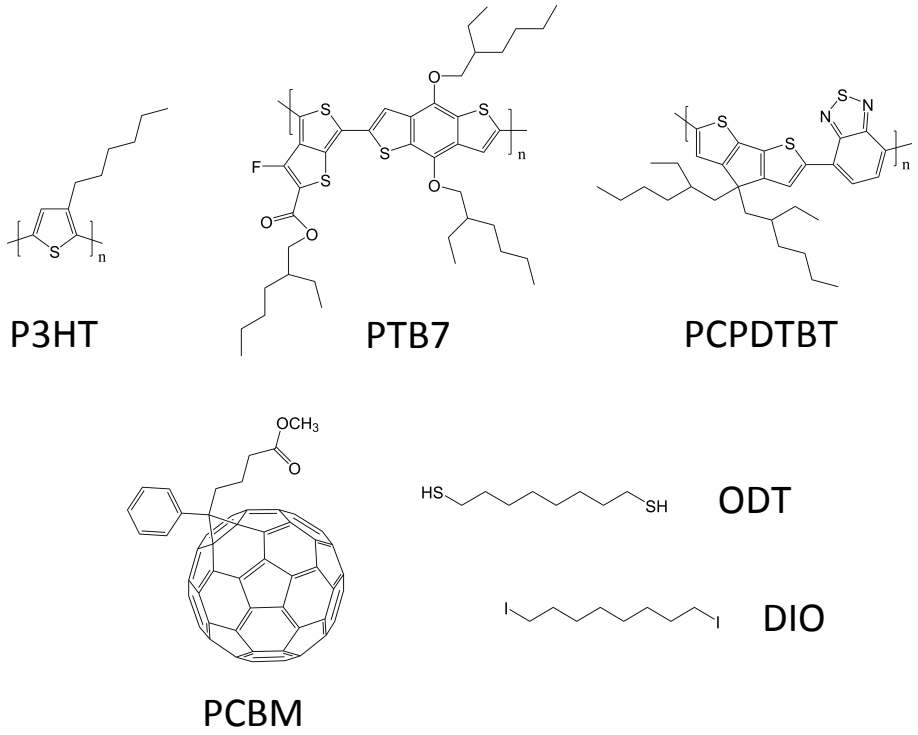

Figure 6.1: Chemical structures of poly(3-hexylthiophene) (P3HT); poly(thieno[3,4-b]thiophene-alt-benzodithiophene) (PTB7); poly[2,6-(4,4-bis-(2-ethylhexyl)-4H-cyclopenta[2,1-b;3,4-b']dithiophene)-alt-4,7(2,1,3-benzothiadiazole)] (PCPDTBT); [6,6]-phenyl-C61-butyric acid methyl ester (PCBM); 1,8-octanedithiol (ODT); and 1,8-diiodooctane (DIO).

fractions (60–70 wt%). However, we find that these devices still show poor electron collection at large film thicknesses. There is no evidence for increased phase separation in the blend – indeed TEM indicates reduced phase separation. SCLC measurements show no improvement in electron mobility in blends with DIO additive. This suggests that electron mobility continues to limit electron collection in blends with DIO, and that some other factor is responsible for the improved Fill Factor at intermediate PCBM weight fractions. Possible factors behind the improvement in FF, such as an increased electron lifetime, are discussed.

Hence, we conclude that even with the use of DIO there remains a strong limit to PCE in the PTB7:PCBM system due to the trade-off between absorption and charge collection, primarily electron collection. We suggest that this is largely due to the low crystallinity of the PTB7 polymer, which leads to a low degree of phase separation, resulting in poor connectivity and ordering in the fullerene phase and a low electron mobility. Novel processing routes to improve the connectivity and ordering of the fullerene in blends with polymers that do not readily order – either involving phase separation or not – therefore offer the prospect of significant advances in OPV performance.

Year	Material	PCE / %	Thickness / nm	Ref.
2005–2010	P3HT	> 4	100–300	[200]
2007	PCPDTBT	5.5	110	[198]
2009	PCDTBT	6.1	80	[195]
2009	PBDTTT-C	6.6	80	[196]
2010	PTB7	7.4	100	[197]
2011	PTB7	8.4	90	[89]

Table 6.1: Unofficial summary of historical 'champion' OPV polymers for polymer:fullerene BHJ devices in the published literature. It can be seen that all systems since P3HT:PCBM are optimised only at film thicknesses $\leq$ 110nm.

The data in this Chapter was collected at Sumitomo Chemical Co., Ltd. The LiF optimisation was performed in collaboration with Toshio Kimura. The impedance spectroscopy measurements were carried out in collaboration with Takayuki Okachi. The TEM images were collected by Akiko Mitani.

6.3 Background

6.3.1 State-of-the-art OPV is limited by charge collection

Improving charge collection efficiency in OPV devices will be critical in efforts to increase PCE beyond 10%. More efficient charge collection allows thicker active layers to be used, as necessary for effective light-harvesting. Currently, state-of-the-art OPV systems waste a significant fraction of the available light. This can be seen by comparing internal quantum efficiencies (IQEs), which have reached over 90% in some systems at peak wavelength [195, 196, 197], with external quantum efficiencies (EQEs), which usually peak at around 50–70% in the same systems [198, 195, 196, 197]. The absorption depth of OPV active layers (over the main absorption range) is of the order 100 nm, meaning that several hundred nm of active layer is enough absorb almost all the available light. However, most OPV systems display a dramatic drop in performance – particularly in electrical Fill Factor (FF) – as the active layer thickness is increased above 100 nm. Hence, approximately one third of the incident usable light is wasted [111], as shown in Figure 6.2, representing a large efficiency penalty. Similar thickness dependences of absorption have been found in other modelling studies [199, 106].

One of the best-performing OPV systems in terms of active layer thickness is P3HT:PCBM. P3HT:PCBM has received a great deal of research attention over the past decade since 2002 [78, 200],

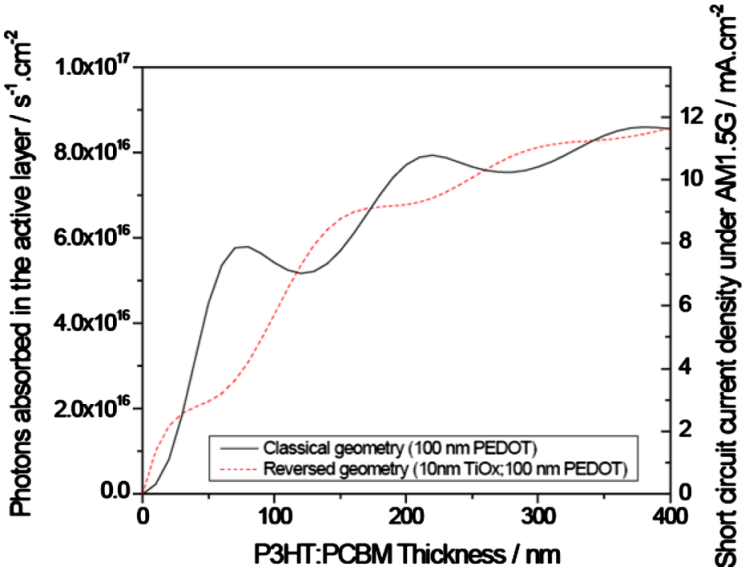

Figure 6.2: Taken from [111]. Example of the thickness dependence of the absorption for a bulk-heterojunction active layer – here modelled for P3HT:PCBM, but representative of all OPV systems. It can be seen that at the first peak near 100 nm, more than one-third of the available incident light is wasted (approximating that the peak between 300 nm and 400 nm is the maximum available). The modulation of the absorption is caused by optical interference effects.

and up to around 2006 was the state-of-the-art OPV system. Although the record efficiencies of over 5% in P3HT:PCBM were found for active layers < 200 nm, high efficiencies over 4% have been seen with active layers up to 300 nm in thickness [200]. A number of separate thickness dependence studies of P3HT:PCBM in the literature have found PCE maxima between 200 nm and 300 nm [199]. This is in clear contrast to subsequent 'champion' OPV systems, as summarised in Table 6.1. Historical records within the published literature include the PCPDTBT:PC71BM [198], PCDTBT:PC71BM [195], PBDTTT:PC71BM [196] and PTB7:PC71BM [197, 89] systems. In each of these cases, the optimum thickness was found to be 80–110nm.

It is generally understood that the requirement for thin layers relates to the problem of transporting the photo-generated charge carriers to the electrodes before they are 'lost' to the competing process of bimolecular recombination [5]. The maximum thickness for a device will depend on the mobility and lifetime of the charges; that is, on how far the charges may move before they recombine. The recombination lifetime will depend on 'microscopic' factors such as the energetics of the recombination process and the molecular structure of the two materials, and also on 'macroscopic' factors which influence mobility, such as the purity and connectivity of the phases. Due to this complexity, to disentangle the precise relationship between microstructure and recombination is challenging, and this has not yet been achieved for any state-of-the-art OPV system. Hence, efforts to unravel

the causes of the reduced performance of active layers >100 nm in thickness are of great importance for the development of commercially-viable OPV.

In this Chapter we choose to focus on PTB7:PCBM as a state-of-the-art OPV system (it is currently the highest PCE polymer:fullerene system published in the literature) which suffers from a strong decrease in charge collection with increasing active layer thickness (as we have previously observed in our laboratory). It is expected that a comparison of PTB7:PCBM with P3HT:PCBM – a system which performs better for large active layer thicknesses – and with PCPDTBT:PCBM – a system whose charge collection properties have been studied in some detail – may yield insight into the mechanisms limiting charge collection at large thicknesses and hence state-of-the-art PCEs.

6.3.2 Studying charge collection and carrier mobility in OPV devices

It was outlined in Section 2.3.1 that OPV device efficiency is critically dependent on effective charge collection. Charge collection at the electrodes requires sufficient mobility in order to compete with bimolecular recombination, which can be characterised by a carrier lifetime. The product of the mobility, lifetime and electric field $\mu\tau$E represents a characteristic distance over which charges travel before recombination. The product $\mu\tau$E is typically of the order of the film thickness ≈100 nm at operating voltages, and recombination is competitive with charge collection. The blend microstructure has a strong influence both on the mobility and on the lifetime. Changes in microstructure due to different processing routes or small changes in chemical structure are often seen to lead to large changes in OPV performance. This also means that in order to explain the improvement, systematic studies correlating microstructure, mobility-lifetime properties and OPV performance are required.

Charge transport in polymer:fullerene bulk heterojunction solar cells has received significant attention, and the carrier mobilities in blend films have been studied by FET, ToF and SCLC measurements, among other techniques. Measurements on some of the first polymer:fullerene blends – based on MDMO-PPV and PCBM – were carried out by a number of groups [101, 109, 201, 18, 202]. With these early measurements, and ever since, there has been debate regarding the relative limitations of hole and electron transport and the dominant mechanism of charge recombination. In configurations optimised for device performance, the groups found using a variety of techniques including SCLC and ToF that electron mobilities were typically 1–2 orders of magnitude higher than hole mobilities.

Transport measurements on blends of other PPVs with PCBM showed electron mobilities in the blend up to three orders of magnitude higher than hole mobilities in the blend [75].

6.3.3 Electron mobility in PCBM and in polymer:PCBM blends

Indeed, the electron mobility in PCBM can be high. The electron mobility in pristine PCBM has been measured at over 10^{-3} cm2/Vs by the SCLC method [101]. FET measurements have shown very high electron mobilities in PCBM of over 10^{-2} cm2/Vs [203] and even over 10^{-1} cm^2/Vs [204]. The high electron mobility in pristine PCBM has been rationalised in terms of the delocalisation of the electron wavefunction over the whole conjugated part of the molecule, the near-spherical shape of which allows efficient electron wavefunction overlap almost isotropically, and in terms of the low torsional relaxation of the molecule as compared with polymers. It has been shown that PCBM in pristine films tends to form a well-ordered structure consisting of densely packed crystalline domains in random crystallographic orientation [180]. The size of the domains depends on the speed of solvent removal; spin-coating tends to lead to nanocrystalline domains, with the formation of larger single crystals possible for very slow solvent removal.

It is clear, however, that a possible weakness of the fullerenes, as in principle for all small molecules, is the connectivity of the phase when mixed with a second material as in a polymer:PCBM blend. Unlike for polymers where neighbouring chromophores are linked covalently into the chain, for small molecules there is no guarantee of close overlap with the neighbouring chromophore. It is well established that the electronic transfer rate between two molecules is strongly dependent on the spatial separation of the occupied and empty states. Mackenzie et al. have calculated that an increase in the intermolecular distance between two fullerenes of 1 Å can reduce the transfer rate by an order of magnitude [182]. It is therefore clear that less dense packing resulting from the disruptive influence of a polymer in the blend has the potential to reduce the electron mobility significantly.

It may therefore be expected that the electron mobility will be influenced by the composition and microstructure of the blend. Composition-dependent studies of electron mobility in MDMO-PPV:PCBM blends support this notion. The mobility measurements in MDMO-PPV:PCBM described above – with electron mobility much larger than hole mobility – correspond to blends with a large excess of PCBM (80 wt%). Tuladhar et al. also studied MDMO-PPV:PCBM blends with decreasing PCBM content, and found a strong decrease in (zero-field) electron mobility from around

10^{-3} cm^2/Vs at 70 wt% PCBM, to around 10^{-4} cm^2/Vs at 50 wt% and to below 10^{-5} cm^2/Vs at 25 wt%.

6.3.4 Influence of polymer crystallinity and PCBM fraction on electron mobility in the blend

The detailed blend microstructure – how intimately the two materials are mixed – is therefore expected to affect the severity of the decrease in electron mobility with decreasing PCBM fraction. A key factor contributing to the blend microstructure is the degree of crystallinity of the polymer. A clear illustration of this is the demonstration of excellent electron mobility in annealed P3HT:PCBM, where the electron mobility in a 50 wt% PCBM blend was shown by Mihailetchi et al. to be above 10^{-3} cm^2/Vs, more than an order of magnitude higher than for the 50 wt% PCBM MDMO-PPV:PCBM blend [47]. It has been shown that this is due to a strong crystallisation of P3HT upon annealing above the glass transition temperature, driving phase separation and the formation of a connected and more ordered PCBM phase. The microstructural changes upon annealing have been elucidated in detail by Campoy-Quiles et al. [90]. The effect on mobility of annealing has been studied using SCLC by Mihailetchi et al. [47]. It was shown that the improvement in OPV performance is, in fact, correlated with a drastic increase in the hole mobility. In pristine P3HT films, the hole mobility was found as 10^{-4} cm^2/Vs, with no change on annealing. In 50 wt% PCBM blends before annealing, however, the hole mobility in P3HT was found to be very low at below 10^{-7} cm^2/Vs. The electron mobility in the blend was found to be around 10^{-4} cm^2/Vs, 1–2 orders of magnitude lower than in pristine PCBM films. On annealing, the hole mobility increased to 10^{-4} cm^2/Vs and the electron mobility to just over 10^{-3} cm^2/Vs; that is, both approximately to the mobility of the pristine materials. This behaviour was also observed in FETs with real-time annealing by Agostinelli et al. [205]. Although the hole transport shows the most significant improvement in this case, it is important to note that a significant decrease in mobility on blending was observed for electrons in the PCBM phase, and that crystallisation of the polymer was observed to lead to an increase in electron mobility.

However, it has become clear that P3HT:PCBM is an extreme case, due to the high tendency towards crystallisation of P3HT. In the case of other polymers, where crystallisation is weak and annealing does not promote phase separation, a higher fraction of PCBM is required to form a connected, ordered PCBM network. This can be seen in the optimised compositions of state-of-the-art

polymer:fullerene blends for OPV. Considering the polymers in Table 6.1, the optimised blends all contain higher fractions of PCBM than P3HT:PCBM. The highest efficiencies for P3HT:PCBM have been found at 45–50 wt% PCBM [199, 200], for PCPDTBT:PC71BM at 67–75 wt% PCBM [198, 100], for PCDTBT:PC71BM at 67–80 wt% PCBM [195], for PBTTT-C:PC71BM at 60 wt% PCBM [196] (no other compositions given) and for PTB7:PC71BM at 50–67 wt% PCBM [197]. We also note that in OPV devices the bulk of the absorption occurs in the polymer phase, and hence these compositions optimised for PCE are likely to be polymer-rich as compared with the compositions optimised purely for charge collection.

The limiting effect of electron transport due to low polymer crystallinity has been described explicitly in the case of PCPDTBT:PC71BM. The first paper on the OPV properties of this system was published by Peet et al. [198]. It was shown that efficient devices required the processing additive octanedithiol (ODT), which was shown to increase both FF and J_{sc} significantly. The group studied the FET mobility of holes for the system, but found no increase in hole mobility with the additive. Thus, they attributed the improvement in device performance to an increase in carrier generation and/or carrier lifetime. Indeed, Clarke et al. [206] and Etzold et al. [207] have since found an increase in carrier generation through processing with ODT. However, Morana et al. later studied the composition dependence of FET mobility for both holes and electrons in PCPDTBT:PC71BM blends processed with and without ODT [100]. They too found no change in hole mobility, but identified an increase in electron mobility of a factor of two. They also found the optimum composition for OPV performance at lower PCBM fractions for blends with ODT, and hence concluded that the effect of ODT is to improve the connectivity of the fullerene network. Similar measurements on FETs by Cho et al. showed improvements in both hole and electron mobility, with the changes in electron mobility larger [208]. Agostinelli et al. have studied the effect of ODT on the same system, also finding evidence for improved percolation in the fullerene network with composition-dependent OPV studies (as well as evidence for less dispersive transport in the polymer phase by ToF) [191]. It is now established that the beneficial effect of ODT is to promote the phase separation of the blend, leading to slightly improved polymer crystallinity and an improved PCBM network [209, 198, 100, 191, 210]. A similar effect can be achieved with other additives, including diiodooctane (DIO), dibromooctane and others [211].

A number of recent publications also support the hypothesis of decreased electron mobility in blends

with less crystallisable polymers. Morana et al. have observed larger electron mobilities in blends of PCBM with silicon bridged Si-PCPDTBT than in blends with carbon-bridged C-PCPDTBT, and have correlated this using X-ray scattering to higher crystallinity in Si-PCPDTBT. Recently, Machui et al. have studied the effect of adding PCPDTBT (with low crystallisability) as a minority third component to P3HT:PCBM devices keeping the fraction of PCBM constant at 50 wt%. Annealed 10:40:50 wt% PCPDTBT:P3HT:PCBM blends showed a SCLC electron mobility of 3×10^{-4} cm^2/Vs, almost an order of magnitude lower than the electron mobility in annealed 50:50 wt% P3HT:PCBM blends of 2×10^{-3} cm^2/Vs. In contrast, the hole mobility in P3HT, which was still able to crystallise and phase separate within the ternary blend, was not affected. This highlights the fact that good connectivity and ordering in the fullerene phase is not possible without either strong polymer crystallisation and a high degree of phase separation or a sufficiently large PCBM fraction.

We further note that while polymer crystallisation appears to be a necessary condition for the formation of a well-connected fullerene phase at 50 wt% PCBM, it is not always a sufficient condition. For example, Cates et al. have studied blends of PBTTT with PCBM [169]. They found that even though PBTTT crystallises rather strongly, a PCBM fraction of 80 wt% was required for optimum OPV performance. It was shown through X-ray diffraction studies that this was due to 'intercalation' of the fullerene into the polymer in the crystalline state. Intercalation describes the process whereby small molecules pack between the side-chains of the polymer. In this way, the polymer 'soaks up' a large fraction of the fullerene and prevents the formation of a well-connected fullerene phase up to large PCBM weight fractions. Cates et al. have shown that intercalation also occurs in the case of MDMO-PPV:PCBM blends [212]. Notwithstanding the particular mechanism, it is clear that if the blends cannot be processed such that PCBM is driven out of the polymer domains to form separate, connected domains – whether a result of low crystallisability of the polymer, fullerene intercalation or both – electron transport will be poor up to high PCBM weight fractions.

6.3.5 PTB7:PCBM is an interesting case for a study of charge collection

We now turn to the system that is the main focus of this Chapter, the PTB7:PCBM blend. There has been little published regarding the transport properties of the system, but a number of papers detailing its OPV properties. It is an important system to study since at the time of writing it is

the highest efficiency polymer:fullerene system published in the literature, with He et al. having achieved 8.4% certified [89] with the PTB7:PC71BM blend. It is also currently limited to devices of approximately 100 nm in thickness, suggesting that improvements in charge collection may allow significant increases in J_{sc} and PCE. It is therefore of great interest to determine the extent to which the microstructural factors discussed above affect charge transport in this case. In the first paper demonstrating PTB7:PC71BM, Liang et al. showed that this system too can be optimised by use of the solvent additive DIO, which leads to an increase in both FF and J_{sc} [197]. The group presented TEM images showing an increased intermixing on the 10–100 nm scale with DIO, and concluded that the effect of the additive was to assist in the 'formation of interpenetrating networks'. They also measured the hole mobility in a pristine polymer film by SCLC, finding a value of 6×10^{-4} cm^2/Vs. Neither the electron mobility nor the hole mobility in the blend has been published.

Other studies have considered the structure and microstructure within the PTB7:PC71BM blend. Hammond et al., modelling X-ray diffraction and polarising absorption spectroscopy data, have found that the PTB7 polymer within the blend is rather disordered, with only around 20% of the polymer showing orientational order [213]. Also employing TEM, they found that the microstructure consists of nanoscale PC71BM-rich aggregates separated by polymer-rich regions. Using various X-ray techniques, Chen et al. have described a complex 'hierarchical' microstructure of nanocrystallites and nanocrystallite aggregates of each material intermixed in fullerene- or polymer-rich domains hundreds of nanometres in size [214]. Each of these studies found that processing with DIO further increased the intermixing to some degree, though the effect was found in most cases to be rather small. Also using X-ray scattering, Lou et al. studied solutions of PTB7:PC71BM in CB with or without DIO, and found a decrease in average PC71BM aggregate radius from 1.2 nm to less than 0.8 nm (the limit of sensitivity of the experiment) [215]. Since the mean diameter of a C60 molecule is of the order 0.7 nm, this finding too is consistent with a very high level of intermixing both with and without DIO. It is clear, therefore, that the effect of DIO in PTB7:PCBM blends is not similar to the effect of ODT in PCPDTBT:PCBM blends. There is no consensus on the precise effect of DIO in PTB7:PCBM blends, but the literature evidence suggests that the additive further promotes the already intimate intermixing on the 1–100 nm scale.

6.4 Results

6.4.1 Identification of charge collection problem in PTB7:PCBM blends

Figure 6.3 shows a series of light current-voltage curves of optimised OPV devices of PTB7:PCBM and P3HT:PCBM for various active layer film thicknesses. We note that these devices and all devices in this Chapter were fabricated with PC61BM rather than PC71BM, as stability and reproducibility were prioritised over PCE values. It can be seen that as the thickness of the PTB7:PCBM active layer is increased, the area enclosed by the curve in the power-generating quadrant is strongly reduced. There is a severe drop in FF. The short-circuit current first increases with thickness from 65 nm to 98 nm and then decreases to 285 nm and 390 nm. The large reverse bias current (towards the saturation regime), however, shows clearly that the charge generation is increasing across the whole thickness range, as expected for the higher absorption in thicker films. Figure 6.4 shows the thickness dependence of the FF in both systems. Comparison with the P3HT:PCBM system shows that the decrease in FF with increasing thickness is much stronger in PTB7:PCBM.

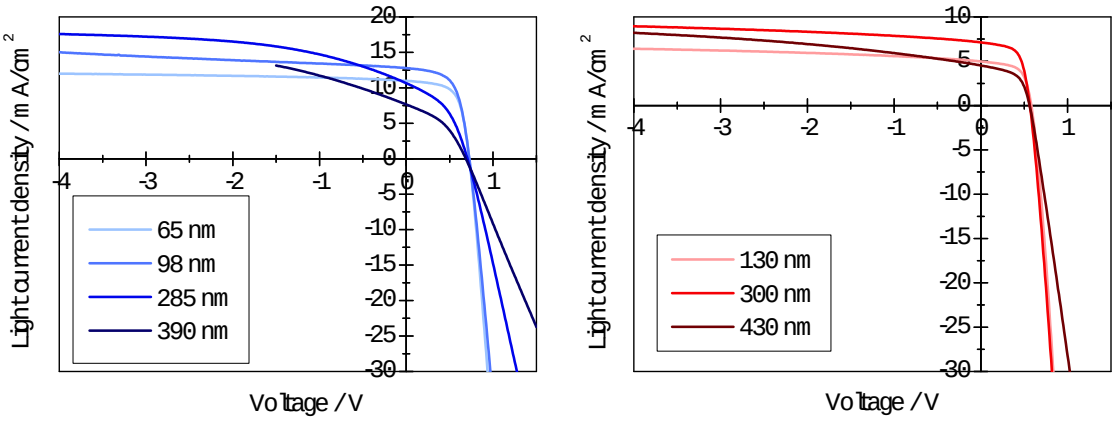

Figure 6.3: Light JV curves demonstrating the strong drop in FF with thickness in PTB7:PCBM devices (left, various blue) as compared with P3HT:PCBM devices (right, various red). The P3HT:PCBM devices were made with 50 wt% PCBM, spin-coated from chlorobenzene and post-annealed at 130°C for 15 mins in nitrogen; the PTB7:PCBM devices were made with 60 wt% PCBM and spin-coated from a chlorobenzene solution with DIO additive, with no annealing.

In Section 2.3.3, several reasons for a low FF were listed, including inefficient charge collection due to low mobility-lifetime product; inefficient charge collection due to an imbalance in hole and electron mobilities and build-up of space-charge; poor extraction at the electrodes; low shunt resistance due to leakage pathways; high external series resistance. Of these reasons, however, only

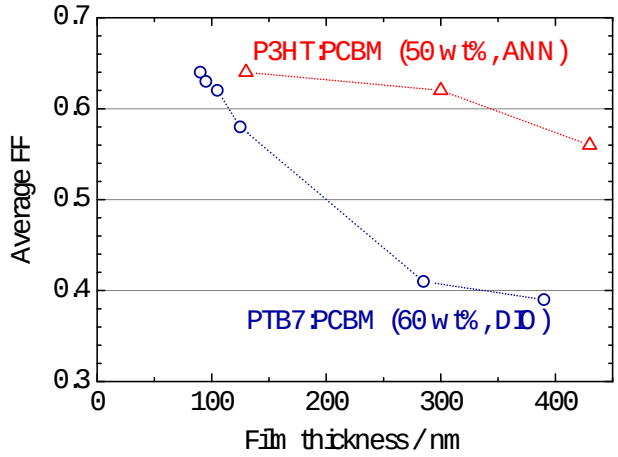

Figure 6.4: Thickness dependence of the FF for the PTB7:PCBM and P3HT:PCBM data shown in Figure 6.3. Additional data points for PTB7:PCBM were not shown in Figure 6.3 for clarity.

the first is expected to lead to a strong and uniform decrease in FF with thickness, as seen for the PTB7:PCBM devices. Space-charge is expected to lead to a low FF even in thin films, which is not the case here. A leakage current is expected to improve (decrease) with film thickness. A limiting external series resistance would lead to a thickness-independent current in high forward bias, which is not seen here. In fact, the current in forward bias strongly decreases with thickness, as expected for a bulk mobility-limited current, and to a greater extent than in the P3HT:PCBM devices. This is consistent with a lower mobility of at least one carrier in PTB7:PCBM than in P3HT:PCBM. Hence, the thickness dependence of the FF shown in Figure 6.4 is strongly suggestive of inefficient charge collection due to a mobility-lifetime problem, and specifically of a reduced mobility relative to P3HT:PCBM.

However, it is not clear at this stage to what extent the suspected mobility difference is responsible for the drop in FF. It is also unclear whether the mobility issue concerns hole transport, electron transport, or a combination of the two. Since these issues are of great interest for the improvement of OPV devices, it is necessary that we should be able to examine the mobility of such devices more directly.

6.4.2 Strategy to correlate mobility and OPV performance

In order to study the effect of charge carrier mobility on the thickness-dependence of OPV device performance, it is necessary to represent the operational conditions within an OPV device

as accurately as possible. Therefore, firstly, we study blend films fabricated with the same processing parameters, in order to ensure comparable microstructure. Since we wish to explain the poor performance of thicker devices, we study both the mobility and OPV performance of films between approximately 100 nm and 400 nm. Secondly, since mobility in organic materials is typically strongly dependent on electric field and charge carrier density [31, 29], we carry out the mobility measurement in a comparable electric field and charge density regime. Of the techniques outlined in Section 2.2, therefore, we expect that space-charge-limited current (SCLC) or impedance spectroscopy (IS) measurements should be appropriate. These techniques are preferable in this case to time-of-flight due to the requirement for the latter of thick films of around a micron or more, where microstructure may be misrepresented. They are preferable in this case to field-effect transistor measurements due to a consideration of charge concentration conditions and transport geometries.

Initial trials of SCLC and IS were carried out. It was found for IS measurements that, in some cases, the mobility could only be derived using films > 400 nm in thickness, as the frequency range of the measurement (up to around 10^6 Hz) was insufficient to measure a transit time faster than around 10^{-6} s. It was deemed necessary that the technique chosen should be able to reproduce the literature mobility values for the 'control' system P3HT:PCBM, as characterised (by SCLC) in [47]. For the electron mobility in this system of around 4×10^{-3} cm^2/Vs, at a typical field of 10^4 V/cm, the minimum transit time observable of approximately 10^{-6} s would require a film thickness of approximately 400 nm. In contrast, the literature shows that such mobilities may be measured by SCLC in films of 100–400 nm thickness, providing that the electrodes perform sufficiently well. Hence, it was decided to pursue the SCLC method.

In order to validate the SCLC measurement method, we have performed initial measurements on the well-studied P3HT:PCBM system. Figure 6.5 shows SCLC data taken with the P3HT:PCBM system, after substantial electrode optimisation. The data were corrected for series resistance as measured on blank substrates and the resulting current-voltage curves were fit to the Murgatroyd equation [76] – Equation 2.14 – with a fixed built-in voltage for each electrode structure. The mobility in such a model is field-dependent. The mobility values presented here (and throughout the Chapter) correspond to an intermediate field of 10^5 V/cm; that is, 1 V for a film of thickness 100 nm. Also shown for comparison is the corresponding literature data [47]. Data points shown are hole and electron mobilities for 50 wt% PCBM blend films of P3HT:PCBM, both before and

after the standard annealing treatment of heating at 130°C for 15 mins; hole mobilities for pristine P3HT films before and after annealing treatment; and electron mobility of a pristine PCBM film after annealing treatment. It can be seen that our experimental values are in very good agreement with the literature values.

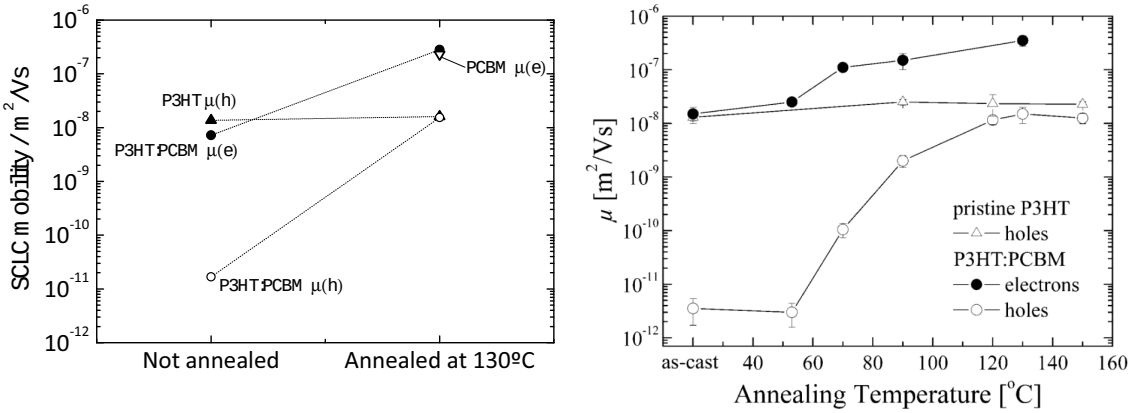

Figure 6.5: Top: SCLC mobility for holes and electrons in non-annealed and annealed P3HT, PCBM and P3HT:PCBM films; bottom: the literature values from [47] (see 'as-cast' and 130°C points) for comparison.

It was found that in order to reproduce the electron mobility data in the literature mentioned above, the injecting electrode choice was critical. A summary graph of representative JV curves from a PCBM film, for three electron-only device structures, is shown in Figure 6.6. The hole-blocking counter-electrode in each case is ITO/TiO_x, but the injecting electrode was one of TiO_x/Al, Ca/Al or LiF/Al. The active layers are nominally identical, and hence the current magnitude is a direct probe of injection capability. It can be seen that LiF/Al cathode gives the largest current, and shows no injection-limited regime. The Ca/Al cathode shows almost as large a current at intermediate fields, and no injection-limited region, but a rather spurious voltage dependence at high fields, weaker than the quadratic dependence expected for SCLC. It should be noted that the performance of Ca/Al varied strongly; sometimes it performed as well as LiF but commonly behaviour such as this was observed. Finally, the TiO_x cathode shows the lowest current. There is a clear injection-limited regime at intermediate voltages, and even when the voltage dependence reduces, the current is seen to be limited to over an order of magnitude lower than that for the LiF/Al cathode. The reason for this is not clear, but it is possible that only a fraction of the electrode area is injecting. Hence, all further electron-only devices were fabricated with LiF/Al as injecting electrode. Hole-only devices were more straightforward, and it was found that a device consisting of

ITO/PEDOT:PSS injecting electrode and Au electron-blocking counter-electrode was sufficient to provide unipolar Ohmic injection of holes into P3HT. This electrode combination was later found also to be sufficient for hole mobility measurements in both PCPDTBT:PCBM and PTB7:PCBM.

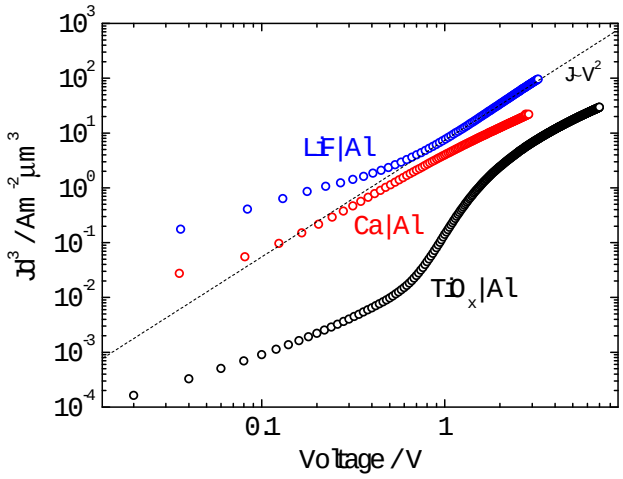

Figure 6.6: Comparison of electron injection capability of TiO_x/Al, Ca/Al and LiF/Al electrodes. The active layer is identical in each case, and consists of 100 nm of PCBM annealed at 130°C for 10 mins.

Hence, the experimental strategy chosen was to fabricate, for each OPV device considered, corresponding hole-only and electron-only devices using the electrodes as shown in Figure 6.7 (TiO_x/Al was found to be sufficient as OPV cathode for electron extraction). The positive bias was applied in each case to the ITO electrode.

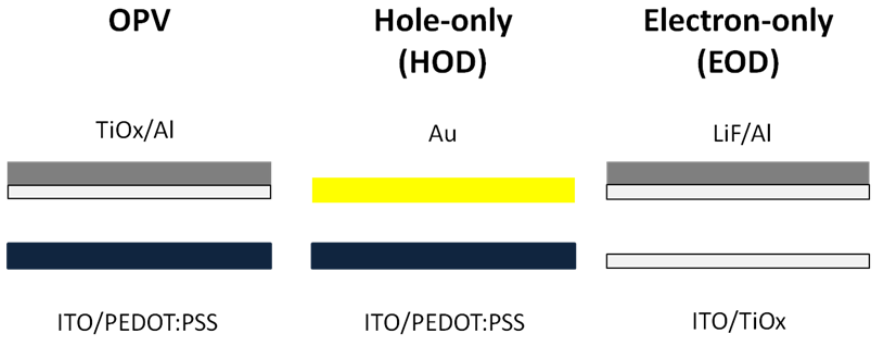

Figure 6.7: Electrodes used for devices of each type in this Chapter.

A further verification experiment was performed in order to test proper functioning of the SCLC devices. It can be seen from Equations 2.13 and 2.14 that the mobility calculated from the JV data

is a strong function of the film thickness, proportional to d^3. If the current is injection-limited, it is not expected to vary strongly with film thickness, since it is limited only by the property of the contacts. If Equation 2.13 or Equation 2.14 is applied – incorrectly – to this JV data, we would thus expect an apparent thickness dependence of the incorrectly-derived mobility roughly proportional to d^3. We may in reality expect the mobility to vary to some degree with film thickness, due to microstructural changes and the properties of dispersive transport, for example, but we do not expect a variation as strong as d^3. Hence, a measurement of the thickness dependence of the mobility derived from Equation 2.14 should provide a further test of sufficient injection and SCLC behaviour.

Thickness dependences of the hole and electron mobility in annealed films of P3HT:PCBM are shown in Figure 6.8. Over the range, the thickness increases by a factor of approximately 4, and so an injection-limited current would be expected to lead to an increase in calculated mobility of approximately $4^3 = 64$. Since the observed variation of the hole and electron mobility is less than a factor of 5, this lends strong support to the assumption of properly-functioning, sufficiently-injecting devices. We observe that the electron mobility in the thinnest film is approximately half of the value at larger thicknesses. This may be due to a slightly injection-limited current; to the larger fractional error in the thickness measurement of thin films; or to a real drop in mobility for some microstructural reason. The slightly increased hole mobility in the thinnest film may similarly be due to an error in the thickness measurement or to a real increase in mobility. However, these deviations of a factor of 2–3 are of the order of the experimental error in the SCLC measurement and fitting procedure.

6.4.3 Processing-dependent electron mobility in PCPDTBT:PCBM

The above section demonstrated a basic verification of the SCLC mobility measurement in a system previously characterised by SCLC. It was thought desirable to further test the method in another well-understood system, but one to which the application of the SCLC method was novel. It was decided that PCPDTBT:PCBM offered a suitable case study, as the hole and electron mobilities have been studied using FET measurements (see details below). Further, these studies considered the mobility in films processed with and without processing additives, of the type used to enhance efficiency in our main system of interest PTB7:PCBM. Hence, it is of interest whether our SCLC method is sensitive to mobility changes for such processing variations.

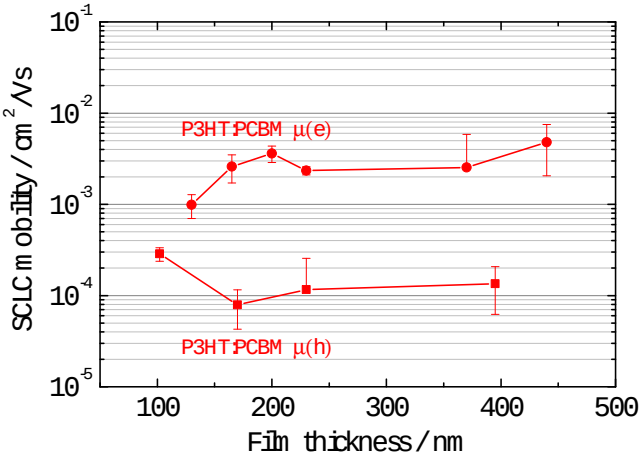

Figure 6.8: Thickness dependence of SCLC hole and electron mobility in annealed P3HT:PCBM. The weak dependence (variation of a factor of <5) over the range 100–450nm suggests that the devices are not injection-limited.

As described in Section 6.3.4, it was shown by Peet et al. that addition of 3 wt% of octanedithiol to the chlorobenzene solvent improved the FF and J_{sc} in PCPDTBT:PCBM blends [198]. This was correlated with increased phase separation and improved local ordering. FET mobilities in the system have previously been measured [198, 100, 208]. Precise findings vary between studies. Increases of between a factor of 2 and 10 in electron mobility with addition of ODT have been observed. Changes in hole mobility with ODT were negligible in two of the studies, and increases of between a factor of 2 and 5 were observed in the third. Figure 6.9 shows SCLC hole and electron mobility data collected from a series of PCPDTBT:PCBM devices with and without ODT, with various fractions of PCBM from 50 wt% to 91 wt%.

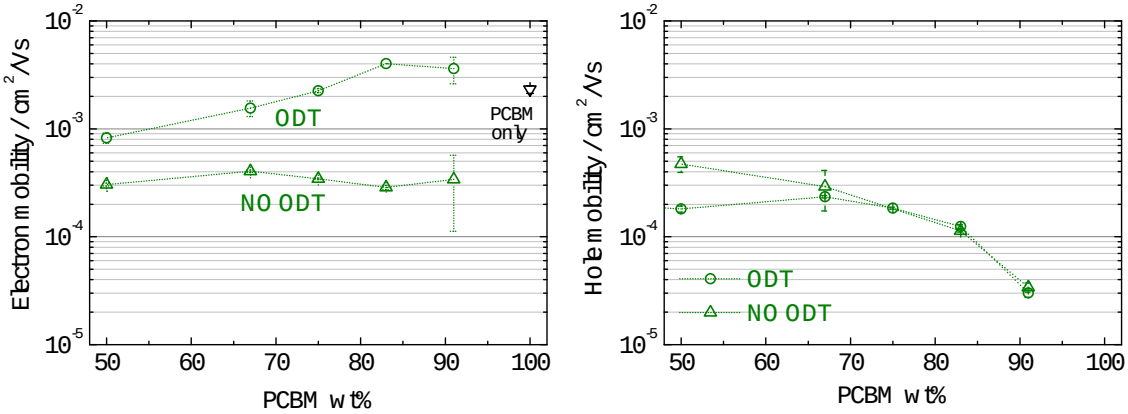

Figure 6.9: Composition dependence of SCLC electron mobility (left) and hole mobility (right) in PCPDTBT:PCBM devices processed without and with ODT.

There are several points of interest. The hole mobility shows very little change on addition of ODT to the processing solvent, with a small decrease for the 50 wt% PCBM blends. This is roughly consistent with the literature. As the PCBM fraction increases, the hole mobility drops relatively weakly up to a PCBM fraction of around 90 wt%, where it drops more sharply. The absolute magnitude of the hole mobility for 50–83 wt% PCBM is very similar to that in P3HT:PCBM, at just over 10^{-4} cm^2/Vs. In contrast, the electron mobility is significantly enhanced by addition of ODT to the processing solvent. For 50 wt% PCBM, the mobility increases by a factor of 3 to nearly 10^{-3} cm^2/Vs. As the PCBM fraction increases, the electron mobility of the film with ODT increases to approximately 4×10^{-3} cm^2/Vs, more than an order of magnitude larger than the mobility in the film without ODT. This value is approximately that found for electrons in pristine PCBM and in annealed P3HT:PCBM films, indicating the formation of a pure or nearly-pure, percolating PCBM phase. Finally, we note that the PCPDTBT:PCBM blend processed without ODT shows a rather low mobility of just over 10^{-4} cm^2/Vs and an absence of composition dependence, with the electron mobility constant within the error of measurement. This may indicate that the two phases are very intimately intermixed, and even up to 90 wt% PCBM a fullerene phase free of the disruptive influence of the polymer is unable to form. This is all consistent with an improvement in the electron transport in the PCBM phase contributing to the improved FF and J_{sc} in PCPDTBT:PCBM blends (with 67 wt% PCBM) with ODT.

Having reproduced the above results for the better-studied systems of P3HT:PCBM and PCPDTBT:PCBM, we now turn to the main subject of this Chapter, the PTB7:PCBM system.

6.4.4 Electron transport as a limiting factor in PTB7:PCBM blends

It was demonstrated in Section 6.4.1 that PTB7:PCBM (we showed devices processed with DIO) exhibit a much worse decrease in FF with thickness than P3HT:PCBM. It was shown that the data suggests a lower mobility-lifetime product, and there was also evidence for a lower bulk mobility. However, from OPV current-voltage curves alone it was not possible to show whether this is an issue of hole or electron mobility or both, and to what extent the low mobility alone (as distinct from carrier lifetime) is responsible for the poor charge collection in thicker devices. We now turn to SCLC measurements on PTB7:PCBM (processed with DIO) to address this.

Figure 6.10 shows a comparison of JV curves of single-carrier devices of PTB7:PCBM and P3HT:PCBM.

PTB7:PCBM films were spin-coated from chlorobenzene solvent with DIO additive with 60 wt% PCBM; P3HT:PCBM films were spin-coated from chlorobenzene with 50 wt% PCBM. It can be seen that the current densities in the hole-only devices are very comparable, with a difference of only a factor of 2–3. In contrast, the current densities in the electron-only devices differ by a factor of more than two orders of magnitude, with the electron mobility in PTB7:PCBM at around 10^{-5} cm^2/Vs. Figure 6.11 shows the thickness dependence of the PTB7:PCBM hole and electron mobilities. This shows very clearly the large difference in magnitude of the electron mobilities, and the close similarity of the hole mobilities, in the two systems. The large difference in the electron mobility between PTB7:PCBM and P3HT:PCBM clearly makes electron transport a strong candidate for the cause of the low Fill Factor in PTB7:PCBM blends with increasing film thickness.

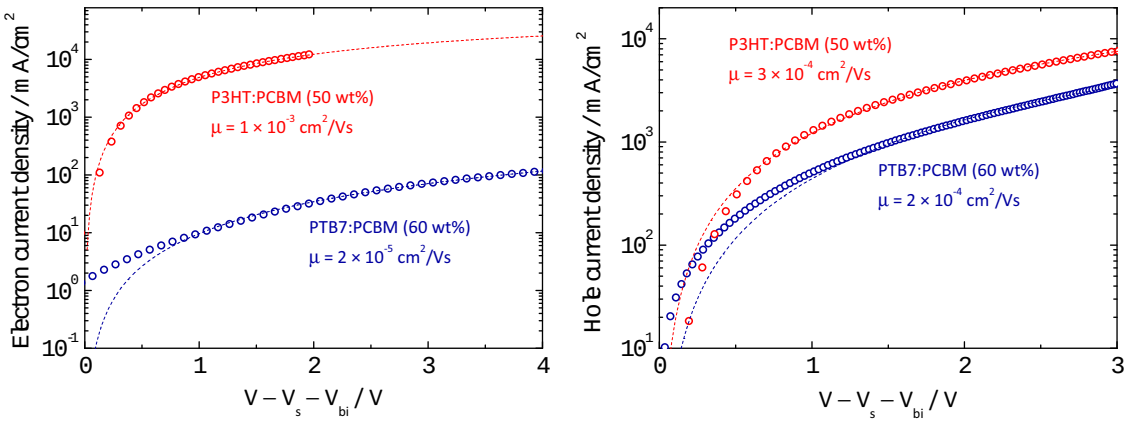

Figure 6.10: Example JV curves of electron-only (left) and hole-only (right) devices, comparing PTB7:PCBM with P3HT:PCBM. Dotted lines are fits to Equation 2.14. Mobilities are given at 10^5 V/cm to account for the field-dependence of the mobility.

It is interesting that despite the fact we have exchanged the polymer, it is the electron transport in the fullerene phase that is different. Therefore, it is clear that the difference in electron mobility between the two systems has its origin in the blend microstructure, rather than in differences of chemical structure. Further, the electron mobility reduces by a remarkably large amount, and this is despite the higher PCBM content in the PTB7:PCBM blend. We propose that the difference is due to the disruptive effect of the polymer on the PCBM network. As discussed in Section 6.3.3, it may be expected that a very fine intermixing between the two materials should have an adverse effect on the packing order and percolation of the fullerene. The literature discussed in Section 6.3.4 – largely X-ray and TEM data – suggests intimate intermixing in PTB7:PCBM. This is supported by the

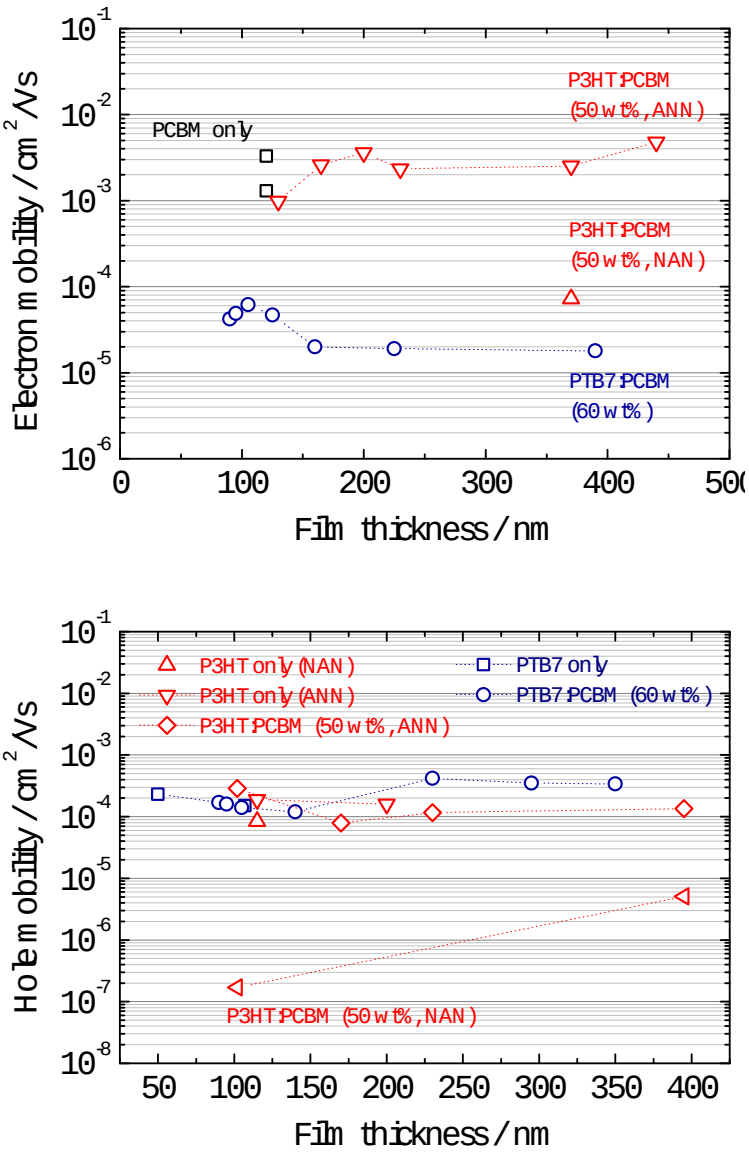

Figure 6.11: Thickness dependences of electron mobility (top) and hole mobility (bottom) in P3HT, PTB7 and blends with PCBM.

comparison of the electron mobility in PTB7:PCBM and that in non-annealed P3HT:PCBM blend, which is known to have a low degree of phase separation and a poorly-formed fullerene network. Figure 6.11 shows that the electron mobility of PTB7:PCBM is much closer to the electron mobility value in non-annealed P3HT:PCBM than that in annealed P3HT:PCBM.

It can be seen that the hole mobility is just over 10^{-4} cm^2/Vs in both pristine PTB7 and PTB7:PCBM blend films. The absence of a reduction in the hole mobility in PTB7:PCBM versus pristine PTB7 can be rationalised by considering that the polymer is less susceptible to percolation problems and

average increases in packing distances than the fullerene due to its macromolecular nature, and the fact that the pristine PTB7 film is not in a crystalline, ordered state even before PCBM is introduced. In order to find support for our hypothesis of low electron mobility in PTB7:PCBM being caused by a low degree of phase separation, we examine the microstructural characteristics of the PTB7:PCBM blend.

6.4.5 Microstructural properties of the PTB7:PCBM blend processed with and without DIO

It is known that solvent additives affect the degree of phase separation in PTB7:PCBM [197, 215, 214, 213]. As described in Section 6.3.5, Liang et al. showed that processing with DIO leads to an increase in both FF and J_{sc} (in 60 wt% PCBM blends 100 nm in thickness). The data presented in the sections above, comparing PTB7:PCBM with P3HT:PCBM, were taken using PTB7:PCBM films processed with DIO, corresponding to the case optimised for OPV power conversion efficiency. Here, we perform experiments to observe ourselves the differences in microstructure of PTB7:PCBM films processed with and without DIO.

Absorption spectra

It has been shown that the addition of solvent additives such as ODT and DIO to PCPDTBT:PCBM blends lead to a significant red-shift in absorption of around 30 nm, indicative of stronger inter-chain interactions. It is thought that the additive allows PCPDTBT to form a more ordered structure, which is thought to be the driving force for phase separation in those blends [198, 100, 191, 209]. Absorption spectra of PTB7:PCBM films processed with or without DIO are shown in Figure 6.12. There is no significant change in the absorption spectrum, and hence no evidence for a change in ordering in the PTB7 phase analogous to the case of PCPDTBT. The absence of a change in the absorption spectrum with DIO has not to our knowledge been explicitly noted in the literature, but it is not inconsistent with previous absorption data [197].

TEM imaging of the microstructure

We have employed TEM to make a direct observation of the microstructure of the PTB7:PCBM films processed both with and without DIO, as shown in Figure 6.13. It is immediately obvious from the images that there is a substantial difference in phase separation on the 100nm scale. In both images the darker regions are attributed to PCBM. In the film processed without DIO, PCBM-rich

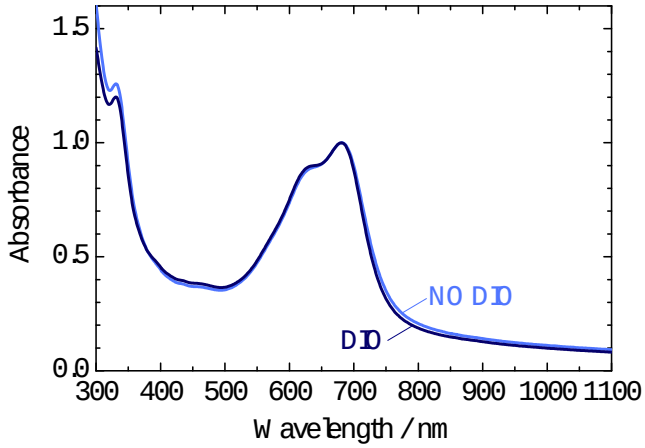

Figure 6.12: Absorption spectra of films of PTB7:PCBM in a 50 wt% PCBM blend processed with and without DIO.

domains of ≈100 nm in size can be seen within the polymer-rich surrounding matrix. Such features are absent in the film processed with DIO, where the largest phase separation is seen on a 1–10 nm scale. Hence, it can be seen that the additive acts to reduce phase separation on the 10–100 nm scale. We note that this behaviour is different from the well-studied behaviour of PCPDTBT:PCBM blends when processed with and without solvent additives such as ODT and DIO, where phase separation is promoted by the additive. However, it can be seen in the film processed without DIO that neither the dark nor the light regions have a uniform appearance. This suggests that there may be significant intermixing on the < 10 nm scale despite the phase separation of fullerene- and polymer-rich regions on the 10–100 nm scale. We note that the TEM images are consistent in these details with the literature [197]. The degree of intermixing was further addressed spectroscopically.

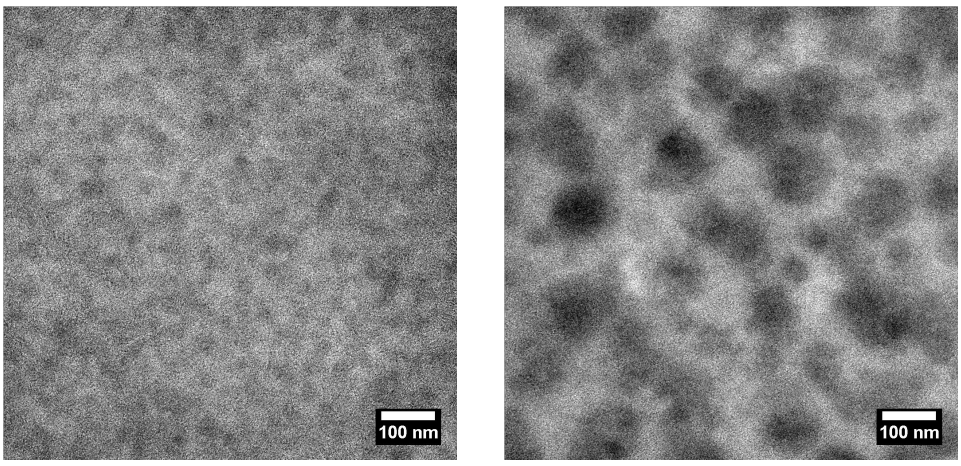

Figure 6.13: TEM images of PTB7:PCBM with 60 wt% PCBM, processed from chlorobenzene with (left) and without (right) DIO additive. The scale bars are 100 nm.

Photoluminescence quenching – a probe of the degree of intermixing

It is interesting to consider the TEM images of the PTB7:PCBM blends with and without DIO additive alongside PL quenching data, as shown in Figure 6.14. PL is a simple but useful tool to semi-quantitatively probe the degree of intermixing on scales below the exciton diffusion length (typically 1–20 nm [82, 83]). Several other factors contribute to the PL quenching in addition to the degree of intermixing, including the exciton diffusion properties and the efficiency of charge separation between polymer and PCBM. However, a comparison of the degree of intermixing can be determined by considering a series of blend films with decreasing PCBM content. At very low PCBM content (for example, 0.1 wt% PCBM), it is assumed that the fullerene molecules are dispersed and that there are no effects of blend microstructure on the PL from the various the polymer:PCBM systems. In this regime, differences in exciton diffusion length and charge separation efficiency between polymer and PCBM dominate. The degree of quenching is rather low, since the probability of an exciton reaching a PCBM acceptor is low. As the PCBM fraction is increased towards 50 wt%, the effects of intermixing become pronounced. If the PCBM is well intermixed, the PL quenching becomes very large, as the probability of an exciton reaching a PCBM acceptor molecule becomes very high. If, in contrast, the phases are separated and not well intermixed, this probability does not increase as quickly or to as high a value, as there remain significant PCBM-free regions where excitons are less likely to be quenched. Hence, a comparison of the PL quenching over a range of PCBM fractions in blends with and without DIO allows the blend microstructure to be probed.

Figure 6.14 shows a comparison of the integrated PL intensity of PTB7:PCBM blends processed with and without DIO, annealed P3HT:PCBM and non-annealed P3HT:PCBM blend films. In each case the integrated signal is normalised to the integrated signal from the corresponding polymer-only film. It is known that the P3HT:PCBM is significantly more intermixed before annealing [200], and hence this difference may be used as a point of comparison. It can be seen that the differences in PL quenching in the 0.1 wt% PCBM blend are rather small. The slightly stronger quenching in P3HT:PCBM (annealed) may reflect a longer exciton diffusion length in the ordered P3HT. However, at larger PCBM fractions, the degree of quenching in the P3HT:PCBM (not annealed) and both PTB7:PCBM blends increases more quickly, and at a certain PCBM fraction the quenching becomes stronger than in the P3HT:PCBM (annealed) blend. We note that the energetic driving force for charge separation is significantly lower in the PTB7:PCBM blends than in

the P3HT:PCBM blend, and hence energetics cannot explain this difference. The difference can be ascribed to a greater extent of intermixing on the < 10 nm scale in both PTB7:PCBM blends relative to both P3HT:PCBM blends. In this detail our findings are consistent with the literature as discussed in Section 6.3.5 [214, 213, 215]. This is also consistent with the relative behaviour in PL quenching of annealed and non-annealed P3HT:PCBM.

It is of interest that the level of PL quenching is slightly stronger in the PTB7:PCBM blend processed without DIO than the blend processed with DIO. This is perhaps surprising given the TEM images above. We note again that the level of PL quenching is dependent not only on the degree of intermixing, but also on the exciton dynamics and the energy and local geometry of charge separation. One potential factor to be explored is the effect of remaining DIO molecules, and whether their presence surrounding fullerene molecules could slow down the electron transfer step. We note that all films were placed under high vacuum to dry before measurement, but this possibility cannot be ruled out. Nonetheless, in the absence of evidence to the contrary, we attribute the change to the degree of intermixing. The stronger quenching in blends without DIO is not in itself inconsistent with the TEM images, but rather requires that the length scales be considered carefully. It appears that increased intermixing on the 10–100 nm scale of the film processed with DIO does not significantly increase the ability for PCBM to quench the polymer emission. It appears that the degree of intermixing on the < 10 nm scale is similar but slightly lower than in the blends processed without DIO. However, we note that this analysis is apparently not consistent with the literature studies listed above (which used X-ray scattering, polarising absorption spectroscopy and energy-filtered TEM techniques). Those studies found a slightly increased degree of intermixing on addition of DIO.

Summary of microstructural measurements on PTB7:PCBM

With the comparison of the PTB7:PCBM and P3HT:PCBM systems, a picture is emerging that the OPV performance, and charge collection efficiency in particular, is closely related to the microstructure of the blend. A worse thickness dependence of the FF in PTB7:PCBM devices compared with P3HT:PCBM devices; a lower SCLC electron mobility in PTB7:PCBM; and indications of a less phase separated microstructure in PTB7:PCBM together suggest that purity and connectivity in the PCBM phase in PTB7:PCBM blends is a problem.

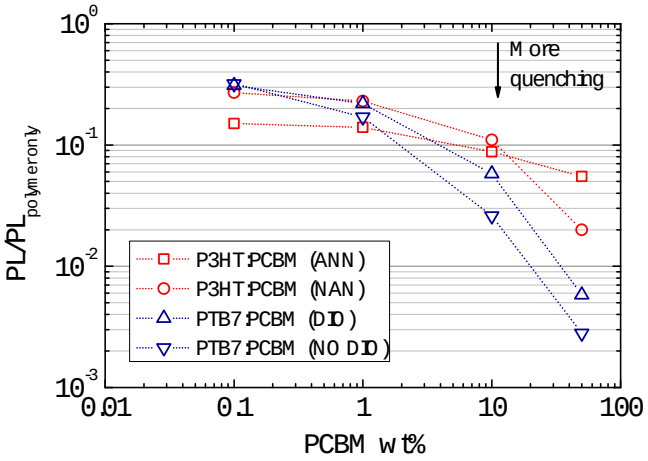

Figure 6.14: Comparison of PL quenching versus polymer only films in non-annealed and annealed P3HT:PCBM and PTB7:PCBM blends with and without solvent additive DIO, with varying polymer:PCBM blend ratios from 0.1 wt% PCBM 50 wt% PCBM. The films are all roughly 100 nm in thickness.

The degree of phase separation appears to be low for the PTB7:PCBM blend processed both with and without DIO. Our own measurements and those in the literature suggest that the PTB7:PCBM blend processed both with and without DIO is highly intermixed on the < 10 nm and even on the < 1 nm scale. Our own PL data and literature structural data are not ostensibly in agreement over the effect of DIO on the degree of intermixing on this scale. However, our TEM measurements and the literature both suggest some level of phase separation into polymer-rich and fullerene-rich domains on the 100 nm scale in blends without DIO, and no such phase separation in blends with DIO.

We will return in a later section to study in more detail the effect of DIO on the PTB7:PCBM blends. At this point we focus on varying the polymer:fullerene ratio of PTB7:PCBM blends (processed without DIO) in order to control the microstructure. We study the correlation between polymer:fullerene ratio, electron and hole carrier mobility and OPV device performance.

6.4.6 Improving the electron transport in PTB7:PCBM by increasing the PCBM content

It was found above that the PTB7:PCBM blend exhibits a two orders of magnitude lower electron mobility than the (annealed) P3HT:PCBM blend, but a very similar hole mobility. TEM and PL experiments suggested that this may be due to a lower degree of phase separation in PTB7:PCBM, leading to poor connectivity and ordering in the PCBM phase. This suggests a simple way of

improving the electron transport: increasing the PCBM content of the blend film. This may be expected to allow the formation of more pure, more ordered and better-connected fullerene domains. Increasing the PCBM fraction may of course be unfavourable for the hole mobility, and hence we consider both electron and hole mobility. Increasing the PCBM fraction will also reduce light harvesting, and hence we consider the OPV performance both in terms of FF and PCE.

We first consider the effect of increasing the PCBM content on the SCLC carrier mobilities. We first study PTB7:PCBM films without DIO additive. Figure 6.15 shows the composition dependence of the electron and hole mobility in PTB7:PCBM blends.

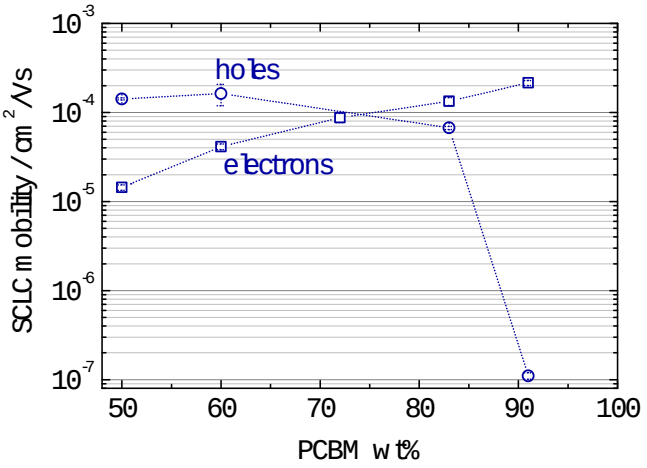

Figure 6.15: SCLC hole and electron mobility of PTB7:PCBM (no DIO additive) as a function of PCBM wt%. All films were ≈100 nm in thickness.

The composition dependence of the electron mobility is strong over the whole range studied. From its initial value of approximately 10^{-5} cm^2/Vs at 50–60 % wt% PCBM, the electron mobility increases by over an order of magnitude to over 10^{-4} cm^2/Vs at 80–90 wt% PCBM. This is not explained by a simple scaling of the SCLC current with the volume fraction of PCBM: a less-than-doubling of the PCBM mass content of the film, from 50 wt% to 91 wt% PCBM, leads to an increase in mobility by a factor of around 15. Rather, the increase in electron mobility must be related to an improvement in packing and/or connectivity. We note that the value of the electron mobility at 90 wt% PCBM is still around one order of magnitude lower than that of pristine PCBM of just above 10^{-3} cm^2/Vs, possibly reflecting the persistent disruptive effect of a small minority of polymer in the blend.

In contrast to the strong composition dependence of the electron mobility over the whole range, the hole mobility varies much less dramatically over approximately 50–80 wt% PCBM. Within this range, the hole mobility remains at around 10^{-4} cm^2/Vs, dropping only by a factor of 2. Above approximately 80–85 wt% PCBM, however, the hole mobility undergoes a sudden dramatic decrease, to around 10^{-7} cm^2/Vs for 90 wt% PCBM. It is likely that this blend corresponds to a polymer content, at 10% by weight and $< 19\%$ by volume (based on [216] and assuming the density of PTB7 is greater than 0.9 g/cm^3), essentially below the percolation threshold. However, the persistence of the high hole mobility of 10^{-4} cm^2/Vs (approximately the same as in an annealed sample of P3HT:PCBM) up to around 80 wt% PCBM suggests that the hole transport in the PTB7:PCBM blend is very robust.

Having found these promising trends for the electron and hole transport, we turn to the OPV performance of such blends. Figure 6.16 shows the composition dependence of the FF and the PCE of OPV devices of PTB7:PCBM processed without DIO to around 100 nm thickness (ie films of the same specification as in the SCLC devices above). It can be seen from Figure 6.16 that the FF is very strongly dependent on the composition of the blend, increasing from around 0.51 for 50–60 wt% PCBM to around 0.60 for 80 wt% PCBM. The increase is approximately uniform between 60 wt% and 80 wt% PCBM. Comparing with the mobility data in Figure 6.15, it can be seen that the increase in FF is correlated closely with an increase in electron mobility (an increase of a factor of 2–3). Over the same range the hole mobility decreases by a factor of approximately 1.5. The difference in electron and hole mobilities is less than one order of magnitude up to 90 wt% PCBM, and hence we may assume that the build-up of space charge does not limit device operation. It may therefore be concluded that the FF at 60 wt% PCBM is limited by poor electron collection. Increasing the PCBM content to 80 wt% allows a significant improvement in electron collection, and does not impact adversely to a significant degree on the hole collection.

Figure 6.16 shows the dependence of PCE on composition. It can be seen that despite the significant increases in FF with increasing PCBM content > 60 wt% the loss in polymer absorption due to replacing polymer with PCBM means that the PCE decreases with increasing PCBM content above 50 wt%. This has a particularly strong effect in this case since we are using PC60BM, and not PC71BM. It may be expected that the improved electron collection may allow thicker active

layers to be used, and that the increase in absorption with thickness may compensate the loss in absorption from using higher PCBM fractions.

Thickness dependences of FF and PCE were carried out for the PTB7:PCBM blends with 60 wt% and 80 wt% PCBM. These are shown in Figure 6.17.

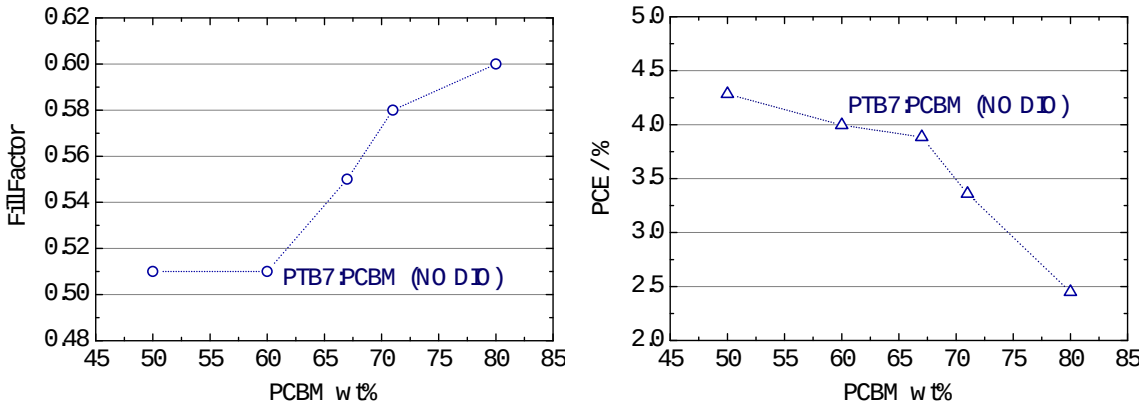

Figure 6.16: Composition dependence of FF (left) and PCE (right) in PTB7:PCBM (processed without DIO additive).

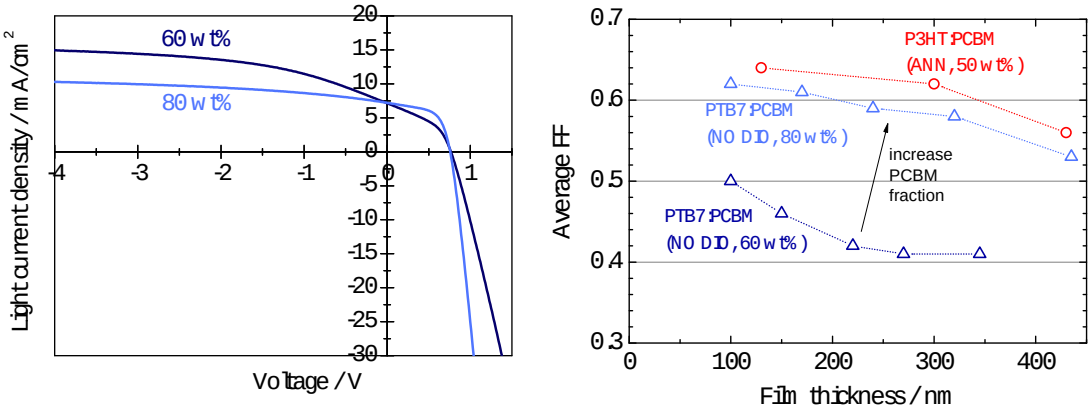

Figure 6.17: Left: Light JV curves showing the improvement in FF of thick devices of PTB7:PCBM (without DIO) by increasing the PCBM content from 60 wt% (270 nm film thickness) to 80 wt% (320 nm film thickness). Right: Improvement of the thickness dependence of the Fill Factor for PTB7:PCBM 80 wt% PCBM as compared with 60 wt% PCBM (both with no DIO additive), and the thickness dependence of P3HT:PCBM for comparison.

The 80 wt% PCBM PTB7:PCBM devices show an impressive improvement in FF relative to the 60 wt% PCBM devices. It can be seen that the thickness performance of the 80 wt% PCBM blend is approximately as good as for the annealed P3HT:PCBM blend, with the FF falling only slightly up

to a thickness of 300 nm and remaining close to 0.6 at this thickness. In contrast, the FF of the 60 wt% PCBM blend starts lower at 0.5 and falls steeply to its limiting value close to 0.4 by a thickness just over 200 nm. The effect of this is that the optimum PCE value of the 80 wt% PCBM blend lies not around 100 nm as for the 60 wt% PCBM blend, but – as a result of the increased absorption – at 320 nm, with the 320 nm device showing a 25% higher PCE than the 100 nm device. This is shown in Figure 6.18.

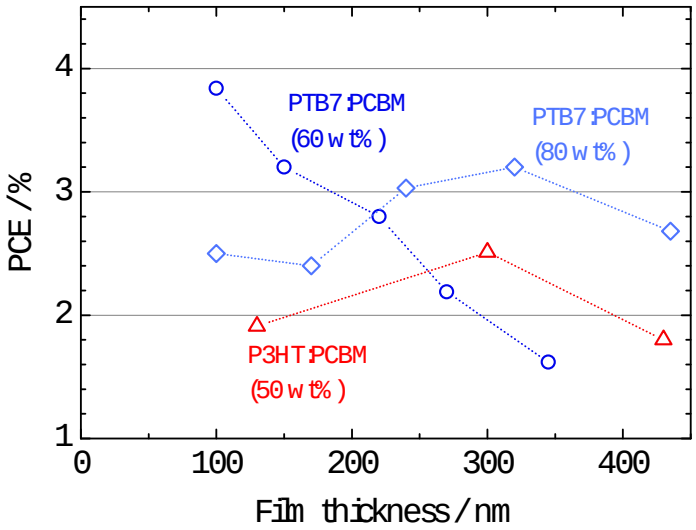

Figure 6.18: Thickness dependences of the PCE for the 60 wt% PCBM and 80 wt% PCBM PTB7:PCBM blends (without DIO), and that of the 50 wt% PCBM P3HT:PCBM blend for comparison. It can be seen that the improved charge collection in the 80 wt% PCBM blend relative to the 60 wt% PCBM blend allows thicker devices to be employed, with a peak PCE at a thickness > 300 nm, similar to the 50 wt% PCBM P3HT:PCBM blend.

This confirms that increasing the PCBM content of the PTB7:PCBM blend to 80 wt% leads to much-improved electron collection (and therefore much-improved overall charge collection). The 80 wt% PCBM blend shows a thickness dependence comparable with the optimised annealed P3HT:PCBM blend. However, it can be seen that even when the thickness of the 80 wt% PCBM blend is 'optimised' to 320 nm, the maximum efficiency obtained is around 20% lower than in the 100 nm 60 wt% PCBM blend, as shown in Figure 6.18. Therefore, we can see that due to the absorption penalty the strategy of increasing PCBM content is unlikely to lead to an overall increase in PCE. We note that this result may be improved by the use of PC71BM, which is absorbs more strongly than PC61BM. This has not been tested here. In any case, this approach has given us a clear picture of the importance of removing the limit to charge collection, and to electron collection in

particular, in the PTB7:PCBM blend.

6.4.7 Effect of DIO solvent additive on PCE and mobility in PTB7:PCBM

It was discussed in Section 6.3.5 that the use of the solvent additive DIO for PTB7:PCBM significantly improves the OPV performance in 60 wt% PCBM blends. As shown in Figure 6.19, the PCE is improved through increases in FF and J_{sc}.

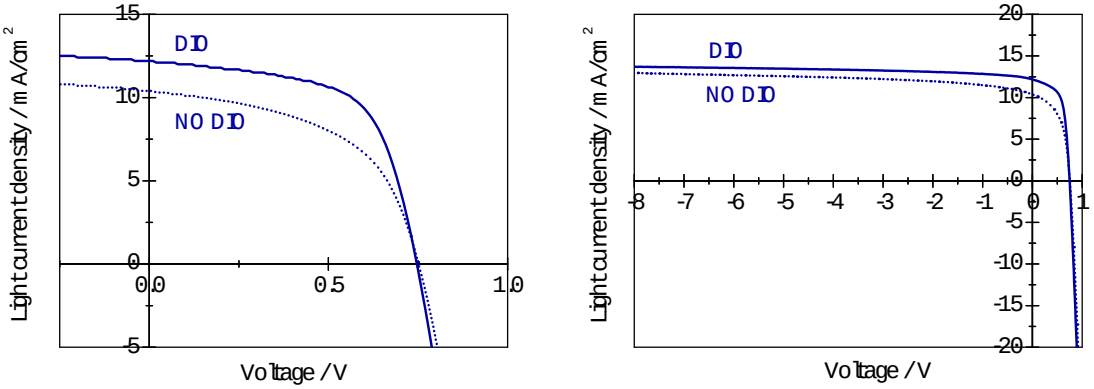

Figure 6.19: Light JV curve (shown on two different scales for clarity) for a comparison of 60 wt% PCBM PTB7:PC60BM blends processed from chlorobenzene with and without a 3wt% 1,8-diiodooctane solvent additive. The PCE increases from 4.1% to 5.6% due to increases in the FF and J_{sc}.

The microstructural changes in the blend film caused by the addition of DIO were discussed in Section 6.4.5. Absorption spectra show no evidence of increased order in the polymer phase. TEM imaging measurements suggest that blends processed without DIO are more phase-separated on the 10–100 nm scale, but remain intermixed on the < 10 nm scale. PL measurements suggest that blends processed without DIO are similarly or slightly more intermixed on the < 10 nm scale.

We have studied the effect of DIO in PTB7:PCBM OPV devices with different PCBM fractions, as shown in Figure 6.20. The corresponding data for devices processed without DIO are shown for comparison.

It is clear that the improvement in FF by processing with DIO seen for the 60 wt% PCBM blends is not uniformly reproduced over the composition range. Rather, the effect of the DIO additive appears to be to shift the optimum composition for FF to a significantly lower PCBM fraction, between 60 wt% and 70 wt%. In devices processed without DIO, the FF increases for increasing

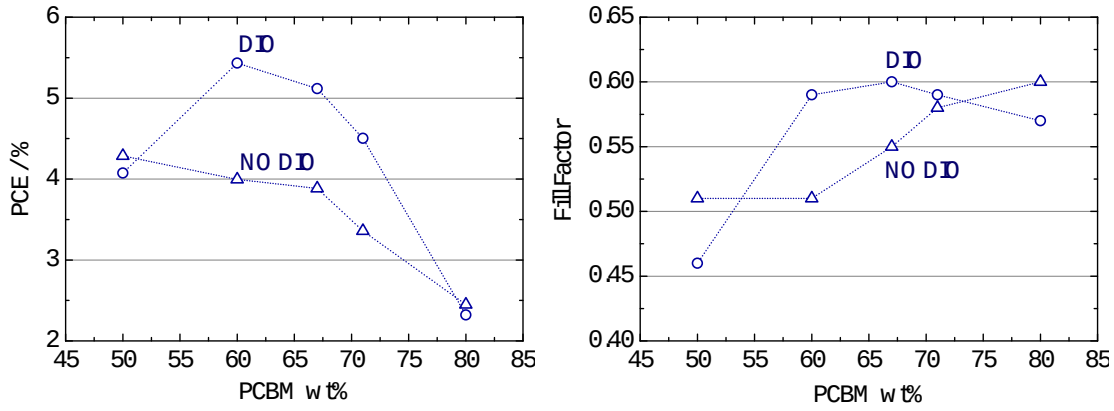

Figure 6.20: Composition dependence of FF (left) and PCE (right) in PTB7:PCBM without and with DIO. All films are ≈100 nm.

PCBM fractions over the whole range, with the fastest increase between PCBM 60 wt% and 70 wt% PCBM. In devices processed with DIO, the fastest increase in FF is between 50 wt% and 60 wt% PCBM, and the FF actually decreases above approximately 70 wt% PCBM. For this system, the FF increase from 50 wt% to 60 wt% PCBM is strong enough that it is not compensated by the reduction in absorption by replacing polymer with PCBM, and the PCE maximum is seen at 60 wt% PCBM. The PCE of this sample at ≈100 nm is larger than that achievable at any thickness and any composition in blends without DIO. Above 70 wt% PCBM, both the FF and the absorption decrease, leading to a strong reduction in PCE.

Given the trend with composition of the FF in the devices processed with DIO, and given our hypothesis as outlined in the above Section 6.4.4 regarding electron collection as the primary problem in the system, we may expect that the effect of DIO is to improve the electron transport at intermediate compositions (60–70 wt%). It is therefore of great interest to characterise the transport directly in the system processed with DIO. Figure 6.21 shows the composition dependences of the SCLC electron and hole mobility in PTB7:PCBM blends processed with DIO alongside the system processed without DIO for comparison.

It can be seen that the blends with DIO additive, like the blends without DIO, show a weak composition dependence of the hole mobility in the range of PCBM fractions 50–83 wt% (we do not have data for the 91 wt% PCBM blend in the case with DIO additive). In fact, it can be seen that the hole mobility in PTB7:PCBM with the DIO additive is essentially unchanged from the case without

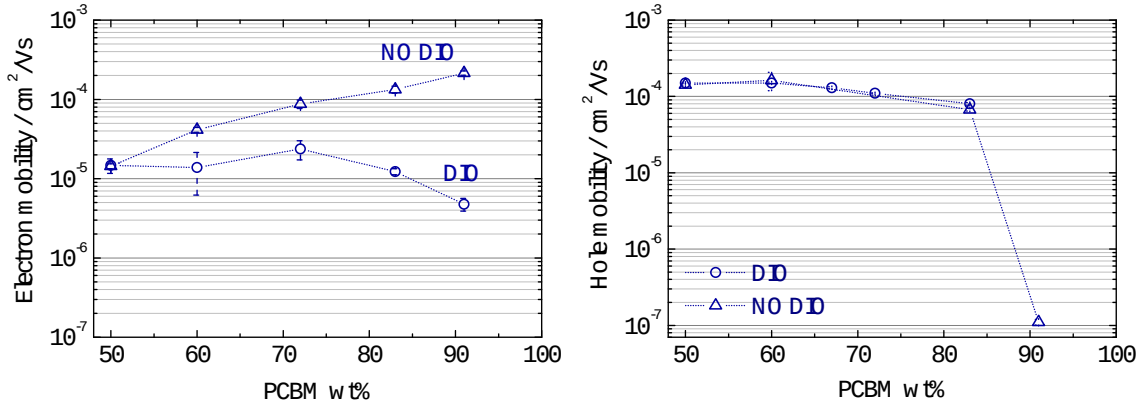

Figure 6.21: Composition dependence of SCLC electron mobility (left) and hole mobility (right) in PTB7:PCBM blends processed with or without DIO. All films are ≈100 nm in thickness.

DIO. The SCLC results therefore suggest that the additive has no effect on the hole transport.

In contrast, the electron mobility shows a significant difference. Whilst the electron mobilities for the 50 wt% PCBM blends are essentially the same with and without DIO, the blends processed with DIO show almost no composition dependence, with a low mobility of around 10^{-5} cm^2/Vs measured for the whole range of PCBM fractions 50–83 wt%. Even a small decrease (by a factor of around 2) is measured for the 90 wt% PCBM blend. This is clearly a very different behaviour from that in the blends without DIO additive, where increasing the PCBM content leads to an increase of over one order of magnitude in electron mobility over the same range. We note that the electron mobility measurements were carried out three times in order to confirm this result; the values obtained were the same to within a factor of two across all compositions each time. We also note that the devices were stored at high vacuum ($< 10^{-6}$ mbar) for at least 30 minutes before contact deposition, and hence rule out any electron-trapping effects of residual DIO additive analogous to the hole trapping effect of ODT as observed in FETs by Cho et al. [208]. It is clear, therefore, that the mobility data does not in this case offer an explanation for the enhanced OPV performance of PTB7:PCBM blends when processed with DIO. The mobility data is also unable to explain the composition dependence of the OPV performance of blends processed with DIO.

The enhancement in FF and the shift in the optimum composition on addition of DIO has been shown only for devices of approximately 100 nm thickness. Figure 6.22 shows the thickness dependence of the FF in 60 wt% PCBM blends processed with and without DIO, and the 80 wt% PCBM blend processed without DIO from Section 6.4.6.

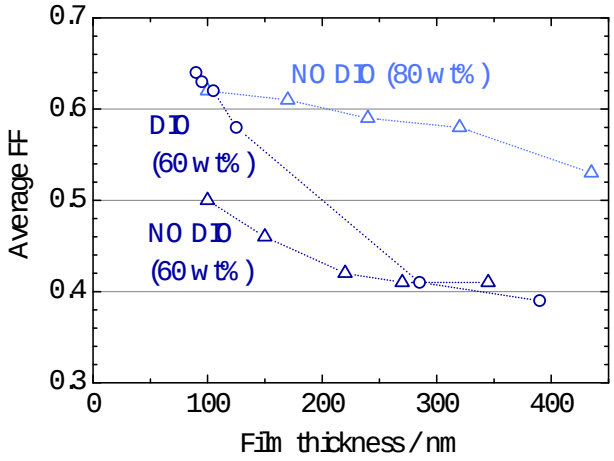

Figure 6.22: Thickness dependence of FF for 60 wt% PCBM PTB7:PCBM blends with and without DIO processing additive, and of 80 wt% PCBM PTB7:PCBM blends without DIO.

Figure 6.22 shows a large improvement in FF with DIO only for devices approximately 100 nm in thickness. The FF drops sharply from over 0.6 at 100 nm to around 0.4 at 250–300 nm. We can see therefore that the charge collection problem is not fully solved by processing with DIO; thick films capable of absorbing all incident useable light still show low PCE. It is clear that processing with DIO is not as advantageous for charge collection as increasing the fullerene content. This is interesting, and supports the findings of the SCLC measurements that the origin of the enhanced FF in 100 nm devices with DIO does not lie in improvements in charge transport. The origin of the enhanced FF cannot be deduced from the data presented.

However, we do know from the data presented in this Chapter that problems in electron collection are the dominant reason for sub-optimal performance in the PTB7:PCBM blend. It may be speculated, therefore, that the effect of the DIO is indeed to improve the collection of electrons, but that the change is not reflected in the SCLC mobility measurements. This could entail, for example, a reduction in the concentration of isolated PCBM nanocrystallites within the polymer-rich phase, or the formation of a 'cleaner' interface between the two materials. From the TEM and PL data above it is clear that in both cases there is a high degree of intermixing and low domain purity, but there may be important differences at the nanoscale which those methods cannot detect. Such changes may not be reflected in SCLC measurements, but may be observable as changes in carrier lifetime. Experiments to test this are now underway. We note, however, that the electron mobility as measured by SCLC in 60 wt% PCBM devices processed with DIO is in fact 2–3 times smaller

than the electron mobility in devices processed without DIO, and hence the increase in lifetime would need to be large to overcompensate this reduction. Further structural and spectroscopic insight into the differences of blends processed with and without DIO should be a priority for future work.

6.5 Conclusions and implications

We have carried out a detailed and systematic study of carrier mobility and OPV device performance, concentrating on the PTB7:PCBM system and comparisons with the P3HT:PCBM and PCPDTBT:PCBM systems. In particular, we set out to address the question of why state-of-the-art OPV systems such as PTB7:PCBM perform so much worse at large active layer thicknesses than P3HT:PCBM. We have shown that the FF of PTB7:PCBM devices decreases steeply from > 0.6 at 100 nm thickness to approximately 0.4 for thicknesses > 300 nm. Annealed P3HT:PCBM devices, in contrast, are able to show FF > 0.6 for thicknesses up to 300–400 nm.

The primary finding of this study is that low electron mobility is the dominant cause of the poor performance of PTB7:PCBM relative to P3HT:PCBM at larger film thicknesses. We have found that the electron mobility in PTB7:PCBM blends is 1–2 orders of magnitude lower than the electron mobility in annealed P3HT:PCBM for all film thicknesses up to 400 nm. The hole mobility, in contrast, was found to be the same to within a factor of approximately three in all devices studied. Many studies addressing charge transport in OPV only explicitly consider hole mobility in the blend, likely a result of the difficulty in obtaining reliable electron mobility values. This study demonstrates that electron transport in the blend must be considered in conjunction with hole transport for a meaningful comparison between different devices.

It is proposed that the low electron mobility in PTB7:PCBM is due to a low degree of phase separation of the polymer and PCBM, such that ordering and connectivity in the fullerene phase are inhibited. Methods described in the literature to control phase separation, including choice of solvent(s), variation of drying time and thermal annealing, have been outlined briefly. Thermal annealing, highly effective in increasing phase separation in P3HT:PCBM [47, 90], has not been effective for blends using the more recent OPV polymers, including PCPDTBT and PTB7. This is likely a result of the lower tendency towards crystallisation of these polymers compared with P3HT.

Solvent additives such as ODT and DIO have been shown to offer an alternative route [198, 197]. We have examined the PCPDTBT:PCBM system for comparison with PTB7:PCBM as a well-studied system which requires solvent additives for optimised PCE [198, 191, 100, 208]. We have found, in agreement with the majority of the literature, that the effect of the ODT additive in this case is to increase the degree of phase separation in the blend. This was found to lead to an increase in electron mobility of nearly an order of magnitude, with no significant change in hole mobility.

It is known that processing PTB7:PCBM with the solvent additive DIO leads to a higher FF in blends with 60 wt% PCBM [197]. We have shown through TEM and PL measurements that PTB7:PCBM blends both with and without DIO display less phase separation on the 1–100 nm scale than annealed P3HT:PCBM. Given the hypothesis that a low degree of phase separation in the 60 wt% blends leads to a low electron mobility, this is consistent with the observation that PTB7:PCBM blends with and without DIO both show a steep decrease in FF for thicknesses above 100 nm. Also in agreement with this hypothesis is the finding using SCLC measurements that the FF enhancement through using DIO is *not* due to a mobility increase for either electrons or holes. We have speculated that the FF enhancement through processing with DIO may be due to an increased purity of the polymer-rich phase or a 'cleaner' interface between the two phases, properties which may be observable as changes in the charge carrier lifetime. Experiments are underway to test this.

In order to confirm the hypothesis that electron collection is the primary limiting factor in PTB7:PCBM blends, we have studied the effect of increasing the fullerene content in PTB7:PCBM blends without DIO additive. We have shown that increasing the PCBM content from the PCE-optimised value of 60 wt% to 80 wt% allows a thickness dependence almost as good as that of annealed P3HT:PCBM. As for annealed P3HT:PCBM, the optimum thickness for PCE of PTB7:PCBM with 80 wt% PCBM is found above 300 nm. This improvement has been correlated using SCLC measurements to an increase in electron mobility, with almost no change observed in hole mobility. Although in this case the loss in absorption due to the replacement of polymer with fullerene overcompensates the gain in electron collection, the result confirms that by improving the electron transport alone efficient electron and hole collection is possible for PTB7:PCBM devices greater than 300 nm in thickness.

Together, therefore, the evidence from the P3HT:PCBM, PCPDTBT:PCBM and PTB7:PCBM

systems suggests that a low electron mobility due to a low degree of phase separation is likely to be a general problem for state-of-the-art OPV systems. It appears that the low degree of phase separation is in turn a result of the low tendency of the polymers to crystallise. A key challenge for OPV researchers is thus to achieve better connectivity and ordering in the fullerene phase in blends without necessitating either (i) a large excess of fullerene or (ii) strong crystallisation of the polymer. Use of solvent additives is one route to achieve this, but novel methods may need to be developed. It may be estimated that approximately one third of the incident available light in state-of-the-art devices is wasted due to the requirement for active layers to be no more than 100 nm in thickness [111]. We have shown that by improving only the electron transport, FF values close to 0.6 are possible for PTB7:PCBM devices > 300 nm in thickness. It may be hypothesised that if active layer thicknesses could be increased in this way without the need for a higher fullerene fraction, PCEs up to 50% larger than the current values for 100 nm devices may be within reach. Making a simple estimate using the current published record PCE of 8.4% for PTB7:PCBM [89] – assuming a 50% increase in J_{sc} and a reduction in FF to only 0.6 for a hypothetical thick device – we obtain a hypothetical PCE of close to 11%. Hence, optimisation of the electron transport properties of state-of-the-art OPV blends should be a topic of high priority for research.

Chapter 7

Conclusions and Future Work

7.1 Hole transport in a family of polyfluorenes

We have achieved our initial aim of explaining the mechanism of mobility enhancement in F8:F4/1 relative to PFO as first observed by Yap et al. [16], and in the process we have set out a clearer picture of the charge transport properties in the polyfluorene family. The mechanism of mobility enhancement in F8:F4/1 has been shown to be a suppression of the formation of minority non-glassy phases, more precisely (i) the beta-phase conformation and (ii) the crystalline phases found in spin-coated PFO films. Spectroscopic, optical, structural and thermal measurements have shown that the shorter, branched side-chain structure in F8:F4/1 prohibits the formation of an analogous beta-phase conformation, and also strongly suppresses crystallisation.

Through careful processing at elevated temperature, we have been able to fabricate the corresponding glassy isotropic film of PFO, and measure in it the high time-of-flight mobility of above 10^{-2} cm^2/Vs seen in F8:F4/1. We are then able to introduce into this glassy isotropic film either the beta-phase or the crystalline phase, in isolation. Remarkably, the presence of the beta-phase alone reduces the mobility by more than two orders of magnitude to around 10^{-4} cm^2/Vs. This is the first time to our knowledge that the trapping effect of a single conformational defect has been elucidated. Introducing the crystalline phase by thermal annealing invariably reduces the mobility to around 10^{-3} cm^2/Vs.

Suggested future work:

- The observation of high mobility in glassy isotropic films offers the exciting prospect of devel-

oping high mobility materials in situations where crystallinity involving cofacial π–stacking is undesirable, such as those requiring efficient luminescence. It is therefore of interest to look for other material systems with low tendencies to π–stack whose mobility may, like PFO, have been limited by minority conformational phases or minority crystalline phases to well below what they can achieve. We suggest that materials which show (i) a large difference between FET mobility and ToF mobility and/or (ii) a large difference between intra-chain TRMC mobility and bulk ToF mobility may be good candidates. Property (i) may be used to identify materials where small minority phases act as traps in ToF experiments and in device operation. Property (ii) suggests revisiting the polymers such as the polyfluorenes, the polyindenofluorenes and the ladder-type polyphenylenes, which show fairly planarised backbones and high intra-chain mobilities. Indeed, Kim et al. [36] have already demonstrated high time-of-flight mobilites in an amorphous indenofluorene-phenanthrene copolymer.

- In cases where the bulk mobility is not limited by trapping species such as the beta-phase or minority crystallites, it is likely to be limited by the fastest percolating inter-chain transfer sites. In the study of Yap et al., these sites were originally suggested to be mediated by the F4/1 units where neighbouring polymers may approach more closely. This thesis shows that whatever the nature of the preferential sites, they are able to occur in PFO as well as in F8:F4/1. It is of interest whether these fast transfer sites are indeed regions of close approach, and if so, how they could be made even faster. Imaginative experiments to address this question may allow the design of non-crystalline polymers with ever higher bulk mobilities.

- We have focused on the possibility of achieving high mobility in glassy amorphous films. However, the study also suggests the possibility of increasing the mobility in polyfluorenes by increasing the fraction of either crystalline phase or beta-phase. Regarding a higher crystalline fraction, it appears that conventional thermal annealing routes will not succeed, and novel routes would be needed. In concurrence with the high intra-chain mobility of beta-phase PFO [124], it may be speculated that a percolating beta-phase may allow extremely high bulk mobility. A recent study succeeded in inducing a beta-phase fraction of almost 50% into a thin film using mixed solvents [137]. With increased understanding of the process of formation of the beta-phase and its spatial uniformity, such experiments may be within reach.

7.2 Electron transport in fullerene multi-adducts

We have used temperature-dependent transport studies to distinguish between the effects on mobility of energetic and configurational disorder in the family of fullerene derivatives PCBM, bis-PCBM and tris-PCBM. The low electron mobility in the multi-adducts bis-PCBM and tris-PCBM has been attributed to one or both of: (i) increased energetic disorder due to the presence of a mixture of isomers with varying LUMO energies, or (ii) increased configurational disorder due to the disruptive effect of the additional side-chains on molecular packing [26, 105].

Our transport measurements reveal large differences in energetic disorder between the fullerenes, roughly consistent with the modelling and electrochemical study of Frost et al. [114] which predicted variations in the LUMO levels of the multi-adduct isomers of up to several 100 meV. The transport measurements also indicate that the variation in configurational disorder between the fullerenes is negligible. The large differences in electron mobility between PCBM, bis-PCBM and tris-PCBM are therefore concluded to be predominantly due to differences in energetic disorder resulting from the isomeric mixture. Where separation of the isomers is precluded, the presence of isomers with different LUMO levels presents a strict limit on the achievable transport properties of fullerene multi-adducts, and thus on their use in OPV devices. Design rules for novel OPV acceptors of any type must include a consideration of energetic disorder introduced through the production of isomers.

Suggested future work:

- An acid test for the above conclusion would be to repeat the transport measurements on separated isomers of the multi-adducts. High purity samples of a single isomer of tris-PCBM ought to show, according to the above findings, a FET electron mobility comparable with that of PCBM. The issue of obtaining a favourable blend microstructure in OPV devices using the multi-adducts may remain [217, 168], but the higher mobility in the fullerene may lead to significantly improved device performance. Alternatively, other multi-adduct structures may lead to isomers without the large variation in LUMO energies, making them more tolerable from a mobility perspective [174].
- Follow-up work is planned using the in-house Imperial transport model as described in Section 4.6.3 to examine whether the large mobility variations between the fullerenes can be explained

by only the differences in energetic disorder measured by Frost et al. [114].

- Further structural evidence may be able to offer support for the notion that configurational disorder is not a significant problem in the multi-adducts. The similar mobility of PCBM, bis-PCBM and tris-PCBM when extrapolated towards infinite temperature implies, surprisingly, that the transfer integral for electron hops is not greatly affected by the additional side-chains. There is some support for this in the study of Guilbert et al., who carried out XRD on blends of P3HT with PCBM, bis-PCBM and tris-PCBM [217] (Supporting Information). While the fullerene signal is very diffuse, there is no evidence of a difference in average packing distance between the different fullerenes. Further structural measurements may be more conclusive.

7.3 Electron transport in polymer:PCBM blends for OPV

We have addressed the question of why state-of-the-art OPV systems such as PTB7:PCBM perform so much worse at large active layer thicknesses than P3HT:PCBM. It may be estimated that approximately one third of the incident available light is wasted due to the requirement for active layers to be no more than 100 nm in thickness [111]. By correlating mobility measurements with OPV device data, we have shown conclusively that low electron mobility in PTB7:PCBM is the main cause of this shortcoming. We have found that the electron mobility in PTB7:PCBM blends is 1–2 orders of magnitude lower than in annealed P3HT:PCBM for all film thicknesses up to 400 nm. The hole mobility, in contrast, was found to be the same to within a factor of approximately three in all devices studied. We propose that the low electron mobility results from the low degree of phase separation of PTB7 and PCBM in the blend, as observed using TEM and PL quenching experiments. It appears that this leads to a disordered and poorly-connected PCBM phase. The low degree of phase separation is likely to be due to the low tendency of PTB7 to crystallise. Since other state-of-the-art OPV polymers show a low tendency to crystallise, we suggest that poor electron transport is the primary reason for the thickness limit across these polymer:PCBM systems.

We have shown that increasing the PCBM content in PTB7:PCBM from the PCE-optimised value of 60 wt% to 80 wt% allows a thickness dependence almost as good as that of annealed P3HT:PCBM, and a FF close to 0.6 above 300 nm. However, not surprisingly, such devices show decreased absorption. Unfortunately, the use of DIO solvent additive, successful in increasing phase separation and electron mobility in PCPDTBT:PCBM blends, does not increase the degree of phase separation or

electron mobility in PTB7:PCBM and does not lead to good electron collection in thick devices. A key challenge for OPV researchers is thus to develop improved methods to ensure connectivity and ordering in the fullerene phase in blends without relying on either (i) a large excess of fullerene or (ii) strong crystallisation of the polymer.

Suggested future work:

- The effect of DIO on PTB7:PCBM remains unclear. We have verified literature TEM data apparently showing less phase separation on the 1–100 nm scale in films processed with DIO, but have seen a slightly decreased level of PL quenching in those films, at odds with the TEM data. In any case, neither observation satisfactorily explains the dramatic effect on FF and PCE of DIO for 60 wt% PCBM devices at low thicknesses. We have suggested that the DIO additive may increase the purity of the polymer phase or lead to a 'cleaner' interface between the two materials, reducing nongeminate recombination and increasing carrier lifetime, but these hypotheses are as yet unsupported. In order to address this further, we have begun a collaboration with the Department of Chemistry at Imperial to examine the PTB7:PCBM blends fabricated with and without DIO using charge extraction and transient photovoltage techniques. These experiments will allow a measurement of effective carrier lifetime and effective carrier mobility under OPV operating conditions.

- Improved methods to ensure ordering and/or connectivity in the fullerene phase may allow drastic increases in device thickness and, therefore, efficiency. In the absence of polymer crystallinity, thermal annealing routes as used for P3HT:PCBM are ineffective. Processing with various solvent additives such as DIO and ODT has shown some excellent results, and this approach will be pursued. Inhibiting the intercalation of fullerenes into the polymer chain by varying fullerene size or sidechain spacing is another way to promote nm-scale phase separation [169], but this does not generally extend to controlling phase separation on a larger scale. The idea of using polymerised fullerenes in OPV devices is intriguing, but a previous attempt gave fairly poor device performance [218]. This vibrant research community will, no doubt, find new solutions.

7.4 List of Publications

Foster S. et al.: *The limiting role of beta-phase in time-of-flight charge transport in poly(9,9-dioctylfluorene), and mobility enhancement through inhibiting its formation*, to be submitted to Adv. Mater.

Foster S. et al.: *Electron collection as a limit to polymer:PCBM solar cell efficiency: effect of blend microstructure on carrier mobility and device performance in PTB7:PCBM*, in preparation

Koch F., Rivnay J., Foster S., Mueller C., Downing J., Buchaca-Domingo E., Westacott P., Yu L., Yuan M., Baklar M., Luscombe C., McLachlan M., Heeney M., Rumbles G., Silva S., Salleo A., Nelson J., Smith P. and Stingelin N.: *Microstructure development with molecular weight in semicrystalline organic semiconductors and its influence on charge transport*, Prog. Polym. Sci., 2013, submitted

Faist M.A., Shoai S., Tuladhar S.M., Dibb G.F.A., Foster S., Gong W., Kirchartz T., Bradley D.D.C., Durrant J.R. and Nelson J.: *Understanding the reduced efficiencies of organic solar cells employing fullerene multiadducts as acceptors*, Adv. Energy Mater., 2013, accepted

Faist M.A., Keivanidis P.E., Foster S., Woebkenberg P.H., Anthopoulos T.D., Bradley D.D.C., Durrant J.R. and Nelson J.: *Effect of multiple adduct fullerenes on charge generation and transport in photovoltaic blends with poly(3-hexylthiophene-2,5-diyl)*, J. Polym. Sci. B Polym. Phys., 2011, 49, 45-51

Agostinelli T, Ferenczi T.A.M., Pires E., Foster S., Maurano A., Mueller C., Ballantyne A., Hampton M., Lilliu S., Campoy-Quiles M., Azimi H., Morana M., Bradley D.D.C., Durrant J.R., Macdonald J.E., Stingelin N. and Nelson J.: *The role of alkane dithiols in controlling polymer crystallization in small band gap polymer:fullerene solar cells*, J. Polym. Sci. B Polym. Phys., 2011, 49, 717-724

Bibliography

[1] T. Hasegawa and J. Takeya, "Organic field-effect transistors using single crystals," *Science and Technology of Advanced Materials*, vol. 10, p. 024314, Apr. 2009.

[2] H. N. Tsao, D. M. Cho, I. Park, M. R. Hansen, A. Mavrinskiy, D. Y. Yoon, R. Graf, W. Pisula, H. W. Spiess, and K. Muellen, "Ultrahigh mobility in polymer field-effect transistors by design," *Journal of the American Chemical Society*, vol. 133, pp. 2605–2612, Mar. 2011.

[3] S. Wang, M. Kappl, I. Liebewirth, M. Mueller, K. Kirchhoff, W. Pisula, and K. Muellen, "Organic field-effect transistors based on highly ordered single polymer fibers," *Advanced Materials*, vol. 24, no. 3, pp. 417–420, 2012.

[4] P. Borsenberger and D. S. Weiss, *Organic receptors for xerography*. New York: Marcel Dekker, Inc., 1998.

[5] J. Benson-Smith and J. Nelson, "Organic donor-acceptor heterojunction solar cells," in *Nanostructured and Photoelectrochemical Systems for Solar Photon Conversion* (M. D. Archer and A. J. Nozik, eds.), ch. 7, Imperial College Press, London, 2008.

[6] R. J. Fessenden, J. S. Fessenden, and M. W. Logue, *Organic Chemistry*. Brooks/Cole Publishing Company, Jan. 1998.

[7] M. Knupfer, J. Fink, and D. Fichou, "Strongly confined polaron excitations in charged organic semiconductors," *Physical Review B*, vol. 63, p. 165203, Apr. 2001.

[8] K. E. Ziemelis, A. T. Hussain, D. D. C. Bradley, R. H. Friend, J. Rhe, and G. Wegner, "Optical spectroscopy of field-induced charge in poly(3-hexyl thienylene) metal-insulator-semiconductor structures: Evidence for polarons," *Physical Review Letters*, vol. 66, pp. 2231–2234, Apr. 1991.

[9] H. Sirringhaus, "Device physics of solution-processed organic field-effect transistors," *Advanced Materials*, vol. 17, no. 20, pp. 2411–2425, 2005.

[10] J.-L. Bredas, D. Beljonne, V. Coropceanu, and J. Cornil, "Charge-transfer and energy-transfer processes in pi-conjugated oligomers and polymers: a molecular picture," *Chemical Reviews*, vol. 104, pp. 4971–5004, Nov. 2004.

[11] V. Coropceanu, J. Cornil, D. A. da Silva Filho, Y. Olivier, R. Silbey, and J.-L. Bredas, "Charge transport in organic semiconductors," *Chemical Reviews*, vol. 107, pp. 926–952, Apr. 2007.

[12] Z. B. Henson, K. Muellen, and G. C. Bazan, "Design strategies for organic semiconductors beyond the molecular formula," *Nature Chemistry*, vol. 4, no. 9, pp. 699–704, 2012.

[13] H. Baessler, "Charge transport in disordered organic photoconductors a monte carlo simulation study," *physica status solidi (b)*, vol. 175, no. 1, pp. 15–56, 1993.

[14] T. Kreouzis, D. Poplavskyy, S. M. Tuladhar, M. Campoy-Quiles, J. Nelson, A. J. Campbell, and D. D. C. Bradley, "Temperature and field dependence of hole mobility in poly(9,9-dioctylfluorene)," *Physical Review B*, vol. 73, p. 235201, June 2006.

[15] J. C. Blakesley, M. Schubert, R. Steyrleuthner, Z. Chen, A. Facchetti, and D. Neher, "Time-of-flight measurements and vertical transport in a high electron-mobility polymer," *Applied Physics Letters*, vol. 99, pp. 183310–183310–3, Nov. 2011.

[16] B. K. Yap, R. Xia, M. Campoy-Quiles, P. N. Stavrinou, and D. D. C. Bradley, "Simultaneous optimization of charge-carrier mobility and optical gain in semiconducting polymer films," *Nature Materials*, vol. 7, no. 5, pp. 376–380, 2008.

[17] S. M. Tuladhar, M. Sims, J. Kirkpatrick, R. C. Maher, A. J. Chatten, D. D. C. Bradley, J. Nelson, P. G. Etchegoin, C. B. Nielsen, P. Massiot, W. N. George, and J. H. G. Steinke, "Influence of alkyl chain length on charge transport in symmetrically substituted poly(2,5-dialkoxy-p-phenylenevinylene) polymers," *Physical Review B*, vol. 79, p. 035201, Jan. 2009.

[18] C. Melzer, E. J. Koop, V. D. Mihailetchi, and P. W. M. Blom, "Hole transport in poly(phenylene vinylene)/Methanofullerene bulk-heterojunction solar cells," *Advanced Functional Materials*, vol. 14, no. 9, pp. 865–870, 2004.

[19] H. Baessler and A. Koehler, "Charge transport in organic semiconductors," in *Unimolecular and Supramolecular Electronics I* (R. M. Metzger, ed.), vol. 312 of *Topics in Current Chemistry*, pp. 1–65, Springer Berlin / Heidelberg, 2012.

[20] A. Miller and E. Abrahams, "Impurity conduction at low concentrations," *Physical Review*, vol. 120, pp. 745–755, Nov. 1960.

[21] D. Hertel and H. Baessler, "Photoconduction in amorphous organic solids," *ChemPhysChem*, vol. 9, no. 5, pp. 666–688, 2008.

[22] R. Coehoorn, W. F. Pasveer, P. A. Bobbert, and M. A. J. Michels, "Charge-carrier concentration dependence of the hopping mobility in organic materials with gaussian disorder," *Physical Review B*, vol. 72, p. 155206, Oct. 2005.

[23] V. I. Arkhipov, E. V. Emelianova, and G. J. Adriaenssens, "Effective transport energy versus the energy of most probable jumps in disordered hopping systems," *Physical Review B*, vol. 64, p. 125125, Sept. 2001.

[24] P. M. Borsenberger, L. T. Pautmeier, and H. Baessler, "Nondispersive-to-dispersive charge-transport transition in disordered molecular solids," *Physical Review B*, vol. 46, pp. 12145–12153, Nov. 1992.

[25] H. Baessler and P. Borsenberger, "The transition from nondispersive to dispersive charge transport in vapor deposited films of 1-phenyl-3-p-diethylamino-styryl-5-p-diethylphenylpyrazoline (DEASP)," *Chemical Physics*, vol. 177, pp. 763–771, Dec. 1993.

[26] M. Lenes, S. W. Shelton, A. B. Sieval, D. F. Kronholm, J. C. K. Hummelen, and P. W. M. Blom, "Electron trapping in higher adduct fullerene-based solar cells," *Advanced Functional Materials*, vol. 19, no. 18, pp. 3002–3007, 2009.

[27] H. C. F. Martens, P. W. M. Blom, and H. F. M. Schoo, "Comparative study of hole transport in poly(p-phenylene vinylene) derivatives," *Physical Review B*, vol. 61, pp. 7489–7493, Mar. 2000.

[28] M. C. J. M. Vissenberg and M. Matters, "Theory of the field-effect mobility in amorphous organic transistors," *Physical Review B*, vol. 57, pp. 12964–12967, May 1998.

[29] W. F. Pasveer, J. Cottaar, C. Tanase, R. Coehoorn, P. A. Bobbert, P. W. M. Blom, D. M. deLeeuw, and M. A. J. Michels, "Unified description of charge-carrier mobilities in disordered semiconducting polymers," *Physical Review Letters*, vol. 94, p. 206601, May 2005.

[30] V. I. Arkhipov, P. Heremans, E. V. Emelianova, G. J. Adriaenssens, and H. Baessler, "Weak-field carrier hopping in disordered organic semiconductors: the effects of deep traps and partly filled density-of-states distribution," *Journal of Physics: Condensed Matter*, vol. 14, pp. 9899–9911, Oct. 2002.

[31] C. Tanase, E. J. Meijer, P. W. M. Blom, and D. M. de Leeuw, "Unification of the hole transport in polymeric field-effect transistors and light-emitting diodes," *Physical Review Letters*, vol. 91, p. 216601, Nov. 2003.

[32] A. Deviis, K. Meerholz, D. Hertel, and V. Gulbinas, "Hierarchical charge carrier motion in conjugated polymers," *Chemical Physics Letters*, vol. 498, pp. 302–306, Oct. 2010.

[33] S. A. Chen and C. S. Liao, "Conductivity relaxation and chain motions in conjugated conducting polymers: neutral poly(3-alkylthiophenes)," *Macromolecules*, vol. 26, pp. 2810–2816, May 1993.

[34] F. Laquai, G. Wegner, and H. Baessler, "What determines the mobility of charge carriers in conjugated polymers?," *Philosophical Transactions of the Royal Society A: Mathematical, Physical and Engineering Sciences*, vol. 365, pp. 1473–1487, June 2007.

[35] D. Hertel, U. Scherf, and H. Baessler, "Charge carrier mobility in a ladder-type conjugated polymer," *Advanced Materials*, vol. 10, no. 14, pp. 1119–1122, 1998.

[36] H. Kim, N. Schulte, G. Zhou, K. Muellen, and F. Laquai, "A high gain and high charge carrier mobility indenofluorene-phenanthrene copolymer for light amplification and organic lasing," *Advanced Materials*, vol. 23, no. 7, pp. 894–897, 2011.

[37] F. C. Grozema and L. D. A. Siebbeles, "Charge mobilities in conjugated polymers measured by pulse radiolysis time-resolved microwave conductivity: From single chains to solids," *The Journal of Physical Chemistry Letters*, vol. 2, pp. 2951–2958, Dec. 2011.

[38] H. Sirringhaus, P. J. Brown, R. H. Friend, M. M. Nielsen, K. Bechgaard, B. M. W. Langeveld-Voss, A. J. H. Spiering, R. a. J. Janssen, E. W. Meijer, P. Herwig, and D. M. d. Leeuw, "Two-dimensional charge transport in self-organized, high-mobility conjugated polymers," *Nature*, vol. 401, pp. 685–688, Oct. 1999.

[39] C. Goh, R. J. Kline, M. D. McGehee, E. N. Kadnikova, and J. M. J. Frechet, "Molecular-weight-dependent mobilities in regioregular poly(3-hexyl-thiophene) diodes," *Applied Physics Letters*, vol. 86, pp. 122110–122110–3, Mar. 2005.

[40] A. M. Ballantyne, L. Chen, J. Dane, T. Hammant, F. M. Braun, M. Heeney, W. Duffy, I. McCulloch, D. D. C. Bradley, and J. Nelson, "The effect of poly(3-hexylthiophene) molecular weight on charge transport and the performance of polymer:fullerene solar cells," *Advanced Functional Materials*, vol. 18, no. 16, pp. 2373–2380, 2008.

[41] R. Kline, M. McGehee, E. Kadnikova, J. Liu, and J. Frechet, "Controlling the field-effect mobility of regioregular polythiophene by changing the molecular weight," *Advanced Materials*, vol. 15, no. 18, pp. 1519–1522, 2003.

[42] J.-F. Chang, J. Clark, N. Zhao, H. Sirringhaus, D. W. Breiby, J. W. Andreasen, M. M. Nielsen, M. Giles, M. Heeney, and I. McCulloch, "Molecular-weight dependence of interchain polaron delocalization and exciton bandwidth in high-mobility conjugated polymers," *Physical Review B*, vol. 74, p. 115318, Sept. 2006.

[43] Y. Kim, S. Cook, S. M. Tuladhar, S. A. Choulis, J. Nelson, J. R. Durrant, D. D. C. Bradley, M. Giles, I. McCulloch, C.-S. Ha, and M. Ree, "A strong regioregularity effect in self-organizing conjugated polymer films and high-efficiency polythiophene:fullerene solar cells," *Nature Materials*, vol. 5, no. 3, pp. 197–203, 2006.

[44] R. Mauer, M. Kastler, and F. Laquai, "The impact of polymer regioregularity on charge transport and efficiency of P3HT:PCBM photovoltaic devices," *Advanced Functional Materials*, vol. 20, no. 13, pp. 2085–2092, 2010.

[45] F. C. Grozema, P. T. van Duijnen, Y. A. Berlin, M. A. Ratner, and L. D. A. Siebbeles, "Intramolecular charge transport along isolated chains of conjugated polymers: effect of torsional disorder and polymerization defects," *The Journal of Physical Chemistry B*, vol. 106, pp. 7791–7795, Aug. 2002.

[46] H. Sirringhaus, N. Tessler, and R. H. Friend, "Integrated optoelectronic devices based on conjugated polymers," *Science*, vol. 280, pp. 1741–1744, June 1998.

[47] V. D. Mihailetchi, H. X. Xie, B. de Boer, L. J. A. Koster, and P. W. M. Blom, "Charge transport and photocurrent generation in poly(3-hexylthiophene): Methanofullerene bulk-heterojunction solar cells," *Advanced Functional Materials*, vol. 16, no. 5, pp. 699–708, 2006.

[48] R. J. O. M. Hoofman, M. P. d. Haas, L. D. A. Siebbeles, and J. M. Warman, "Highly mobile electrons and holes on isolated chains of the semiconducting polymer poly(phenylene vinylene)," *Nature*, vol. 392, pp. 54–56, Mar. 1998.

[49] A. R. Inigo, C. C. Chang, W. Fann, J. D. White, Y.-S. Huang, U.-S. Jeng, H. S. Sheu, K.-Y. Peng, and S.-A. Chen, "Enhanced hole mobility in poly-(2-methoxy-5-(2-ethylhexoxy)-1,4-phenylenevinylene) by elimination of nanometer-sized domains," *Advanced Materials*, vol. 17, no. 15, pp. 1835–1838, 2005.

[50] L. Bozano, S. A. Carter, J. C. Scott, G. G. Malliaras, and P. J. Brock, "Temperature- and field-dependent electron and hole mobilities in polymer light-emitting diodes," *Applied Physics Letters*, vol. 74, pp. 1132–1134, Feb. 1999.

[51] S. Shaked, S. Tal, Y. Roichman, A. Razin, S. Xiao, Y. Eichen, and N. Tessler, "Charge density and film morphology dependence of charge mobility in polymer field-effect transistors," *Advanced Materials*, vol. 15, no. 11, pp. 913–916, 2003.

[52] P. Prins, F. C. Grozema, F. Galbrecht, U. Scherf, and L. D. A. Siebbeles, "Charge transport along coiled conjugated polymer chains," *The Journal of Physical Chemistry C*, vol. 111, pp. 11104–11112, July 2007.

[53] M. Redecker, D. D. C. Bradley, M. Inbasekaran, and E. P. Woo, "Nondispersive hole transport in an electroluminescent polyfluorene," *Applied Physics Letters*, vol. 73, pp. 1565–1567, Sept. 1998.

[54] M. Redecker, D. D. C. Bradley, M. Inbasekaran, and E. P. Woo, "Mobility enhancement through homogeneous nematic alignment of a liquid-crystalline polyfluorene," *Applied Physics Letters*, vol. 74, pp. 1400–1402, Mar. 1999.

[55] T. Yasuda, K. Fujita, T. Tsutsui, Y. Geng, S. W. Culligan, and S. H. Chen, "Carrier transport properties of monodisperse glassy-nematic oligofluorenes in organic field-effect transistors," *Chemistry of Materials*, vol. 17, pp. 264–268, Jan. 2005.

[56] H. T. Nicolai, G. A. H. Wetzelaer, M. Kuik, A. J. Kronemeijer, B. de Boer, and P. W. M. Blom, "Space-charge-limited hole current in poly(9,9-dioctylfluorene) diodes," *Applied Physics Letters*, vol. 96, pp. 172107–172107–3, Apr. 2010.

[57] P. Prins, F. C. Grozema, J. M. Schins, S. Patil, U. Scherf, and L. D. A. Siebbeles, "High intrachain hole mobility on molecular wires of ladder-type poly(p-phenylenes)," *Physical Review Letters*, vol. 96, p. 146601, Apr. 2006.

[58] P. Prins, F. C. Grozema, J. M. Schins, T. J. Savenije, S. Patil, U. Scherf, and L. D. A. Siebbeles, "Effect of intermolecular disorder on the intrachain charge transport in ladder-type poly(p-phenylenes)," *Physical Review B*, vol. 73, p. 045204, Jan. 2006.

[59] J. L. Bredas, B. Themans, J. G. Fripiat, J. M. Andre, and R. R. Chance, "Highly conducting polyparaphenylene, polypyrrole, and polythiophene chains: An ab initio study of the geometry and electronic-structure modifications upon doping," *Physical Review B*, vol. 29, pp. 6761–6773, June 1984.

[60] W. Graupner, G. Leditzky, G. Leising, and U. Scherf, "Shallow and deep traps in conjugated polymers of high intrachain order," *Physical Review B*, vol. 54, pp. 7610–7613, Sept. 1996.

[61] M. D. McGehee, E. K. Miller, D. Moses, and A. J. Heeger, "Twenty years of conducting polymers: From fundamental science to applications," in *Advances in Synthetic Metals: Twenty Years of progress in science and technology*, p. 98, Lausanne, Switzerland: Elsevier Science S.A., 1999.

[62] B. Van Averbeke and D. Beljonne, "Conformational effects on excitation transport along conjugated polymer chains," *The Journal of Physical Chemistry A*, vol. 113, pp. 2677–2682, Mar. 2009.

[63] A. J. Campbell, D. D. C. Bradley, and H. Antoniadis, "Dispersive electron transport in an electroluminescent polyfluorene copolymer measured by the current integration time-of-flight method," *Applied Physics Letters*, vol. 79, pp. 2133–2135, Oct. 2001.

[64] S. A. Choulis, Y. Kim, J. Nelson, D. D. C. Bradley, M. Giles, M. Shkunov, and I. McCulloch, "High ambipolar and balanced carrier mobility in regioregular poly(3-hexylthiophene)," *Applied Physics Letters*, vol. 85, pp. 3890–3892, Oct. 2004.

[65] P. Blom and M. Vissenberg, "Charge transport in poly(p-phenylene vinylene) light-emitting diodes," *Materials Science and Engineering: R: Reports*, vol. 27, pp. 53–94, May 2000.

[66] H. T. Nicolai, M. Kuik, G. a. H. Wetzelaer, B. d. Boer, C. Campbell, C. Risko, J. L. Bredas, and P. W. M. Blom, "Unification of trap-limited electron transport in semiconducting polymers," *Nature Materials*, vol. 11, no. 10, pp. 882–887, 2012.

[67] R. J. Kline and M. D. McGehee, "Morphology and charge transport in conjugated polymers," *Journal of Macromolecular Science, Part C: Polymer Reviews*, vol. 46, no. 1, pp. 27–45, 2006.

[68] I. McCulloch, M. Heeney, C. Bailey, K. Genevicius, I. MacDonald, M. Shkunov, D. Sparrowe, S. Tierney, R. Wagner, W. Zhang, M. L. Chabinyc, R. J. Kline, M. D. McGehee, and M. F. Toney, "Liquid-crystalline semiconducting polymers with high charge-carrier mobility," *Nature Materials*, vol. 5, no. 4, pp. 328–333, 2006.

[69] Y. Li, Y. Wu, P. Liu, M. Birau, H. Pan, and B. S. Ong, "Poly(2,5-bis(2-thienyl)-3,6-dialkylthieno [3,2-b]thiophene)s–High-Mobility semiconductors for thin-film transistors," *Advanced Materials*, vol. 18, no. 22, pp. 3029–3032, 2006.

[70] I. Osaka, G. Sauve, R. Zhang, T. Kowalewski, and R. D. McCullough, "Novel thiophene-thiazolothiazole copolymers for organic field-effect transistors," *Advanced Materials*, vol. 19, no. 23, pp. 4160–4165, 2007.

[71] P. P. Infelta, M. P. de Haas, and J. M. Warman, "The study of the transient conductivity of pulse irradiated dielectric liquids on a nanosecond timescale using microwaves," *Radiation Physics and Chemistry (1977)*, vol. 10, no. 5-6, pp. 353–365, 1977.

[72] F. C. Grozema, R. J. O. M. Hoofman, L. P. Candeias, M. P. de Haas, J. M. Warman, and L. D. A. Siebbeles, "The formation and recombination kinetics of positively charged poly(phenylene vinylene) chains in pulse-irradiated dilute solutions," *The Journal of Physical Chemistry A*, vol. 107, pp. 5976–5986, Aug. 2003.

[73] A. Rose, "Space-charge-limited currents in solids," *Physical Review*, vol. 97, pp. 1538–1544, Mar. 1955.

[74] A. M. Goodman and A. Rose, "Double extraction of uniformly generated electron:hole pairs from insulators with noninjecting contacts," *Journal of Applied Physics*, vol. 42, pp. 2823–2830, June 1971.

[75] V. D. Mihailetchi, J. Wildeman, and P. W. M. Blom, "Space-charge limited photocurrent," *Physical Review Letters*, vol. 94, p. 126602, Apr. 2005.

[76] P. N. Murgatroyd, "Theory of space-charge-limited current enhanced by frenkel effect," *Journal of Physics D: Applied Physics*, vol. 3, pp. 151–156, Feb. 1970.

[77] B. A. Gregg, S. E. Gledhill, and B. Scott, "Can true space-charge-limited currents be observed in pi-conjugated polymers?," *Journal of Applied Physics*, vol. 99, pp. 116104–116104–3, June 2006.

[78] G. Dennler, M. C. Scharber, and C. J. Brabec, "Polymer-fullerene bulk-heterojunction solar cells," *Advanced Materials*, vol. 21, no. 13, pp. 1323–1338, 2009.

[79] J. Nelson, "polymer:fullerene bulk heterojunction solar cells," *Materials Today*, vol. 14, pp. 462–470, Oct. 2011.

[80] C. J. Brabec, N. S. Sariciftci, and J. C. Hummelen, "Plastic solar cells," *Advanced Functional Materials*, vol. 11, no. 1, pp. 15–26, 2001.

[81] G. Yu, J. Gao, J. C. Hummelen, F. Wudl, and A. J. Heeger, "Polymer photovoltaic cells: Enhanced efficiencies via a network of internal donor-acceptor heterojunctions," *Science*, vol. 270, pp. 1789–1791, Dec. 1995.

[82] O. V. Mikhnenko, H. Azimi, M. Scharber, M. Morana, P. W. M. Blom, and M. A. Loi, "Exciton diffusion length in narrow bandgap polymers," *Energy & Environmental Science*, vol. 5, no. 5, p. 6960, 2012.

[83] P. E. Shaw, A. Ruseckas, and I. D. W. Samuel, "Exciton diffusion measurements in poly(3-hexylthiophene)," *Advanced Materials*, vol. 20, no. 18, pp. 3516–3520, 2008.

[84] A. Maurano, R. Hamilton, C. G. Shuttle, A. M. Ballantyne, J. Nelson, B. ORegan, W. Zhang, I. McCulloch, H. Azimi, M. Morana, C. J. Brabec, and J. R. Durrant, "Recombination dynamics as a key determinant of open circuit voltage in organic bulk heterojunction solar cells: A comparison of four different donor polymers," *Advanced Materials*, vol. 22, no. 44, p. 49874992, 2010.

[85] D. Credgington, R. Hamilton, P. Atienzar, J. Nelson, and J. R. Durrant, "Non-geminate recombination as the primary determinant of open-circuit voltage in Polythiophene:Fullerene blend solar cells: an analysis of the influence of device processing conditions," *Advanced Functional Materials*, vol. 21, no. 14, p. 27442753, 2011.

[86] R. Mauer, I. A. Howard, and F. Laquai, "Effect of nongeminate recombination on fill factor in Polythiophene/Methanofullerene organic solar cells," *The Journal of Physical Chemistry Letters*, vol. 1, pp. 3500–3505, Dec. 2010.

[87] R. Mauer, I. A. Howard, and F. Laquai, "Effect of external bias on nongeminate recombination in Polythiophene/Methanofullerene organic solar cells," *The Journal of Physical Chemistry Letters*, vol. 2, pp. 1736–1741, July 2011.

[88] F. Etzold, I. A. Howard, R. Mauer, M. Meister, T.-D. Kim, K.-S. Lee, N. S. Baek, and F. Laquai, "Ultrafast exciton dissociation followed by nongeminate charge recombination in PCDTBT:PCBM photovoltaic blends," *Journal of the American Chemical Society*, vol. 133, pp. 9469–9479, June 2011.

[89] Z. He, C. Zhong, X. Huang, W.-Y. Wong, H. Wu, L. Chen, S. Su, and Y. Cao, "Simultaneous enhancement of open-circuit voltage, short-circuit current density, and fill factor in polymer solar cells," *Advanced Materials*, vol. 23, no. 40, pp. 4636–4643, 2011.

[90] M. Campoy-Quiles, T. Ferenczi, T. Agostinelli, P. G. Etchegoin, Y. Kim, T. D. Anthopoulos, P. N. Stavrinou, D. D. C. Bradley, and J. Nelson, "Morphology evolution via self-organization and lateral and vertical diffusion in polymer:fullerene solar cell blends," *Nature Materials*, vol. 7, no. 2, pp. 158–164, 2008.

[91] B. A. Gregg, M. A. Fox, and A. J. Bard, "Photovoltaic effect in symmetrical cells of a liquid crystal porphyrin," *The Journal of Physical Chemistry*, vol. 94, pp. 1586–1598, Feb. 1990.

[92] P. Langevin *Annales de Chimie et de Physique*, vol. 28, p. 433, 1903.

[93] C. Deibel, A. Wagenpfahl, and V. Dyakonov, "Origin of reduced polaron recombination in organic semiconductor devices," *arXiv:0907.2428*, July 2009. Phys. Rev. B 80, 075203 (2009).

[94] A. Pivrikas, N. S. Sariciftci, G. Juska, and R. Oesterbacka, "A review of charge transport and recombination in polymer/fullerene organic solar cells," *Progress in Photovoltaics: Research and Applications*, vol. 15, no. 8, pp. 677–696, 2007.

[95] G. Juska, K. Genevicius, N. Nekrasas, and G. Sliauzys, "Two-dimensional langevin recombination," *physica status solidi (c)*, vol. 7, no. 3-4, pp. 980–983, 2010.

[96] R. Hamilton, C. G. Shuttle, B. O'Regan, T. C. Hammant, J. Nelson, and J. R. Durrant, "Recombination in annealed and nonannealed Polythiophene/Fullerene solar cells: Transient photovoltage studies versus numerical modeling," *The Journal of Physical Chemistry Letters*, vol. 1, pp. 1432–1436, May 2010.

[97] T. M. Clarke, D. B. Rodovsky, A. A. Herzing, J. Peet, G. Dennler, D. DeLongchamp, C. Lungenschmied, and A. J. Mozer, "Significantly reduced bimolecular recombination in a novel silole-based polymer: Fullerene blend," *Advanced Energy Materials*, vol. 1, no. 6, pp. 1062–1067, 2011.

[98] T. M. Clarke, J. Peet, P. Denk, G. Dennler, C. Lungenschmied, and A. J. Mozer, "Non-langevin bimolecular recombination in a silole-based polymer:PCBM solar cell measured by time-resolved charge extraction and resistance-dependent time-of-flight techniques," *Energy & Environmental Science*, vol. 5, no. 1, p. 5241, 2012.

[99] T. Kirchartz and J. Nelson, "Meaning of reaction orders in polymer:fullerene solar cells," *Physical Review B*, vol. 86, p. 165201, Oct. 2012.

[100] M. Morana, M. Wegscheider, A. Bonanni, N. Kopidakis, S. Shaheen, M. Scharber, Z. Zhu, D. Waller, R. Gaudiana, and C. Brabec, "Bipolar charge transport in PCPDTBT-PCBM bulk-heterojunctions for photovoltaic applications," *Advanced Functional Materials*, vol. 18, no. 12, pp. 1757–1766, 2008.

[101] S. M. Tuladhar, D. Poplavskyy, S. A. Choulis, J. R. Durrant, D. D. C. Bradley, and J. Nelson, "Ambipolar charge transport in films of methanofullerene and poly(phenylenevinylene)/Methanofullerene blends," *Advanced Functional Materials*, vol. 15, no. 7, pp. 1171–1182, 2005.

[102] V. D. Mihailetchi, L. J. A. Koster, P. W. M. Blom, C. Melzer, B. de Boer, J. K. J. van Duren, and R. a. J. Janssen, "Compositional dependence of the performance of poly(p-phenylene vinylene):Methanofullerene bulk-heterojunction solar cells," *Advanced Functional Materials*, vol. 15, no. 5, p. 795801, 2005.

[103] M. Morana, H. Azimi, G. Dennler, H.-J. Egelhaaf, M. Scharber, K. Forberich, J. Hauch, R. Gaudiana, D. Waller, Z. Zhu, K. Hingerl, S. S. van Bavel, J. Loos, and C. J. Brabec, "Nanomorphology and charge generation in bulk heterojunctions based on low-bandgap dithiophene polymers with different bridging atoms," *Advanced Functional Materials*, vol. 20, no. 7, pp. 1180–1188, 2010.

[104] H. Azimi, A. Senes, M. C. Scharber, K. Hingerl, and C. J. Brabec, "Charge transport and recombination in low-bandgap bulk heterojunction solar cell using bis-adduct fullerene," *Advanced Energy Materials*, vol. 1, no. 6, pp. 1162–1168, 2011.

[105] M. A. Faist, P. E. Keivanidis, S. Foster, P. H. Woebkenberg, T. D. Anthopoulos, D. D. C. Bradley, J. R. Durrant, and J. Nelson, "Effect of multiple adduct fullerenes on charge generation and transport in photovoltaic blends with poly(3-hexylthiophene-2,5-diyl)," *Journal of Polymer Science Part B: Polymer Physics*, vol. 49, no. 1, pp. 45–51, 2011.

[106] F. M. Braun, *Modelling of light-trapping structures and their application in organic photovoltaic devices*. Ph.D., University of London, 2007.

[107] M. M. Mandoc, L. J. A. Koster, and P. W. M. Blom, "Optimum charge carrier mobility in organic solar cells," *Applied Physics Letters*, vol. 90, pp. 133504–133504–3, Mar. 2007.

[108] T. Kirchartz, B. E. Pieters, K. Taretto, and U. Rau, "Mobility dependent efficiencies of organic bulk heterojunction solar cells: Surface recombination and charge transfer state distribution," *Physical Review B*, vol. 80, p. 035334, July 2009.

[109] S. A. Choulis, J. Nelson, Y. Kim, D. Poplavskyy, T. Kreouzis, J. R. Durrant, and D. D. C. Bradley, "Investigation of transport properties in polymer/fullerene blends using time-of-flight photocurrent measurements," *Applied Physics Letters*, vol. 83, pp. 3812–3814, Nov. 2003.

[110] P. W. M. Blom, V. D. Mihailetchi, L. J. A. Koster, and D. E. Markov, "Device physics of polymer:fullerene bulk heterojunction solar cells," *Advanced Materials*, vol. 19, no. 12, pp. 1551–1566, 2007.

[111] J. Peet, L. Wen, P. Byrne, S. Rodman, K. Forberich, Y. Shao, N. Drolet, R. Gaudiana, G. Dennler, and D. Waller, "Bulk heterojunction solar cells with thick active layers and high fill factors enabled by a bithiophene-co-thiazolothiazole push-pull copolymer," *Applied Physics Letters*, vol. 98, pp. 043301–043301–3, Jan. 2011.

[112] G. F. A. Dibb, F. C. Jamieson, A. Maurano, J. Nelson, and J. R. Durrant, "Limits on the fill factor in organic photovoltaics: Distinguishing nongeminate and geminate recombination mechanisms," *The Journal of Physical Chemistry Letters*, vol. 4, pp. 803–808, Mar. 2013.

[113] M. Lenes, G.-J. A. H. Wetzelaer, F. B. Kooistra, S. C. Veenstra, J. C. Hummelen, and P. W. M. Blom, "Fullerene bisadducts for enhanced open-circuit voltages and efficiencies in polymer solar cells," *Advanced Materials*, vol. 20, no. 11, pp. 2116–2119, 2008.

[114] J. M. Frost, M. A. Faist, and J. Nelson, "Energetic disorder in higher fullerene adducts: A quantum chemical and voltammetric study," *Advanced Materials*, vol. 22, no. 43, pp. 4881–4884, 2010.

[115] D. Neher, "Polyfluorene homopolymers: Conjugated liquid-crystalline polymers for bright blue emission and polarized electroluminescence," *Macromolecular Rapid Communications*, vol. 22, no. 17, pp. 1365–1385, 2001.

[116] U. Scherf and E. List, "Semiconducting polyfluorenes - towards reliable structure-property relationships," *Advanced Materials*, vol. 14, no. 7, pp. 477–487, 2002.

[117] P. Chen, G. Yang, T. Liu, T. Li, M. Wang, and W. Huang, "Optimization of opto-electronic property and device efficiency of polyfluorenes by tuning structure and morphology," *Polymer International*, vol. 55, no. 5, pp. 473–490, 2006.

[118] M. Jaiswal and R. Menon, "Polymer electronic materials: a review of charge transport," *Polymer International*, vol. 55, no. 12, pp. 1371–1384, 2006.

[119] J. H. Burroughes, D. D. C. Bradley, A. R. Brown, R. N. Marks, K. Mackay, R. H. Friend, P. L. Burns, and A. B. Holmes, "Light-emitting diodes based on conjugated polymers," *, Published online: 11 October 1990; | doi:10.1038/347539a0*, vol. 347, pp. 539–541, Oct. 1990.

[120] D. Braun and A. J. Heeger, "Visible light emission from semiconducting polymer diodes," *Applied Physics Letters*, vol. 58, pp. 1982–1984, May 1991.

[121] U. Scherf and K. Muellen, "Polyarylenes and poly(arylenevinylenes), 7. a soluble ladder polymer via bridging of functionalized poly(p-phenylene)-precursors," *Die Makromolekulare Chemie, Rapid Communications*, vol. 12, no. 8, pp. 489–497, 1991.

[122] H. Reisch, U. Wiesler, U. Scherf, and N. Tuytuylkov, "Poly(indenofluorene) (PIF), a novel low band gap polyhydrocarbon," *Macromolecules*, vol. 29, pp. 8204–8210, Jan. 1996.

[123] F. Laquai, A. K. Mishra, K. Muellen, and R. H. Friend, "Amplified spontaneous emission of poly(ladder-type phenylene)s - the influence of photophysical properties on ASE thresholds," *Advanced Functional Materials*, vol. 18, no. 20, pp. 3265–3275, 2008.

[124] P. Prins, F. C. Grozema, B. S. Nehls, T. Farrell, U. Scherf, and L. D. A. Siebbeles, "Enhanced charge-carrier mobility in beta-phase polyfluorene," *Physical Review B*, vol. 74, p. 113203, Sept. 2006.

[125] J. Zaumseil and H. Sirringhaus, "Electron and ambipolar transport in organic field-effect transistors," *Chemical Reviews*, vol. 107, pp. 1296–1323, Apr. 2007.

[126] S. H. Chen, A. C. Su, C. H. Su, and S. A. Chen, "Crystalline forms and emission behavior of poly(9,9-di-n-octyl-2,7-fluorene)," *Macromolecules*, vol. 38, pp. 379–385, Jan. 2005.

[127] M. Grell, D. D. C. Bradley, M. Inbasekaran, and E. P. Woo, "A glass-forming conjugated main-chain liquid crystal polymer for polarized electroluminescence applications," *Advanced Materials*, vol. 9, no. 10, pp. 798–802, 1997.

[128] M. Grell, D. Bradley, X. Long, T. Chamberlain, M. Inbasekaran, E. Woo, and M. Soliman, "Chain geometry, solution aggregation and enhanced dichroism in the liquidcrystalline conjugated polymer poly(9,9-dioctylfluorene)," *Acta Polymerica*, vol. 49, no. 8, pp. 439–444, 1998.

[129] M. Grell, D. D. C. Bradley, G. Ungar, J. Hill, and K. S. Whitehead, "Interplay of physical structure and photophysics for a liquid crystalline polyfluorene," *Macromolecules*, vol. 32, pp. 5810–5817, Sept. 1999.

[130] M. Grell, D. Bradley, M. Inbasekaran, G. Ungar, K. Whitehead, and E. Woo, "Intrachain ordered polyfluorene," *Synthetic Metals*, vol. 111-112, pp. 579–581, June 2000.

[131] M. Ariu, M. Sims, M. D. Rahn, J. Hill, A. M. Fox, D. G. Lidzey, M. Oda, J. Cabanillas-Gonzalez, and D. D. C. Bradley, "Exciton migration in beta-phase poly(9,9-dioctylfluorene)," *Physical Review B*, vol. 67, p. 195333, May 2003.

[132] S. H. Chen, A. C. Su, and S. A. Chen, "Noncrystalline phases in poly(9,9-di-n-octyl-2,7-fluorene)," *The Journal of Physical Chemistry B*, vol. 109, pp. 10067–10072, May 2005.

[133] K. Becker and J. M. Lupton, "Dual species emission from single polyfluorene molecules: signatures of stress-induced planarization of single polymer chains," *Journal of the American Chemical Society*, vol. 127, pp. 7306–7307, May 2005.

[134] E. Da Como, K. Becker, J. Feldmann, and J. M. Lupton, "How strain controls electronic linewidth in single -phase polyfluorene nanowires," *Nano Letters*, vol. 7, pp. 2993–2998, Oct. 2007.

[135] D. D. C. Bradley, M. Grell, X. Long, H. Mellor, A. W. Grice, M. Inbasekaran, and E. P. Woo, "Influence of aggregation on the optical properties of a polyfluorene," *Proc. SPIE: Optical probes of conjugated polymers*, vol. 3145, p. 254, 1997.

[136] M. Ariu, D. G. Lidzey, M. Sims, A. J. Cadby, P. A. Lane, and D. D. C. Bradley, "The effect of morphology on the temperature-dependent photoluminescence quantum efficiency of the conjugated polymer poly(9, 9-dioctylfluorene)," *Journal of Physics: Condensed Matter*, vol. 14, pp. 9975–9986, Oct. 2002.

[137] J. Peet, E. Brocker, Y. Xu, and G. C. Bazan, "Controlled beta-phase formation in poly(9,9-di-n-octylfluorene) by processing with alkyl additives," *Advanced Materials*, vol. 20, no. 10, pp. 1882–1885, 2008.

[138] D. W. Bright, F. B. Dias, F. Galbrecht, U. Scherf, and A. P. Monkman, "The influence of alkyl-chain length on beta-phase formation in polyfluorenes," *Advanced Functional Materials*, vol. 19, no. 1, pp. 67–73, 2009.

[139] W. Chunwaschirasiri, B. Tanto, D. L. Huber, and M. J. Winokur, "Chain conformations and photoluminescence of poly(di-n-octylfluorene)," *Physical Review Letters*, vol. 94, p. 107402, Mar. 2005.

[140] W. C. Tsoi, A. Charas, A. J. Cadby, G. Khalil, A. M. Adawi, A. Iraqi, B. Hunt, J. Morgado, and D. G. Lidzey, "Observation of the beta-phase in two short-chain oligofluorenes," *Advanced Functional Materials*, vol. 18, no. 4, pp. 600–606, 2008.

[141] A. L. T. Khan, P. Sreearunothai, L. M. Herz, M. J. Banach, and A. Koehler, "Morphology-dependent energy transfer within polyfluorene thin films," *Physical Review B*, vol. 69, p. 085201, Feb. 2004.

[142] A. Hayer, A. L. T. Khan, R. H. Friend, and A. Koehler, "Morphology dependence of the triplet excited state formation and absorption in polyfluorene," *Physical Review B*, vol. 71, p. 241302, June 2005.

[143] A. J. Cadby, P. A. Lane, H. Mellor, S. J. Martin, M. Grell, C. Giebeler, D. D. C. Bradley, M. Wohlgenannt, C. An, and Z. V. Vardeny, "Film morphology and photophysics of polyfluorene," *Physical Review B*, vol. 62, pp. 15604–15609, Dec. 2000.

[144] M. Sims, K. Zheng, M. C. Quiles, R. Xia, P. N. Stavrinou, D. D. C. Bradley, and P. Etchegoin, "On the use of optical probes to monitor the thermal transitions in spin-coated poly(9,9-dioctylfluorene) films," *Journal of Physics: Condensed Matter*, vol. 17, pp. 6307–6318, Oct. 2005.

[145] P. N. Stavrinou, G. Ryu, M. Campoy-Quiles, and D. D. C. Bradley, "The change in refractive index of poly(9,9-dioctylfluorene) due to the adoption of the beta-phase chain conformation," *Journal of Physics: Condensed Matter*, vol. 19, p. 466107, Nov. 2007.

[146] G. Ryu, P. N. Stavrinou, and D. D. C. Bradley, "Spatial patterning of the beta-phase in poly(9,9-dioctylfluorene): A metamaterials-inspired molecular conformation approach to the fabrication of polymer semiconductor optical structures," *Advanced Functional Materials*, vol. 19, no. 20, pp. 3237–3242, 2009.

[147] H.-F. Shi, Y. Nakai, S.-J. Liu, Q. Zhao, Z.-F. An, T. Tsuboi, and W. Huang, "Improved energy transfer through the formation of the phase for polyfluorenes containing phosphorescent iridium(III) complexes," *The Journal of Physical Chemistry C*, vol. 115, pp. 11749–11757, June 2011.

[148] S. Janietz, D. D. C. Bradley, M. Grell, C. Giebeler, M. Inbasekaran, and E. P. Woo, "Electrochemical determination of the ionization potential and electron affinity of poly(9,9-dioctylfluorene)," *Applied Physics Letters*, vol. 73, pp. 2453–2455, Oct. 1998.

[149] B. K. Yap, *A study of the underlying processes that impact on conjugated polymer device stability and efficiency*. Ph.D., Imperial College London, UK, 2008.

[150] L.-Y. Chen, W.-Y. Hung, Y.-T. Lin, C.-C. Wu, T.-C. Chao, T.-H. Hung, and K.-T. Wong, "Enhancement of bipolar carrier transport in oligofluorene films through alignment in the liquid-crystalline phase," *Applied Physics Letters*, vol. 87, pp. 112103–112103–3, Sept. 2005.

[151] L.-Y. Chen, T.-H. Ke, C.-C. Wu, T.-C. Chao, K.-T. Wong, and C.-C. Chang, "Anisotropic ambipolar carrier transport and high bipolar mobilities up to 0.1 cm^2/vs in aligned liquid-crystal glass films of oligofluorene," *Applied Physics Letters*, vol. 91, pp. 163509–163509–3, Oct. 2007.

[152] Z.-Q. Lin, N.-E. Shi, Y.-B. Li, D. Qiu, L. Zhang, J.-Y. Lin, J.-F. Zhao, C. Wang, L.-H. Xie, and W. Huang, "Preparation and characterization of polyfluorene-based supramolecular pi-conjugated polymer gels," *The Journal of Physical Chemistry C*, vol. 115, pp. 4418–4424, Mar. 2011.

[153] J.-H. Chen, C.-S. Chang, Y.-X. Chang, C.-Y. Chen, H.-L. Chen, and S.-A. Chen, "Gelation and its effect on the photophysical behavior of poly(9,9-dioctylfluorene-2,7-diyl) in toluene," *Macromolecules*, vol. 42, pp. 1306–1314, Feb. 2009.

[154] F. Laquai, G. Wegner, C. Im, H. Bssler, and S. Heun, "Comparative study of hole transport in polyspirobifluorene polymers measured by the charge-generation layer time-of-flight technique," *Journal of Applied Physics*, vol. 99, pp. 023712–023712–7, Jan. 2006.

[155] F. Laquai and D. Hertel, "Influence of hole transport units on the efficiency of polymer light emitting diodes," *Applied Physics Letters*, vol. 90, pp. 142109–142109–3, Apr. 2007.

[156] M. Sims, S. M. Tuladhar, J. Nelson, R. C. Maher, M. Campoy-Quiles, S. A. Choulis, M. Mairy, D. D. C. Bradley, P. G. Etchegoin, C. Tregidgo, K. Suhling, D. R. Richards, P. Massiot, C. B. Nielsen, and J. H. G. Steinke, "Correlation between microstructure and charge transport in poly(2,5-dimethoxy-p-phenylenevinylene) thin films," *Physical Review B*, vol. 76, p. 195206, Nov. 2007.

[157] M. Zhang, H. N. Tsao, W. Pisula, C. Yang, A. K. Mishra, and K. Muellen, "Field-effect transistors based on a benzothiadiazole-cyclopentadithiophene copolymer," *Journal of the American Chemical Society*, vol. 129, pp. 3472–3473, Mar. 2007.

[158] H. N. Tsao, D. Cho, J. W. Andreasen, A. Rouhanipour, D. W. Breiby, W. Pisula, and K. Muellen, "The influence of morphology on high-performance polymer field-effect transistors," *Advanced Materials*, vol. 21, no. 2, pp. 209–212, 2009.

[159] A. R. Inigo, Y. F. Huang, J. D. White, Y.-S. Huang, W. Fann, K.-Y. Peng, and S.-A. Chen, "Review of morphology dependent charge carrier mobility in MEH-PPV," *J. Chin. Chem. Soc.*, vol. 57, no. 3B, 2010.

[160] S. Athanasopoulos, J. Kirkpatrick, D. Martinez, J. M. Frost, C. M. Foden, A. B. Walker, and J. Nelson, "Predictive study of charge transport in disordered semiconducting polymers," *Nano Letters*, vol. 7, pp. 1785–1788, June 2007.

[161] C. J. Brabec, A. Cravino, D. Meissner, N. S. Sariciftci, T. Fromherz, M. T. Rispens, L. Sanchez, and J. C. Hummelen, "Origin of the open circuit voltage of plastic solar cells," *Advanced Functional Materials*, vol. 11, no. 5, pp. 374–380, 2001.

[162] M. C. Scharber, D. Muehlbacher, M. Koppe, P. Denk, C. Waldauf, A. J. Heeger, and C. J. Brabec, "Design rules for donors in bulk-heterojunction solar cells–towards 10 % energy-conversion efficiency," *Advanced Materials*, vol. 18, no. 6, pp. 789–794, 2006.

[163] H. Azimi, M. Morana, T. Ameri, B. Dastmalchi, M. Scharber, K. Hingerl, and C. J. Brabec, "Determining the internal quantum efficiency of organic bulk heterojunctions based on mono and bis-adduct fullerenes as acceptor," *Solar Energy Materials and Solar Cells*, vol. 95, pp. 3093–3098, Nov. 2011.

[164] G. Zhao, Y. He, and Y. Li, "6.5% efficiency of polymer solar cells based on poly(3-hexylthiophene) and indene-c60 bisadduct by device optimization," *Advanced Materials*, vol. 22, no. 39, pp. 4355–4358, 2010.

[165] Y. He, G. Zhao, B. Peng, and Y. Li, "High-yield synthesis and electrochemical and photovoltaic properties of indene-c70 bisadduct," *Advanced Functional Materials*, vol. 20, no. 19, pp. 3383–3389, 2010.

[166] X. Gong, T. Yu, Y. Cao, and A. Heeger, "Large open-circuit voltage polymer solar cells by poly(3-hexylthiophene) with multi-adducts fullerenes," *SCIENCE CHINA Chemistry*, vol. 55, no. 5, pp. 743–748, 2012.

[167] C.-L. Chang, C.-W. Liang, J.-J. Syu, L. Wang, and M.-k. Leung, "Triphenylamine-substituted methanofullerene derivatives for enhanced open-circuit voltages and efficiencies in polymer solar cells," *Solar Energy Materials and Solar Cells*, vol. 95, pp. 2371–2379, Aug. 2011.

[168] M. A. Faist, *Spectroscopic studies of the charge transfer state and device performance of polymer:fullerene photovoltaic blends*. Ph.D., Imperial College London, UK, 2012.

[169] N. C. Cates, R. Gysel, Z. Beiley, C. E. Miller, M. F. Toney, M. Heeney, I. McCulloch, and M. D. McGehee, "Tuning the properties of polymer bulk heterojunction solar cells by adjusting fullerene size to control intercalation," *Nano Letters*, vol. 9, pp. 4153–4157, Dec. 2009.

[170] J. M. Ball, R. K. M. Bouwer, F. B. Kooistra, J. M. Frost, Y. Qi, E. B. Domingo, J. Smith, D. M. de Leeuw, J. C. Hummelen, J. Nelson, A. Kahn, N. Stingelin, D. D. C. Bradley, and T. D. Anthopoulos, "Soluble fullerene derivatives: The effect of electronic structure on transistor performance and air stability," *Journal of Applied Physics*, vol. 110, pp. 014506–014506–9, July 2011.

[171] N. S. Sariciftci, L. Smilowitz, A. J. Heeger, and F. Wudl, "Photoinduced electron transfer from a conducting polymer to buckminsterfullerene," *Science*, vol. 258, pp. 1474–1476, Nov. 1992.

[172] N. S. Sariciftci, D. Braun, C. Zhang, V. I. Srdanov, A. J. Heeger, G. Stucky, and F. Wudl, "Semiconducting polymer:buckminsterfullerene heterojunctions: Diodes, photodiodes, and photovoltaic cells," *Applied Physics Letters*, vol. 62, pp. 585–587, Feb. 1993.

[173] J. C. Hummelen, B. W. Knight, F. LePeq, F. Wudl, J. Yao, and C. L. Wilkins, "Preparation and characterization of fulleroid and methanofullerene derivatives," *The Journal of Organic Chemistry*, vol. 60, pp. 532–538, Feb. 1995.

[174] J. M. Frost, *Computational modelling and design of conjugated molecular electronic materials*. Ph.D., University of London, 2010.

[175] P. A. Troshin, H. Hoppe, J. Renz, M. Egginger, J. Y. Mayorova, A. E. Goryachev, A. S. Peregudov, R. N. Lyubovskaya, G. Gobsch, N. S. Sariciftci, and V. F. Razumov, "Material solubility-photovoltaic performance relationship in the design of novel fullerene derivatives for bulk heterojunction solar cells," *Advanced Functional Materials*, vol. 19, no. 5, pp. 779–788, 2009.

[176] S. C. Rifkin and D. H. Evans, "General equation for voltammetry with step-functional potential changes applied to differential pulse voltammetry," *Analytical Chemistry*, vol. 48, pp. 1616–1618, Sept. 1976.

[177] J. J. Kwiatkowski, J. M. Frost, and J. Nelson, "The effect of morphology on electron field-effect mobility in disordered c60 thin films," *Nano Letters*, vol. 9, pp. 1085–1090, Mar. 2009.

[178] T. B. Singh, N. S. Sariciftci, H. Yang, L. Yang, B. Plochberger, and H. Sitter, "Correlation of crystalline and structural properties of c60 thin films grown at various temperature with charge carrier mobility," *Applied Physics Letters*, vol. 90, pp. 213512–213512–3, May 2007.

[179] S. Kobayashi, T. Takenobu, S. Mori, A. Fujiwara, and Y. Iwasa, "Fabrication and characterization of c60 thin-film transistors with high field-effect mobility," *Applied Physics Letters*, vol. 82, pp. 4581–4583, June 2003.

[180] X. Yang, J. K. J. van Duren, M. T. Rispens, J. C. Hummelen, R. a. J. Janssen, M. a. J. Michels, and J. Loos, "Crystalline organization of a methanofullerene as used for plastic solar-cell applications," *Advanced Materials*, vol. 16, no. 9-10, pp. 802–806, 2004.

[181] R. K. M. Bouwer, G.-J. A. H. Wetzelaer, P. W. M. Blom, and J. C. Hummelen, "Influence of the isomeric composition of the acceptor on the performance of organic bulk heterojunction P3HT:bis-PCBM solar cells," *Journal of Materials Chemistry*, vol. 22, no. 30, p. 15412, 2012.

[182] R. C. I. MacKenzie, J. M. Frost, and J. Nelson, "A numerical study of mobility in thin films of fullerene derivatives," *The Journal of Chemical Physics*, vol. 132, pp. 064904–064904–6, Feb. 2010.

[183] Y. He, H.-Y. Chen, J. Hou, and Y. Li, "Indene-C60 bisadduct: A new acceptor for high-performance polymer solar cells," *Journal of the American Chemical Society*, vol. 132, pp. 1377–1382, Feb. 2010.

[184] H. Azimi, D. Fournier, M. Wirix, E. Dobrocka, T. Ameri, F. Machui, S. Rodman, G. Dennler, M. C. Scharber, K. Hingerl, J. Loos, C. J. Brabec, and M. Morana, "Nano-morphology characterization of organic bulk heterojunctions based on mono and bis-adduct fullerenes," *Organic Electronics*, vol. 13, pp. 1315–1321, Aug. 2012.

[185] C. Mueller, T. A. M. Ferenczi, M. Campoy-Quiles, J. M. Frost, D. D. C. Bradley, P. Smith, N. Stingelin-Stutzmann, and J. Nelson, "Binary organic photovoltaic blends: A simple rationale for optimum compositions," *Advanced Materials*, vol. 20, no. 18, pp. 3510–3515, 2008.

[186] S. M. Tuladhar, *Charge Transport in Polymer and Polymer/Fullerene Blends: Influence of Chemical Structure, Morphology and Blend Composition.* Ph.D., University of London, UK, 2006.

[187] J. M. Frost, F. Cheynis, S. M. Tuladhar, and J. Nelson, "Influence of polymer-blend morphology on charge transport and photocurrent generation in donor-acceptor polymer blends," *Nano Letters*, vol. 6, pp. 1674–1681, Aug. 2006.

[188] V. Mihailetchi, J. van Duren, P. Blom, J. Hummelen, R. Janssen, J. Kroon, M. Rispens, W. Verhees, and M. Wienk, "Electron transport in a methanofullerene," *Advanced Functional Materials*, vol. 13, no. 1, pp. 43–46, 2003.

[189] H. Antoniadis and E. A. Schiff, "Transient photocharge measurements and electron emission from deep levels in undoped a-Si:H," *Physical Review B*, vol. 46, pp. 9482–9492, Oct. 1992.

[190] R. Oesterbacka, G. Juska, K. Arlauskas, and H. Stubb, "Time-of-flight measurements in langmuir-blodgett films of poly(3-hexylthiophene)," pp. 389–394, Dec. 1997.

[191] T. Agostinelli, T. A. M. Ferenczi, E. Pires, S. Foster, A. Maurano, C. Mueller, A. Ballantyne, M. Hampton, S. Lilliu, M. Campoy-Quiles, H. Azimi, M. Morana, D. D. C. Bradley, J. Durrant, J. E. Macdonald, N. Stingelin, and J. Nelson, "The role of alkane dithiols in controlling polymer crystallization in small band gap polymer:fullerene solar cells," *Journal of Polymer Science Part B: Polymer Physics*, vol. 49, no. 10, pp. 717–724, 2011.

[192] A. Bruno tech. rep., Imperial College London, 2011.

[193] T. D. Anthopoulos, D. M. de Leeuw, E. Cantatore, P. van 't Hof, J. Alma, and J. C. Hummelen, "Solution processible organic transistors and circuits based on a c70 methanofullerene," *Journal of Applied Physics*, vol. 98, p. 054503, Sept. 2005.

[194] N. I. Craciun, J. Wildeman, and P. W. M. Blom, "Universal arrhenius temperature activated charge transport in diodes from disordered organic semiconductors," *Physical Review Letters*, vol. 100, p. 056601, Feb. 2008.

[195] S. H. Park, A. Roy, S. Beaupre, S. Cho, N. Coates, J. S. Moon, D. Moses, M. Leclerc, K. Lee, and A. J. Heeger, "Bulk heterojunction solar cells with internal quantum efficiency approaching 100%," *Nature Photonics*, vol. 3, no. 5, pp. 297–302, 2009.

[196] J. Hou, H.-Y. Chen, S. Zhang, R. I. Chen, Y. Yang, Y. Wu, and G. Li, "Synthesis of a low band gap polymer and its application in highly efficient polymer solar cells," *Journal of the American Chemical Society*, vol. 131, pp. 15586–15587, Nov. 2009.

[197] Y. Liang, Z. Xu, J. Xia, S.-T. Tsai, Y. Wu, G. Li, C. Ray, and L. Yu, "For the bright Future–Bulk heterojunction polymer solar cells with power conversion efficiency of 7.4%," *Advanced Materials*, vol. 22, no. 20, pp. E135–E138, 2010.

[198] J. Peet, J. Y. Kim, N. E. Coates, W. L. Ma, D. Moses, A. J. Heeger, and G. C. Bazan, "Efficiency enhancement in low-bandgap polymer solar cells by processing with alkane dithiols," *Nature Materials*, vol. 6, no. 7, pp. 497–500, 2007.

[199] A. J. Moule, J. B. Bonekamp, and K. Meerholz, "The effect of active layer thickness and composition on the performance of bulk-heterojunction solar cells," *Journal of Applied Physics*, vol. 100, pp. 094503–094503–7, Nov. 2006.

[200] M. T. Dang, L. Hirsch, and G. Wantz, "P3HT:PCBM, best seller in polymer photovoltaic research," *Advanced Materials*, vol. 23, no. 31, pp. 3597–3602, 2011.

[201] J. Nelson, "Diffusion-limited recombination in polymer-fullerene blends and its influence on photocurrent collection," *Physical Review B*, vol. 67, p. 155209, Apr. 2003.

[202] J. K. J. van Duren, X. Yang, J. Loos, C. W. T. Bulle-Lieuwma, A. B. Sieval, J. C. Hummelen, and R. a. J. Janssen, "Relating the morphology of poly(p-phenylene vinylene)/Methanofullerene blends to solar-cell performance," *Advanced Functional Materials*, vol. 14, no. 5, pp. 425–434, 2004.

[203] T. D. Anthopoulos, C. Tanase, S. Setayesh, E. J. Meijer, J. C. Hummelen, P. W. M. Blom, and D. M. de Leeuw, "Ambipolar organic field-effect transistors based on a solution-processed methanofullerene," *Advanced Materials*, vol. 16, no. 23-24, pp. 2174–2179, 2004.

[204] P. H. Woebkenberg, D. D. Bradley, D. Kronholm, J. C. Hummelen, D. M. de Leeuw, M. Colle, and T. D. Anthopoulos, "High mobility n-channel organic field-effect transistors based on soluble c60 and c70 fullerene derivatives," *Synthetic Metals*, vol. 158, pp. 468–472, July 2008.

[205] T. Agostinelli, S. Lilliu, J. G. Labram, M. Campoy-Quiles, M. Hampton, E. Pires, J. Rawle, O. Bikondoa, D. D. C. Bradley, T. D. Anthopoulos, J. Nelson, and J. E. Macdonald, "Real-time investigation of crystallization and phase-segregation dynamics in P3HT:PCBM solar cells during thermal annealing," *Advanced Functional Materials*, vol. 21, no. 9, pp. 1701–1708, 2011.

[206] T. Clarke, A. Ballantyne, F. Jamieson, C. Brabec, J. Nelson, and J. Durrant, "Transient absorption spectroscopy of charge photogeneration yields and lifetimes in a low bandgap polymer/fullerenefilm," *Chemical Communications*, pp. 89–91, Dec. 2008.

[207] F. Etzold, I. A. Howard, N. Forler, D. M. Cho, M. Meister, H. Mangold, J. Shu, M. R. Hansen, K. Muellen, and F. Laquai, "The effect of solvent additives on morphology and excited-state dynamics in PCPDTBT:PCBM photovoltaic blends," *Journal of the American Chemical Society*, vol. 134, pp. 10569–10583, June 2012.

[208] S. Cho, J. K. Lee, J. S. Moon, J. Yuen, K. Lee, and A. J. Heeger, "Bulk heterojunction bipolar field-effect transistors processed with alkane dithiol," *Organic Electronics*, vol. 9, pp. 1107–1111, Dec. 2008.

[209] Y. Gu, C. Wang, and T. P. Russell, "Multi-length-scale morphologies in PCPDTBT/PCBM bulk-heterojunction solar cells," *Advanced Energy Materials*, vol. 2, no. 6, pp. 683–690, 2012.

[210] S. Chambon, R. Mens, K. Vandewal, E. Clodic, M. Scharber, L. Lutsen, J. Gelan, J. Manca, D. Vanderzande, and P. Adriaensens, "Influence of octanedithiol on the nanomorphology of PCPDTBT:PCBM blends studied by solid-state NMR," *Solar Energy Materials and Solar Cells*, vol. 96, pp. 210–217, Jan. 2012.

[211] J. K. Lee, W. L. Ma, C. J. Brabec, J. Yuen, J. S. Moon, J. Y. Kim, K. Lee, G. C. Bazan, and A. J. Heeger, "Processing additives for improved efficiency from bulk heterojunction solar cells," *Journal of the American Chemical Society*, vol. 130, pp. 3619–3623, Mar. 2008.

[212] N. C. Cates, R. Gysel, J. E. P. Dahl, A. Sellinger, and M. D. McGehee, "Effects of intercalation on the hole mobility of amorphous semiconducting polymer blends," *Chemistry of Materials*, vol. 22, pp. 3543–3548, June 2010.

[213] M. R. Hammond, R. J. Kline, A. A. Herzing, L. J. Richter, D. S. Germack, H.-W. Ro, C. L. Soles, D. A. Fischer, T. Xu, L. Yu, M. F. Toney, and D. M. DeLongchamp, "Molecular order in high-efficiency Polymer/Fullerene bulk heterojunction solar cells," *ACS Nano*, vol. 5, pp. 8248–8257, Oct. 2011.

[214] W. Chen, T. Xu, F. He, W. Wang, C. Wang, J. Strzalka, Y. Liu, J. Wen, D. J. Miller, J. Chen, K. Hong, L. Yu, and S. B. Darling, "Hierarchical nanomorphologies promote exciton dissociation in Polymer/Fullerene bulk heterojunction solar cells," *Nano Letters*, vol. 11, pp. 3707–3713, Sept. 2011.

[215] S. J. Lou, J. M. Szarko, T. Xu, L. Yu, T. J. Marks, and L. X. Chen, "Effects of additives on the morphology of solution phase aggregates formed by active layer components of high-efficiency organic solar cells," *Journal of the American Chemical Society*, vol. 133, pp. 20661–20663, Dec. 2011.

[216] C. Bulle-Lieuwma, W. van Gennip, J. van Duren, P. Jonkheijm, R. Janssen, and J. Niemantsverdriet, "Characterization of polymer solar cells by TOF-SIMS depth profiling," *Applied Surface Science*, vol. 203-204, pp. 547–550, Jan. 2003.

[217] A. A. Y. Guilbert, L. X. Reynolds, A. Bruno, A. MacLachlan, S. P. King, M. A. Faist, E. Pires, J. E. Macdonald, N. Stingelin, S. A. Haque, and J. Nelson, "Effect of multiple adduct fullerenes on microstructure and phase behavior of P3HT:Fullerene blend films for organic solar cells," *ACS Nano*, vol. 6, pp. 3868–3875, May 2012.

[218] M. Drees, H. Hoppe, C. Winder, H. Neugebauer, N. S. Sariciftci, W. Schwinger, F. Schffler, C. Topf, M. C. Scharber, Z. Zhu, and R. Gaudiana, "Stabilization of the nanomorphology of polymerfullerene bulk heterojunction blends using a novel polymerizable fullerene derivative," *Journal of Materials Chemistry*, vol. 15, pp. 5158–5163, Dec. 2005.